Novel Osteobiologics for Bone Tissue Engineering

A Dissertation Presented for the
Doctor of Philosophy
Degree
The University of Tennessee, Knoxville

Austin J. Bow
December 2019

Copyright © 2019 by Austin J. Bow
All rights reserved.

DEDICATION

I dedicate this work to the family, friends, and teachers, both here and in memory, that were there for support throughout my career. From you came the unwavering strength to find sure-footing regardless of terrain.

ACKNOWLEDGEMENTS

A special thanks is in order for my mentor Madhu Dhar, without whose guidance this work would not have been possible. Similarly, the support and advice from colleagues in the lab, in particular Steven Newby and Lisa Amelse, and throughout the department of Large Animal Clinical Sciences, with emphasis on valuable input received from David Anderson, was crucial in the development and execution of this research. Furthermore, help from both Kim Rutherford and Stephen Kania in navigating the requirements of the Comparative and Experimental Medicine (CEM) program and the University of Tennessee, Knoxville Graduate School was invaluable and deserves recognition. I would also like to extend my gratitude to the members of my committee for their time and help in molding my research to focus its scope and streamline methodologies.

Additionally, I would like to thank the multiple funding sources that made this research feasible. First and foremost, the funding received through the Department of Defense via the U.S. Army Medical Research and Material Command (MRMC), which permitted my position as a graduate research assistant in the CEM program and covered in large the expenses associated with much of the detailed research. Further funding through OsteoScience foundation and the Center of Excellence program facilitated various studies that produced data of unique value to be later built upon.

For those portions of this work that have been published I would like to thank the editors, reviewers, and publishers for their time and patience.

Lastly, I would like to recognize the vital role of the collaborative research teams with which I have had the pleasure of working. The material design and development team based in the Center for Integrative Nanotech. Sciences at the University of Arkansas at Little Rock (UALR) characterized and provided all materials utilized in this research. The metabolomics division within the Biological and Small Molecule Mass Spectrometry Core (BSMMSC) and the Department of Chemistry at the University of Tennessee, Knoxville provided critical efforts in both operation of equipment and expertise in small molecule analysis.

ABSTRACT

The field of bone tissue engineering features a wide variety of biomaterials designed to facilitate repair and restoration of injured bone tissue. Due to the complex nature of bone, these graft materials face unique challenges in accommodating this highly dynamic environment in which internal structures are being constantly remodeled via osteoblastic and osteoclastic functions. Therefore, effective graft designs must incorporate compositional elements that are capable of promoting and facilitating such activity to permit successful integration with native tissue. These osteobiologic characteristics, including osteo-conduction, osteo-induction, and osseo-integration, are key factors in determining a materials osteogenic capacity and its potential as a bone graft technology. The comprised studies focus on the development and biological assessment of a construct that incorporates osteobiologic components, nano-hydroxyapatite (nHA) and decellularized bone particles (DBPs), within a polymeric binder to form osteogenic matrices for enhancing bone repair. A battery of *in vitro* and *in vivo* assessments of this osteogenic platform were carried out at various stages of the development process to characterize the impact of this biomaterial on multiple cell lines, both immortalized and naïve, as well as in different rodent bone defect models, in both long bone and oromaxillofacial applications. Promising *in vitro* and *in vivo* data at early stages paved the way for more extensive testing, in particular the examination of target proteins expressed in treated tissue, through immunohistochemical techniques, and of the molecular impact of the graft material, using both metabolomic and transcriptomics. Positive detection of key proteins associated with osteogenic and cell attachment functions further supported evidence that scaffolds served as effective matrices for cellular migration and subsequent osteo-differentiation. Additionally, the development of potential pathways of effect for these constructs on exposed naïve cells provided key targets for future studies, which may elucidate the precise mechanisms responsible for the observed biological responses. Furthermore, this multi-omics methodology presents a powerful tool for the evaluation of new graft technologies, promoting the potential of intelligent biomaterial design for specific applications.

TABLE OF CONTENTS

Chapter I: Introduction to Osteobiologics 1

A Brief Introduction to Bone 2

Osteobiologic Products 3
Allografts Products 3
Xenografts Products 7
Synthetic Graft Products 11
Bioactive Graft Products 12

Conclusion 14

References 17

Appendix 24

Chapter II: *In Vitro* Assessment of Immortalized Pre-osteoblast Cells on Polyurethane Matrices Impregnated with Nano-hydroxyapatite 27

Abstract 28

Introduction 29

Material Film *In Vitro* Work 31
MC 3T3-E1 Cell Culture Parameters 31
Viability and Proliferation 31
Morphological Assessment 32

Conclusion 33

References 36

Appendix 39

Chapter III: *In Vivo* Biocompatibility Assessment of Polyurethane/Nano-hydroxyapatite Film-derived Osteobiologic Platforms Using a Rat Unicortical Bone Defect 44

Abstract 45

Introduction 46

3D Scaffold *In Vitro* Analysis 48
Viability and Proliferation 48
qPCR Assessment 49

3D Scaffold Rat *In Vivo* Analysis 51
Tibial Defect Model 51
CT Analysis 52
Histological Analysis 53
New Bone Analysis 54

Conclusion 56

References 58

Appendix 63

Chapter IV: *In Vivo* Comparison of Osteobiologic Platforms with Predicate Devices Using a Rat Critically-size Bone Defect 76

Abstract 77

Introduction 78

Examined Graft Materials 79
Experimental Materials 79
Predicate Materials 80

In Vivo Graft Comparative Analysis 80
Mandibular Defect Model 80
CT Analysis 81
Histological Analysis 81
Immunohistochemisty Analysis 82

Conclusion 82

References 85

Appendix 89

Chapter V: *In Vivo* Assessment of Advanced Osteobiologics Platforms Utilizing a Rat Unicortical Bone Defect 101

Abstract 102

Introduction 102

Advanced Materials 103
Super-hydratable Scaffold Design 103
Injectable Scaffold Design 104
Predicate Device Comarisons 104

Advanced Material *In Vitro* Analysis 105
Caprine Mesenchymal Stem Cell Culture Parameters 105
Viability and Proliferation 106

Advanced Material *In Vivo* Analysis 106
Tibial Defect Model 106
Advanced Material Handling 107
CT Analysis 108
Histological Analysis 108
Immunohistochemisty Analysis 108

Conclusion 109

References 111

Appendix 113

Chapter VI: Multi-omics Assessment of Molecular Mechanisms Associated with Adhesion and Osteogenic Functions of Human Mesenchymal Stem Cells Exposed to an Osteobiologic Platform 123

Abstract 124

Introduction 125

Human Mesenchymal Stem Cell *In Vitro* Work 127
Human Mesenchymal Stem Cell Isolation and Expansion 127
Viability and Proliferation 127
Cytocompatibility 128

Transcriptomics 128
PCR Profiler Microarrays 128
Data Correlation 129

Metabolomics 129
LC-MS Analysis 129
Metabolite Data Analysis 130

Fundamental Pathway Development.....131
Pathway Correlation Databases 131
Network Mapping Software.....132

Conclusion 132

References.....135

Appendix 139

Chapter VII: Conclusions and Future Direction 154

Introduction 155

Future Research.....159

Conclusion 159

References.....160

Appendix 162

Vita 165

LIST OF TABLES

Table 1.1. Overview of bone graft materials 26

Table 3.1: CT qualitative and quantitative statistical analysis 66

Table 6.1. List of up-regulated genes associated with human skeletal development, categorized by function 142

Table 6.2: List of up-regulated genes associated with human bone mineral metabolism, categorized by function.....143

Table 6.3. List of up-regulated genes associated with human cell adhesion molecules, categorized by function.....144

Table 6.4: List of up-regulated genes from associated with human signal transduction pathways, categorize by function 145

Table 6.5. Pathways of interest list generated using IMPaLA software.....149

Table 6.6: Pathways of interest list generated using DAVID software for up-regulated genes from osteogenesis and signal transduction arrays 150

LIST OF FIGURES

Figure 1.1. Generalized flow chart diagram for demineralization of bone tissue . 24

Figure 1.2. Generalized flow chart diagram for decellularization of bone tissue . 25

Figure 2.1. Cell viability/proliferation using Calcein-AM staining 39

Figure 2.2. Cell morphology using DiI staining 40

Figure 2.3. Cell nodule identification utilizing ImageJ processing of DiI stained samples 41

Figure 2.4. Nodule formation tracking utilizing DiI fluorescent labeling 42

Figure 2.5. 80/20 material film seeded with MC 3T3-E1 cells and stained with Alizarin Red reagent 43

Figure 3.1. Day 7 DiI imaging of MC 3T3-E1 cells on 3D scaffold 63

Figure 3.2. Gene expression of S-1 and S-2 treated cells cultures 64

Figure 3.3. *In vivo* model timeline 65

Figure 3.4. S-1 and S-2 untreated/treated defect CT imaging 67

Figure 3.5. Defect orientation for histological imaging 68

Figure 3.6. H&E imaging of S-1 and S-2 treated and untreated defects 69

Figure 3.7. Toluidine Blue imaging of S-1 and S-2 treated and untreated defects 70

Figure 3.8. H&E-based bone surface area measurements 71

Figure 3.9. Oxytet fluorescence imaging of S-1 and S-2 treated and untreated defects 72

Figure 3.10. Fluorescent area analysis 73

Figure 3.11. DAPI fluorescence imaging of S-1 and S-2 treated and untreated defects 74

Figure 3.12. Oxytet fluorescence imaging of defects treated with scaffolds derived from 70/30 and 60/40 PU-nHA films 75

Figure 4.1. Mandibular defect model CT 3D renders 89

Figure 4.2. Graphical representation of mandibular CT area (a) and density (b) data..... 90

Figure 4.3. Masson's Trichrome images of M-1 at 1 and 2 months after implantation 91

Figure 4.4. Masson's Trichrome images of Bio-Oss Collagen® at 1 and 2 months after implantation 92

Figure 4.5. Masson's Trichrome images of Syntoss® at 1 and 2 months after implantation 93

Figure 4.6. Masson's Trichrome images of S-1 at 1 and 2 months after implantation 94

Figure 4.7. Graphical representation of early collagen/bone formation surface area data 95

Figure 4.8. Overview of IHC protocol 96

Figure 4.9. IHC staining for OPN in M-1 (a-c) and S-1 (d-f) samples at 2 months after implantation 97

Figure 4.10. IHC staining for Sp7 in M-1 (a-c) and S-1 (d-f) samples at 2 months after implantation 98

Figure 4.11. IHC staining for CD34 in M-1 (a-c) and S-1 (d-f) samples at 2 months after implantation 99

Figure 4.12. IHC staining for FN in M-1 (a-c) and S-1 (d-f) samples at 2 months after implantation 100

Figure 5.1. Calcein-AM imaging of bmcMSCs exposed and unexposed to injectable materials and corresponding predicate device 113

Figure 5.2. MTS proliferative assay for bmcMSCs seeded to injectable scaffold designs 114

Figure 5.3. CT 3D renders (a,b) and cross-sectional images (c,d) for expandable design treated tibial defects 115

Figure 5.4. CT 3D renders (a-c) and cross-sectional images (d-f) for injectable design treated tibial defects 116

Figure 5.5. Masson's Trichrome Images of BioOss Collagen® treated defect .. 117

Figure 5.6. Masson's Trichrome images of Expand-o-graft treated defect 118

Figure 5.7. Masson's Trichrome images of Veragraft® treated defect 119

Figure 5.8. Masson's Trichrome Images of I-1 treated defect 120

Figure 5.9. Masson's Trichrome images of I-2 treated defect 121

Figure 5.10. IHC imaging for Expand-o-graft treated tibial defects 122

Figure 6.1. Calcein-AM proliferation assay conducted at day 3, 5, and 7 time points 139

Figure 6.2. DiI fluorescent images of cells seeded to scaffolds at day 3 and 7 time points 140

Figure 6.3. Heatmap (a,c) and gene primer layout with expression values (b,d) generated from human osteogenesis (a-b) and signal transduction arrays (c-d) 141

Figure 6.4. sPLS-DA plot and driving metabolites for cell-based group 146

Figure 6.5. sPLS-DA plot and driving metabolites for material-based group 147

Figure 6.6. Heatmaps depicting metabolite abundance variations 148

Figure 6.7. ConsensusPathDB network map generated from up-regulated osteogenesis and signal transduction array expression data 151

Figure 6.8. ConsensusPathDB network map generated from metabolite abundance data 152

Figure 6.9. Osteogenic signal pathway interaction schematic 153

Figure 7.1. Early in vitro MC 3T3-E1 cell seeding density optimization 162

Figure 7.2. nHA content interference with Alizarin Red staining 163

Figure 7.3. Research workflow overview 164

LIST OF ABBREVIATIONS

1. adhMSCs ..... Adipose-derived Human Mesenchymal Stem Cells
2. β-TCP ..... β-Tricalcium Phosphate
3. bmcMSCs ..... Bone Marrow-derived Caprine Mesenchymal Stem Cells
4. BMP ..... Bone Morphogenic Protein
5. BMP-2 ..... Bone Morphogenic Protein-2
6. BSMMSC ..... Biological and Small Molecule Mass Spectrometry Core
7. BSP ..... Bone Sialoprotein
8. CaP ..... Calcium Phosphate
9. CD ..... Cluster of Differentiation
10. cDNA ..... Complimentary DNA
11. CEJ ..... Cementoenamel Junction
12. CEM ..... Comparative and Experimental Medicine
13. CHO ..... Chinese Hamster Ovary
14. cMSCs ..... Caprine Mesenchymal Stem Cells
15. cmRNAs ..... Chemically-modified RNAs
16. CPDB ..... ConsensusPath Database
17. CT ..... Computed Tomography
18. DAVID ..... Database for Annotation, Visualization, and Integrated Discovery
19. DBM ..... Demineralized Bone Matrix
20. DBPs ..... Decellularized Bone Particles
21. dPU ..... Degradable Polyurethane
22. ECM ..... Extracellular Matrix
23. E. Coli ..... Escherichia Coli
24. ESI ..... Electrospray Ionization
25. FDA ..... Food and Drug Administration
26. FN ..... Fibronectin
27. GEM ..... Growth-factor-enhanced Matrix
28. H&E ..... Hematoxylin & Eosin
29. HA ..... Hydroxyapatite
30. HH ..... Hedgehog
31. HRP ..... Horseradish Peroxidase
32. ICBG ..... Iliac Crest Bone Graft
33. IHC ..... Immunohistochemistry
34. IMPaLA ..... Integrated Molecular Pathway Level Analysis
35. KEGG ..... Kyoto Encyclopedia of Genes and Genomes
36. MAVEN ..... Metabolomic Analysis and Visualization Engine
37. LC-MS ..... Liquid Chromatography-Mass Spectrometer
38. mmRNAs ..... Modified Messenger RNAs
39. MOIs ..... Metabolites of Interest
40. mRNA ..... Messenger RNA
41. MSCs ..... Mesenchymal Stem Cells
42. nHA ..... Nano-Hydroxyapatite

43. OCN ..... Osteocalcin
44. ON ..... Osteonectin
45. OPN ..... Osteopontin
46. PCR ..... Polymerase Chain Reaction
47. pDNA ..... Plasmid DNA
48. PF127 ..... Pluronic f-127
49. PLS-DA ..... Partial Least Squares Discriminant Analysis
50. POIs ..... Pathways of Interest
51. PU ..... Polyurethane
52. qPCR ..... Real-time Polymerase Chain Reaction
53. rhPDGF-BB ..... Recombinant Human Platelet-derived Growth Factor BB
54. ROI ..... Region of Interest
55. ROS ..... Reactive Oxygen Species
56. sPLS-DA ..... Sparse Partial Least Squares Discriminant Analysis
57. SQ ..... Subcutaneous
58. UALR ..... University of Arkansas at Little Rock

CHAPTER I:
INTRODUCTION TO OSTEOBIOLOGICS

A version of this chapter was originally published by Austin J. Bow:

Bow, A., Anderson, D. E., & Dhar, M. (2019). Commercially available bone graft substitutes: the impact of origin and processing on graft functionality. *Drug Metabolism Reviews*, 1-12. doi:10.1080/03602532.2019.1671860

This is an article published by Taylor & Francis in a special issue of the Journal of Drug Metabolism Reviews October 2019, available online: https://doi.org/10.1080/03602532.2019.1671860. Copyrights have been obtained for using content from this originally published work in the following chapter.

A Brief Introduction to Bone

Far from the static structure that it is sometimes portrayed, bone comprises of a highly dynamic system regularly undergoing remodeling based on skeletal force distribution. This process relies on specialized cells, namely osteoclasts and osteoblasts, capable of resorbing existing substrate and depositing new bone respectively. Osteoclasts, which are multinucleated cell bodies formed from hematopoietic precursors of monocytic and macrophagic lineage, operate to degrade existing structures enzymatically exposing mature osteocytes embedded within matrix (Lemma et al., 2016). Osteoblasts, which form epithelioid structures along the surface of existing bone, modulate secretion of bone organic matrix and mineralization at this interface (Blair et al., 2017). During this deposition process, osteoblasts become encased within the newly formed mineral construct and mature to osteocytes, which comprise over 90% of the cellular content of bone and has demonstrated the ability to regulate the balance between remodeling agents (Bellido, 2014; Hasan et al., 2018). The operation and coordination of function for these critical structural remodeling agents is heavily reliant on the flux of chemical signals produced by the extracellular matrix (ECM) in the form of proteins and growth factors, which stimulate highly specific reactionary cascades. These signaling cascades are largely responsible for the recruitment and differentiation of precursor cells through-out the repair process (Majidinia et al., 2018).

The complex interaction of the described mechanisms can be credited for the impressive regenerative capacity of bone, with functional repair and restoration possible for even large tissue trauma. However, for injuries that exceed the healing capabilities of the tissue, what is known as a critically-sized defect, spontaneous regeneration and repair will not be possible. It is therefore necessary for such cases to implement a graft material to facilitate cellular migration and signaling through the defect region permitting effective repair (Noori et al., 2017). For this reason, the development of effective bone graft materials has been a major research focus, resulting in a wide range of scaffold designs with varying advantages and disadvantages.

Osteobiologic Products

In designing an optimal graft material for bone tissue engineering applications, the product should display key osteobiologic characteristics (Cornell, 2004), such as osteo-conductive, osteo-inductive, and osseo-integrative attributes, to be capable of facilitating and promoting growth of new bone tissue, as well as integration with native tissue. Biomaterials that mimic or utilize the natural architecture of bone therefore offer superior function for not only encouraging the migration of local progenitor cells, but also to serve as a substrate for tissue development. Additionally, the combination of micro- and nano-scale topographical elements have been observed to significantly impact the interaction with and activity of exposed cells (Zhu et al., 2017; Jackson et al., 2018). The current gold standard for grafting material is the use of autologous bone, tissue harvested from a donor site of the individual receiving the graft, as this does not pose concerns of immune response or disease transmission while presenting an optimal construct for tissue in-growth (Azi et al., 2016). However, autologous grafts are limited with respect to available source material and raise concerns of donor site morbidity (Lee et al., 2018). For this reason, the use of allogenic, xenogeneic, and synthetic graft materials offer attractive alternatives with regard to availability and cost parameters. Furthermore, the application of bioactive agents such as proteins and growth factors closely associated with osteogenesis or genetic manipulation through both viral and non-viral methods have demonstrated the potential to enhance existing scaffold technologies, as well as act as effective stand-alone treatments (Hasan et al., 2018).

This section will explore commonly employed, commercially available bone graft and bioactive materials of both organic and synthetic origin found through a rudimentary web-based search of PubMed and Medline databases. The examined materials, assessed based on origin and matrix composition, will be separated into allogenic, xenogeneic, synthetic, and bioactive graft classifications. Evaluation of the advantages and disadvantages associated with each graft type will be driven by comparison of material processing methods and tissue interaction post-implantation. The application of explored commercially available materials in combination with experimental elements, such as cell-based delivery platforms or polymer binder additions, will not be addressed further in this article (Rao and Stegemann, 2013; Lei et al., 2018).

Allograft Products

Allografts comprise of scaffolds and particles derived from human cadavers, thereby maintaining architecture and extracellular proteins identical to that observed in the native bone tissue. For this reason, this category of grafting material demonstrates strong osteoconductive and integrative capabilities, as well as varying degrees of osteo-inductive potential based on the processing method utilized (Drosos et al., 2015; Kadam et al., 2016). The primary concern with allografts is the risk of disease transmission or immune response due to same

species transplantation. To address this, the harvested samples are most commonly subjected to a freeze-drying procedure to eliminate the cellular component of the tissue. Removal of this element permits a drastic reduction in the risk factors associated with allografts. The remaining extracellular matrix can then be applied as a scaffold material or reduced to particles of specific size ranges for void filling applications. By varying the duration and number of freeze-dry cycles, the resulting scaffold can have significantly altered mechanical stability and surface protein characteristics (Kadam et al., 2016), making it suitable for new bone repair and regeneration

Further processing of harvested human allograft bone can be conducted using an acid extraction to produce demineralized bone matrix (DBM), the general process of which can be observed in **Figure 1.1**. DBM is comprised of the organic elements of the bone, including proteins and other growth factors, which maintain the osteoconductive and osteo-inductive characteristics while removing the mineral structural components of the matrix. This permits the product to be implemented in a variety of means including granular particles, powders, or putties for filling void spaces (Kadam et al., 2016). Additionally, the process of demineralization reduces antigenic structures that may cause an immunological response, though this will still vary depending on the extent of the demineralization (Drosos et al., 2015).

Commonly used and characterized commercially available allograft materials include both freeze-dried and DBM products, as well as different material forms for some products. [The products: Grafton®, MinerOss®, RaptOs®, Cancellous Chips, Puros®, and RegenerOss®, were selected though a basic web-based search of commonly implemented allogenic grafts.]

Grafton® DBM (BioHorizons)

Grafton® DBM is an allogenic graft material produced and distributed by BioHorizons that provides a scaffold matrix encompassing both osteoconductive and osteo-inductive properties. As noted in Kadam et al. (2016), Grafton® DBM has been implemented in a wide variety of applications including sclerosis, cervical spine, and lumbar fusion applications. It is intended to be applied as in cases requiring bone graft extensions, substitute, or filler that are not directly related to structural stability or weightbearing sites. This is due to the DBM grafts maintaining low mechanical strength as compared to the compression forces observed in weightbearing skeletal structures. For this reason, a particularly attractive application of Grafton® DBM is in oromaxillofacial surgical applications, such as in alveolar ridge augmentation. The graft material is designed to be absorbed and replaced by native tissue during normal remodeling of the defect region. A prospective randomized clinical trial comparing Grafton® DBM with an autologous graft material harvested from the iliac crest bone (ICBG) was conducted to determine efficiency in fusion with local bone. The study conducted by Kang et al. (2012), assessed the 2-year follow-up of 41 patients that had received either the Grafton® DBM (n=28) or ICBG (n=13) for final fusion rates. There was no

significant difference between the two groups (Kang et al., 2012), Indicating that the Grafton® DBM material may be capable of facilitating comparable repair to autogenic graft materials for bone injuries where fusion is required.

MinerOss® Chips (BioHorizons)

MinerOss® particles are an allogenic graft product produced and distributed by BioHorizons that are derived from either cortical bone, cancellous bone, or a blend. The freeze-dry process used for this product results in a mineralized particulate material with both strong osteoconductive properties and enhanced surface area for tissue interaction. These particle materials (particle size ranging from 600µm to 1250 µm) are intended, as per the product page, for implementation as a defect filler in ridge/sinus augmentation and socket grafting to act as a mineral matrix for native tissue in-growth. A study was conducted to assess MinerOss® particles as a primary grafting material for a sinus augmentation procedure and was followed for a post-operative period of 6 months. Bone core biopsies harvested during implant placement permitted histological evaluation of graft-tissue integration. Implants placed in graft-filled defects (n=39) demonstrated satisfactory stability, with only one implant failing, and histologic analysis revealed strong osseo-integration characteristics (Avila et al., 2010).

RaptOs® (Citagenix)

RaptOs® is an allogenic graft block product produced and distributed by Citagenix derived from cortico-cancellous bone. As per product page, the graft material is intended for filling bony void space in non-weightbearing osseous defects, since compressive mechanical forces of skeletal bone exceed those observed in allogenic products produced through freeze-dry processes. In a study conducted by Kaya et al. (2015), RaptOs® was evaluated histologically for bone reparative characteristics in a tibial defect model alongside two other graft materials of different origins, BioOss® (xenogeneic) and β-tricalcium phosphate (synthetic). Generated in both tibias of 28 Wistar rats, the defects measured 10mm in length, 3mm in depth, and 2mm in width. Each rat was one of the three grafts in both legs, or left void for control samples, with one site receiving a pretreatment with a commonly employed antibiotic, rifampin. 21 days post-operatively rats were sacrificed, and samples were harvested for histological sectioning. Defects treated with RaptOs®, without inclusion of the antibiotic, demonstrated partial unions and early stage development of woven bone, as indicated by the presence of collagen fibers within the site. Despite the low cellular activity observed, these samples did maintain a consistently higher degree of cell activity as compared to the unfilled control samples and displayed the presence of bone marrow along the periphery of the material (Kaya et al., 2015). This study indicated that the human allograft product was capable of acting as a supplemental matrix within the defects to permit early-stage repair.

Cancellous Chips (Musculoskeletal Transplant Foundation)

Cancellous chips are a common allograft material and for human use can be procured readily from organizations such as the Musculoskeletal Transplant Foundation. The process of production of this graft material, described earlier, involves the use of freeze-dry cycles and irradiation to counteract the disease transmission and immune reactivity risks associated with allografts. The degradation of surface proteins and growth factors within the bone matrix during this process results in the final porous scaffold product exhibiting severely reduced or no osteo-inductive capabilities. Therefore, cancellous bone chips are primarily utilized as osteoconductive filler matrices within non-weightbearing osseous defects. A study conducted by Hall et al. (2018), assessed cancellous chips derived from canine bone as a predicate material against a synthetic graft material in a critically-sized axial defect in the proximal humorous of 13 hound-type dogs. The administered cancellous chips ranged from 1-4mm and were acquired from Veterinary Transplant Services, Inc. The humeri harvested at sacrifice (3 samples at 6 weeks, 5 samples at 13 weeks, and 5 samples at 26 weeks) were examined histologically to evaluate new mineralized bone and fibrous tissue formation. Analysis of 13-week and 26-week samples revealed that cancellous chip treated defects did exhibit enhanced healing and integration with native tissue at the periphery of the implanted material, yet fibrous tissue formations were observed at the center region of these defects. These formations were attributed to the poor inductive ability of the allograft material resulting reduced capacity to facilitate repair of critically-sized defects (Hall et al., 2018). Additional analysis of compressive mechanical strengths of samples and percentage of residual material compliment this finding with cancellous chip treated samples showing lower mechanical strength and greater volumes of remaining material as compared to the synthetic graft. As allograft products such as cancellous chips have been observed to require as much as 1 to 3 years for complete healing of the treated injury, it possible that the 26-week time point utilized in this study may account for the low level of repair observed in this study (Hall et al., 2018).

Puros® (Zimmer Biomet)

Puros® is a mineralized cancellous bone allograft produced and distributed by Zimmer Biomet and utilizes a Tutoplast® processing method. This process provides a scaffold structure with preserved internal porous structure, surface proteins, and matrix growth factors of the natural bone. The preservation of matrix proteins and growth factors enable the grafting material to have osteo-inductive capabilities in addition to the osteoconductive properties of the basal structure, making such a material an attractive alternative to autologous grafts. A study conducted by Reddy et al. (2016) assessed Puros® with relation to the effectiveness of autologous bone grafts for treating periodontal intra osseous defects over 6 months. Patients included in the study (n=10) were divided at random into either Group A, receiving Puros® treatment (n=5), or Group B, receiving autologous bone graft (n=5). The primary assessment was conducted

through radiography of the defect region by evaluating changes in the defect depth (DD) at 1, 3, and 6 months post-operative intervals. Each timepoint was compared to baseline measurements. DD was determined based on parameters associated with the cementoenamel junction (CEJ), the region of the interface between enamel and cementum, including the relation to the most apical point of the defect and to the most coronal point of the alveolar crest. Defects treated with Puros® demonstrated significant decreases in depth size over each analyzed time point and was found to be comparable to autologous bone in the percentage of defect filled at the 6-month interval. It was concluded that both the Puros® and autologous bone promote predictable periodontal regeneration (Reddy et al., 2016).

RegenerOss® (Zimmer Biomet)

RegenerOss® is a partially demineralized, freeze-dried allogeneic product produced and distributed by Zimmer Biomet that undergoes processing methods designed to remove unwanted cellular elements while preserving lipids in the tissue. The resulting product is recommended for primarily oral and maxillofacial surgical procedures such as alveolar ridge augmentation, sinus floor elevation, and tooth socket preservation, as per product page. As with previously discussed allograft materials, RegenerOss® is not capable to provide sufficient mechanical stability alone for use in weightbearing bony defects. Available product particle sizes can range from 200-800µm and therefore offer variation in both surface area and topographical elements that may aid in promoting osteoconductive capabilities. In a case-controlled study by Eskan et al. (2017), 14 patients were treated with the allogeneic bone graft in conjunction with a bioresorbable matrix membrane for covering the defect region, and then placed into one of two groups, those receiving primary wound flap closure and those with the primary wound left exposed. The primary objective of the study was to assess the impact of initial wound exposure with relation to regenerative and reparative capacities, as well as to evaluate the effectiveness of the allograft material with membrane cover. Treatments were analyzed based on alveolar ridge widths, with baseline measurements conducted at initial surgical entry and final values taken after 4 months healing time during dental implant placement. Despite a lack of significance between study groups in alveolar ridge width increase over the 4-month period, all defects treated with the RegenerOss® product in conjunction with the bioresorbable matrix membrane demonstrated a significant increase in mean alveolar ridge width, indicating effective application of the allograft for osteo-reparative functions in this model (Eskan et al., 2017).

Xenograft Products

Xenografts comprise of scaffolds and particles derived from non-human species and therefore encompass a wide array of structural and protein compositional characteristics. Xenografts have been an attractive alternative to human-derived graft materials primarily due to manufacturing costs and enhanced

availability of source material (Qiao et al., 2018). Additionally, the risk of disease transmission is greatly reduced since the transplant material is no longer human in origin, yet this also results in the material having a greater risk of evoking an immune response due to foreign proteins and elements. To address this risk, raw xenogeneic materials are subjected to the processes discussed earlier with allogenic grafts, namely freeze-drying and demineralization procedures. Materials that have undergone extensive freezing and lyophilization cycles to remove the organic components of the tissue matrix are considered “anorganic” and offer an inexpensive substitute for apatite structures that possess strong osteoconductive characteristics (Lee et al., 2014). The general process utilized for this decellularization of tissue can be observed in **Figure 1.2**. As these constructs do not maintain effective/intact proteins within the matrix, products prepared through this method do not generally demonstrate osteo-inductive capabilities. Currently, the most prolifically utilized xenograft materials are of bovine origin; however, grafts derived from porcine tissue have shown promise, due to architectural and compositional similarities to human bone (Qiao et al., 2018).

The explored commercially available xenogeneic grafts consist of products from both bovine and porcine origins, with varying processing methods. The products: MinerOss XP®, BioOss®, InterOss®, and Gen-Os®, were selected through a basic web-based search for commonly employed xenograft materials.

MinerOss XP® (BioHorizons)

MinerOss XP® is a porcine-derived bone particulate graft material produced and distributed by BioHorizons. Similar to the previously discussed MinerOss® allogenic chips, MinerOss XP® is designed to act as a filler agent for bony defects that are non-weightbearing, as in cases as ridge and sinus augmentation. Source tissue undergoes extensive washing and fat stripping processes to remove the organic elements, including surface and matrix proteins, to eliminate factors that may elicit a reaction in native tissue surrounding the implant site. The resulting anorganic matrix is highly porous and maintains strong osteoconductive functions, providing an environment favorable for new bone formation. The efficiency of MinerOss XP® to form new bone (osteoid) was examined against a bone grafting material of bovine origin, which is currently more commonly utilized for xenograft applications, in a case study conducted by Guarnieri et al. (2017). The study consisted of a comparative histological assessment of new bone formation in two sockets that had received either the bovine or porcine-derived graft material. Core samples from the sockets were taken 6 months initial extraction and material application, during implant placement. Histological evaluation of the samples indicated that the porcine-derived product resulted in an increased formation of new bone as compared to the bovine-derived material, with percentage osteoid being 32.19% and 26.85% respectively. Additionally, the porcine-derived material demonstrated a reduced level of residual grafting material, an important consideration for xenogeneic graft materials as it is indicative of ability of the host to breakdown and resorb the graft (Guarnieri et al., 2017). Both materials utilized

in the study demonstrated osteoconductive attributes and did not impede bone formation at the defect site.

BioOss® (Geistlich)

Produced and distributed by Geistlich, BioOss® is a deproteinized bone mineral particulate product of bovine origin. Deproteinization through common processes such as calcination, the removal of non-mineral elements by thermal degradation, or chemical treatments offer resulting graft products that consist primarily of the mineral phase structures (Su et al., 2018). These structures have inherently high porosities with varying pore sizes and intricate connecting channels, which are essential attributes for material intended to provide osteo-conductive effects. BioOss® has demonstrated significant enhancement of new bone development when implemented in non-weightbearing bony defects, particularly when incorporated as a supportive element to autologous bone particulate. In a systematic review by Aludden et al. (2017) the comparative impact of BioOss® as a standalone grafting material was assessed in relation to the bovine-derived products' coupling with autologous bone particulate in a selection of human lateral ridge augmentation procedures conducted between January 1990 and May 2016. The study evaluated effectiveness of treatment options based on two primary outcome criteria, the "survival of the suprastructure" and the "survival of the implant" (Aludden et al., 2017). If the suprastructure integrity, the newly formed bone matrix within the defect site, was determined to be compromised, this was defined as a "total loss" as the implant site could not then be assessed. Permitting that suprastructure was intact, the implant site was evaluated based on integration with native tissue and impact on surrounding tissue. To further support primary outcome classifications, measurements of histologically assessed new bone formation, ridge dimensional elements, and patient-reported outcomes were also incorporated into the study. It was determined that the variation in study design of the non-comparative evaluations of BioOss® treatments that were evaluated by Aludden et al. (2017) complicated the ability to accurately compare the individual study results in a systematic review. Therefore, the review heavily relied on secondary assessment characteristics to compare the two treatment modalities. Histological results and ridge dimensional assessments, both two dimensional and volumetric, indicated that there was not a significant difference between the treatments. Furthermore, comparison of characteristics of BioOss® mixed with autologous bone particulate against the application of purely autograft material did not yield a significant variation in implant survivability, thereby indicating the potential of BioOss® and similar xenogeneic-based graft materials as effective alternatives.

InterOss® (Sigma Graft)

InterOss®, similar to BioOss®, is an anorganic bovine-derived bone particulate graft material developed and distributed through SigmaGraft. The process utilized for deproteinization consists of initial chemical treatment of the

origin tissue with NaOH and H_2O_2 solutions, followed by calcination at 350℃. The resulting highly porous mineral structure is then capable of providing an osteoconductive substrate for application in non-weightbearing bony defects. The design and function of this material closely mimics the previously described BioOss® graft material, which is the basis for a comparative study conducted by Lee et al. (2014) of the SigmaGraft research and development department. The study primarily focused on comparing the physical and chemical characteristics of both materials including the surface area, porosity, and protein residue measurements. Results of the evaluation of the products indicated that the mineral composition and surface area of structures were not significantly different. Likewise, the crude protein residue content was not significantly different between the two materials, though it was speculated that the relatively lower content observed in InterOss® may have been a result of the extended annealing process (Lee et al., 2014). Another comparative study of these two graft materials was conducted by Kim et al. (2017) to evaluate the impact of these materials when applied to a complex *in vivo* system. The preclinical study utilized a critically-sized mandibular alveolar ridge defect in canines and was assessed at 4, 8, and 12 weeks post treatment. 54 defects in 27 animals received either treatment with InterOss®, BioOss®, or left empty. Histological and microcomputed tomography were used to evaluate the new bone development at defect sites and indicated that both materials were effective at facilitating new bone growth in relation to the negative control group, though there was no significant difference between products (Kim et al., 2017).

Gen-Os® (Tecnoss Dental)

Gen-Os® is a porcine-derived cortico-cancellous xenogeneic graft product developed and distributed by Tecnoss Dental primarily for oromaxillofacial applications. Conservation of origin tissue matrix structure enables graft particles to serve as highly porous substrate material for facilitating osteoconductive functions, much like previously described xenogeneic grafts. Additionally, Gen-Os® processing preserves the collagen content of the origin tissue, which promotes osseo-integrative and osteo-inductive capacities. The inherent hydrophilic nature of the product due to the collagen content is also emphasized as a potential carrier mechanism for select drugs (Figueiredo et al., 2013; Fischer et al., 2015). A study evaluating the effectiveness of Gen-Os® as treatment in a select population of healthy chronic periodontitis patients, with individuals receiving graft product after debridement or only receiving open flap debridement. Treatments were assessed through clinical rankings, including plague index, gingival index, and pocket depth, and radiographical measurements of bone density. Comparison of baseline values with results at 6 and then 12 months post operation demonstrated that Gen-Os® significantly enhanced both clinical and radiological outcomes (Attia, 2017).

Synthetic Graft Products

Synthetic bone graft substitutes are those that are derived from non-organic sources and consist of a broad spectrum of materials with varying characteristics. Though many of these materials are polymeric-based, these constructs are susceptible to high variability during synthesis and will not be further discussed in this article. Focusing primarily on commonly employed ceramic-based grafting materials, these materials consist of dense mineral structures that can be modified to adjust porosity and surface topography. Such materials have demonstrated promise in bone tissue regenerative application due to their ability to mimic the structure of native bone and provide an osteoconductive substrate for tissue in-growth. However, these materials do not inherently contain proteins or growth factors that would allow for osteo-inductive functions and therefore must be coupled with other materials or biological agents to elicit such activity.

The selected synthetic graft materials consist of ceramic-based mineral products intended to act as osteoconductive constructs. The explored products include hydroxyapatite nanocrystals, Chronos®, Syntoss®, and Vitoss® Synthetic, and were produced via a rudimentary web-based search for commercially available synthetic bone grafts.

Hydroxyapatite Nanocrystals (Berkley Advanced Biomaterials)

Synthetic hydroxyapatite nanocrystals (nHA) are a commonly employed calcium-phosphate (CaP) salt that is identical in composition to naturally forming hydroxyapatite (HA), which is a primary mineral element in bone (Sadat-Shojai et al., 2013). nHA can be readily synthesized through simple chemical processing to generate bulk quantities for a variety of applications. Additionally, pre-synthesized nHA products are commercially available, such as products generated and distributed by Berkley Advanced Biomaterials, for application as a standalone material or in conjunction with other materials for enhancement of properties. The nano-scale of this CaP significantly increases the surface area as compared to micro-scale HA, thereby heavily impacting the osteo-conductivity of the material. However, the high surface energy associated with the nanoparticles results in a propensity for particles to agglomerate and form macrostructures with significantly different characteristics (Fu et al., 2017). These varying microscale topographical landscapes can result in substantially different cell-material interactions and influence both cytocompatibility and cell differentiation characteristics (Jackson et al., 2018). nHA has demonstrated strong biocompatibility and is readily internalized by native cells, resulting in modulative effects on gene expression (Ha et al., 2015; Santos et al., 2017). These particles can also be readily incorporated with various material structures as a surface coating or integrative component, permitting design of composite graft materials that facilitate new bone formation (Bow et al., 2019).

ChronOs® (DePuy Synthes)

ChronOs® is a synthetic β-tricalcium phosphate (β-TCP) bone grafting material produced and distributed by DePuy Synthes. β-TCPs are a commonly implemented material for bone grafting applications due to inherent biocompatibility, as well as resorbable and osteo-conductive functions (Arbez and Libouban, 2017). As with the previously described synthetic nHA material, β-TCPs like ChronOs® are often used in conjunction with other mineral or bioactive components. In materials such as Syntoss®, a bone graft substitute produced by Dental Solutions Israel, β-TCP is combined with HA for an osteo-conductive porous structure (no available peer reviewed publications for Syntoss®). However, as a standalone grafting material ChronOs® has demonstrated effectiveness as a readily available bone void filling agent in non-weightbearing structures. In a study conducted by Bonardi et al. (2018), ChronOs® was examined alongside autogenous bone grafts and BioOss® in a human maxillary sinus bone augmentation procedure. The results indicated that ChronOs® was not significantly different from autogenous bone grafts in new bone formation, residual material, or area of connective tissue; however, ChronOs® did display significantly less residual material than those treated with BioOss®. ChronOs® therefore offers an attractive alternative bone grafting material, particularly when coupled with autogenous bone particulate which can provide an osteo-inductive characteristic (Bonardi et al., 2018).

Vitoss® Synthetic (Stryker)

Vitoss® is a synthetic cancellous bone developed and distributed by Stryker as a bone graft substitute for bony voids in intrinsically non-weightbearing structures. This CaP grafting material is designed to be highly porous with complex inter-pore channels to mimic the structure of natural bone. The matrix composition and structure enable Vitoss® to exhibit both biocompatible and osteo-conductive characteristics, and when coupled with bioactive agents can serve as an osteogenic substrate. In a prospective multi-cohort study conducted by Epstein et al. (2015), Vitoss® is compared to NanOss, a bioactive material composed of nano-scale CaP and porcine-derived collagen matrix, to assess the effectiveness of the materials in patients receiving laminectomies followed by posterior cervical fusions. The first cohort (n=72), were treated with a combination of autografts, bone marrow aspirate, and Vitoss®, while the second cohort (n=20) received the NanOss® in place of Vitoss®. Findings indicated that both examined material treatments yielded comparable fusion times and did not demonstrate significantly different fusion characteristics (Epstein, 2015).

Bioactive Graft Products

Bioactive materials comprise of a wide array of compounds ranging from osteogenic-related proteins, such as bone morphogenic protein-2 (BMP-2), to genetic manipulation of native cells using nucleic acid, i.e. plasmid DNA (pDNA) and chemically-modified RNA (cmRNA), or viral-based approaches. For this

reason, the application of bioactive materials varies dramatically based on the type of compound with many requiring a delivery mechanism to enhance effectiveness or duration of effect. This coupling with existing technologies permits development of finely-tuned grafts capable of facilitating bone repair via a tailored set of mechanisms, and therefore offers a highly attractive alternative to traditional bone graft substitutes. For this reason, the application of bioactive molecules in combination with traditional osteobiologic substrates has garnered the focus of many researchers in the field of bone tissue engineering. However, many of these agents are restricted in commercialization potential due to inherent costs and time associated with developing materials classified as drugs by the U.S. Food and Drug Administration (FDA) (Hasan et al., 2018). Furthermore, treatments utilizing bioactive materials may in some cases increase the risk of side effects in the local tissues or lead to tumorigenic growth. Therefore, limited products in this category are readily available commercially, which consequently results in products themselves being expensive, and are restricted to specific applications.

The bioactive graft materials selected for this review consist of growth factor-based molecules added to traditional osteobiologic grafts, such as those discussed above, in order to enhance or better regulate osteogenic activity. The products described here include Infuse™ and GEM 21S®, which were produced via a rudimentary web-based search for commercially available FDA-approved bioactive materials.

Infuse™ (Medtronic)

BMP-2 has been demonstrated to be closely associated with osteogenesis (Schuberth et al., 2009), particularly with relation to mineralization, and is the only FDA-approved osteo-inductive growth factor currently available for bone grafts (James et al., 2016). The Infuse™ product produced and distributed by Medtronic, consists of an absorbable collagen sponge scaffold seeded with recombinant human BMP-2 generated using a hamster oocyte production cell line for protein recombination. Chinese hamster ovary (CHO) cell-derived rhBMP-2 maintains potent osteo-inductive potential, but, as a consequence of production costs, remains an expensive product. Comparative studies examining the osteo-inductive potential of CHO cell-derived rhBMP-2 with a relatively cheaper manufacture process utilizing Escherichia Coli (E. Coli)-derived rhBMP-2, which permits increased protein yield, have thus far indicated that the CHO cell-derived protein boast superior osteo-inductive potential (Jin et al., 2019). As per the Infuse™ product page, the bioactive product is indicated for only specific applications in spinal fusion procedures and acute tibial shaft fractures. The primary reason for the observed limited application of the product are likely related to the potential side-effects associated with administering growth factor doses *in vivo*. As discussed in James et al. (2016), adverse effects of BMP-2 can range from surgical site inflammation to ectopic bone formation. This is particularly concerning when considering applications related to spinal fusion and further stresses the importance of adherence to product guidelines.

GEM 21S® (Lynch Biologics)

GEM 21S® is a growth-factor-enhanced matrix (GEM) material produced and distributed by Lynch Biologics for use in dental therapy applications. The bioactive product is comprised of purified recombinant human platelet-derived growth factor-BB (rhPDGF-BB), derived from yeast cultures, seeded to a β-tricalcium phosphate (β-TCP) (Singh and Suresh, 2012), similar in design to the previously discussed ChronOs®. PDGF-BB is strongly associated with angiogenesis and has been demonstrated to be produced by osteoclasts during osteogenesis for recruitment of precursor cells (Xie et al., 2014). The combination of the growth factor with an osteoconductive matrix, β-TCP, is intended to promote healthy bone repair by recruitment of progenitor cells and formation of vasculature within the scaffold. In a study conducted by Young et al. (2009), the GEM 21S® product was examined for protein release dynamics in vivo using a calvarial defect in rats. It was observed that the protein underwent a rapid burst release, with complete depletion of the protein by 72 hours post-implantation (Young et al., 2009). Despite the release rate of the protein it was observed that the rhPDGF-BB was still bioactive in the surrounding tissue. A separate comparative study examined the use of GEM 21S® with a collagen membrane for dental recession defects to determine if the product was capable of enhancing root coverage as compared with a collagen membrane alone (Singh and Suresh, 2012). Though root coverage in the GEM 21S® treated samples appeared improved, the researchers noted that no significant difference was observed between the study test groups.

Conclusion

The bone graft materials discussed in this section (**Table 1.1**), represent a small portion of currently available biomaterials for bone tissue engineering applications; however, these products demonstrate the fundamental osteobiologic characteristics for materials designed to act as effective bone tissue engineering grafts. Though, as the different processing methods used to generate these products result in an array of grafts that display highly variable reparative functions, an ideal bone substitute graft is still yet to be developed. This is further echoed in the low mechanical structural integrity of these materials restricting application primarily to non-weightbearing injury sites. For these reasons, the previously described materials serve as the more commonly applied bone grafts substitutes and are utilized as basal elements of more complex scaffold composite designs. As the majority of these products exhibited osteo-conductive and biocompatibility qualities, coupling bioactive components, such as growth factors, with the materials can offer enhanced functions including osteo-inductive and osseo-integrative characteristics (Zhao et al., 2017). Furthermore the implementation of cell-based or gene therapy-based approaches can serve to generate osteogenic environments capable of facilitating finely-tuned bone repair (Hasan et al., 2018). Utilizing polymer-based additives to matrix compositions can result in grafts with

both hard mineral and pliable elastic regions, thereby mimicking mechanical diversity in natural bone. Additionally, hydratable polymers may provide optimal means for carrying and eluting drugs at the site of interest. Drugs capable of preventing infection of the treated site or stimulating the native tissue to facilitate enhanced reparative characteristics, can be readily incorporated into multi-composite structures comprised of any number of the discussed materials and a polymeric binding agent to develop a scaffold material that could far exceed the capabilities of even autologous grafts. Such novel combinations of available technologies provide an ever-expanding arsenal of graft options for treating bone injuries and represent the impressive potential of bone tissue engineering. However, determining the optimal graft technology for replacement of autografts will require continued concentrated research efforts in both benchtop and clinical trial settings to ensure an effective and superior osteobiologic product.

The experimental osteobiologic materials discussed in this work were designed for enhancing the repair and restoration time frame of bone injuries, in both endochondral and intramembranous sites, as compared with currently available graft technologies. Furthermore, the various composites offer a relatively inexpensive and readily synthesizable alternative. The majority of the composite materials discussed will be comprised of polyurethane (PU), nano-hydroxyapatite (nHA), and decellularized bone particles (DBPs) in varying ratios and with multiple fabrications techniques. Of these materials, most iterations employ a degradable PU known as D3 (https://plastics.ulprospector.com/datasheet/e155789/hydromed-d3), while the variant utilizes a PU with enhanced hydrophilicity to provide for increased material swelling. Additionally, two materials were examined that implement a combinatorial design of nHA and Pluronic f-127 (PF127) (http://phm.utoronto.ca/~ddubins/MSDS/Poloxamer_407_MSDS.pdf) also known as Poloxamer 407, with one iteration also including quaternized chitosan (Luan et al. 2018). These alternative designs were intended to provide an osteobiologic matrix that was injectable, as the PF127 is a thermosensitive block polymer capable of reversible gelling.

To accurately and completely assess these graft materials for biocompatibility, osteogenic potential, and general effectiveness, a wide array of experimental techniques was utilized, each with appropriate controls and study design. These processes will be discussed in-depth within respective chapters but range from in vitro characterization techniques, such as cellular viability stains and polymerase chain reaction (PCR), to tissue assessment through immunohistochemistry (IHC). Controls for these experiments were tailored to elucidate material action on a particular system, either *in vitro* or *in vivo*, or to draw comparisons with commercially available grafts. For comparative studies, predicate devices were selected that best resembled the structure and application method of the examined test article.

The application and assessment of a wide array of materials including experimental iterations, predicate devices, the basal construct components of these (both mineral and organic), and the potential of incorporating various biologic

additives has demonstrated the expansiveness of the bone tissue engineering field. The improvement of existing technologies in this field, either through combination of currently available components or the synthesis of new additives and fabrication methods, offers an ever-advancing arsenal of biomedical tools for treating and restoring function of complex bone injuries and diseases. This work represents a minute fraction of this advancement yet serves as an example of the investigative effort required to effectively assess a previously unexamined bone graft design.

References

Aludden, H. C., Mordenfeld, A., Hallman, M., Dahlin, C., & Jensen, T. (2017). Lateral ridge augmentation with Bio-Oss alone or Bio-Oss mixed with particulate autogenous bone graft: a systematic review. *Int J Oral Maxillofac Surg, 46*(8), 1030-1038. doi:10.1016/j.ijom.2017.03.008

Arbez, B., & Libouban, H. (2017). Behavior of macrophage and osteoblast cell lines in contact with the beta-TCP biomaterial (beta-tricalcium phosphate). *Morphologie, 101*(334), 154-163. doi:10.1016/j.morpho.2017.03.006

Attia, A. (2017). Clinical and radiographic evaluation of cortico-cancellous bone mix xenograft (osteobiol Gen-Os) in the treatment of human periodontal intrabony defects. *Egyptian Dental Journal, 63*.

Avila, G., Neiva, R., Misch, C. E., Galindo-Moreno, P., Benavides, E., Rudek, I., & Wang, H. L. (2010). Clinical and histologic outcomes after the use of a novel allograft for maxillary sinus augmentation: a case series. *Implant Dent, 19*(4), 330-341. doi:10.1097/ID.0b013e3181e59b32

Azi, M. L., Aprato, A., Santi, I., Kfuri, M., Jr., Masse, A., & Joeris, A. (2016). Autologous bone graft in the treatment of post-traumatic bone defects: a systematic review and meta-analysis. *BMC Musculoskelet Disord, 17*(1), 465. doi:10.1186/s12891-016-1312-4

Bellido, T. (2014). Osteocyte-driven bone remodeling. *Calcified Tissue International, 94*(1), 25-34. doi:10.1007/s00223-013-9774-y

Blair, H. C., Larrouture, Q. C., Li, Y., Lin, H., Beer-Stoltz, D., Liu, L., . . . Nelson, D. J. (2017). Osteoblast Differentiation and Bone Matrix Formation In Vivo and In Vitro. *Tissue engineering. Part B, Reviews, 23*(3), 268-280. doi:10.1089/ten.TEB.2016.0454

Bomback, D. A., Grauer, J. N., Lugo, R., Troiano, N., Patel, T., & Friedlaender, G. E. (2004). Comparison of posterolateral lumbar fusion rates of Grafton Putty and OP-1 Putty in an athymic rat model. *Spine (Phila Pa 1976), 29*(15), 1612-1617.

Bonardi, J. P., Pereira, R. D. S., Boos Lima, F., Faverani, L. P., Griza, G. L., Okamoto, R., & Hochuli-Vieira, E. (2018). Prospective and Randomized Evaluation of ChronOS and Bio-Oss in Human Maxillary Sinuses: Histomorphometric and Immunohistochemical Assignment for Runx 2, Vascular Endothelial Growth Factor, and Osteocalcin. *J Oral Maxillofac Surg, 76*(2), 325-335. doi:10.1016/j.joms.2017.09.020

Bow, A., Newby, S., Rifkin, R., Jackson, B. K., Matavosian, A., Griffin, C., . . . Dhar, M. (2019). Evaluation of a Polyurethane Platform for Delivery of Nanohydroxyapatite and Decellularized Bone Particles in a Porous Three-Dimensional Scaffold. *ACS Applied Bio Materials, 2*(5), 1815-1829. doi:10.1021/acsabm.8b00670

Brecevich, A. T., Kiely, P. D., Yoon, B. V., Nguyen, J. T., Cammisa, F. P., & Abjornson, C. (2017). Efficacy comparison of Accell Evo3 and Grafton demineralized bone matrix putties against autologous bone in a rat posterolateral spine fusion model. *Spine J, 17*(6), 855-862. doi:10.1016/j.spinee.2017.01.012

Drosos, G. I., Touzopoulos, P., Ververidis, A., Tilkeridis, K., & Kazakos, K. (2015). Use of demineralized bone matrix in the extremities. *World J Orthop, 6*(2), 269-277. doi:10.5312/wjo.v6.i2.269

Epstein, N. E. (2015). Preliminary documentation of the comparable efficacy of vitoss versus NanOss bioactive as bone graft expanders for posterior cervical fusion. *Surg Neurol Int, 6*(Suppl 4), S164-171. doi:10.4103/2152-7806.156559

Eskan, M. A., Girouard, M.-E., Morton, D., & Greenwell, H. (2017). The effect of membrane exposure on lateral ridge augmentation: a case-controlled study. *International Journal of Implant Dentistry, 3*(1), 26. doi:10.1186/s40729-017-0089-z

Figueiredo, A., Coimbra, P., Cabrita, A., Guerra, F., & Figueiredo, M. (2013). Comparison of a xenogeneic and an alloplastic material used in dental implants in terms of physico-chemical characteristics and in vivo inflammatory response. *Mater Sci Eng C Mater Biol Appl, 33*(6), 3506-3513. doi:10.1016/j.msec.2013.04.047

Fischer, K. R., Stavropoulos, A., Calvo-Guirado, J. L., Schneider, D., & Fickl, S. (2015). Influence of local administration of pamidronate on extraction socket healing--a histomorphometric proof-of-principle pre-clinical in vivo evaluation. *Clin Oral Implants Res, 26*(10), 1135-1142. doi:10.1111/clr.12483

Fu, L., Wang, Z., Dong, S., Cai, Y., Ni, Y., Zhang, T., . . . Zhou, Y. (2017). Bilayer Poly(Lactic-co-glycolic acid)/Nano-Hydroxyapatite Membrane with Barrier Function and Osteogenesis Promotion for Guided Bone Regeneration. *Materials, 10*(3), 257. doi:10.3390/ma10030257

Greenspan, D. C. (2012). Physical and Chemical Properties of Commercially Available Mineralized Bone Allograft. *Zimmer Dental Inc, Carlsbad*, 1-8.

Guarnieri, R., DeVilliers, P., Grande, M., Stefanelli, L. V., Di Carlo, S., & Pompa, G. (2017). Histologic evaluation of bone healing of adjacent alveolar sockets grafted with bovine- and porcine-derived bone: a comparative case report in humans. *Regenerative Biomaterials, 4*(2), 125-128. doi:10.1093/rb/rbx002

Ha, S.-W., Jang, H. L., Nam, K. T., & Beck, G. R. (2015). Nano-hydroxyapatite modulates osteoblast lineage commitment by stimulation of DNA methylation and regulation of gene expression. *Biomaterials, 65*, 32-42. doi:10.1016/j.biomaterials.2015.06.039

Hall, D. J., Turner, T. M., & Urban, R. M. (2018). Healing bone lesion defects using injectable CaSO4 /CaPO4 -TCP bone graft substitute compared to cancellous allograft bone chips in a canine model. *J Biomed Mater Res B Appl Biomater*. doi:10.1002/jbm.b.34132

Hasan, A., Byambaa, B., Morshed, M., Cheikh, M. I., Shakoor, R. A., Mustafy, T., & Marei, H. E. (2018). Advances in osteobiologic materials for bone substitutes. *Journal of Tissue Engineering and Regenerative Medicine, 12*(6), 1448-1468. doi:10.1002/term.2677

Jackson, B. K., Bow, A. J., Kannarpady, G., Biris, A. S., Anderson, D. E., Dhar, M., & Bourdo, S. E. (2018). Polyurethane/nano-hydroxyapatite composite films as osteogenic platforms. *J Biomater Sci Polym Ed, 29*(12), 1426-1443. doi:10.1080/09205063.2018.1464264

James, A. W., LaChaud, G., Shen, J., Asatrian, G., Nguyen, V., Zhang, X., . . . Soo, C. (2016). A Review of the Clinical Side Effects of Bone Morphogenetic Protein-2. *Tissue Eng Part B Rev, 22*(4), 284-297. doi:10.1089/ten.TEB.2015.0357

Jin, Y. Z., Zheng, G. B., & Lee, J. H. (2019). Escherichia coli BMP-2 showed comparable osteoinductivity with Chinese hamster ovary derived BMP-2 with demineralized bone matrix as carrier. *Growth Factors*, 1-10. doi:10.1080/08977194.2019.1596905

Kadam, A., Millhouse, P. W., Kepler, C. K., Radcliff, K. E., Fehlings, M. G., Janssen, M. E., . . . Vaccaro, A. R. (2016). Bone substitutes and expanders in Spine Surgery: A review of their fusion efficacies. *Int J Spine Surg, 10*, 33. doi:10.14444/3033

Kang, J., An, H., Hilibrand, A., Yoon, S. T., Kavanagh, E., & Boden, S. (2012). Grafton and local bone have comparable outcomes to iliac crest bone in instrumented single-level lumbar fusions. *Spine (Phila Pa 1976), 37*(12), 1083-1091. doi:10.1097/BRS.0b013e31823ed817

Kanter, A. S., Gandhoke, G. S., Welch, W. C., Arnold, P. M., Cheng, J. S., & Okonkwo, D. O. (2016). A prospective, multi-center clinical and radiographic outcomes evaluation of ChronOS strip for lumbar spine fusion. *J Clin Neurosci, 25*, 36-40. doi:10.1016/j.jocn.2015.08.012

Kaya, A., Kaya, B., Aktas, A., & Fırat, E. T. (2015). Effect of rifampin in combination with allogeneic, alloplastic, and heterogenous bone grafts on bone regeneration in rat tibial bone defects. *Journal of Oral and Maxillofacial Surgery, Medicine, and Pathology, 27*(1), 20-28. doi:https://doi.org/10.1016/j.ajoms.2013.08.001

Kim, D. M., Hong, H., Lin, J. C., & Nevins, M. (2017). Evaluation of the Bone-Regenerating Effects of Two Anorganic Bovine Bone Grafts in a Critical-Sized Alveolar Ridge Defect Model. *Int J Periodontics Restorative Dent, 37*(4), e234-e244. doi:10.11607/prd.3305

Kolerman, R., Nissan, J., Rahmanov, M., Calvo-Guirado, J. L., Green, N. T., & Tal, H. (2019). Sinus augmentation analysis of the gradient of graft consolidation: a split-mouth histomorphometric study. *Clin Oral Investig*. doi:10.1007/s00784-018-2793-3

Kumar, M., Chopra, S., Das, D., Gupta, M., Memoalia, J., & Verma, G. (2018). Direct Maxillary Sinus Floor Augmentation for Simultaneous Dental Implant Placement. *Ann Maxillofac Surg, 8*(2), 188-192. doi:10.4103/ams.ams_168_18

Kumaran, S. T., Arun, K. V., Sudarsan, S., Talwar, A., & Srinivasan, N. (2010). Osteoblast response to commercially available demineralized bone matrices--an in-vitro study. *Indian J Dent Res, 21*(1), 3-9. doi:10.4103/0970-9290.62796

Lee, D. S. H., Pai, Y., & Chang, S. (2014). Physicochemical characterization of InterOss® and Bio-Oss® anorganic bovine bone grafting material for oral surgery – A comparative study. *Materials Chemistry and Physics, 146*(1), 99-104. doi:https://doi.org/10.1016/j.matchemphys.2014.03.004

Lee, L. N., Quatela, O., & Bhattacharyya, N. (2018). The epidemiology of autologous tissue grafting in primary and revision rhinoplasty. *Laryngoscope*. doi:10.1002/lary.27551

Lei, B., Guo, B., Rambhia, K. J., & Ma, P. X. (2018). Hybrid polymer biomaterials for bone tissue regeneration. *Front Med*. doi:10.1007/s11684-018-0664-6

Lemma, S., Sboarina, M., Porporato, P. E., Zini, N., Sonveaux, P., Di Pompo, G., . . . Avnet, S. (2016). Energy metabolism in osteoclast formation and activity. *Int J Biochem Cell Biol, 79*, 168-180. doi:10.1016/j.biocel.2016.08.034

Majidinia, M., Sadeghpour, A., & Yousefi, B. (2018). The roles of signaling pathways in bone repair and regeneration. *J Cell Physiol, 233*(4), 2937-2948. doi:10.1002/jcp.26042

Noori, A., Ashrafi, S. J., Vaez-Ghaemi, R., Hatamian-Zaremi, A., & Webster, T. J. (2017). A review of fibrin and fibrin composites for bone tissue engineering. *Int J Nanomedicine, 12*, 4937-4961. doi:10.2147/IJN.S124671

Potres, Z., Deshpande, S., Kloeppel, H., Voss, K., & Klineberg, I. (2016). Assisted Wound Healing and Vertical Bone Regeneration with Simultaneous Implant Placement: A Histologic Pilot Study. *Int J Oral Maxillofac Implants, 31*(1), 45-54. doi:10.11607/jomi.3951

Pujari-Palmer, S., Chen, S., Rubino, S., Weng, H., Xia, W., Engqvist, H., Tang, L. and Ott, M. K. (2016). In vivo and in vitro evaluation of hydroxyapatite nanoparticle morphology on the acute inflammatory response. *Biomaterials, 90*, 1-11. doi:10.1016/j.biomaterials.2016.02.039

Qiao, W., Liu, R., Li, Z., Luo, X., Huang, B., Liu, Q., . . . Chen, Z. (2018). Contribution of the in situ release of endogenous cations from xenograft bone driven by fluoride incorporation toward enhanced bone regeneration. *Biomater Sci, 6*(11), 2951-2964. doi:10.1039/c8bm00910d

Rao, R. R., & Stegemann, J. P. (2013). Cell-based approaches to the engineering of vascularized bone tissue. *Cytotherapy, 15*(11), 1309-1322. doi:10.1016/j.jcyt.2013.06.005

Reddy, B. R., Sudhakar, J., Rajesh, N., Sandeep, V., Reddy, Y. M., & Gnana Sagar, W. R. (2016). Comparative clinical and radiographic evaluation of mineralized cancellous bone allograft (puros((R))) and autogenous bone in the treatment of human periodontal intraosseous defects: 6-months follow-up study. *J Int Soc Prev Community Dent, 6*(Suppl 3), S248-s253. doi:10.4103/2231-0762.197207

Sadat-Shojai, M., Khorasani, M.-T., Dinpanah-Khoshdargi, E., & Jamshidi, A. (2013). Synthesis methods for nanosized hydroxyapatite with diverse

structures. *Acta Biomaterialia, 9*(8), 7591-7621. doi:https://doi.org/10.1016/j.actbio.2013.04.012

Santos, C., Gomes, P., Duarte, J. A., Almeida, M. M., Costa, M. E., & Fernandes, M. H. (2017). Development of hydroxyapatite nanoparticles loaded with folic acid to induce osteoblastic differentiation. *Int J Pharm, 516*(1-2), 185-195. doi:10.1016/j.ijpharm.2016.11.035

Schuberth, J. M., DiDomenico, L. A., & Mendicino, R. W. (2009). The utility and effectiveness of bone morphogenetic protein in foot and ankle surgery. *J Foot Ankle Surg, 48*(3), 309-314. doi:10.1053/j.jfas.2009.01.011

Singh, P., & Suresh, D. K. (2012). Clinical evaluation of GEM 21S((R)) and a collagen membrane with a coronally advanced flap as a root coverage procedure in the treatment of gingival recession defects: A comparative study. *J Indian Soc Periodontol, 16*(4), 577-583. doi:10.4103/0972-124x.106919

Sohn, D. S., & Moon, Y. S. (2018). Histomorphometric study of rabbit's maxillary sinus augmentation with various graft materials. *Anat Cell Biol, 51*(Suppl 1), S1-s12. doi:10.5115/acb.2018.51.S1.S1

Su, F. Y., Pang, S., Ling, Y. T. T., Shyu, P., Novitskaya, E., Seo, K., . . . McKittrick, J. (2018). Deproteinization of Cortical Bone: Effects of Different Treatments. *Calcif Tissue Int, 103*(5), 554-566. doi:10.1007/s00223-018-0453-x

Walsh, W., Christou, C., Low, A., Yu, Y., Oliver, R., Bertollo, N., . . . Ahn, E. (2013). *Bone graft materials: a comparison of NanOss Bioactive 3d and VitOss BA in a challenging model.* Paper presented at the Orthopaedic Proceedings.

Xie, H., Cui, Z., Wang, L., Xia, Z., Hu, Y., Xian, L., . . . Cao, X. (2014). PDGF-BB secreted by preosteoclasts induces angiogenesis during coupling with osteogenesis. *Nat Med, 20*(11), 1270-1278. doi:10.1038/nm.3668

Xu, A. T., Qi, W. T., Lin, M. N., Zhu, Y. H., & He, F. M. (2019). The optimization of sintering treatment on bovine-derived bone grafts for bone regeneration: in vitro and in vivo evaluation. *J Biomed Mater Res B Appl Biomater*. doi:10.1002/jbm.b.34387

Young, C. S., Ladd, P. A., Browning, C. F., Thompson, A., Bonomo, J., Shockley, K., & Hart, C. E. (2009). Release, biological potency, and biochemical integrity of recombinant human platelet-derived growth factor-BB (rhPDGF-BB) combined with Augment(TM) Bone Graft or GEM 21S beta-tricalcium

phosphate (beta-TCP). *J Control Release, 140*(3), 250-255. doi:10.1016/j.jconrel.2009.06.030

Zhao, R., Xie, P., Zhang, K., Tang, Z., Chen, X., Zhu, X., . . . Zhang, X. (2017). Selective effect of hydroxyapatite nanoparticles on osteoporotic and healthy bone formation correlates with intracellular calcium homeostasis regulation. *Acta Biomaterialia, 59*, 338-350. doi:https://doi.org/10.1016/j.actbio.2017.07.009

Zhu, Y., Zhang, K., Zhao, R., Ye, X., Chen, X., Xiao, Z., . . . Zhang, X. (2017). Bone regeneration with micro/nano hybrid-structured biphasic calcium phosphate bioceramics at segmental bone defect and the induced immunoregulation of MSCs. *Biomaterials, 147*, 133-144. doi:https://doi.org/10.1016/j.biomaterials.2017.09.018

Appendix

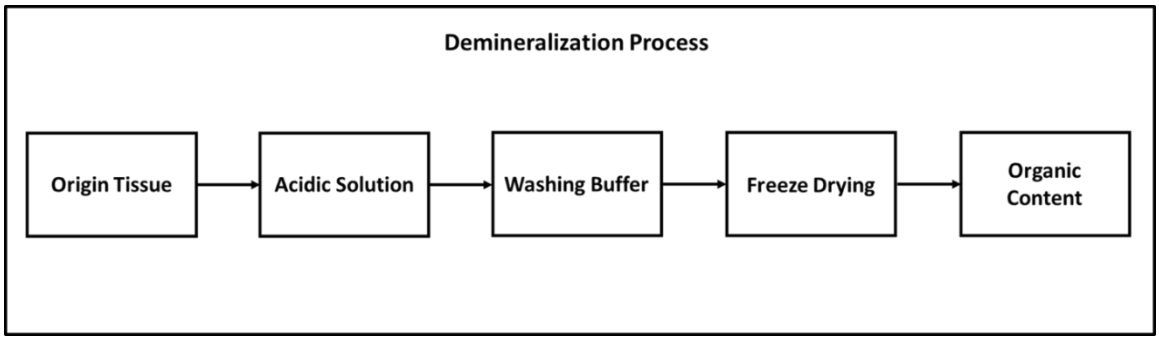

Figure 1.1. Generalized flow chart diagram for demineralization of bone tissue. Process moves from origin bone tissue to low mineral/high organic content product.

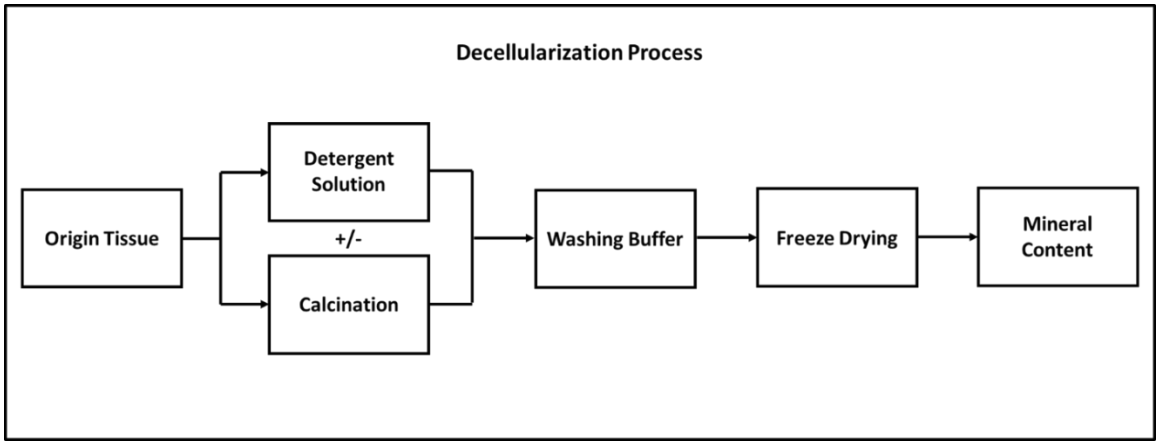

Figure 1.2. Generalized flow chart diagram for decellularization of bone tissue. Process moves from origin bone tissue to high mineral/low organic content product.

Table 1.1. Overview of bone graft materials. List detailing general information and characteristics of discussed bone graft technologies. In addition to graft type and source, material content and application references are listed.

Graft Material	Company	Graft Type	Graft Source	Inorganic Content	Organic Content	*In Vitro* Application Reference(s)	*In Vivo* Application Reference(s)
Grafton DBM	BioHorizons	Allogenic	Homo Sapien	No	Yes	Kumaran et al. 2010	Bomback et al. 2004; Brecevich et al. 2017; Kadam et al. 2016; Kang et al. 2012
MinerOss	BioHorizons	Allogenic	Homo Sapien	Yes	No	Greenspan 2012	Avila et al. 2010; Potres et al. 2016
RaptOs	Citragenix	Allogenic	Homo Sapien	Yes	No		Kaya et al. 2015; Kolerman et al. 2019
Cancellous Chips	Musculoskeletal Transplant Foundation	Allogenic	Homo Sapien	Yes	No		Hall et al. 2018
Puros	Zimmer Biomet	Allogenic	Homo Sapien	Yes	Yes	Greenspan 2012	Reddy et al. 2016
RegenerOss	Zimmer Biomet	Allogenic	Homo Sapien	Yes	Yes		Eskan et al. 2017
MinerOss XP	BioHorizons	Xenogeneic	Porcine	Yes	No		Guarnieri et al. 2017
BioOss	Geistlich	Xenogeneic	Bovine	Yes	No	Jackson et al. 2018; Xu et al. 2019	Aludden et al. 2017; Bow et al. 2019; Kumar et al. 2018; Sohn and Moon 2018; Xu et al. 2019
InterOss	Sigma Graft	Xenogeneic	Bovine	Yes	No	Lee et al. 2014	Kim et al. 2017
Gen-Os	Tecnoss Dental	Xenogeneic	Porcine	Yes	Yes		Attia 2017; Figueiredo et al. 2013; Fischer et al. 2015
Nano-Hydroxyapatite	Berkley Adv. Biomaterials	Synthetic	N/A	Yes	No	Fu et al. 2017; Ha et al. 2015; Jackson et al. 2018; Santos et al. 2017	Bow et al. 2019; Pujari et al. 2016
ChronOs	Depuy Synthes	Synthetic	N/A	Yes	No	Arbez and Libouban 2017	Bonardi et al. 2018; Kanter et al. 2016
Vitoss	Stryker	Synthetic	N/A	Yes	No		Epstein 2015; Walsh et al. 2013
nanOss	rti Surgical	Synthetic	N/A	Yes	No		Epstein 2015; Walsh et al. 2013

CHAPTER II:
IN VITRO ASSESSMENT OF IMMORTALIZED PRE-OSTEOBLAST CELLS ON POLYURETHANE MATRICES IMPREGNATED WITH NANO-HYDROXYAPATITE

A version of this chapter was originally published by Bailey K. Jackson and Austin J. Bow:

Jackson, B. K., Bow, A. J., Kannarpady, G., Biris, A. S., Anderson, D. E., Dhar, M., & Bourdo, S. E. (2018). Polyurethane/nano-hydroxyapatite composite films as osteogenic platforms. *J Biomater Sci Polym Ed, 29*(12), 1426-1443. doi:10.1080/09205063.2018.1464264

This is an article published by Taylor & Francis in Journal of Biomaterials Science, Polymer Edition on 02 May 2018, available online: tandfonline.com/doi/abs/10.1080/09205063.2018.1464264. Copyrights have been obtained for using content from this originally published work in the following chapter. Material fabrication and characterization of physical and chemical properties were carried out by listed authors from the Center for Integrative Nanotechnology Sciences at the University of Arkansas at Little Rock (UALR). The biologic assessment of the material through *in vitro* experimentation was conducted by Austin Bow at the University of Tennessee in Knoxville. As such this chapter will address only the biologic analyses and conclusions drawn from these data.

Abstract

A wide variety of biomaterials are utilized in tissue engineering to promote cell proliferation in vitro or tissue growth in vivo. The combination of cells, extracellular matrices, and biocompatible materials may make it possible to grow functional living tissues ranging from bone to nerve cells. In bone regeneration, polymeric scaffolds can be enhanced by the addition of bioactive materials. To this end, this study designed several ratios of polyurethane (PU) and nano-hydroxyapatite (nHA) composites (PU-nHA ratios: 100/0, 90/10, 80/20, 70/30, 60/40 w/w). The physical and mechanical properties of these composites and their relative cellular compatibility in vitro were determined by the research team at UALR. The results showed a significant increase in surface roughness and a decrease in contact angle when the nHA concentration increased above 20%, resulting in a significant increase in hydrophilicity. These surface property changes influenced cellular behavior when MC 3T3-E1 cells were seeded on the composites. All composites were cytocompatible. There was a linear increase in cell proliferation on the 80/20 and 70/30 composites only, whereas subjective evaluation demonstrated noticeable clusters or nodules of cells (considered hallmarks of osteogenic differentiation) in the absence of any osteogenic inducers only on the 90/10 and 80/20 composites. Cellular data suggests that the 80/20 composite was an optimal environment for cell adhesion, proliferation, and, potentially, osteogenic differentiation in vitro.

Introduction

Tissue engineering, a field that merges engineering with medical research, utilizes materials with complex bio-physico-chemical properties and living cells to either generate tissue *in vitro* or promote rapid tissue growth *in vivo*. With the development of materials that have tunable characteristics, new areas of research have emerged related to the regeneration of missing tissues due to trauma, disease, or military exercises. Within this field, bone tissue engineering focuses on assisting bone growth, healing, or regeneration. Bone injuries often require prolonged periods of time to heal and can cause long-term problems if they do not heal properly. Simple fractures usually heal without complicated therapies, but complex fractures involving shattered or missing bone often require void filling, a scaffold to guide healing, or a construct to support the area and/or assist in healing. Several types of scaffolds are used in bone tissue engineering, from collagen-based materials (Ferreira, Gentile, Chiono, & Ciardelli, 2012; Sun, Zhu, Hu, & Krebsbach, 2014; Bayer et al., 2013) and polymer composites (Lou et al., 2015; Goncalves et al., 2015; Liao, Cui, Zhang, & Feng, 2004; Hutmacher, 2000) to particle-based pastes and cements (Kobayashi et al., 1998; Harper & Bonfield, 2000). Porosity and mechanical integrity are important properties of a successful scaffold (Liu, Hunziker, Randall, de Groot, & Layrolle, 2003; Biswas et al., 2010; O'Brien, 2011). Bone tissues have inherent properties that create a porous environment while still providing strength and rigidity. However, these properties vary significantly based on the location of the osseous tissue in the body. Therefore, increased research attention has been given to matching the properties of the scaffold used in regenerative applications with the characteristics of the tissues to be regrown. Bone scaffolds can be improved through biomimetics (Su et al., 2016), the study and imitation of naturally occurring properties. In the past, biomimicry has not been a significant factor in bone tissue engineering, but recently, it has led to the creation of successful bone scaffolds. Bones are hierarchical materials, meaning that they are composed of layers containing large components, which are made up of smaller components. Specifically, bone is comprised of “brick and mortar” structures, with a hard, plate-like inorganic substance supported by a softer organic component (Gao, 2006; Egan, Sinko, LeDuc, & Keten, 2015; Meyers, McKittrick, & Chen, 2013). These brick and mortar structures add mechanical stability to bone by dispersing forces through the matrix, especially when a plate-like material is arranged preferentially in load-bearing directions (Egan, Sinko, LeDuc, & Keten, 2015). To mimic these components of natural bone, scaffolds can be constructed using polymers with various sizes of particles loaded into them, thereby creating a composite matrix. The advantages of such materials are significant—they can be formed in different shapes, have tunable mechanical properties, can support cellular proliferation, and may be biodegradable.

Many current composite bone scaffolds must be removed after the bone is healed or to allow the bone to complete the healing process, in order to prevent

residual materials from damaging the body. The scaffolds used in this study were designed with biocompatible polyurethane (PU) and nano-hydroxyapatite (nHA) as the soft and hard components, respectively. Generally, PU degrades via hydrolysis, but the overall process is complex and highly dependent on its structure and chemical composition (Adhikari et al., 2008; Zhang et al., 2016). The PU used in this study was desirable because it is biologically stable for up to 30 days after implantation. This limited durability will give the scaffold structural stability during the initial stage of natural bone growth, after which it slowly, safely degrades. HA is a crystalline structure that is naturally occurring in bone but can also be generated synthetically. As such, HA does not generally cause any adverse effects on the body and should assist in bone cell viability with the potential to be integrated into the natural bone. It has been reported that nano-hydroxyapatite exhibits better cellular response for bone regeneration compared to microHA (Christenson et al., 2007). Therefore, our intent is to evaluate several composites with varied ratios of nHA that are incorporated into a polyurethane that serves as a binding agent to hold the nHA particles together. To this aim, we can determine an optimal concentration from *in vitro* cellular proliferation studies which would then assist in the design of 3-dimensional scaffolds for *in vivo* studies.

Vital to the development of biomaterials is the assessment of the cytocompatibility and effect on cell activity of the material (Salgado, Coutinho, & Reis, 2004). This is accomplished through *in vitro* evaluation of cell response utilizing commercially available cells, such as the MC 3T3-E1 cell line (ATCC). MC 3T3-E1 is a cell line of mouse (Mus musculus) calvaria preosteoblast cells commonly used in studies related to bone differentiation and is one of the most convenient and physiologically relevant systems for study of osteogenic control of osteoblasts. A spontaneously immortalized cell line, MC 3T3-E1 behaves as immature, committed osteoblast cells. The cell phenotype is very stable and rigorously maintained (Towler & Arnaud, 2002).

In this study, we utilized a commercially available, biocompatible, and solution processible ether based polyurethane and incorporated nano-hydroxyapatite in a simple mixing process. We hypothesized that by varying the concentrations of nHA, we will generate composites of similar mechanical stability and mineral type, but varying in their surface properties, which will affect cellular behavior. These evaluations will focus on generating platforms for bone tissue engineering. To test our hypothesis, we generated four compositions of PU-nHA composite films (in addition to a 100/0 PU-nHA that served as a control), which were characterized by the material research team at UALR using mechanical and physicochemical techniques. Characterization techniques provided information on the consistency of the films' chemical, physical, and mechanical properties. Subsequently, mouse preosteoblast and immortalized MC 3T3-E1 cells were seeded on these films to evaluate the films' cytocompatibility and cell behavior. These studies were performed to determine the best composite ratio that should be used to generate a 3D bone scaffold.

Material Film *In Vitro* Work

MC 3T3-E1 Cell Culture Parameters

Commercially obtained MC 3T3-E1 cells (ATCC) were seeded in tissue culture polystyrene-treated flasks and cultured at 37°C and 5% CO_2 in αMEM media with 10% fetal bovine serum and 1% penicillin streptomycin. The αMEM media along with the serum and the antibiotics constitute the growth medium. Media was replaced every 2–3 days, and the cells were passaged when they were approximately 90–95% confluent. Confluent cells were exposed to 0.25% Trypsin-ethylenediaminetetraacetic acid solution for 2 minutes at 37°C and collected. Cells were counted using a hemocytometer with Trypan Blue staining. For osteogenic differentiation, growth medium was supplemented with 50 µg/mL ascorbic acid, 10 mmol/L β-glycerophosphate, and 10 nmol/L dexamethasone.

For cell culture, the PU-nHA-layered coverslips were placed material-side down into individual wells of a non-tissue culture-treated plate and exposed to growth media for at least 1 hour to separate the material film from the coverslip, at which point the glass coverslip was removed from the well. This was done to ensure that the cells adhered to the material films only. Finally, the cells were seeded on the films. Seeding density and culturing parameters were dependent on the type of experiment.

Each *in vitro* assay was carried out simultaneously, using an equal number of cells seeded on the films and the polystyrene tissue culture surfaces. Cells seeded on the polystyrene surfaces served as positive controls, and negative controls were materials and polystyrene surfaces without any cells. Each assay was performed at least twice with each sample in triplicate.

Commercially available MC 3T3-E1 cells adhered to all the iterations tested, and initial evaluations showed that the cells proliferated on all films except the 60/40 iteration. Visual inspection indicated that cells were not healthy and non-proliferative, and hence, the 60/40 iteration was not used in subsequent *in vitro* assays. Furthermore, 60/40 was not used to quantitate cell proliferation using the calcein-am assay.

Viability and Proliferation

Calcein-AM staining, coupled with the quantitation of fluorescent intensity, was used to assess cell proliferation and viability on the PU-nHA films. A fluorescence assay was carried out in black-walled 24-well plates to eliminate potential auto-fluorescence. 40,000 cells were seeded per film (1 film per well), and the cells were incubated in growth media for 3, 5, and 7 days. For evaluation, samples were incubated with 0.5 mL of staining solution, containing 10 µg/ml calcein-AM reconstituted with dimethyl sulfoxide, at 37°C for 5 minutes, and the fluorescence intensity was measured using a microplate reader set at an excitation wavelength of 485 nm and an emission wavelength of 528 nm. Sample readings were adjusted using the negative control readings. Replicates of materials were averaged, and a graph of fluorescence intensity over the experimental timeframe

was generated. Simultaneously, fluorescent images of all samples at each time point were taken to verify the presence of cells and their viability.

Cell proliferation and viability was confirmed on the 100/0, 90/10, 80/20 and 70/30 composites using Calcein-AM staining over a period of 7 days (**Figure 2.1**). Calcein-AM is a hydrophobic, non-fluorescent dye that infiltrates live, intact cells, and is hydrolyzed by intracellular esterases, a process that converts the Calcein-AM to calcein. Calcein-AM is hydrophilic, has strong green fluorescence, and is retained by the cytoplasm of the cell, making it an indicator of cell health. Fluorescence intensity is proportional to the quantity of viable cells, and therefore, quantitative measurements of change in total fluorescence intensities over a given period are indicative of cell proliferation (Crisan et al., 2015). As a result, Calcein-AM staining serves a dual purpose of imaging viable cells and measuring their proliferation. This strategy becomes particularly valuable when cells are seeded on composite films, which cannot be imaged using standard microscopic methods. Green fluorescent imaging (**Figure 2.1**) and quantification confirmed that all four iterations of the films were biocompatible with the MC 3T3-E1 cells. As judged by the fluorescence intensities of cells, there was a linear increase in cell proliferation ($R^2 > 0.9$) on the 80/20 and 70/30 films only (**Figure 2.1**). Though there was an increase in cell fluorescence on the 90/10 film on day 3, the intensity changes were not linear over days 5 and 7. 100/0 films demonstrated no linearity among time points, with values initially increasing before a slight reduction.

Morphological Assessment

Direct labeling of MC3T3-E1 cells with DiI (1,1'-dioctadecyl-3,3,3',3'-tetramethylindocarbocyanine perchlorate) was used to assess cell morphology on the films. In a typical labeling reaction, 50 µg/ml DiI was used to label 1 million cells. Cells were incubated at 37°C for 15 minutes and excess DiI was removed by washing with HBSS (Hank's balanced salt solution). Cells were then re-suspended in complete growth media. As described above, 40,000 cells were seeded per film (per well) in a 24-well plate then incubated in growth media for 7 days. Images of five random areas on each sample and the corresponding controls were taken once a day for seven days to visualize and track the growth patterns and morphology of cells. The exposure time and magnification were kept constant during imaging.

Cell morphology and viability over time were confirmed using the red-fluorescent cytoplasmic DiI stain (**Figure 2.2**). DiI staining does not compromise the integrity of the cellular membrane and allows us to image the same cells in real time. This eliminates the need to harvest or fix cells to visualize changes in morphology using microscopy. The formation of clusters of cells or “nodules” is considered the hallmark of osteogenic differentiation and demonstrates bone metabolic activity (Declercq, Verbeeck, De Ridder, Schacht, & Cornelissen, 2005). Therefore, changes in cell morphology, indicative of osteogenic differentiation profiles, were evaluated subjectively and quantitatively by imaging the nodules formed when the MC 3T3-E1 cells adhered and proliferated on the films.

Quantitative measurements were conducted using ImageJ software to categorize nodules by size based on reference nodules in cultures on 100% PU films stained with alizarin red for calcium content (**Figure 2.3**). Particular attention was given to nodules in the Rank 4 category, designated as large nodules, and the average area of these nodules was examined in cell-seeded material across time points (**Figure 2.4**). Over time, cells on 90/10 and 80/20, PU-nHA films presented signs of cell-cell communication and formation of dense nodular structures. Cells seeded on the 70/30 composite films did show some signs of cell-cell communication, but the pattern was not as striking as observed on the 90/10 and 80/20 films. All three film iterations demonstrated an increase in large nodule area coverage between day 3 and day 7 time points (**Figure 2.4**). Cells exposed to 60/40 and 100/0 films did not display similar interactions, appearing as static, spherical elements suspended in the films.

Since, the MC3T3 E1 cells showed evidence of cell clusters and communication, we next investigated the cell morphology changes on 90/10 and 80/20 films in presence of the osteogenic differentiation medium (**Figure 2.2**). Nodular structures observed in growth media supplemented with osteogenic inducers, dexamethasone, beta-glycerophosphate, and ascorbic acid differed in appearance from structures observed in presence of growth medium alone. Cells seeded on the films and osteogenic differentiation medium exhibited signs of stress. Structures present on samples in presence of the osteogenic inducers displayed a lack of cell-cell communication and were not as dense as clusters present in samples exposed to the films in the absence of osteogenic inducers. This indicates that the cells in samples supplemented with differentiation medium may have been exposed to culture conditions leading to excessive stress and sporadic differentiation. Taken together, all data suggest that the cells seeded on 90/10 and 80/20 PU-nHA films show signs of osteogenic differentiation in the absence of any osteogenic inducers.

Conclusion

In conclusion, our results demonstrated that by varying the nHA content, the cellular response is affected, and by evaluating this response, we were able to identify a composite which could potentially be used to design a 3D scaffold for future *in vivo* studies. The chemical, physical, and mechanical properties of all the composite films showed consistency and reproducibility for each preparation. While the mechanical properties did not exhibit any significant changes, there were statistically significant differences in the surface roughness and the contact angle of the composites. The cellular response to each iteration can thus, be attributed to this composition change as well as surface topography.

In vitro assessment of MC 3T3-E1 cells on these films presented inherent challenges resulting from the compositional make-up of the material. The inclusion of PU and nHA within the nanocomposite prevented use of common assays for proliferation (MTS assay) and differentiation (Alizarin Red staining). Formazan

crystal products were unable to be readily released into the surrounding media when subjecting solutions to MTS reagent, thereby resulting in unreliable readings for proliferation of cells on the films. To circumvent this issue the earlier describe Calcein-AM fluorescent analysis was conducted to determine cell viability and proliferation. Similarly, the presence of nHA in the material demanded an alternative method to traditional alizarin red staining for evaluating the osteogenic differentiation potential of cells on films. As this reagent works by staining calcium to identify mineralized regions, the presence of calcium-rich additive in the material resulted in prolific background that heavily obscured signal (**Figure 2.5**). Initially, an alkaline phosphatase kit was attempted to assess osteogenic differentiation potential, yet this assay appeared to face similar issues as the previously attempted MTS assay and results were determined to be unreliable. The use of the earlier described DiI fluorescent stain was therefore implemented to track cell morphology over the study time course and attempt to correlate nodule formation observed on films with similar nodules in PU-only material iterations and cell monolayers to examine the osteogenic potential of film iterations.

The proliferation on different film compositions (as described above) showed that all of the composites are cytocompatible. This claim is supported by observation of cells through two separate stains, Calcein AM and DiI (**Figures 2.1-2.2**). Proliferative ability of cells exposed to 70/30 and 80/20 compositions appeared normal and unhindered, based on their linearity. The early spike and sequential plateauing of readings for cells exposed to 90/10 may be due to the relatively low surface roughness in the film (**Figure 2.1**) which may not be conducive to cell proliferation, and hence, lack reactivity in the proliferation assay. The exact reason for the initial increase is not known at this time and is beyond the scope of this study. Clustering and cell-to-cell communication of MC 3T3-E1 cells on 90/10 and 80/20 films suggest that the cells are probably undergoing osteogenic differentiation in the absence of any inducers, which can be proved using *in vivo* models. This is further supported by the fact that during proliferation, cells exhibited healthy morphology and cell-cell communication, in contrast to the effects observed in the presence of osteogenic differentiation medium.

Our data suggests that the material properties, and specifically the nHA content do influence cell behavior, which we could subjectively evaluate using the cellular assays described in this study. Even though the 90/10, 80/20, and 70/30 composites all supported cellular proliferation, only the 90/10 and 80/20 showed clustering of cells. In contrast, cells did adhere to the 60/40 composite, but, did not proliferate, and hence, did not demonstrate any clusters or cell-to-cell communication. This was an unexpected finding because an increase in the percentage of nHA should promote cell adherence and osteogenic differentiation.

There are many published reports where authors have demonstrated that surface roughness can significantly affect cell attachment, proliferation, apoptosis and osteogenic differentiation. Studies have demonstrated that surface roughness is a very important aspect of a biomaterial which can significantly modulate cell behavior and hence, an optimal surface roughness has to be identified (Deng et

al., 2015). More specifically, osteogenesis, induced by osteoblastic cells, is characterized by a sequence of events, involving cell attachment and cell proliferation, followed by the expression of osteoblast phenotype, is highly dependent on the surface topography of biomaterials. It has been suggested that the surface composition and structure of biomaterials can influence the adsorption of the extracellular matrix proteins including fibronectin and vitronectin, which play a very significant biological role in cell adhesion. Modulation of the osteogenic differentiation process by various surface textures has been demonstrated by evaluating changes in the alkaline phosphatase activity or in the expression profiles of osteogenic-specific genes using immortalized (MC3T3E1 or MG-63 cells) or primary (mesenchymal stem cells) cell lines.

In view of these reports, we believe that the high surface roughness in the 60/40 composites affect the cellular adherence and thus, proliferation which could potentially affect osteogenic differentiation. Taken together, linearity in cell proliferation coupled with changes in morphology and formation of cell clusters, suggests that the composite containing 20% nHA and 80% PU presents an environment conducive for cells to adhere, proliferate and form clusters suggesting osteogenic differentiation. Future *in vivo* experiments using these 80/20 films should be investigated in order to further assess the osteogenic potential of cells on such composites in an *in vivo* bone defect model.

As the current thin film form of the material does not resemble or address the complex architecture of bone, or lend to ease of application, a 3D construct design was developed based on both the 80/20 and 90/10 films. The new scaffold material comprised of layers of these films interspersed with decellularized bone particles (DBPs) to fabricate two scaffolds with inherent porosity that contains micro- and nano-architectural elements. Scaffolds based on the 80/20 material were designated as S-1, while those based on 90/10 films were S-2. This design was hypothesized to maintain the cytocompatibility and potential osteogenic functions of the film material while providing a more clinically applicable material for treating bone injuries. To test this hypothesis, both in vitro and in vivo assessment of the 3D scaffold design was performed, first to verify cytocompatibility on the layered structure, and then to determine biocompatibility and osteogenic capacity in an animal model. Since rodent models are a well-established method for early-stage biocompatibility studies, due to availability, cost, and low inter-animal variance, a unicortical tibial defect model in rats was utilized. This work and resulting data are detailed in the following chapter.

References

Adhikari, R., Gunatillake, P. A., Griffiths, I., Tatai, L., Wickramaratna, M., Houshyar, S., . . . Carbone, T. (2008). Biodegradable injectable polyurethanes: synthesis and evaluation for orthopaedic applications. *Biomaterials, 29*(28), 3762-3770. doi:10.1016/j.biomaterials.2008.06.021

Bayer, I. S., Ghosh, A., Labriola, M., Biris, A. S., Dervishi, E., Watanabe, F., . . . Biswas, A. (2013). Fabrication of bionanocomposites comprising flat nanocrystals of calcium in collagen fibers exhibiting hardness comparable to metal. *RSC Advances, 3*(43), 20315-20323. doi:10.1039/C3RA43121E

Biswas, A., Bayer, I. S., Zhao, H., Wang, T., Watanabe, F., & Biris, A. S. (2010). Design and synthesis of biomimetic multicomponent all-bone-minerals bionanocomposites. *Biomacromolecules, 11*(10), 2545-2549. doi:10.1021/bm1009359

Christenson, E. M., Anseth, K. S., van den Beucken, J. J., Chan, C. K., Ercan, B., Jansen, J. A., . . . Mikos, A. G. (2007). Nanobiomaterial applications in orthopedics. *J Orthop Res, 25*(1), 11-22. doi:10.1002/jor.20305

Crisan, L., Crisan, B., Soritau, O., Baciut, M., Biris, A. R., Baciut, G., & Lucaciu, O. (2015). In vitro study of biocompatibility of a graphene composite with gold nanoparticles and hydroxyapatite on human osteoblasts. *J Appl Toxicol, 35*(10), 1200-1210. doi:10.1002/jat.3152

Declercq, H. A., Verbeeck, R. M., De Ridder, L. I., Schacht, E. H., & Cornelissen, M. J. (2005). Calcification as an indicator of osteoinductive capacity of biomaterials in osteoblastic cell cultures. *Biomaterials, 26*(24), 4964-4974. doi:10.1016/j.biomaterials.2005.01.025

Deng, Y., Liu, X., Xu, A., Wang, L., Luo, Z., Zheng, Y., . . . Wei, S. (2015). Effect of surface roughness on osteogenesis in vitro and osseointegration in vivo of carbon fiber-reinforced polyetheretherketone-nanohydroxyapatite composite. *Int J Nanomedicine, 10*, 1425-1447. doi:10.2147/ijn.S75557

Egan, P., Sinko, R., LeDuc, P. R., & Keten, S. (2015). The role of mechanics in biological and bio-inspired systems. *Nature Communications, 6*, 7418. doi:10.1038/ncomms8418

Ferreira, A. M., Gentile, P., Chiono, V., & Ciardelli, G. (2012). Collagen for bone tissue regeneration. *Acta Biomater, 8*(9), 3191-3200. doi:10.1016/j.actbio.2012.06.014

Gao, H. (2006, 2006//). *Application of fracture mechanics concepts to hierarchical biomechanics of bone and bone-like materials.* Paper presented at the Advances in Fracture Research, Dordrecht.

Goncalves, F., Bentini, R., Burrows, M. C., Carreira, A. C. O., Kossugue, P. M., Sogayar, M. C., & Catalani, L. H. (2015). Hybrid Membranes of PLLA/Collagen for Bone Tissue Engineering: A Comparative Study of Scaffold Production Techniques for Optimal Mechanical Properties and Osteoinduction Ability. *Materials (Basel), 8*(2), 408-423. doi:10.3390/ma8020408

Harper, E. J., & Bonfield, W. (2000). Tensile characteristics of ten commercial acrylic bone cements. *J Biomed Mater Res, 53*(5), 605-616.

Hutmacher, D. W. (2000). Scaffolds in tissue engineering bone and cartilage. *Biomaterials, 21*(24), 2529-2543. doi:10.1016/s0142-9612(00)00121-6

Kobayashi, M., Nakamura, T., Okada, Y., Fukumoto, A., Furukawa, T., Kato, H., . . . Kikutani, T. (1998). Bioactive bone cement: comparison of apatite and wollastonite containing glass-ceramic, hydroxyapatite, and beta-tricalcium phosphate fillers on bone-bonding strength. *J Biomed Mater Res, 42*(2), 223-237.

Liao, S. S., Cui, F. Z., Zhang, W., & Feng, Q. L. (2004). Hierarchically biomimetic bone scaffold materials: nano-HA/collagen/PLA composite. *J Biomed Mater Res B Appl Biomater, 69*(2), 158-165. doi:10.1002/jbm.b.20035

Liu, Y., Hunziker, E. B., Randall, N. X., de Groot, K., & Layrolle, P. (2003). Proteins incorporated into biomimetically prepared calcium phosphate coatings modulate their mechanical strength and dissolution rate. *Biomaterials, 24*(1), 65-70. doi:10.1016/s0142-9612(02)00252-1

Lou, c.-w., Huang, C.-L., Chen, C.-K., Liu, C.-F., Wen, S.-P., & Lin, J.-H. (2015). Effect of Different Manufacturing Methods on the Conflict between Porosity and Mechanical Properties of Spiral and Porous Polyethylene Terephthalate/Sodium Alginate Bone Scaffolds. *Materials, 8*, 8768-8779. doi:10.3390/ma8125488

Meyers, M. A., McKittrick, J., & Chen, P. Y. (2013). Structural biological materials: critical mechanics-materials connections. *Science, 339*(6121), 773-779. doi:10.1126/science.1220854

O'Brien, F. J. (2011). Biomaterials & scaffolds for tissue engineering. *Materials Today, 14*(3), 88-95. doi:https://doi.org/10.1016/S1369-7021(11)70058-X

Salgado, A. J., Coutinho, O. P., & Reis, R. L. (2004). Bone tissue engineering: state of the art and future trends. *Macromol Biosci, 4*(8), 743-765. doi:10.1002/mabi.200400026

Su, T., Liu, Y., He, H., Li, J., Lv, Y., Zhang, L., . . . Hu, C. (2016). Strong Bioinspired Polymer Hydrogel with Tunable Stiffness and Toughness for Mimicking the Extracellular Matrix. *ACS Macro Letters, 5*(11), 1217-1221. doi:10.1021/acsmacrolett.6b00702

Sun, H., Zhu, F., Hu, Q., & Krebsbach, P. H. (2014). Controlling stem cell-mediated bone regeneration through tailored mechanical properties of collagen scaffolds. *Biomaterials, 35*(4), 1176-1184. doi:https://doi.org/10.1016/j.biomaterials.2013.10.054

Towler, D. A., & Arnaud, R. S. (2002). Chapter 88 - Use of Cultured Osteoblastic Cells to Identify and Characterize Transcriptional Regulatory Complexes. In J. P. Bilezikian, L. G. Raisz, & G. A. Rodan (Eds.), *Principles of Bone Biology (Second Edition)* (pp. 1503-1527). San Diego: Academic Press.

Zhang, X., Battiston, K. G., McBane, J. E., Matheson, L. A., Labow, R. S., & Santerre, J. P. (2016). 3 - Design of biodegradable polyurethanes and the interactions of the polymers and their degradation by-products within in vitro and in vivo environments. In S. L. Cooper & J. Guan (Eds.), *Advances in Polyurethane Biomaterials* (pp. 75-114): Woodhead Publishing.

Appendix

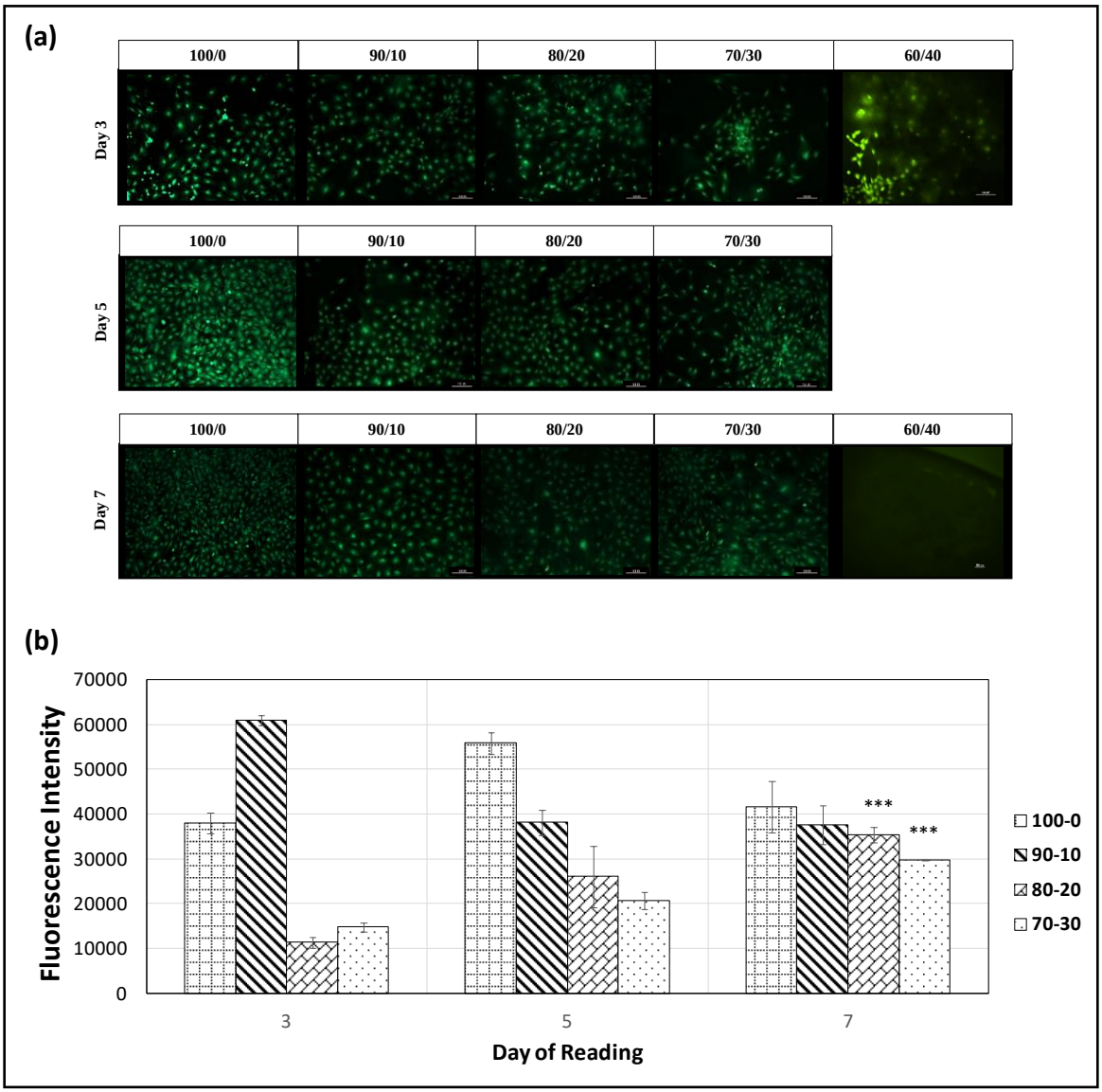

Figure 2.1. Cell viability/proliferation using Calcein-AM staining. (a.) Calcein-AM and (b.) Calcein AM staining fluorescence intensities. Asterisks indicate significant linear increases in fluorescence intensities over a period of 7 days. Note: All samples were subjected to an initial evaluation where only days 3 and 7 were analyzed. As the 60/40 sample did not exhibit healthy proliferation and therefore was not included in the more extensive follow-up study of 3,5, and 7 days nor was statistical analysis performed. However, the preliminary images from the 60/40 film are presented for reference.

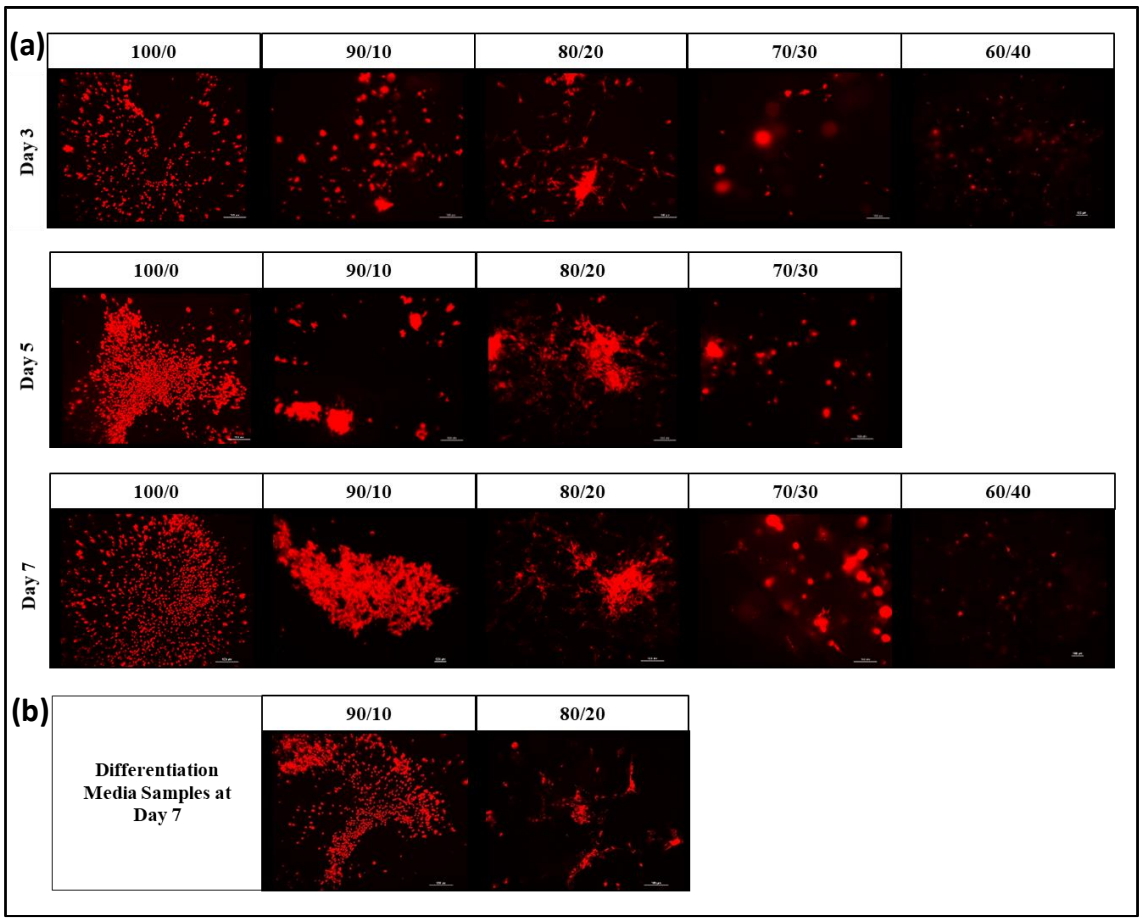

Figure 2.2. Cell morphology using DiI staining. DiI fluorescently labeled cells exposed to 100/0, 90/10, 80/20, 70/30, and 60/40 films in growth media (a). Note: All samples were subjected to an initial evaluation where only days 3 and 7 were analyzed. As it was determined that the 60/40 sample did not exhibit healthy proliferation and therefore was not included in the more extensive follow-up study of 3,5, and 7 days. However, the images from the 60/40 film are presented for reference. DiI fluorescently labeled cells exposed to 90/10 and 80/20 films in osteogenic differentiation media (b) (supplemented with osteogenic inducers, dexamethasone, beta-glycerophosphate, and ascorbic acid) shown for reference at day 7 only.

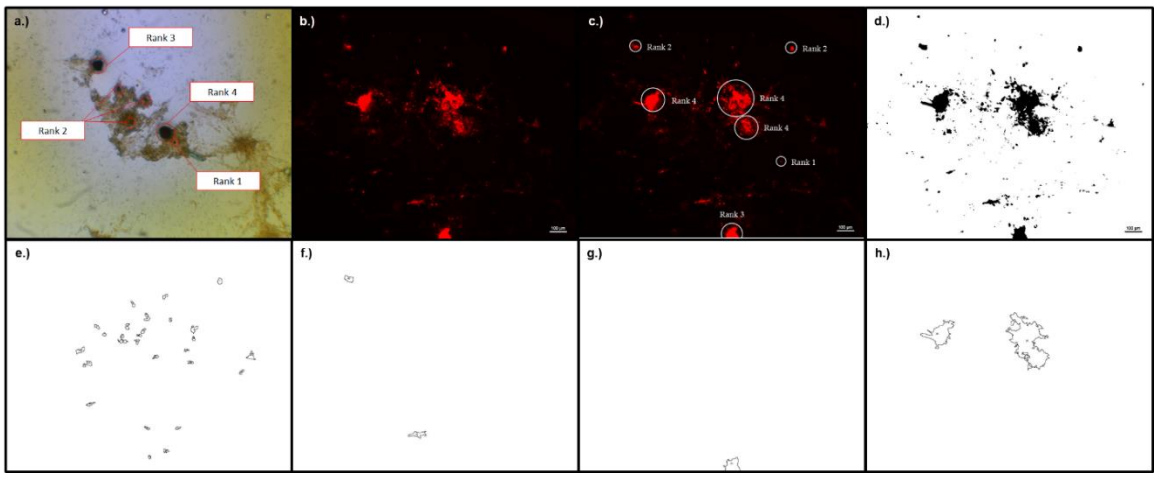

Figure 2.3. Cell nodule identification utilizing ImageJ processing of DiI stained samples. (a) Reference nodule sizes from cell cultures on 100% PU films were used to assess fluorescently labeled cells by assigning nodules in (b) original fluorescent image with (c) ranks. (d) Binary masks for images were generated with ImageJ and (e-h) nodules were isolated based on size ranking.

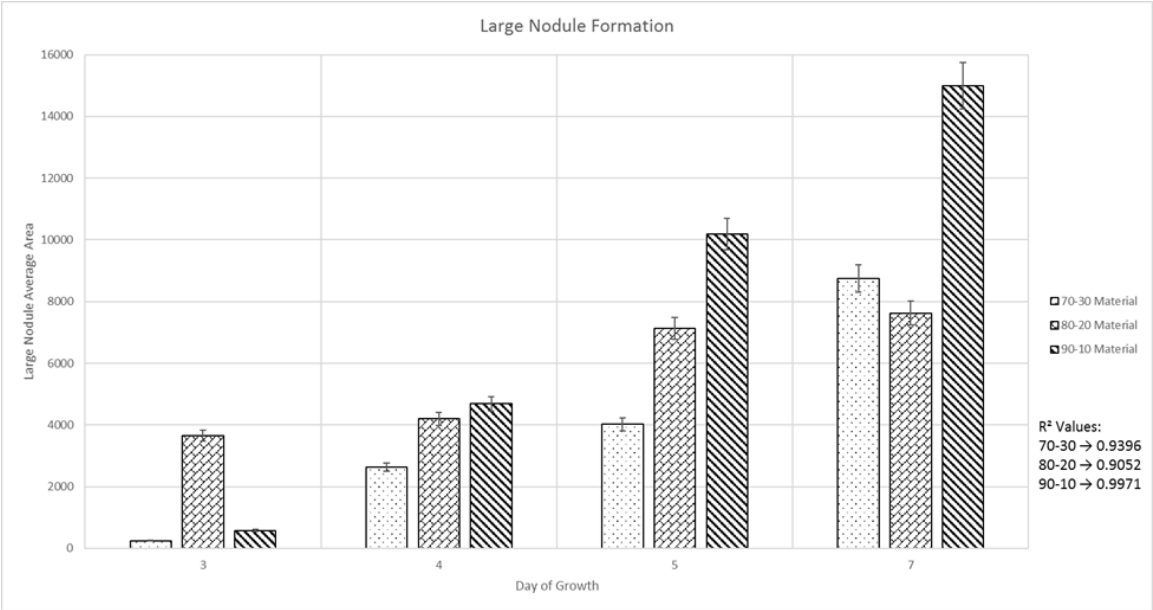

Figure 2.4. Nodule formation tracking utilizing DiI fluorescent labeling. Average area of large nodule formations in DiI labeled samples for three material iterations. The 60-40 material film iteration was not utilized due to observed unhealthy cellular activity.

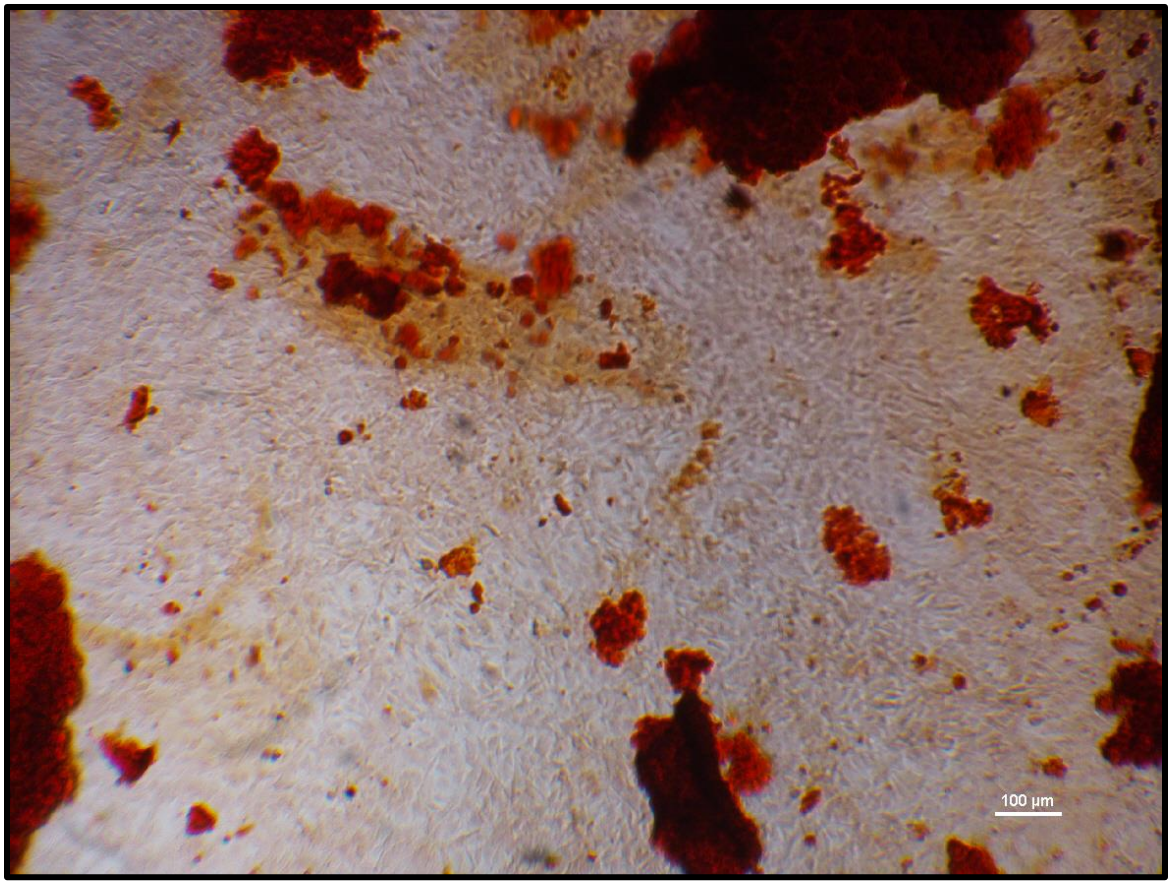

Figure 2.5. 80/20 material film seeded with MC 3T3-E1 cells and stained with Alizarin Red reagent. Uptake of staining solution by nHA content of material presented as dark red generated large level of background that prevented accurate assessment of cell mineralization.

CHAPTER III:
IN VIVO BIOCOMPATIBILITY ASSESSMENT OF POLYURETHANE/NANO-HYDROXYAPATITE FILM-DERIVED OSTEOBIOLOGIC PLATFORMS USING A RAT UNICORTICAL BONE DEFECT

A version of this chapter was originally published by Austin J. Bow:

Bow, A., Newby, S., Rifkin, R., Jackson, B. K., Matavosian, A., Griffin, C., . . . Dhar, M. (2019). Evaluation of a Polyurethane Platform for Delivery of Nanohydroxyapatite and Decellularized Bone Particles in a Porous Three-Dimensional Scaffold. *ACS Applied Bio Materials, 2*(5), 1815-1829. doi:10.1021/acsabm.8b00670

This article was published by ACS publications in the journal of Applied Bio Materials on 26 March 2019, and has been reprinted with permission from Bow, A.; Newby, S.; Rifkin, R.; Jackson, B.; Matavosian, A.; Griffin, C.; King, W.; Alghazali, K.; Madhi, A.; Berryhill, S.; Morello, R.; Hecht, S.; Biris, A.; Anderson, D.; Bourdo, S.; Dhar, M. Evaluation of a polyurethane platform for delivery of nanohydroxyapatite and decellularized bone particles in a porous three-dimensional scaffold. ACS Applied Bio Materials. **2019**, 2(5), 1815-1829: doi: 10.1021/acsabm.8b00670. Copyright 2019 American Chemical Society. Material fabrication and characterization of physical and chemical properties were carried out by listed authors from the Center for Integrative Nanotechnology Sciences at the University of Arkansas at Little Rock (UALR). The biologic assessment of the material through *in vitro* and *in vivo* experimentation was conducted at the University of Tennessee in Knoxville. As such this chapter will address only the biologic analyses and conclusions drawn from these data.

Abstract

The complex dynamic nature of bone tissue presents a unique challenge for developing optimal biomaterials within the field of bone tissue engineering. Materials based on biological and physiological characteristics of natural bone have shown promise for inducing and promoting effective bone repair. Design of multi-composite scaffolds that incorporate both malleable and hard mineral components allow for intricate structures with nano- and macro-sized mineral components to provide architectural elements that promote osteogenesis. The examined scaffolds are multi-layered constructs differing only in the compositional ratio of nano-hydroxyapatite (nHA) and decellularized bone particles (DBPs), and incorporate previously studied nHA/polyurethane films interspersed with macro-sized bone DBPs to stimulate integration with native tissue and induce osteogenic activity. In vitro assessment of cytocompatibility and osteo-stimulatory characteristics indicated that the scaffolds did not negatively impact cell health and demonstrated osteogenic effects. When the constructs were implanted *in vivo*, in a rat tibial defect model, the biocompatibility and osteogenic impact were confirmed. Futhermore, those treated with S-1 scaffolds exhibited greater levels of new bone formation. These results indicate that, while both scaffold designs were biocompatible, S-1 constructs demonstrate an optimal biologically relevant nano-/macro- mineral architectural elements.

Introduction

Design of an effective material for replacing and restoring function of damaged bone has been an evasive and a complex challenge, which can be attributed to the highly dynamic nature of the organ. As bone naturally possesses self-regenerative ability, the main application of such materials will fall to cases that exceed the inherent capabilities of this reparative mechanism (Deng et al., 2008; Zhu et al., 2017; Kruyt Moyo et al., 2006). Currently, the most effective treatment option utilizes autologous bone taken from a donor site of the individual. This offers the ability to restore function without biocompatibility concerns yet relies on a limited source and raises risk to the individual due to multiple surgical incisions (Kruyt Moyo et al., 2006). To circumvent these restrictions, recent progress in bone tissue engineering has turned to natural and synthetic scaffolds designed for bone regeneration (Salgado, Coutinho, & Reis, 2004; Roseti et al., 2017). Production of an ideal scaffold that can be readily synthesized, implanted, and facilitate bone restoration similar, or superior, to an autograft offers an attractive alternative. The optimal synthetic material should permit, or promote, existing progenitor cells to integrate into the structure and provide a basal substrate for natural remodeling to occur. Scaffolds fabricated using components derived from, or similar to, those present in natural bone offer potential for inducing such integrative properties without concern regarding biocompatibility. A bone tissue regenerative scaffold should be composed of materials capable of osteo-conduction and osseo-integration, as well as osteo-inductive potential when cells or growth factors are delivered (Agrawal & Ray, 2001; Albrektsson & Johansson, 2001). Considering these characteristics, calcium-phosphate (CaP) ceramics are one the commonly used “active” component within biomaterial constructs (Zhu et al., 2017). Hydroxyapatite (HA), a widely investigated CaP, has pronounced osteo-conductive capabilities and has demonstrated good biocompatibility within *in vivo* environments, as well as indications of bioactivity *in vitro (*Zhu et al., 2017; Habibovic et al., 2006; Kubasiewicz-Ross et al., 2017; Yu, Xia, Teramoto, & Ni, 2018; Fu et al., 2017; Fu et al., 2017). HA degradation may act to supply calcium and phosphorous ions vital to new bone formation, and therefore acts to promote osteogenesis in exposed cells (Fu et al., 2017).

Recent research in the field of material science, using both *in vitro* and *in vivo* studies, has emphasized the importance of nano-biomaterial substitutes for bone tissue engineering, as they may provide a more efficacious option compared to their macro or micro sized counterparts (Christenson et al., 2007; Ha, Jang, Nam, & Beck, 2015; Pujari-Palmer, 2016). Nano-biomaterials may present an improved biological environment for facilitating osteo-inductive, osteo-conductive and osseo-integrative functions. This is exemplified by the promise nano-hydroxyapatite (nHA) has shown in stimulating osteogenesis, alone, or when it is incorporated into matrix substrates (Liu et al., 2012; Ha, Jang, Nam, & Beck, 2015). nHA particle deposition within material constructs can significantly influence the topographical features of the surfaces of the material, such as enhanced surface

area (Huang et al., 2004). However, increasing nHA content beyond a certain limit, can lead to agglomeration and “chaotic” surface morphology, which can negatively impact cellular activity. This indicates that tailoring of the nanocomposite surface structures and roughness is vital to generating a material with optimal and reproducible cellular growth and maturation (Danish et al., 2015). It has also been suggested that incorporation of nHA into a material construct further enhances adsorption of specific serum proteins due to high surface area/energy of nanoparticles (Zhao et al., 2017; Mohsen-Nia, Massah Bidgoli, Behrashi, & Mohsen Nia, 2012), which in turn promotes cellular adhesion to the substrate. The porosity of such structures can also drastically impact efficient cellular ingrowth and bone formation, with porosities ranging from 50-800 μm being optimal (Unosson, Montufar, Engqvist, Ginebra, & Persson, 2016; Torstrick, Evans, Stevens, Gall, & Guldberg, 2016; Chang et al., 2016; Hing, Best, Tanner, Bonfield, & Revell, 2004). Therefore, by optimizing the combination of nano- and macro-components with specific physicochemical properties it is possible to develop a nanocomposite capable of stimulating osteogenesis (Wang et al., 2018). Despite the osteogenic potential, the *in vivo* toxicity of these nanomaterials should not be disregarded, and hence, must be evaluated prior to clinical application.

We have previously reported that a 2D nanocomposite containing 80% polyurethane (PU) and 20% nHA was cytocompatible and demonstrated a linear increase in proliferation of MC3T3-E1 cells *in vitro* (Jackson et al., 2018). Interestingly, the MC3T3E1 cells adhered to this composite in clusters and appeared to form nodules which are considered as hallmarks of osteogenic differentiation within 5 days of seeding and in the absence of any osteogenic inducing reagents. Data suggested that the physical and chemical properties of this nanocomposite seemed to present an ideal environment for cell adhesion, proliferation, and osteogenic differentiation *in vitro*. Comparatively, a 2D nanocomposite consisting of 90% PU and 10% nHA, despite lack of a linear increase in cell proliferation, demonstrated cell-cell communication and clustering similar to the 80% PU and 20% nHA composite[25] and provided a comparative basal element for design of a 3D construct.

In the present study, we synthesized a 3D scaffold containing a combination of a carbon-based organic polymer, PU, and mineral components, nHA and decellularized bone particles (DBPs) (Geistlich), in such a way that the resulting scaffold consists of a complex nano-/macro-matrix with malleable and mineral components. It has been suggested that for the human trabecular and cortical bones taken together, the organic component ranges between 20-30% of the mineral weight thus, a scaffold with a ratio of 1:2 – 1:4 of these components might prove efficacious in bone healing and repair (Lees & Prostak, 1988; Yerramshetty & Akkus, 2008; Raviraj Havaldar, 2012). PU, acting mechanically as a substitute for the organic constituents in natural bone, is a biocompatible polymer which provides the structure and flexibility to the scaffold. Incorporation of the inorganic, mineral components, nHA and DBPs (nHA+DBPs) into this polymeric matrix generates an environment compatible for integration with natural bone. nHA,

provides the nano-content, is osteo-stimulatory and promotes an osteogenic environment. The DBPs act as bioactive compounds to provide an osteo-conductive macro-content to guide new bone formation. DBPs have been demonstrated to have limited osteogenic potential alone and hence, are typically complexed with other polymers to generate osteogenic scaffolds (De Santis et al., 2017; DeNicolo et al., 2015). The resulting 3D scaffold is porous, pliable, maintains structural integrity, and consists of nano- and macro-components which, together, should generate an environment favorable to cellular migration and osteogenesis (Huang et al., 2004).

We designed an *in vivo* rodent model to evaluate the osteo-conductive and osseo-integrative nature of the scaffold, as well as determine biocompatibility. Based on our *in vitro* results, and published information, we hypothesized that a 3D scaffold containing 80% PU / 20% nHA films with interspersed DBPs will be biocompatible and will present an environment conducive for *in vivo* bone regeneration. Our objectives were to fabricate and characterize a complex 3D scaffold, assess this scaffold *in vitro*, and subsequently, evaluate its biocompatibility and efficacy *in vivo*. To test our hypothesis, we first engineered, manufactured, and characterized a 3D scaffold, verified cell adhesion, morphology and cytocompatibility *in vitro* and, subsequently evaluated the osteogenic potential and biocompatibility *in vivo* using a rat model with a unicortical tibial bone defect. 3D scaffolds comprised of 80% PU / 20% nHA material films interspersed with DBPs, referred to as S-1, were evaluated alongside scaffolds comprised of 90% PU / 10% nHA films interspersed with DBPs, referred to as S-2, to elucidate the impact on the osteogenic environment of a scaffold due to variations in nano-/macro-structural element compositions.

3D Scaffold *In Vitro* Analysis

Viability and Proliferation

Commercially obtained MC3T3-E1 cells were used for all *in vitro* assays as described previously (Jackson et al., 2018). Cells were expanded in tissue culture polystyrene flasks, at 37°C and 5% CO_2 in αMEM media with 10% fetal bovine serum and 1% penicillin streptomycin, which was replaced every 2-3 days. Cell cultures reaching approximately 90% confluency were enzymatically released from growth substrate using 0.25% Trypsin-EDTA solution for 2 minutes at 37°C, collected, and allocated to tissue culture flasks or experimental set-ups. Cells collected during passage were counted using a hemocytometer after 0.4% Trypan Blue staining to ensure accurate seeding concentrations.

Individual plugs of both S-1 and S-2 were obtained from the bulk blocks (30 mm x 30 mm x 5 mm) using a 2mm biopsy punch. Each scaffold plug was placed into individual wells of a non-tissue culture treated plate and exposed to growth media for at least 1 hour prior to cell seeding. This was done to ensure scaffold expansion and uniform exposure of material to media. Finally, the cells were seeded to scaffolds with a seeding density of $5x10^5$ cells/scaffold.

Cell adhesion and morphology was confirmed *in vitro* on the 3D scaffolds using previously described methods (Jackson et al., 2018). The commonly used assessment techniques to measure cell proliferation and viability, including the use of 3-(4,5-dimethylthiazol-2-yl)-5- (3-carboxymethoxyphenyl)-2-(4-sulfophenyl)-2H-tetrazolium (MTS) and the calcein-am and propidium iodide stains, could not be used because of interference by the components of the 3D scaffolds. As a result, cell adhesion and morphological changes were observed using the fluorescent cytoplasmic stain, DiI. Since, DiI is retained in the cytoplasm of living cells, DiI staining was also used to demonstrate cytocompatibility of the scaffolds. Cells seeded on the S-1 and S-2 scaffolds were compared to cells cultured on tissue-culture polystyrene dishes as positive controls, and to scaffolds in media alone without cells, as negative controls.

In vitro evaluation of DiI stained MC3T3-E1 cells demonstrated that cells adhered to the 3D scaffolds and exhibited clustering dynamics within 5-7 days of seeding, suggesting osteogenic differentiation (**Figure 3.1**). Cell behavior was similar to our observations on 2D PU/nHA films as described earlier (Jackson et al., 2018). Cells adhered and formed clusters on the 3D scaffolds within 5 days of seeding and in the absence of any differentiating reagents (dexamethasone, beta glycerophosphate and ascorbic acid) (Jackson et al., 2018). Monitoring of cellular morphology and proliferation through fluorescent microscopy demonstrated cell adhesion and supports cytocompatibility of the materials. As this stain does not effectively act as a means of assessing cytotoxicity, *in vivo* application was necessary to demonstrate biocompatibility. Additionally, as described earlier, the mineral components of the scaffolds prevented the use of alizarin red and alkaline phosphatase staining, to demonstrate osteogenesis. Hence, morphological observations and analysis of gene expression were used for *in vitro* evaluation of scaffolds. Based on the morphologic characteristics and cell-to-cell communication observed at 5 days after cell seeding, all *in vitro* assays with the 3D scaffolds described in this study were carried out at this time point.

qPCR Assessment

We were unable to utilize Alizarin red and alkaline phosphatase assays because of extensive interference from non-specific staining caused by the presence of nHA. The background interference obscured the true values. As a result, we used gene expression analysis of osteogenic markers to assess osteo-differentiation of cells.

Total RNAs were extracted from the cell/scaffold constructs 5 days post seeding and analyzed for the expression of osteogenic-specific genes (Chou, 2005). Total RNA was isolated using the Trizol extraction agent (ThermoFisher) as per the manufacturer's protocol with certain modifications to increase the yield of RNA (Lee, 2011). Briefly, all media was removed, and cell/scaffold constructs were washed. 0.3 mL Trizol was added to each 2 mm scaffold and sonicated. An additional 0.2 mL Trizol agent was applied post-sonication to inhibit the potential entrapment of RNA by calcium precipitates from the scaffold material. Total RNA

was further purified using RNeasy mini kit (Qiagen) and concentrations were measured using a biophotometer. cDNA was prepared using a high-capacity cDNA reverse transcription kit (Applied Biosystems). qPCR analysis of the expression of the bone development markers osteopontin (OPN) and osteocalcin (OCN) was carried out using SYBR green master mix (ThermoFisher) with GAPDH serving as the housekeeping gene control (Agilent). Primer sequences and qPCR conditions for each of the genes were as described earlier[31]. Relative fold differences in the expression of osteogenic genes were calculated using $\Delta\Delta$Ct quantitation method (2008 Applied Biosystems). Averaged Ct values obtained from MxPro PCR software for each sample per target gene were normalized using GAPDH expression. Inclusion of blanks i.e. samples lacking template DNA, allowed determination of maximum acceptable sample Ct values, with values greater than 30 considered to be negative for the gene expression.

Total RNA extraction and purification, cDNA synthesis, and qPCR conditions and analysis were all optimized using MC3T3-E1 cells differentiated on polystyrene surface. MC3T3-E1 cells were differentiated in presence of the osteogenic differentiation medium (growth media supplemented with 10 mM beta glycerophosphate, 10 nM dexamethasone, 100 nM ascorbic acid) and the expression profiles of OPN and OCN were evaluated after 7, 14, and 21 days post induction. This was carried out to confirm osteogenesis and thus, the expression of osteogenic-specific genes in MC3T3-E1 cells under conditions already standardized on tissue culture polystyrene substrates in the absence of scaffolds.

MC3T3-E1 cells were cultured and differentiated towards osteogenesis on tissue culture polystyrene substrates using standard protocols (Jackson et al., 2018). As described earlier, these cells served as controls and ensured the validation of RNA quality, cDNA synthesis, and real time PCR conditions for OPN and OCN genes. The expression of the two osteogenic-specific gene markers was evaluated in MC3T3-E1 cells after 7, 14, and 21 days in presence of differentiation medium to confirm their osteogenic lineage. Using PCR conditions and the primer sequences reported in **Table 3.1**, the expression profiles of OPN and OCN were as expected during osteogenesis on tissue culture polystyrene substrates in the absence of scaffolds. High mineral content of the scaffold constructs required modifications of traditional extraction methods to improve yield and sample purity (Lee, 2011). Total RNA from cell/scaffold constructs at 5 days, when cultured with media having osteogenic-inducing agents, showed consistently poor yields and low integrity. Therefore, total RNAs were isolated from the cell/scaffold constructs only after 5 days post cell seeding in the absence of any differentiating media.

Real time PCR data demonstrating the expression of OPN and OCN genes in cells seeded on the S-1 and S-2 scaffolds confirmed that the cells were indeed of osteogenic lineage and that this was observed within 5 days of seeding and in the absence of any differentiating reagents (**Figure 3.2**). When the expression of these two genes was compared to cells that were differentiated on polystyrene substrate, in the presence of osteogenic inducers for a period of 21-28 days (Towler & Arnaud, 2002), there was a significant up-regulation of OPN expression,

whereas the OCN expression did not change. OPN expression is associated with early-stage bone remodeling processes, while OCN is more closely associated with mineralization and late-stage bone development (Chou, 2005). The significant up-regulation of OPN gene expression relative to cells differentiated on polystyrene substrate for 21-28 days using osteogenic inducers may indicate an enhanced degree of cellular remodeling within the scaffolds as this marker is strongly correlated with osteoblastic activity. The lack of change observed in expression of OCN at an early time point (day 5) may be due to the presence of naïve bone cells, which have not matured to stages of bone mineralization and ossification (Elkhenany et al., 2017). These late-stage processes are difficult to achieve in static cultures for the short duration of 5 days.

The Ct values for cells seeded on both the scaffolds indicated that both genes were expressed under the specified culture conditions, confirming that both the S-1 and S-2 scaffolds attenuated osteogenesis spontaneously without any induction, and within 5 days. Furthermore, comparison of expression between the two scaffolds showed a significant up-regulation of both the OPN and OCN expression when cells adhered and proliferated on S-1, thus, supporting a greater osteogenic induction potential of S-1 relative to S-2.

3D Scaffold *In Vivo* Analysis

Tibial Defect Model

8-10-week-old Sprague Dawley rats were commercially obtained (Harlan Laboratories). Animal procedures were performed in accordance with protocols approved by the University of Tennessee, Institutional Animal Care and Use Committee. An overview of the study design is depicted in **Figure 3.3**.

A unicortical, non-critical sized, defect of rat tibia was used as a model to test the *in vivo* biocompatibility and osseointegration potential of the two scaffolds, S-1 and S-2. Surgical procedures were carried out on four separate days to ensure quality of the operative conditions, with equal numbers of sample groups per day. Surgical procedures were as previously described (Elkhenany et al., 2017). Briefly, under anesthesia, a 5 mm long incision was made above the tibial crest and the periosteum was gently deflected to expose the bone surface. A uniform unicortical defect was generated using a 3 mm burr (Stoelting). One tibia defect per animal was treated with a scaffold, while the contralateral defect was left untreated to act as a comparative control. This was alternated for every animal to randomize the scaffold-treated tibia. Sites were closed with monofilament suture and animals were monitored once daily for at least 7 days post-surgery to track incision site appearance and overall animal health. 24 hours prior to sacrifice, animals were given 20 mg/kg Oxytetracycline HCl subcutaneously (SQ) as a fluorescent bone label. Animals were sacrificed 30 days after surgery.

CT Analysis

After sacrifice, animals were scanned using computed tomography (CT) to evaluate the defect sites. Animals were positioned in sternal recumbency on the CT table with hind limbs fully extended to allow for optimal imaging of regions of interest (ROI). Scanning parameters were limited to hind limbs and pelvis of each animal. Files containing sectional scans and 3D renderings of ROI were collected and analyzed by a board-certified radiologist, blinded to the sample groups. Quantitative analysis of the area and density, and qualitative assessment of periosteal reaction, sclerosis, swelling, mineralization, and gap healing of the defect sites were obtained.

Quantitative and qualitative CT data were examined using SPSS statistical software (IBM). Specifically, density and area measurements were assessed utilizing Student's t-test for significance. Periosteal reaction, sclerosis, swelling, mineralization, and gap healing qualitative rankings were evaluated using the Wilcoxon-Mann-Whitney test to determine significance for each characteristic among study groups. Oxytetracycline fluorescence was compared using Student's t-test. For all data, $P<0.05$ was considered significant.

In vivo CT scans were obtained and analyzed to assess mineralization and defect characteristics, 30 days post scaffold treatment. Analysis of cross-sectional and 3D rendered images (**Table 3.1**, **Figure 3.4**) was conducted to produce quantitative and qualitative data for the treated and untreated tibias of each animal. Quantitative data, which included the area of the defect and density of the defect tissue, were compiled and statistically analyzed. In this model of unicortical bone defect of the tibia, the defects healed in both treated and the untreated control bones. Qualitative rankings for periosteal reaction, sclerosis, swelling, mineralization, and gap healing at defect sites were assigned. All qualitative rankings, except sclerosis, were statistically significant between both S-1 and S-2 treated defects and their respective untreated controls, with rankings for periosteal reaction, swelling, and mineralization greater and gap healing lower in the scaffold-treated defects. The enhanced mineralization could be attributed to late-stage bone development for both S-1 and S-2 treated sites. These observations are supported by *in vitro* findings of Chou *et al*. in which biomimetic apatite structures stimulated a significant upregulation of OCN expression at 4 weeks. Increased expression of OCN is closely correlated with ECM mineralization and may be indicative of scaffolds facilitating osteoblastic maturation and osteo-conductive capacities (Chou, 2005). Osteo-conduction, the ability of a scaffold to support bone grows on (on-growth) or through (in-growth) the structure, is a vital characteristic of an effective bone tissue regenerative scaffold. We used a non-critical sized bone defect to compare bone healing with and without the presence of scaffold treatment. The lack of significant difference in area and density measurements between treated and respective controls suggests that scaffolds did not impair tissue repair and confirm that the scaffolds are biocompatible. Despite variation present in qualitative rankings between treated and untreated groups, these patterns were not abnormal and could be expected when a

biomaterial or a scaffold is surgically implanted *in vivo*. Periosteal reaction and swelling of tissue surrounding defect sites are commonly associated with surgical implantation procedures (Shi, 2016; Yang, 2015; Bandyopadhyay, 2013), and, in our study, do not pose concern of infection, as inflammatory agents were not observed upon histological examination, further confirming the biocompatibility of the scaffolds.

Histological Analysis

After CT, tibial sections were harvested and stored in 70% ethanol for histomorphometry (Orthopaedic Histology and Histomorphometry Laboratory, New Haven, CT). Undecalcified sections of 5 μm thickness were obtained for each tibia. Sections from each bone sample were stained with Hematoxylin and Eosin (H&E) and Toluidine Blue O. ImageJ software was used to generate mask overlays of samples for quantitative assessment of H&E stained samples (Egan, Brennan, & Pignolo, 2012; Stepan, 2002). Bone surface area in the defects were first compared between the scaffold-treated with their respective untreated or control groups. Subsequently, the treatments between the S-1 and S-2 scaffold groups were evaluated.

Using both the H&E and Toluidine Blue stains, the orientation of the defect was first established (**Figures 3.5-3.7**). All samples displayed healthy cellular activity and formation of new bone matrix within defect site. Cellular activity throughout the defect indicated that endogenous cell migration was not impeded by scaffold implementation. Small regions of mineralization were detected, yet no indication of inflammation or inflammatory agents were observed. Additionally, the absence of inflammation, giant cell formation, and fibrous encapsulation further supported the biocompatibility of scaffolds. The presence of osteoblasts, osteoclasts and osteocytes within the defect further supported this biocompatibility and indicated that scaffolds were capable of osseo-integration. Osseo-integration, the stable anchorage and melding of a scaffold with native tissue, is an essential characteristic for regenerative bone tissue technologies as permits the ability for restoration of tissue function through direct bone-to-implant contact. Bone surface area measurements from images of H&E stained samples using ImageJ software showed lack of significant difference among treated groups and respective untreated controls, as well as between the two scaffold-treated groups (**Figure 3.8**). This was not surprising and corroborated the CT findings (**Table 3.1**).

In vivo histological and CT observations (**Figures 3.4, 3.6-3.8**) for S-1 and S-2 treated defects also appeared to compliment *in vitro* gene expression profiles. Enhanced new bone formation in the S-1 treated tibias may indicate an increased level of early-stage remodeling evidenced by an increase in OPN expression *in vitro*, further suggests the osteo-conductive characteristics of this construct. The presence of crystalline structures observed in the H&E staining and the increased mineralization rankings in the CT analysis, predominantly associated with soft tissue capping above the defect may represent a combination of remnants of apatite crystals/DBPs (Shi, 2016) and newly mineralized bone in the scaffold

treated samples. This enhanced mineralization could be attributed to late-stage bone development for both S-1 and S-2 treated sites. These observations are supported by *in vitro* findings of Chou *et al*. in which biomimetic apatite structures stimulated a significant upregulation of OCN expression at 4 weeks. Increased expression of OCN is closely correlated with ECM mineralization and may be indicative of scaffolds facilitating osteoblastic maturation (Chou, 2005)**.**

New Bone Analysis

The use of a bone fluorochrome, i.e. a bone label, known as Oxytetracycline was used to evaluate new bone formation. For each tibia sample, total fluorescent area of regions directly above, center, and the innermost area of the defect was measured. Furthermore, three separate slides of each specimen were imaged, and data was quantitated to develop a comprehensive fluorescent analysis. Quantitation of Oxytetracycline fluorescent area in the ROI on unstained histological sections was conducted with ImageJ software through generation of binary masks for images, permitting measurement of fluorescent area relative to total image area. Fluorescent areas expressed as a percentage of the total area of images were averaged and statistical relations among groups were obtained. Fluorescent values for both the S-1 and S-2 treated samples were first compared to their respective untreated control samples, and subsequently to each other.

Oxytetracycline SQ injections given to rats 24 hours prior to sacrifice offer a mechanism for analyzing relative formation of new bone between the treated and untreated tibias at that time point because it binds to the newly deposited calcium (Nkenke, 2002). The antibiotic fluoresces with an emission wavelength of 512 nm when excited by a wavelength of 390 nm. As the fluorescent compound is strictly excluded from bone except during bone formation, areas exhibiting fluorescence can be strongly correlated to regions of new bone activity (Blair et al., 2017). Imaging followed by the quantitation of the oxytetracycline fluorescence, showed that the S-1 treated tibias demonstrated significantly higher fluorescence compared to both the respective untreated group and the S-2 treated samples (**Figures 3.9-3.10**). The lack of significance between the untreated control groups supported the validity of the bone model used in this study.

The significant increase in fluorescent readings for S-1 represent enhanced new bone formation in defects treated with this scaffold as compared to untreated controls and defects treated with S-2. Given that the primary variation in structural design between the nanocomposites resides in the compositional nHA level, the significant increase in new bone formation for S-1 treated defect sites can be attributed to the 10% greater nHA content of basal PU-nHA films as compared to S-2. As nHA has been shown to demonstrate bioactive characteristics, the enhanced incorporation of nHA coupled with the conserved presence of DBPs, which offer macro structures to support cellular interaction, may provide a superior biological environment for recruitment of endogenous cells. The high adsorption capacity of nHA may be a driving factor for cellular migration and activity (Mohsen-Nia, Massah Bidgoli, Behrashi, & Mohsen Nia, 2012); however, this can also lead

to particle agglomeration and formation of chaotic surface structures (Fu et al., 2017), and hence, the concentration of nHA seems to be critical. S-1 appears to demonstrate an optimal balance of compositional nHA, producing an effective and biocompatible environment for bone repair with both osteo-conductive and osseo-integrative capacities.

These results combined with those from previously described *in vitro* and *in vivo* studies suggest that, while scaffolds containing nano- (nHA) and macro-sized (DBPs) components bound with a polymeric matrix (PU) do provide a stable platform for tissue regeneration, cell behavior is significantly different between S-1 and S-2, despite compositional dynamics being similar. We conclude that S-1 demonstrated the most significant findings with regards to early-stage remodeling gene expression (*in vitro*) and new bone formation (*in vivo*). This indicated that, in addition to the biocompatibility exhibited by both scaffold iterations, S-1 also offers modulative effects on exposed cells. CT analysis of S-1 treated defects demonstrated that material did not elicit any abnormal tissue reaction above what would be expected from implantation of a novel biomaterial, and the mineralized regions seem to correspond to the presence of bone particles in scaffold, though it may also be an evidence of late-stage bone development from induced cells.

The success of a 3D bone tissue engineering scaffold is largely dependent on efficient cell seeding, proliferation, viability, distribution and infiltration. *In vitro*, when cells are seeded onto a newly synthesized 3D bone tissue engineering scaffold, we expect the cells to be viable, proliferate, spread uniformly, and undergo osteogenesis, thereby demonstrating the cytocompatability of the scaffold. Fluorescent staining confirmed cell adhesion, clustering and cytocompatibility. Additionally, we were able to evaluate the osteogenic nature of MC3T3-E1 cells by demonstrating the expression of two important and commonly used osteogenic genes, OPN and OCN by real time PCR. The *in vitro* results gave us the confidence to implant the scaffolds *in vivo* and to establish the biocompatibility and the osteoconductive potential of the platform. With this focus, we used a relatively simple biocompatibility rat model utilizing a unicortical defect in the tibia. The significant differences detected between the two scaffolds using the bone fluorochrome, supported confidence of both the model and the study design. Furthermore, DAPI staining of histological sections verified cellular migration into the material, as nuclei were detected throughout scaffold treated defects (**Figure 3.11**). Utilizing this combination of *in vitro* and *in vivo* strategies, we proved our hypothesis and demonstrated that the scaffolds were biocompatible with one scaffold displaying an osteogenic effect. Future experiments will involve testing the scaffold S-1 in segmental defect models where mechanical integrity of newly formed bone can be assessed.

Conclusion

The designed synthetic scaffolds are intended to provide a supportive and modulatory environment for endogenous cells to enhance bone repair. *In vitro* and *in vivo* assessment of scaffolds appeared to confirm that both material iterations, primarily S-1, were biocompatible and displayed key attributes for a bone graft biomaterial. Significant new bone formation in S-1 treated defects demonstrated that this combination of PU with both nano- (nHA) and macro-sized (DBPs) components, was optimal for generating a biocompatible environment that is both osteo-conductive and osseo-integrative. From these findings, the S-1 construct shows great potential as an effective substitute graft material for damaged/injured bone, and warrants continued investigation utilizing models that may more appropriately simulate common injuries observed in human medicine.

An additional *in vivo* assessment utilizing this tibial model was conducted to compare both the S-1 and S-2 iterations with scaffolds constructed using the 70/30 and 60/40 PU-nHA films discussed in the earlier chapter. This was done to confirm that the S-1 scaffold maintained preferable characteristics to these constructs as in the case of their respective films. In an attempt to avoid the degree of spontaneous healing observed in the previous *in vivo* evaluation, the time frame of this study was reduced from 30 to 15 days. Results from this analysis yielded largely similar data with regards to S-1 and S-2 treated groups. Interestingly, defects treated with scaffolds derived from 70/30 and 60/40 films exhibited substantial fluorescence intensities; however, histological assessment revealed large crystalline mineral structures throughout these treated defects (**Figure 3.12**). These regions also appeared to be responsible for the high fluorescence intensity. Based on these findings it was determined that, despite fluorescence intensity values, the scaffolds derived from these films were not suitable for *in vivo* application. As this study verified that the S-1 scaffold maintained preferable characteristics to other iterations, this nanocomposite would be the primary candidate for continued assessment.

To further examine the efficacy of S-1 as a bone graft substitute material as well as its potential for application in the field of craniomaxillofacial surgery, the material was subject to another rodent *in vivo* study. For this assessment a 5mm mandibular defect model was utilized to observe the capacity of the scaffold to integrate with surrounding native tissue and to facilitate tissue development throughout the construct matrix. In place of the void defects used in the previous in vivo tibial defect model, two predicate devices were implemented to permit comparison of the test article to current commercially available products. Additionally, another iteration of the scaffold fabricated with a modified method was tested evaluate if the new fabrication method would enhance or alter the biological functionality of the material. Verification of biocompatibility and osteogenic capacity via this mandibular model would serve to concrete function of the material within a complex system, while also circumventing some of the limitations observed in the unicortical tibial model, primarily defect parameter consistency and

spontaneous defect closure. This work and resulting data are detailed in the following chapter.

References

Agrawal, C. M., & Ray, R. B. (2001). Biodegradable polymeric scaffolds for musculoskeletal tissue engineering. *J Biomed Mater Res, 55*(2), 141-150.

Albrektsson, T., & Johansson, C. (2001). Osteoinduction, osteoconduction and osseointegration. *Eur Spine J, 10 Suppl 2*, S96-101. doi:10.1007/s005860100282

Amit Bandyopadhyay, S. B. (2013). *Charcterization of Biomaterials* (1 ed.): Elsevier.

Blair, H. C., Larrouture, Q. C., Li, Y., Lin, H., Beer-Stoltz, D., Liu, L., . . . Nelson, D. J. (2017). Osteoblast Differentiation and Bone Matrix Formation In Vivo and In Vitro. *Tissue engineering. Part B, Reviews, 23*(3), 268-280. doi:10.1089/ten.TEB.2016.0454

Chang, B., Song, W., Han, T., Yan, J., Li, F., Zhao, L., . . . Zhang, Y. (2016). Influence of pore size of porous titanium fabricated by vacuum diffusion bonding of titanium meshes on cell penetration and bone ingrowth. *Acta Biomater, 33*, 311-321. doi:10.1016/j.actbio.2016.01.022

Chou, Y., Dunn, J. C. Y. and Wu, B. M. (2005). In Vitro Response of MC3T3-E1 Preosteoblasts within ThreeDimensional Apatite-Coated PLGA Scaffolds. *Journal of Biomedical Materials Research Part B: Applied Biomaterials, 75B*(Issue 1), 81–90 doi:10.1002/jbm.b.30261

Christenson, E. M., Anseth, K. S., van den Beucken, J. J., Chan, C. K., Ercan, B., Jansen, J. A., . . . Mikos, A. G. (2007). Nanobiomaterial applications in orthopedics. *J Orthop Res, 25*(1), 11-22. doi:10.1002/jor.20305

Danish, N., Carol-Anne, S., Matthew, J. D., Meek, R. M. D., Sien, L., Gang, L., & Bo, S. (2015). Three-dimensional CaP/gelatin lattice scaffolds with integrated osteoinductive surface topographies for bone tissue engineering. *Biofabrication, 7*(1), 015005. Retrieved from http://stacks.iop.org/1758-5090/7/i=1/a=015005

De Santis, E., Lang, N. P., Ferreira, S., Rangel Garcia Jr, I., Caneva, M., & Botticelli, D. (2017). Healing at implants installed concurrently to maxillary sinus floor elevation with Bio-Oss® or autologous bone grafts. A histo-morphometric study in rabbits. *Clinical Oral Implants Research, 28*(5), 503-511. doi:10.1111/clr.12825

Deng, Z. L., Sharff, K. A., Tang, N., Song, W. X., Luo, J., Luo, X., . . . He, T. C. (2008). Regulation of osteogenic differentiation during skeletal development. *Front Biosci, 13*, 2001-2021.

DeNicolo, P. J., Guyton, M. K., Cuenin, M. F., Hokett, S. D., Sharawy, M., Borke, J., & McPherson, J. C., 3rd. (2015). Histologic Evaluation of Osseous Regeneration Following Combination Therapy With Platelet-Rich Plasma and Bio-Oss in a Rat Calvarial Critical-Size Defect Model. *J Oral Implantol, 41*(5), 543-549. doi:10.1563/aaid-joi-d-12-00075

Egan, K. P., Brennan, T. A., & Pignolo, R. J. (2012). Bone histomorphometry using free and commonly available software. *Histopathology, 61*(6), 1168-1173. doi:10.1111/j.1365-2559.2012.04333.x

Elkhenany, H., Bourdo, S., Hecht, S., Donnell, R., Gerard, D., Abdelwahed, R., . . . Dhar, M. (2017). Graphene nanoparticles as osteoinductive and osteoconductive platform for stem cell and bone regeneration. *Nanomedicine, 13*(7), 2117-2126. doi:10.1016/j.nano.2017.05.009

Fu, C., Bai, H., Zhu, J., Niu, Z., Wang, Y., Li, J., . . . Bai, Y. (2017). Enhanced cell proliferation and osteogenic differentiation in electrospun PLGA/hydroxyapatite nanofibre scaffolds incorporated with graphene oxide. *PLOS ONE, 12*(11), e0188352. doi:10.1371/journal.pone.0188352

Ha, S.-W., Jang, H. L., Nam, K. T., & Beck, G. R. (2015). Nano-hydroxyapatite modulates osteoblast lineage commitment by stimulation of DNA methylation and regulation of gene expression. *Biomaterials, 65*, 32-42. doi:10.1016/j.biomaterials.2015.06.039

Habibovic, P., Yuan, H., van den Doel, M., Sees, T. M., van Blitterswijk, C. A., & de Groot, K. (2006). Relevance of Osteoinductive Biomaterials in Critical-Sized Orthotopic Defect. *Journal of Orthopaedic Research, 24*(5), 867-876. doi:10.1002/jor.20115

He, F., Qian, G., Ren, W., Ke, J., Fan, P., Shi, X., Cheng, Y., Wu, S., Deng, X. and Ye, J. (2017). Preparation and characterization of iron/β-tricalcium phosphate biocermets for load-bearing bone substitutes. *Ceramics International, 43*(11), 8348-8355. doi:10.1016/j.ceramint.2017.03.173

Hing, K. A., Best, S. M., Tanner, K. E., Bonfield, W., & Revell, P. A. (2004). Mediation of bone ingrowth in porous hydroxyapatite bone graft substitutes. *J Biomed Mater Res A, 68*(1), 187-200. doi:10.1002/jbm.a.10050

Huang, J., Best, S. M., Bonfield, W., Brooks, R. A., Rushton, N., Jayasinghe, S. N., & Edirisinghe, M. J. (2004). In vitro assessment of the biological response to nano-sized hydroxyapatite. *Journal of Materials Science: Materials in Medicine, 15*(4), 441-445. doi:10.1023/B:JMSM.0000021117.67205.cf

Jackson, B. K., Bow, A. J., Kannarpady, G., Biris, A. S., Anderson, D. E., Dhar, M., & Bourdo, S. E. (2018). Polyurethane/nano-hydroxyapatite composite films as osteogenic platforms. *J Biomater Sci Polym Ed, 29*(12), 1426-1443. doi:10.1080/09205063.2018.1464264

Juliana Tsz Yan Lee, W. H. T., King Lau Chow. (2011). Simple Modifications to Standard TRIzol® Protocol Allow High-Yield RNA Extraction from Cells on Resorbable Materials. *Journal of Biomaterials and Nanobiotechnology, 2*, 41-48.

Kruyt Moyo, C., Dhert Wouter, J. A., Yuan, H., Wilson Clayton, E., van Blitterswijk Clemens, A., Verbout Abraham, J., & de Bruijn Joost, D. (2006). Bone tissue engineering in a critical size defect compared to ectopic implantations in the goat. *Journal of Orthopaedic Research, 22*(3), 544-551. doi:10.1016/j.orthres.2003.10.010

Kubasiewicz-Ross, P., Hadzik, J., Seeliger, J., Kozak, K., Jurczyszyn, K., Gerber, H., . . . Kunert-Keil, C. (2017). New nano-hydroxyapatite in bone defect regeneration: A histological study in rats. *Ann Anat, 213*, 83-90. doi:10.1016/j.aanat.2017.05.010

Lees, S., & Prostak, K. (1988). The locus of mineral crystallites in bone. *Connect Tissue Res, 18*(1), 41-54.

Liu, X., Zhao, M., Lu, J., Ma, J., Wei, J., & Wei, S. (2012). Cell responses to two kinds of nanohydroxyapatite with different sizes and crystallinities. *Int J Nanomedicine, 7*, 1239-1250. doi:10.2147/IJN.S28098

Mohsen-Nia, M., Massah Bidgoli, M., Behrashi, M., & Mohsen Nia, A. (2012). Human Serum Protein Adsorption onto Synthesis Nano-Hydroxyapatite. *The Protein Journal, 31*(2), 150-157. doi:10.1007/s10930-011-9384-3

Nkenke, E., Kloss, F., Wiltfang, J., Schultze-Mosgau, S., Radespiel-Troger, M., Loos, K. and Neukam, F. W. (2002). Histomorphometric and fluorescence microscopic analysis of bone remodelling after installation of implants using an osteotome technique. *Clinical Oral Implants Research, 13*(6), 595-602. doi:10.1034/j.1600-0501.2002.130604.x

Pujari-Palmer, S., Chen, S., Rubino, S., Weng, H., Xia, W., Engqvist, H., Tang, L. and Ott, M. K. (2016). In vivo and in vitro evaluation of hydroxyapatite nanoparticle morphology on the acute inflammatory response. *Biomaterials, 90*, 1-11. doi:10.1016/j.biomaterials.2016.02.039

Raviraj Havaldar, S. C. P., B. B. Putti. (2012). Effects of Ageing on Bone Mineral Composition and Bone Strength. *IOSR Journal of Dental and Medical Sciences, 1*(3), 12-16.

Roseti, L., Parisi, V., Petretta, M., Cavallo, C., Desando, G., Bartolotti, I., & Grigolo, B. (2017). Scaffolds for Bone Tissue Engineering: State of the art and new perspectives. *Mater Sci Eng C Mater Biol Appl, 78*, 1246-1262. doi:10.1016/j.msec.2017.05.017

Salgado, A. J., Coutinho, O. P., & Reis, R. L. (2004). Bone tissue engineering: state of the art and future trends. *Macromol Biosci, 4*(8), 743-765. doi:10.1002/mabi.200400026

Shi, J., Sun, J., Zhang, W., Liang, H., Shi, Q., Li, X., Chen, Y., Zhuang, Y. and Dai, J. (2016). Demineralized Bone Matrix Scaffolds Modified by CBD-SDF-1α Promote Bone Regeneration via Recruiting Endogenous Stem Cells. *ACS Applied Materials & Interfaces, 8(41)*, 27511–27522. doi:10.1021/acsami.6b08685

Sing, K. S. W. (1985). Reporting physisorption data for gas/solid systems with special reference to the determination of surface area and porosity (Recommendations 1984). In *Pure and Applied Chemistry* (Vol. 57, pp. 603).

Stepan, J. J. (2002). Techniques for measuring bone mineral density. *International Congress Series, 1229*, 63-68. doi:10.1016/s0531-5131(01)00477-0

Torstrick, F. B., Evans, N. T., Stevens, H. Y., Gall, K., & Guldberg, R. E. (2016). Do Surface Porosity and Pore Size Influence Mechanical Properties and Cellular Response to PEEK? *Clin Orthop Relat Res, 474*(11), 2373-2383. doi:10.1007/s11999-016-4833-0

Towler, D. A., & Arnaud, R. S. (2002). Chapter 88 - Use of Cultured Osteoblastic Cells to Identify and Characterize Transcriptional Regulatory Complexes. In J. P. Bilezikian, L. G. Raisz, & G. A. Rodan (Eds.), *Principles of Bone Biology (Second Edition)* (pp. 1503-1527). San Diego: Academic Press.

Unosson, J., Montufar, E. B., Engqvist, H., Ginebra, M. P., & Persson, C. (2016). Brushite foams--the effect of Tween(R) 80 and Pluronic(R) F-127 on foam porosity and mechanical properties. *J Biomed Mater Res B Appl Biomater, 104*(1), 67-77. doi:10.1002/jbm.b.33355

Wang, X., Zhang, G., Qi, F., Cheng, Y., Lu, X., Wang, L., . . . Zhao, B. (2018). Enhanced bone regeneration using an insulin-loaded nano-hydroxyapatite/collagen/PLGA composite scaffold. *Int J Nanomedicine, 13*, 117-127. doi:10.2147/ijn.S150818

Yang, L. (2015). *Nanotechnology-Enhanced Orthopedic Materials*: Woodhead Publishing.

Yerramshetty, J. S., & Akkus, O. (2008). The associations between mineral crystallinity and the mechanical properties of human cortical bone. *Bone, 42*(3), 476-482. doi:10.1016/j.bone.2007.12.001

Yu, J., Xia, H., Teramoto, A., & Ni, Q. Q. (2018). The effect of hydroxyapatite nanoparticles on mechanical behavior and biological performance of porous shape memory polyurethane scaffolds. *J Biomed Mater Res A, 106*(1), 244-254. doi:10.1002/jbm.a.36214

Zhao, R., Xie, P., Zhang, K., Tang, Z., Chen, X., Zhu, X., . . . Zhang, X. (2017). Selective effect of hydroxyapatite nanoparticles on osteoporotic and healthy bone formation correlates with intracellular calcium homeostasis regulation. *Acta Biomaterialia, 59*, 338-350. doi:https://doi.org/10.1016/j.actbio.2017.07.009

Zhu, Y., Zhang, K., Zhao, R., Ye, X., Chen, X., Xiao, Z., . . . Zhang, X. (2017). Bone regeneration with micro/nano hybrid-structured biphasic calcium phosphate bioceramics at segmental bone defect and the induced immunoregulation of MSCs. *Biomaterials, 147*, 133-144. doi:https://doi.org/10.1016/j.biomaterials.2017.09.018

Appendix

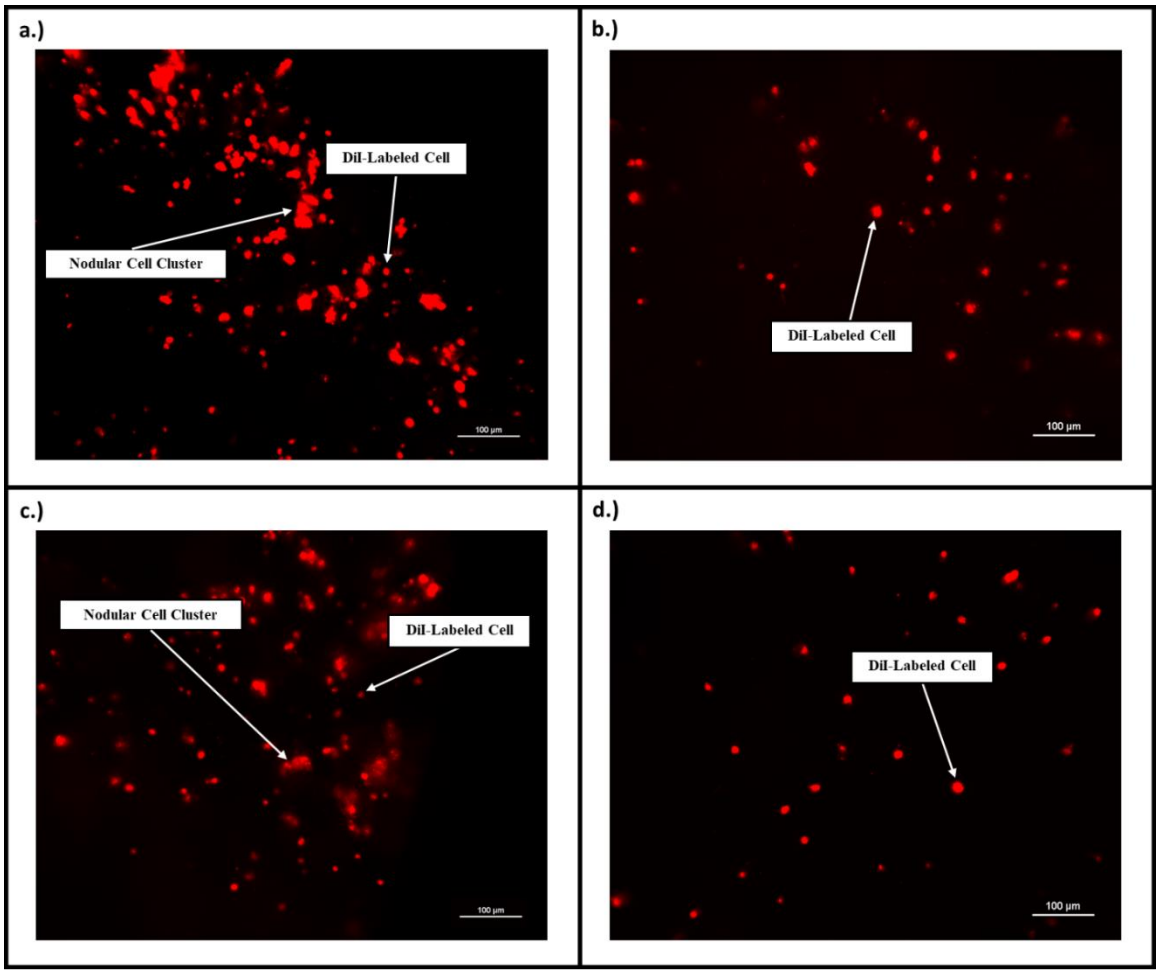

Figure 3.1. Day 7 DiI imaging of MC 3T3-E1 cells on 3D scaffold. Representative images depicting DiI-labeled cells 7 days post-seeding to S-1 cultured in media with and without osteo-differentiation inducing agents (a and b) and to S-2 cultured in media with and without osteo-differentiation inducing agents (c and d).

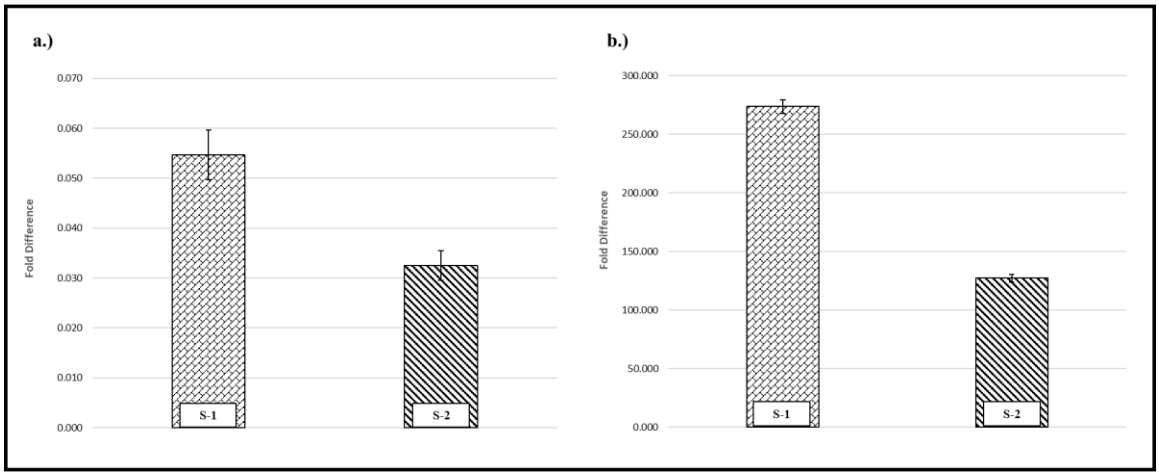

Figure 3.2. Gene expression of S-1 and S-2 treated cells cultures. PCR fold differences for OCN (a) and OPN (b) expression in S-1 and S-2 exposed cell cultures as compared to cultures on polystyrene surfaces in presence of the osteogenic differentiation reagents for 28 days. Gene expression was normalized with GAPDH expression

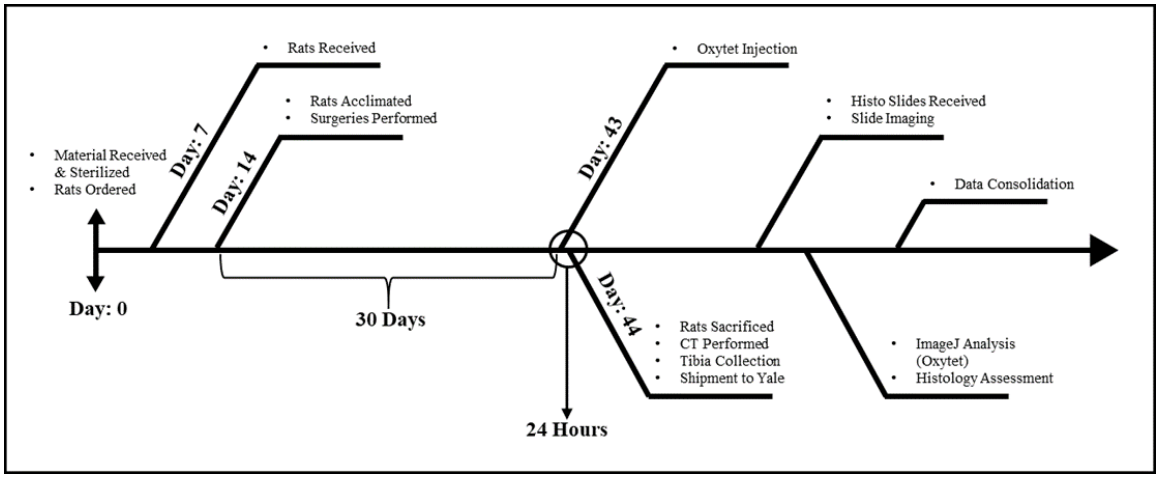

Figure 3.3. *In vivo* model timeline. Major study checkpoints of *in vivo* assessment of scaffold are indicated by branches, and time point objectives are detailed by bulleted lists. The studied sample groups include the S-1 (n=10) and S-2 (n=10) scaffold treated and untreated limbs (n=20).

Table 3.1. CT qualitative and quantitative statistical analysis. Assessment of qualitative CT scoring utilized non-parametric Wilcoxon-Mann-Whitney statistical test (Top). Exact significance values display significant differences among sample groups. Assessment of quantitative CT values for area and density utilized parametric Student's t-test (Bottom). P-values were considered significant if <0.05. The studied sample groups include S-1 treated (n=10), S-1 untreated (n=10), S-2 treated (n=10), and S-2 untreated (n=10).

Wilcoxon-Mann-Whitney	**Periosteal**	**Sclerosis**	**Swelling**	**Mineralization**	**Gap Healing**
S-1 Treated/Untreated (p-value)	0.143	0.165	<0.005	<0.005	0.011
S-2 Treated/Untreated (p-value)	0.052	0.280	0.001	0.001	0.023
S-1/S-2 Treated (p-value)	0.315	0.353	1.000	0.739	0.393

Student's t-test	**Area (mm^2)**	**Density (HU)**
S-1 Treated/Untreated (p-value)	0.481	0.057
S-2 Treated/Untreated (p-value)	0.081	0.321
S-1/S-2 Treated (p-value)	0.168	0.273

6

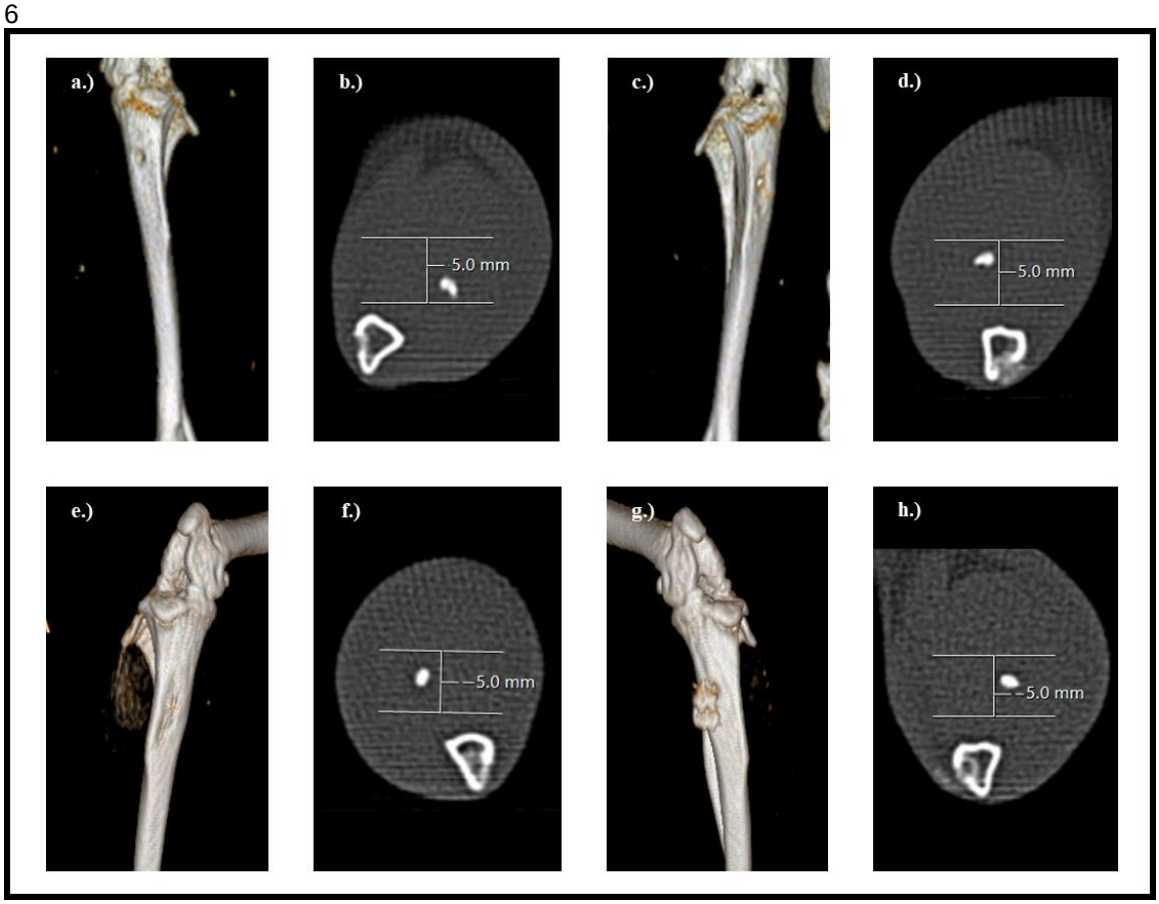

Figure 3.4. S-1 and S-2 untreated/treated defect CT imaging. Representative images depicting CT 3D rendered model for S-1 (a and c) and S-2 (e and g) groups and cross-sectional for S-1 (b and d) and S-2 (f and h) groups. Untreated (a,b,e,f) and treated (c,d,g,h) sample (n=10). The callus formation observed in the S-2 treated limb (g) indicates an increased mineralization due to material exposure.

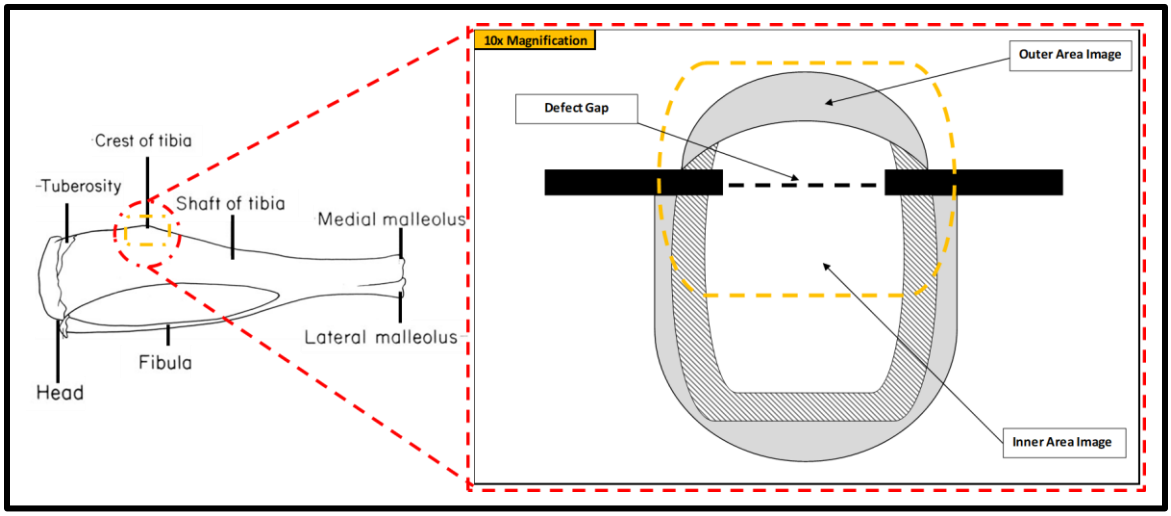

Figure 3.5. Defect orientation for histological imaging.

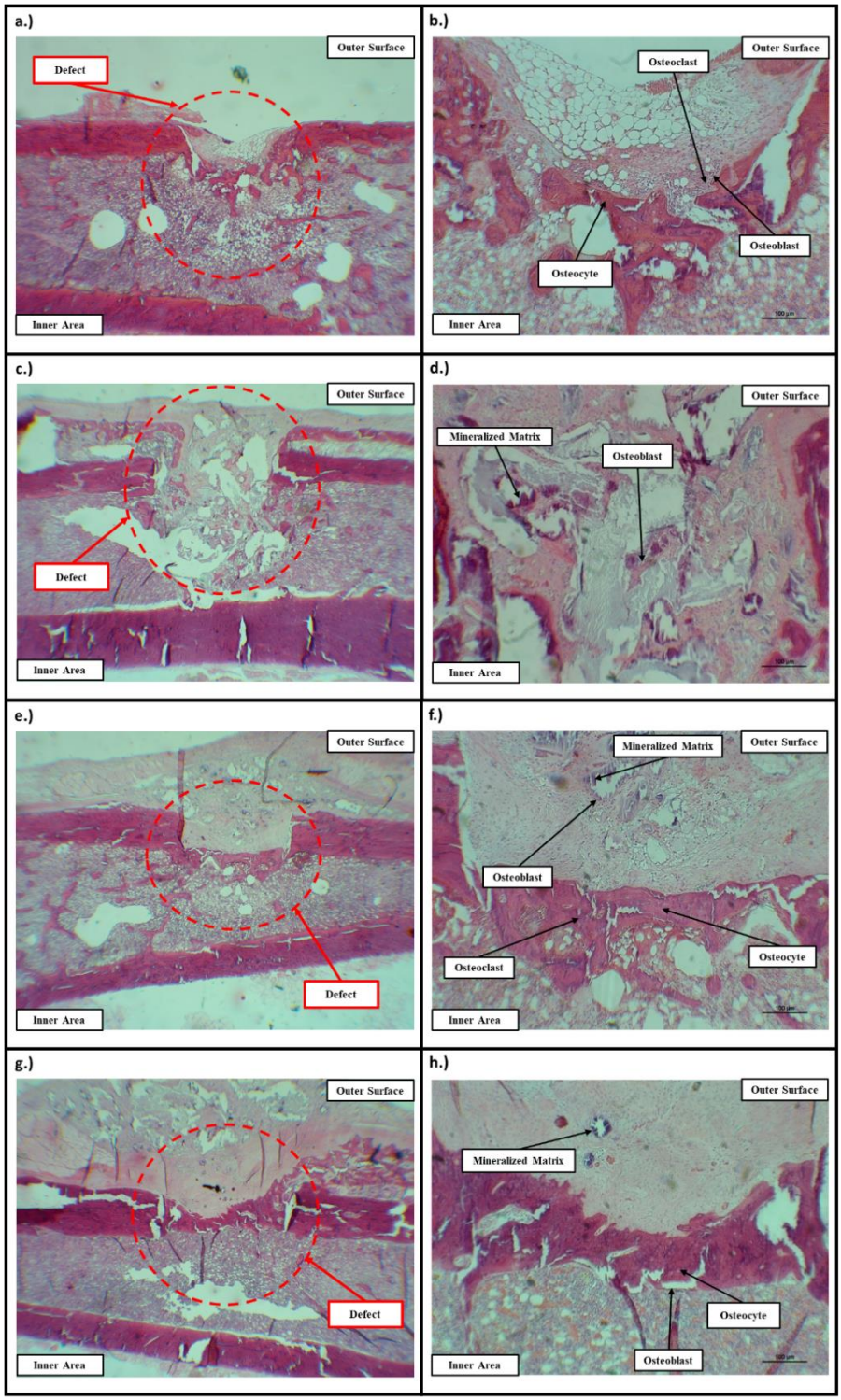

Figure 3.6. H&E imaging of S-1 and S-2 treated and untreated defects. Representative images depicting H&E stained histological sections from S-1 untreated (n=7) and treated (n=7) samples (a-b, e-f) and S-2 untreated (n=6) and treated (n=6) samples (c-d, g-h). Images displaying defect are at 5x (a,c,e,g) and 10x (b,d,f,h) magnifications.

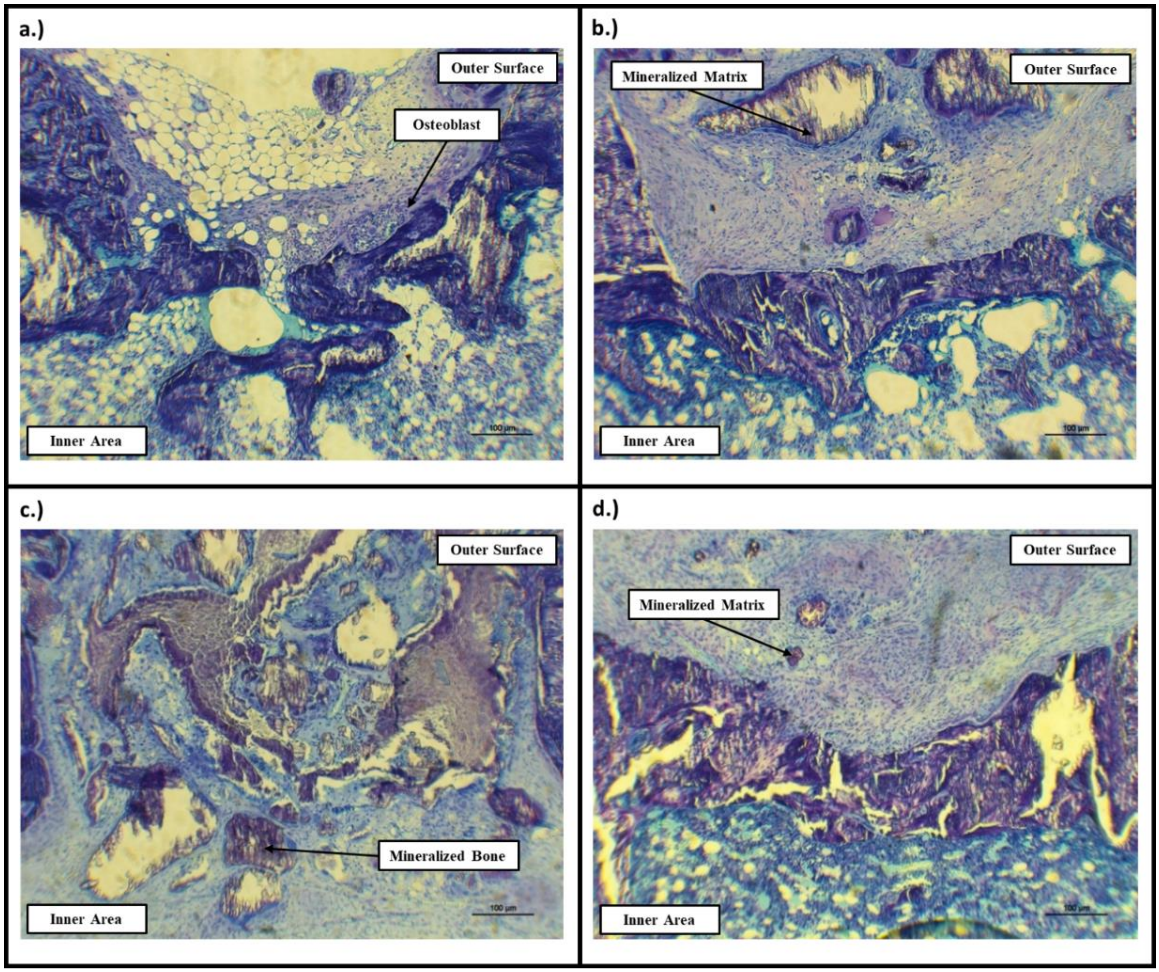

Figure 3.7. Toluidine Blue imaging of S-1 and S-2 treated and untreated defects. Representative images depicting Toluidine Blue O stained histological sections from S-1 untreated (n=7) and treated (n=7) samples (a and b) and S-1 untreated (n=6) and treated (n=6) samples (c and d).

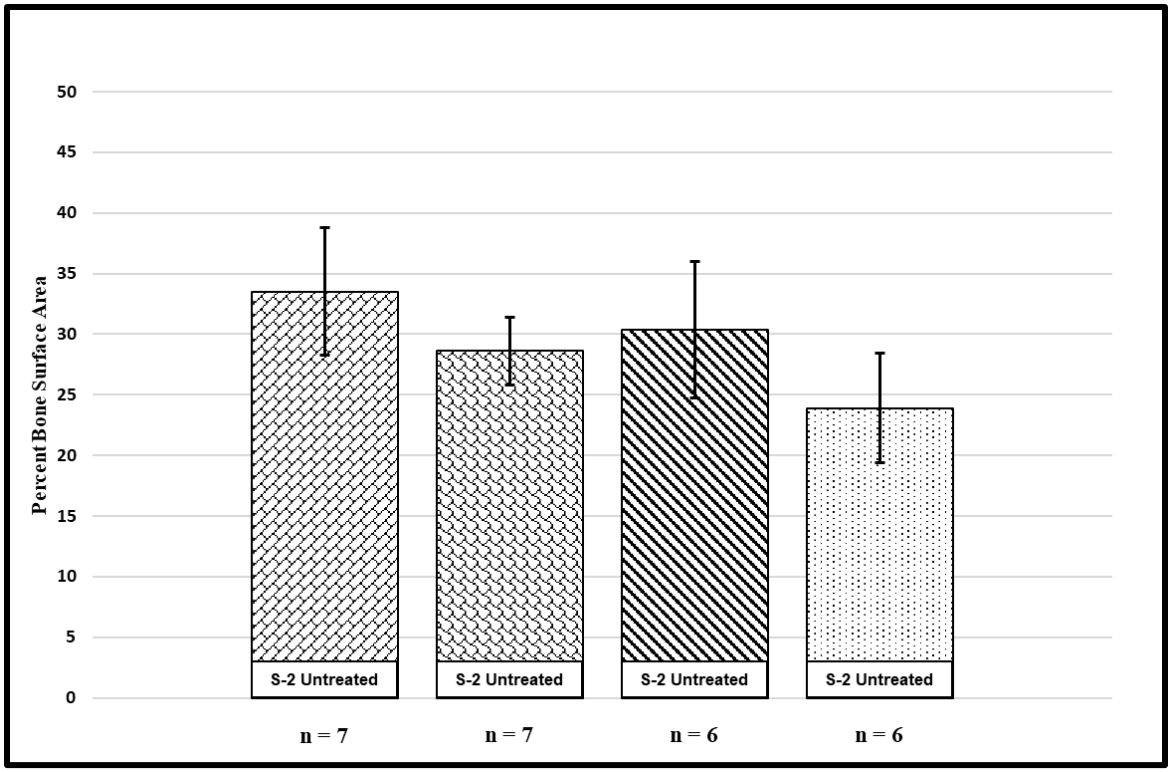

Figure 3.8. H&E-based bone surface area measurements. Percent area coverage data from ImageJ generated binary masks of H&E stained samples.

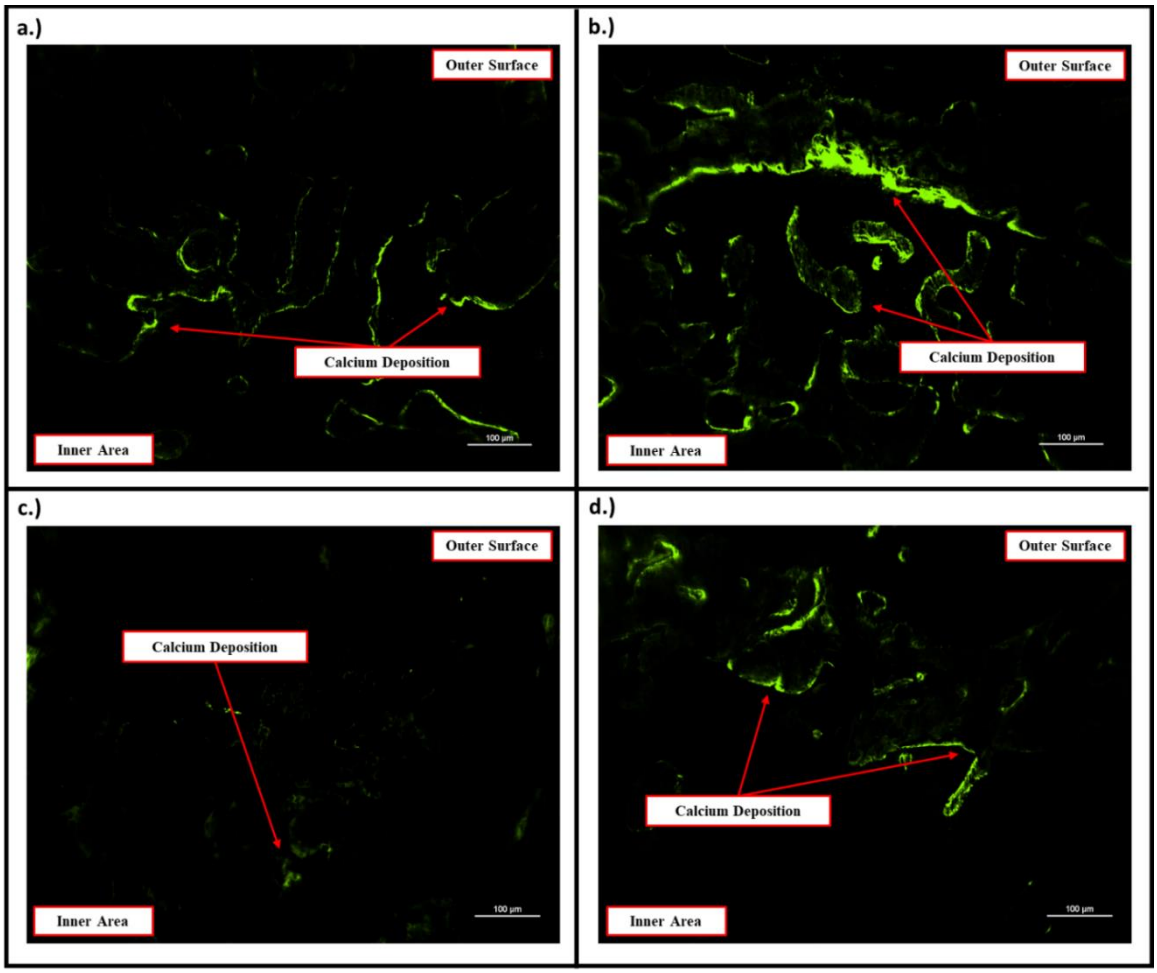

Figure 3.9. Oxytet fluorescence imaging of S-1 and S-2 treated and untreated defects. Representative images depicting Oxytet fluorescence of unstained histological slides for S-1 untreated (n=8) and treated (n=8) samples (a and b), and S-2 untreated (n=9) and treated (n=9) samples (c and d).

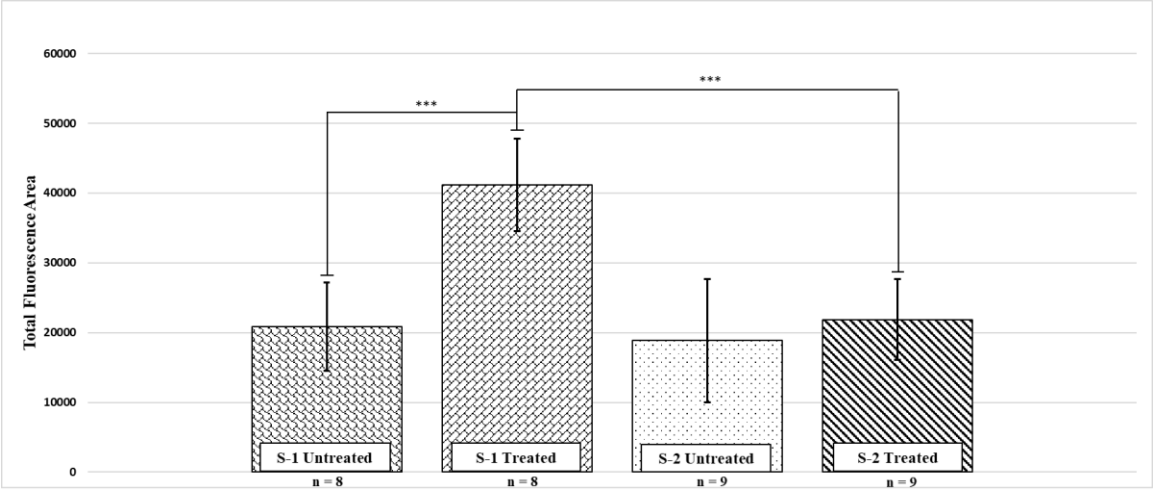

Figure 3.10. Fluorescent area analysis. Oxytet average fluorescent area data comparing treated and untreated groups for S-1 and S-2 constructs. Total fluorescent area derived from averaging of regions of interest directly above, center of, and innermost area of defects. Sample size displayed below respective groups.

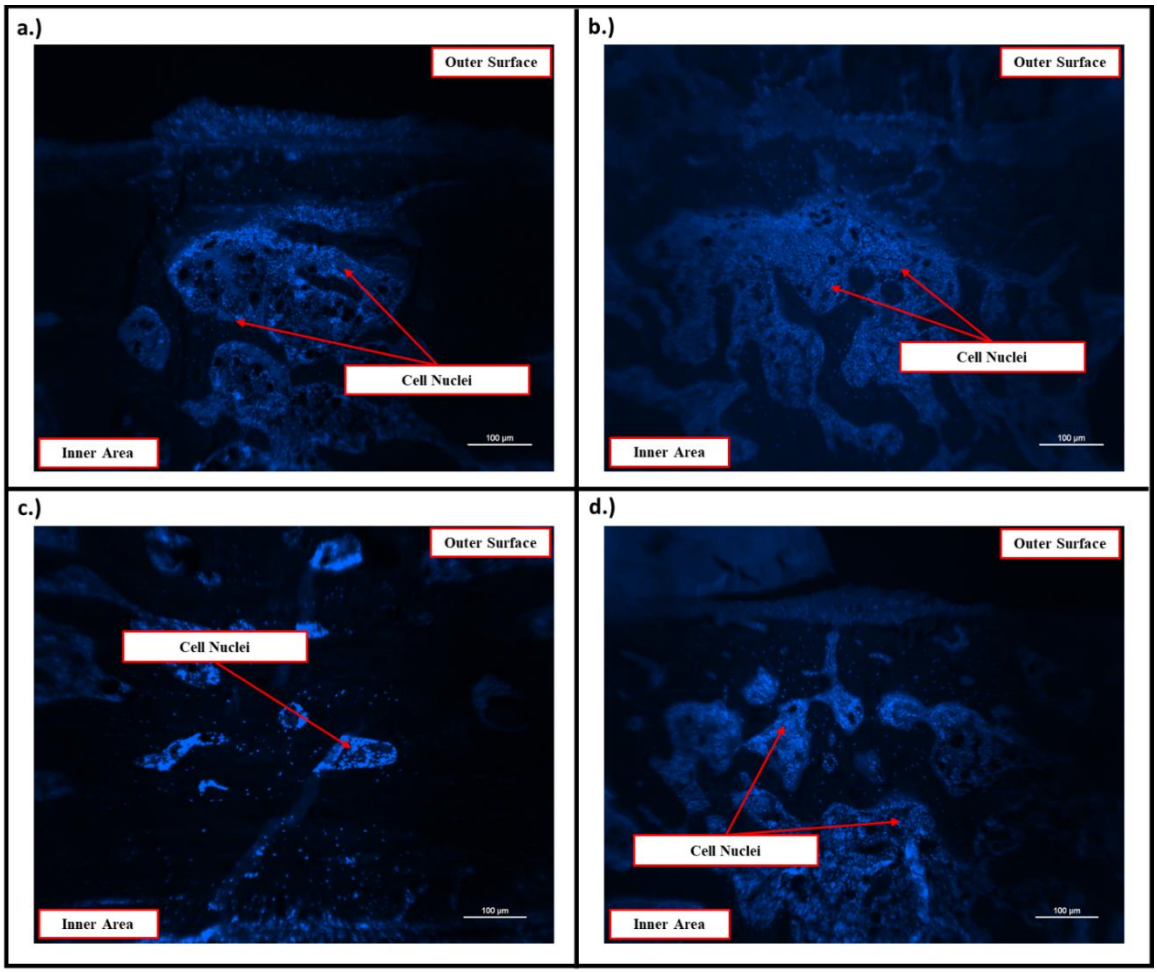

Figure 3.11. DAPI fluorescence imaging of S-1 and S-2 treated and untreated defects. Representative images depicting fluorescence of histological slides stained with DAPI for visualization of cell nuclei within defect. S-1 untreated (n=8) and treated (n=8) samples (a and b) and S-2 untreated (n=9) and treated (n=9) samples (c and d) are shown. DAPI detection within scaffold treated defects indicates cellular migration into material.

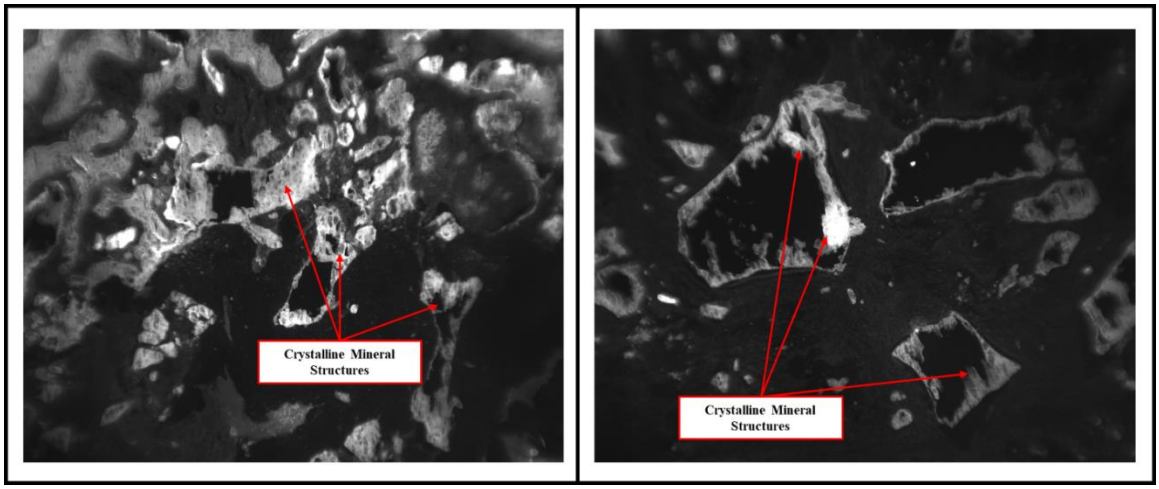

Figure 3.12. Oxytet fluorescence imaging of defects treated with scaffolds derived from 70/30 and 60/40 PU-nHA films. Representative images depicting Oxytet fluorescence of unstained histological slides demonstrate large crystalline mineral structures present in these treated defects. Images have been left as black and white fluorescent camera captures to emphasize crystalline strucutres.

CHAPTER IV:
IN VIVO COMPARISON OF OSTEOBIOLOGIC PLATFORMS WITH PREDICATE DEVICES USING A RAT CRITICALLY-SIZE BONE DEFECT

Abstract

The development of effective bone graft substitute biomaterials has been a critical pursuit in addressing the demand for alternatives to autogenous bone that are both cost effective and readily synthesized. This challenge is further complicated in the treatments associated with oral/maxillofacial injuries due to the complex anatomical nature of flat bone. As a result, a wide assortment of biomaterial designs has been implemented with varying effect characteristics and magnitudes, stemming from differences in physical and chemical properties of the matrix. Therefore, it is essential to develop assessment techniques to objectively compare new osteogenic platforms with existing medical technologies that have well-documented effects. This study examines a previously reported layer-by-layer synthesized nanocomposite, comprised of polyurethane (PU)/nano-hydroxyapatite (nHA) films interspersed with bovine-derived decellularized bone particles, as well as a variation employing a modified synthesis method. Utilizing a 5mm mandibular defect model in rats, these two scaffold iterations were tested *in vivo* for their osseo-integrative capacity and ability to facilitate new bone formation within the defect site as compared to multiple predicate devices. BioOss Collagen® (Geistlich), a xenograft comprised of decellularized bovine bone particles and porcine collagen, and Syntoss® (Dental Solutions Isreal), a synthetic graft comprised of β-tricalcium phosphate (β-TCP) and hydroxyapatite (HA), were used as predicate groups. Rats were randomly divided into 4 treatment groups and the mandibular defects in each group were treated with one of the four composite materials. Rats were sacrificed and subjected to computed tomography (CT) at 30- and 60-days post-treatment. Ultimately, the flat bones were harvested and subjected to histomorphometric analyses. Histological sections were stained with H&E and Masson's trichrome for tissue analysis. Unstained sections were used for immunohistochemical evaluation. Quantitative and qualitative CT data provided by a certified radiologist indicated that the two nanocomposites were not significantly different from the predicate devices. Histological assessment utilizing ImageJ software for the Masson's trichrome stain indicated a significantly enhanced level of collagen and early bone formation in defects treated with the modified synthesis method nanocomposite. Additionally, observational analysis of stained sections appeared to demonstrate effective osseo-integrative capacities of both the nanocomposites. Immunohistochemistry (IHC) of samples furthermore established the presence of the hematopoietic stem cell marker, CD34, within the defect region of specimens treated with the experimental materials. These findings suggest that, though both examined nano-composites display biocompatible and osseo-integrative characteristics comparable to common predicate devices, the iteration utilizing a modified synthesis method may offer an effective and superior design for an osteogenic platform.

Introduction

The development of effective biomaterials for repairing and restoring functionality of bony defects has remained a major area of research within the field of regenerative medicine. This is largely due to the complex and dynamic nature of native bone, which undergoes constant remodeling through osteoblastic and osteoclastic functions. Though the regular restructuring activity of these processes are capable of repairing minor tissue injuries, damage to tissue that exceeds natural repair limitations necessitate application of a grafting material that can facilitate and promote regeneration of the defect (Zhu et al., 2017). However, the inherent hierarchical architecture of native bone complicates design of an optimal bone graft substitute material. Comprised of an intricate matrix of organic and inorganic elements in both nano- and macro-structural configurations, the tissue presents unique challenges to bio-mimicry of the mechanical and biological environment (Thula et al., 2011). The current gold standard for repair of these defects, therefore, remains the use of autologous bone grafts, tissue collected from a donor site of the individual receiving treatment. Despite the highly effective nature of autografts, the requirement of multiple surgery sites and the potential for donor site morbidity pose risks to patients. Therefore, a wide variety of grafts derived from allogenic, xenogeneic, and synthetic origins have been implemented with the goal of achieving similar or superior reparative characteristics (Salgado et al., 2004; Sheikh et al., 2017).

A noted high degree of variability has been observed in the processing methods utilized by different material developers for biologically-based grafts, those from allogenic and xenogeneic origin. This can be observed in the wide array of protocols employed for decellularizing, which is the elimination of organic components to isolate the inorganic/mineral construct, source tissue, resulting in varying degrees of residual organic compounds. This in turn may substantially dictate the ability of a material to integrate within native tissue and promote repair (Saulacic et al., 2015). This inconsistency among these biologically-derived bone graft products has further driven demand for synthetic scaffold designs that utilize simple manufacturing methods and readily available compositional elements. These composites generally attempt to resemble aspects of native bone either in chemical composition, for example similar mineral content, or in physical attributes, such as porosity and tensile/compression dynamics. Some of the most common compositional additives are hydroxyapatite (HA) and beta-tricalcium phosphate (β-TCP), which are both mineral compounds that resemble formations within native bone and maintain osteo-conductive functions (Sohn et al., 2018; Gorla et al., 2015; Ramalingam et al., 2016). Other graft designs have implemented more organic components, such as collagen or osteo-related growth factors, to serve bio-active functions post-implantation (Kim et al., 2015; Sun et al., 2014).

Recently, application of nano-scale particles in combination with marco-scale scaffold architecture has demonstrated promise in generating integrative cellular environments. Particularly, the use of nano-hydroxyapatite (nHA) particles

offer potential as an osteo-inductive component, capable of inducing native progenitor cells toward a bone cell lineage, and serve to promote cell migration and tissue in-growth through rapid adsorption of serum proteins (Mohsen-Nia et al., 2012; Jackson et al., 2018; Bow et al., 2019). Combining such components with other bio-active materials and incorporating these into a polymeric matrix allows for production of biologically effective scaffolds that maintain ideal mechanical properties. A previously examined scaffold that encompasses this scaffold design strategy is comprised of a mix of nHA and decellularized bone particles (DBPs) dispersed within a degradable polyurethane matrix (Bow et al., 2019). The present study intends to further evaluate this composite that is synthesized using a layer-by-layer method, as well as a variant design that employs a salt-leeching technique to form scaffold pores.

Apart from design and development of scaffolds, increased importance is being attributed to the selection of appropriate evaluation techniques. Particularly for in vivo assessment of test articles, the selection of a suitable model is critical and will be largely dependent on the intended application for the graft material, i.e oromaxillofacial or long bone repair (Bigham et al., 2015). Rodent models serve as a well-established means of examining treatment methods with minimal animal to animal variance, allowing for implementation of necessary control groups. A mandibular model described by Higuchi et al. (1999) offers the potential to assess material graft designs in a consistently-sized circular defect in flat bone, which should be indicative of a graft's effectiveness in oromaxillofacial operations. As discussed in Tatara et al. (2016), the current standard treatment for a critically-sized mandibular injury is the use of a free fibular flap, which involves transplanting a segment of the patient's fibular with native vasculature at the defect site. As mentioned previously, such treatments, though effective, result in increased risk to the patient, thereby stimulating development of substitute grafting materials. As defect sizes within this mandibular model exceeding 3mm are considered to be "critically-sized", the implementation of a 5mm dimeter defect will permit assessment of the ability of treatment materials to facilitate repair and restoration of tissue that has been damaged beyond its natural reparative capacity (Kustro et al., 2018). The present study evaluates two test articles with similar compositions as compared with reparative capacity of two currently commercially available and commonly utilized scaffolds, BioOss Collagen® and Syntoss®. The conducted comparative analysis with predicate devices permits an efficient and relevant evaluative technique for development of optimized graft materials.

Examined Graft Materials

Experimental Materials

The previously assessed 3D osteogenic platform designated as S-1 was utilized in this study to further examine its effectiveness in repair of a 5mm mandibular defect as compared to current predicate devices (Bow et al., 2019). Additionally, an iteration of this scaffold design implementing a modified fabrication

method was included in this comparative material assessment. The S-1 scaffold, as described in the previous chapter, utilized a layer-by-layer manufacturing technique, while the modified design, designated M-1, was constructed through a salt-subtraction method. Both S-1 and M-1 are composed primarily of nano-hydroxyapatite (nHA) and decellularized bone particles (Sigma-Graft), with a degradable polyurethane (PU) as a binder.

Predicate Materials

Produced and distributed by Geistlich, BioOss Collagen® is a composite of deproteinized cancellous bone particulate product of bovine origin and 10% porcine collagen fiber. BioOss Collagen® has demonstrated significant enhancement of new bone development when implemented in non-weightbearing bony defects, particularly when incorporated as a supportive element to autologous bone particulate (Aludden et al., 2017; Araujo et al., 2010; Lee et al., 2014).

Syntoss® is a synthetic bone graft substitute comprised of 60% β-TCP and 40% HA that is produced and distributed by Dental Solutions Israel. Similar to characteristics of the previously described synthetic grafting materials, this product maintains strong biocompatibility and osteo-conductivity, largely due to the high mineral content and porous structure. As per product site, Syntoss® grafts are capable of ionic release of Ca and phosphate ions that can stimulate native tissue to enhance osseo-integration.

In Vivo Graft Comparative Analysis

Mandibular Defect Model

Sprague Dawley rats were received and maintained at facilities for 7 days prior to surgeries for acclimation. Pre-surgical analgesic application of buprenorphine was administered, and animals were anesthetized with isoflurane delivered via inhalation for the duration of the surgery. Sterile prep of the surgery site was performed through removal of hair and application of 70% ethanol, chlorohexidine, and betadine solutions respectively. Surgical operations were then carried out. Briefly, a linear incision through epidermal and subcutaneous tissues was made to expose the lower portion of the masseter muscle. A single incision was then made through the masseter muscle using the parotid duct as a guide parameter to expose the mandibular ramus and angle of the mandible. Utilizing a trephine drill bit, a 5mm circular defect was generated on this surface with the ridge of the mandibular ramus as a guide parameter to maintain consistency of defect location. Resulting defect void space was then filled with treatment material cut to appropriate size. Treatment groups consisted of two test materials with similar composition but varied synthesis procedures and two predicate materials, BioOss Collagen® and Syntoss®, acting as controls. Post-implantation, sites were closed through initial suturing of muscle layer and then of subcutaneous tissue. Animals were monitored closely to verify recovery and then

transferred to housing room. Regular monitoring of animals was then carried out for 1 and 2-months post-operation with primary diet of soft gel food for the first 2 weeks before switching to standard dry pellet diet. At 1 and 2-month post-operation time points animals were sacrificed as per protocol and CT scans of region of interest were taken. Treated mandibles were then harvested from specimens for histological sectioning and staining, with tissue stored prior to sectioning in Decal A solution.

CT Analysis

CT scans were performed on animals after sacrificed at 1 and 2-month post-operation time points. 3D renders were generated and collected scans were evaluated by a certified radiologist for both quantitative and qualitative parameters. Measurements for area and density comprised the quantitative element and were coupled with a set of qualitative characteristics developed and employed in a previous study. These parameters include subjective rankings of 0 (negligible) to 3 (severe) for periosteal reaction, sclerosis, swelling, and mineralization, as well as healing with scores ranging from 0 (no closure) to 3 (completely healed).

CT imaging verified that defect generation was successful, and materials persist within the site (**Figure 4.1**). Early tissue formation was observed throughout defect sites treated with both test materials, with possible indication of new bone formation. Quantitative results for area and density were averaged within groups to generate comparative values. Area data for test materials at both time points showed no statistically significant variation from each other. Additionally, test materials did not appear to differ substantially from values of exhibited by predicate materials at respective time points (**Figure 4.2**). Density data did demonstrate significant variation among groups; however, this was expected due to the observed mineral content difference between test and predicate materials. This is illustrated particularly well in the enhanced density measurement of Syntoss® samples, designated S1 and S2 in **Figure 4.2**, which can be correlated to the dense mineral content of the β-TCP/HA matrix.

Histological Analysis

Histological sections were cut from paraffin-embedded decalcified tissue samples at 1-5um thickness. Sets of sections included one slide stained with H&E for general cellular reaction assessment, one slide stained with Masson's Trichrome for evaluation of present tissue types, and 3-5 unstained slides for immunohistochemistry (IHC). Masson's Trichrome stained slides were used to generate semi-quantitative data for new early collagen/bone tissue surface area. Captured images were processed through ImageJ software to create binary masks highlighting tissue of interest, which were subsequently measured as a ratio of highlighted area to total area (Schindelin et al., 2012).

Gross evaluation of H&E stained sections showed an absence of inflammatory signs indicating that all materials were biocompatible. Preliminary Masson's Trichrome imaging resulted in observational differences in tissue content

within the defect (**Figures 4.3-4.6**), and therefore necessitated further assessment via ImageJ software. Semi-quantitative data for early collagen/bone formation surface area demonstrated that test materials exhibited significant increase in surface area from 1-month to 2-month time points. Additionally, one test material, designated as M-1 in **Figure 4.7**, was found have significantly enhanced surface area as compared to all other material types by the 2-month time point.

Immunohistochemistry Analysis

Unstained histological sections of test article samples were subjected to deparaffinization using xylenes and prepped for immune-staining to determine presence and intensity of specific proteins related to angiogenesis, cell attachment, and bone formation. Prepped samples received primary antibodies for the marker of interest, which were then subjected to a biotinylated secondary antibody. A tertiary staining solution conjugated with an avidin-horseradish peroxidase (HRP) molecule capable of strong binding with biotin was utilized to permit detection through a Nova Red staining kit. For contrasting target protein stain during high magnification imaging, hematoxylin staining was implemented, which presents as a blue stain localized to the cell nuclei. An overview of this IHC protocol can be observed in **Figure 4.8**.

Preliminary imaging of IHC stained sections showed promise in detecting specific markers within sample tissue. M-1 and S-1 treated 2-month sections stained for cell attachment and osteo-related markers, including osteopontin (OPN), Sp7, CD34, and fibronectin (FN), demonstrated positive detection and were compared observationally for distribution and organization of protein expression (**Figures 4.9-4.12**).

Conclusion

Examination of H&E stained slides demonstrated that the test articles and the comparative predicate devices were biocompatible with the surrounding native tissue. This was consistent with previously published data evaluating the Scaf-B, which utilized the layer-by-layer synthesis method, and with expectation for the Scaf-K experimental article based on the similar composition. As the two implemented predicate devices are commercially available products for use in oromaxillofacial surgery, and therefore were not anticipated to induce any biocompatibility complications. At 1-month post-implantation, samples for all treatment groups did not display significant differences for area or early collagen/bone formation values indicating that the materials maintained similar reparative characteristics at this time point. However, as evident in stained sections, both H&E and Masson's Trichrome, of the Syntoss® treated defects, there was a notable reduction in the level of tissue in-growth to the injury site as compared with other treatment groups. This reduced tissue in-growth is pronounced in 2-month samples as compared with other treatments and resulted in a significantly lower surface area coverage by early collagen/bone tissue, as

observed in **Figure 4.7**. Apart from Syntoss®, all treatment groups appeared to demonstrate similar tissue in-growth through gross histologic observation and no statistical differences were detected within the 2-month time point samples. Substantial variation among groups in density analysis of CT data was determined to more closely correlate with the initial material mineral content, which is exemplified by the Syntoss® material at both time points, as opposed to new bone formation. The comparable regenerative capacity between experimental materials and BOC, as observed in quantitative and observation data, gives strong indication that the test articles are capable of generating an effective osteogenic environment.

To further assess this, IHC of bio-markers targeting osteogenic, cell attachment, and angiogenic elements was employed. As the primary purpose of this assessment was to observe the presence, distribution, and organization of these select proteins in defects treated with the test articles, focus was place on examining 2-month samples treated with these scaffolds only. Prominent detection of the osteo-related transcription factor, Sp7 (Osterix), and the early bone formation marker, OPN, strongly supported the ability of the test articles to facilitate both osteo-conductive and osteo-inductive functions (Kague et al., 2016). Sp7 is one of the primary regulating factors for osteogenic differentiation of cells along with the RUNX2 and stimulates the upregulation of key osteo-associated proteins including bone sialoprotein (BSP), osteocalcin (OCN), osteonectin (ON), and OPN (Rahman et al., 2015; Pinero et al., 1995). Detection of this transcription factor in defects treated with both test articles therefore illustrates the osteobiologic capacity of the scaffold technologies. However, while this protein was observed through-out the defects, it appeared more concentrated in tissue immediately surrounding structures determined to be remaining DBPs, which indicates that these sites may possess strong osteo-inductive properties. OPN, which is key cell attachment protein in bone and synthesized by preosteoblasts, osteoblasts, and osteocytes, demonstrated prolific presence within and surrounding the defect region, with distribution forming concentric rings that appeared to emanate from the center of the defect (Butler, 1989). These well-defined fronts are characteristic of OPN, which is concentrated at cement lines, and represent potential bone formation fronts, as it operates as a critical matrix organization protein in concert with OCN (Singh et al., 2018; Blair et al., 2017; Foster et al., 2018). Regions stained for OPN resemble those stained for FN in pattern and organization, demonstrating that both proteins play crucial roles in coordinating cell attachment and matrix organization throughout the defect (Brown et al., 1992). FN has been shown to have a major role in the formation and organization of extracellular matrix and cell to cell communication networks, particularly within craniomaxillofacial tissue repair (Al-Qattan et al., 2014; Kim et al., 2015), so the strong intensity of protein in stained samples indicates cellular communication both within the scaffold treated defect and at the scaffold-native bone interface, which further supports the osteo-integrative capacity of the nanocomposites. In addition to these osteogenic and cell attachment proteins, prominent detection was observed for the

transmembrane protein CD34, which is associated with hematopoietic stem cells, enhanced progenitor activity, and early vasculature development (Sidney et al., 2014). Furthermore, cells positive for this surface protein are capable of facilitating environments that promote both angiogenesis and osteogenesis, as they maintain the potential to differentiate to both endothelial and osteoblastic cells (Kuroda et al., 2014). Therefore, the expression of CD34 throughout defects treated with both scaffold iterations demonstrate healthy reparative function. As in the case of Sp7 stained samples, CD34 appears to be most prolific surrounding residual DBPs within the scaffold matrix, which further indicates that these particles may serve as stimulatory surfaces for osteogenic differentiation and new tissue development. Notably, the expression of both Sp7 and CD34 appear to be more organized and pronounced in the samples treated with the modified fabrication method scaffold, which may be due to a more uniform distribution of construct contents.

The detection of these crucial proteins throughout scaffold treated defects, in addition to the enhanced levels of early collagen/bone formation in M-1 treated defects as determined by evaluation of Masson's trichrome stained samples, indicates that this scaffold material utilizing the modified fabrication method is capable of providing an effective osteogenic platform. As such the mechanisms responsible for the observed osteogenic capacity of the bone graft material were of great interest and will be explored in a later chapter. The effective nature of this osteobiologic scaffold encouraged the development of relatively advanced graft materials for more specialized applications that utilized similar compositional elements. These materials included an injectable gelling material with nHA incorporated and a super-hydratable variant of the M-1 scaffold capable of substantial swelling when wetted. Similar assessment methods were used as in the mandibular defect model to assess early collagen/bone formation surfaces and determined the presence of key proteins associated with osteogenic and cell attachment functions. As the primary purpose of these studies was to evaluate the biocompatibility of these advanced materials, the previously described rodent unicortical defect model was used. Additionally, this model was necessary as compared to the mandibular model due to the nature of the injectable material, which would be challenging to maintain at the defect site. The super-hydratable scaffold, being comprised of similar materials to S-1 and M-1 iterations, was anticipated to be cytocompatible and therefore was only subjected to a brief DiI staining assessment in vitro verify similar morphological characteristics to previously examined scaffolds. However, further in vitro work was required for the injectable material as the basal components varied from previously assessed grafts. The in vitro, and subsequent in vivo, evaluation of these advanced materials is encompassed in the following chapter.

References

Al-Qattan, M. M., AlShomer, F., Alqahtani, A., & Alhadlg, A. (2014). Fibronectin and craniofacial surgery. *Ann Plast Surg, 73*(6), 716-720. doi:10.1097/SAP.0b013e3182858812

Aludden, H. C., Mordenfeld, A., Hallman, M., Dahlin, C., & Jensen, T. (2017). Lateral ridge augmentation with Bio-Oss alone or Bio-Oss mixed with particulate autogenous bone graft: a systematic review. *Int J Oral Maxillofac Surg, 46*(8), 1030-1038. doi:10.1016/j.ijom.2017.03.008

Araújo, M. G., Liljenberg, B., & Lindhe, J. (2010). Dynamics of Bio-Oss® Collagen incorporation in fresh extraction wounds: an experimental study in the dog. *Clinical Oral Implants Research, 21*(1), 55-64. doi:10.1111/j.1600-0501.2009.01854.x

Bigham-Sadegh, A., & Oryan, A. (2015). Selection of animal models for pre-clinical strategies in evaluating the fracture healing, bone graft substitutes and bone tissue regeneration and engineering. *Connect Tissue Res, 56*(3), 175-194. doi:10.3109/03008207.2015.1027341

Blair, H. C., Larrouture, Q. C., Li, Y., Lin, H., Beer-Stoltz, D., Liu, L., . . . Nelson, D. J. (2017). Osteoblast Differentiation and Bone Matrix Formation In Vivo and In Vitro. *Tissue engineering. Part B, Reviews, 23*(3), 268-280. doi:10.1089/ten.TEB.2016.0454

Bow, A., Newby, S., Rifkin, R., Jackson, B. K., Matavosian, A., Griffin, C., . . . Dhar, M. (2019). Evaluation of a Polyurethane Platform for Delivery of Nanohydroxyapatite and Decellularized Bone Particles in a Porous Three-Dimensional Scaffold. *ACS Applied Bio Materials, 2*(5), 1815-1829. doi:10.1021/acsabm.8b00670

Brown, L. F., Berse, B., Van de Water, L., Papadopoulos-Sergiou, A., Perruzzi, C. A., Manseau, E. J., . . . Senger, D. R. (1992). Expression and distribution of osteopontin in human tissues: widespread association with luminal epithelial surfaces. *Mol Biol Cell, 3*(10), 1169-1180. doi:10.1091/mbc.3.10.1169

Butler, W. T. (1989). The nature and significance of osteopontin. *Connect Tissue Res, 23*(2-3), 123-136.

Foster, B. L., Ao, M., Salmon, C. R., Chavez, M. B., Kolli, T. N., Tran, A. B., . . . Somerman, M. J. (2018). Osteopontin regulates dentin and alveolar bone

development and mineralization. *Bone, 107*, 196-207. doi:10.1016/j.bone.2017.12.004

Gorla, L. F., Spin-Neto, R., Boos, F. B., Pereira Rdos, S., Garcia-Junior, I. R., & Hochuli-Vieira, E. (2015). Use of autogenous bone and beta-tricalcium phosphate in maxillary sinus lifting: a prospective, randomized, volumetric computed tomography study. *Int J Oral Maxillofac Surg, 44*(12), 1486-1491. doi:10.1016/j.ijom.2015.07.003

Higuchi, T., Kinoshita, A., Takahashi, K., Oda, S., & Ishikawa, I. (1999). Bone regeneration by recombinant human bone morphogenetic protein-2 in rat mandibular defects. An experimental model of defect filling. *J Periodontol, 70*(9), 1026-1031. doi:10.1902/jop.1999.70.9.1026

Jackson, B. K., Bow, A. J., Kannarpady, G., Biris, A. S., Anderson, D. E., Dhar, M., & Bourdo, S. E. (2018). Polyurethane/nano-hydroxyapatite composite films as osteogenic platforms. *J Biomater Sci Polym Ed, 29*(12), 1426-1443. doi:10.1080/09205063.2018.1464264

Kague, E., Roy, P., Asselin, G., Hu, G., Simonet, J., Stanley, A., . . . Fisher, S. (2016). Osterix/Sp7 limits cranial bone initiation sites and is required for formation of sutures. *Developmental biology, 413*(2), 160-172. doi:10.1016/j.ydbio.2016.03.011

Kim, S. G., Lee, D. S., Lee, S., & Jang, J. H. (2015). Osteocalcin/fibronectin-functionalized collagen matrices for bone tissue engineering. *J Biomed Mater Res A, 103*(6), 2133-2140. doi:10.1002/jbm.a.35351

Kuroda, R., Matsumoto, T., Kawakami, Y., Fukui, T., Mifune, Y., & Kurosaka, M. (2014). Clinical impact of circulating CD34-positive cells on bone regeneration and healing. *Tissue engineering. Part B, Reviews, 20*(3), 190-199. doi:10.1089/ten.TEB.2013.0511

Kustro, T., Kiss, T., Chernohorskyi, D., Chepurnyi, Y., Helyes, Z., & Kopchak, A. (2018). Quantification of the mandibular defect healing by micro-CT morphometric analysis in rats. *J Craniomaxillofac Surg, 46*(12), 2203-2213. doi:10.1016/j.jcms.2018.09.022

Lee, D. S. H., Pai, Y., & Chang, S. (2014). Physicochemical characterization of InterOss® and Bio-Oss® anorganic bovine bone grafting material for oral surgery – A comparative study. *Materials Chemistry and Physics, 146*(1), 99-104. doi:https://doi.org/10.1016/j.matchemphys.2014.03.004

Mohsen-Nia, M., Massah Bidgoli, M., Behrashi, M., & Mohsen Nia, A. (2012). Human Serum Protein Adsorption onto Synthesis Nano-Hydroxyapatite. *The Protein Journal, 31*(2), 150-157. doi:10.1007/s10930-011-9384-3

Pinero, G. J., Farach-Carson, M. C., Devoll, R. E., Aubin, J. E., Brunn, J. C., & Butler, W. T. (1995). Bone matrix proteins in osteogenesis and remodelling in the neonatal rat mandible as studied by immunolocalization of osteopontin, bone sialoprotein, alpha 2HS-glycoprotein and alkaline phosphatase. *Arch Oral Biol, 40*(2), 145-155.

Rahman, M. S., Akhtar, N., Jamil, H. M., Banik, R. S., & Asaduzzaman, S. M. (2015). TGF-β/BMP signaling and other molecular events: regulation of osteoblastogenesis and bone formation. *Bone Research, 3*, 15005. doi:10.1038/boneres.2015.5

Ramalingam, S., Al-Rasheed, A., ArRejaie, A., Nooh, N., Al-Kindi, M., & Al-Hezaimi, K. (2016). Guided bone regeneration in standardized calvarial defects using beta-tricalcium phosphate and collagen membrane: a real-time in vivo micro-computed tomographic experiment in rats. *Odontology, 104*(2), 199-210. doi:10.1007/s10266-015-0211-8

Salgado, A. J., Coutinho, O. P., & Reis, R. L. (2004). Bone tissue engineering: state of the art and future trends. *Macromol Biosci, 4*(8), 743-765. doi:10.1002/mabi.200400026

Saulacic, N., Bosshardt, D. D., Jensen, S. S., Miron, R. J., Gruber, R., & Buser, D. (2015). Impact of bone graft harvesting techniques on bone formation and graft resorption: a histomorphometric study in the mandibles of minipigs. *Clin Oral Implants Res, 26*(4), 383-391. doi:10.1111/clr.12357

Schindelin, J., Arganda-Carreras, I., Frise, E., Kaynig, V., Longair, M., Pietzsch, T., . . . Cardona, A. (2012). Fiji: an open-source platform for biological-image analysis. *Nature Methods, 9*, 676. doi:10.1038/nmeth.2019. https://www.nature.com/articles/nmeth.2019#supplementary-information

Sheikh, Z., Hamdan, N., Ikeda, Y., Grynpas, M., Ganss, B., & Glogauer, M. (2017). Natural graft tissues and synthetic biomaterials for periodontal and alveolar bone reconstructive applications: a review. *Biomater Res, 21*, 9. doi:10.1186/s40824-017-0095-5

Sidney, L. E., Branch, M. J., Dunphy, S. E., Dua, H. S., & Hopkinson, A. (2014). Concise review: evidence for CD34 as a common marker for diverse progenitors. *Stem Cells, 32*(6), 1380-1389. doi:10.1002/stem.1661

Singh, A., Gill, G., Kaur, H., Amhmed, M., & Jakhu, H. (2018). Role of osteopontin in bone remodeling and orthodontic tooth movement: a review. *Progress in orthodontics, 19*(1), 18-18. doi:10.1186/s40510-018-0216-2

Sohn, D. S., & Moon, Y. S. (2018). Histomorphometric study of rabbit's maxillary sinus augmentation with various graft materials. *Anat Cell Biol, 51*(Suppl 1), S1-s12. doi:10.5115/acb.2018.51.S1.S1

Sun, Y. X., Sun, C. L., Tian, Y., Xu, W. X., Zhou, C. L., Xi, C. Y., . . . Wang, X. T. (2014). A comparison of osteocyte bioactivity in fine particulate bone powder grafts vs larger bone grafts in a rat bone repair model. *Acta Histochem, 116*(6), 1015-1021. doi:10.1016/j.acthis.2014.04.004

Tatara, A. M., Shah, S. R., Demian, N., Ho, T., Shum, J., van den Beucken, J., . . . Mikos, A. G. (2016). Reconstruction of large mandibular defects using autologous tissues generated from in vivo bioreactors. *Acta Biomater, 45*, 72-84. doi:10.1016/j.actbio.2016.09.013

Thula, T. T., Rodriguez, D. E., Lee, M. H., Pendi, L., Podschun, J., & Gower, L. B. (2011). In vitro mineralization of dense collagen substrates: a biomimetic approach toward the development of bone-graft materials. *Acta Biomater, 7*(8), 3158-3169. doi:10.1016/j.actbio.2011.04.014

Wittenburg, G., Volkel, C., Mai, R., & Lauer, G. (2009). Immunohistochemical comparison of differentiation markers on paraffin and plastic embedded human bone samples. *J Physiol Pharmacol, 60 Suppl 8*, 43-49.

Zhu, Y., Zhang, K., Zhao, R., Ye, X., Chen, X., Xiao, Z., . . . Zhang, X. (2017). Bone regeneration with micro/nano hybrid-structured biphasic calcium phosphate bioceramics at segmental bone defect and the induced immunoregulation of MSCs. *Biomaterials, 147*, 133-144. doi:https://doi.org/10.1016/j.biomaterials.2017.09.018

Appendix

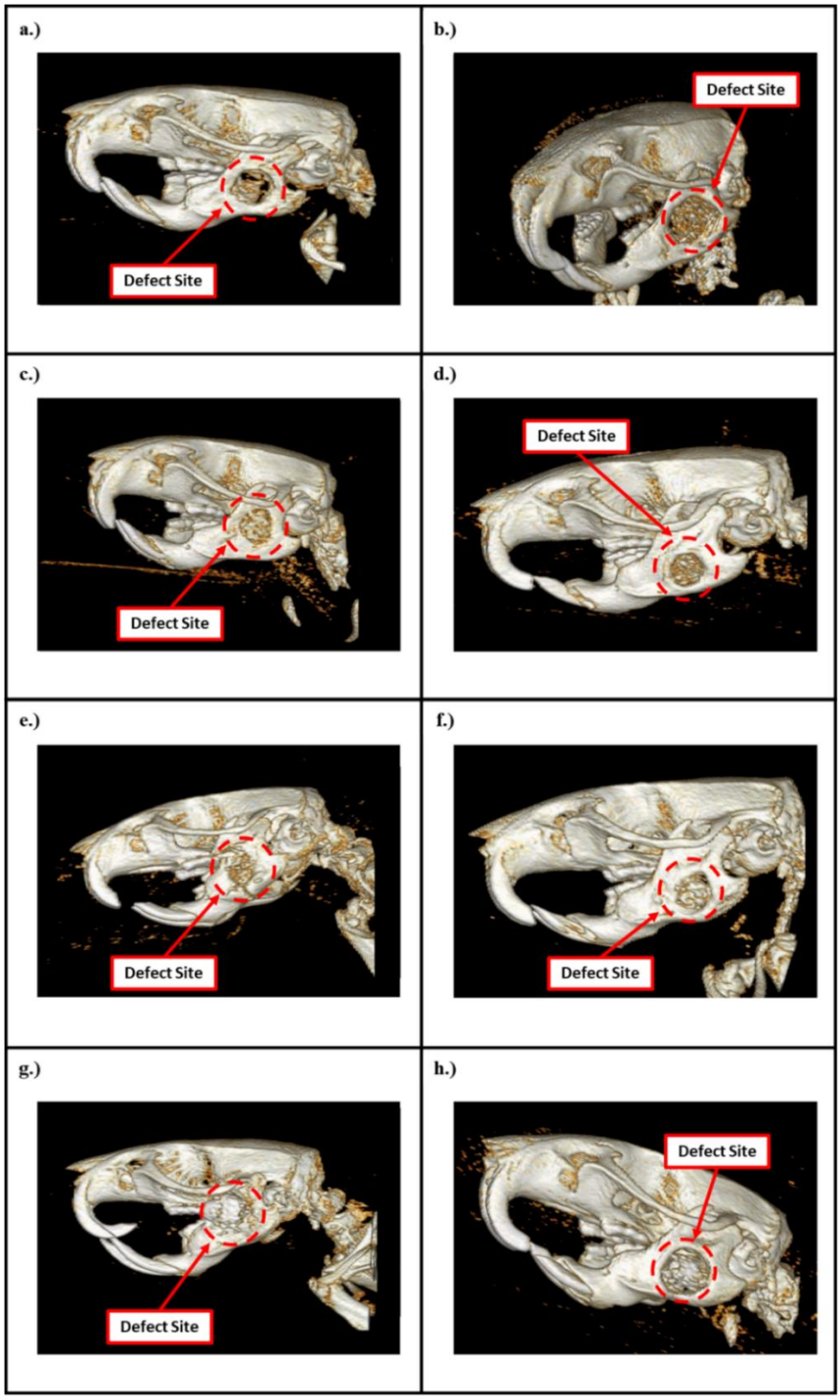

Figure 4.1. Mandibular defect model CT 3D renders. Test articles designated M-1 (a & b) and S-1 (c & d) at as compared with predicate materials, BioOss Collagen® (e & f) and Syntoss® (g & h) at 1-month and 2-month time points respectively.

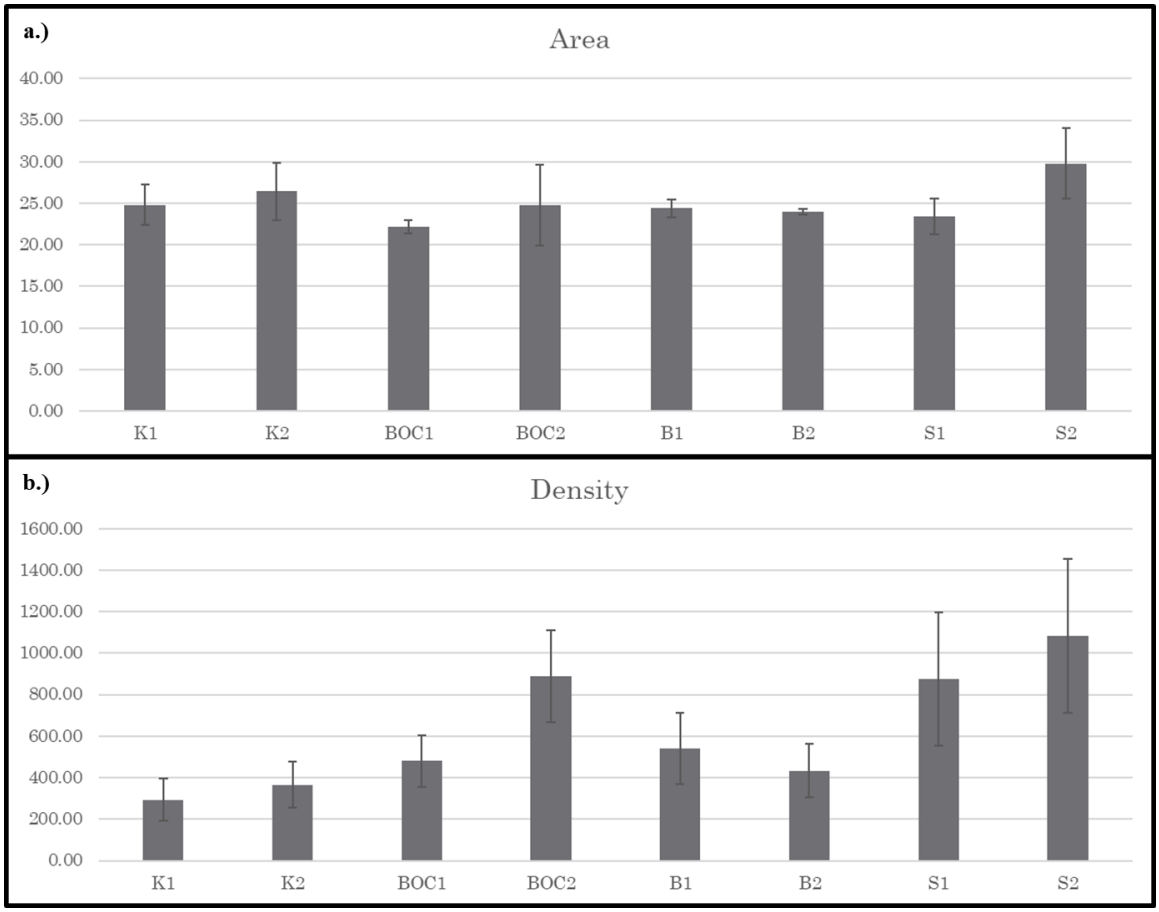

Figure 4.2. Graphical representation of mandibular CT area (a) and density (b) data. Test articles, M-1 (K) and S-1 (B), and predicate materials, BioOss Collagen® (BOC) and Syntoss® (S), are shown. Numerical designation following letter code indicates study time point, either 1-month (1) or 2-month (2).

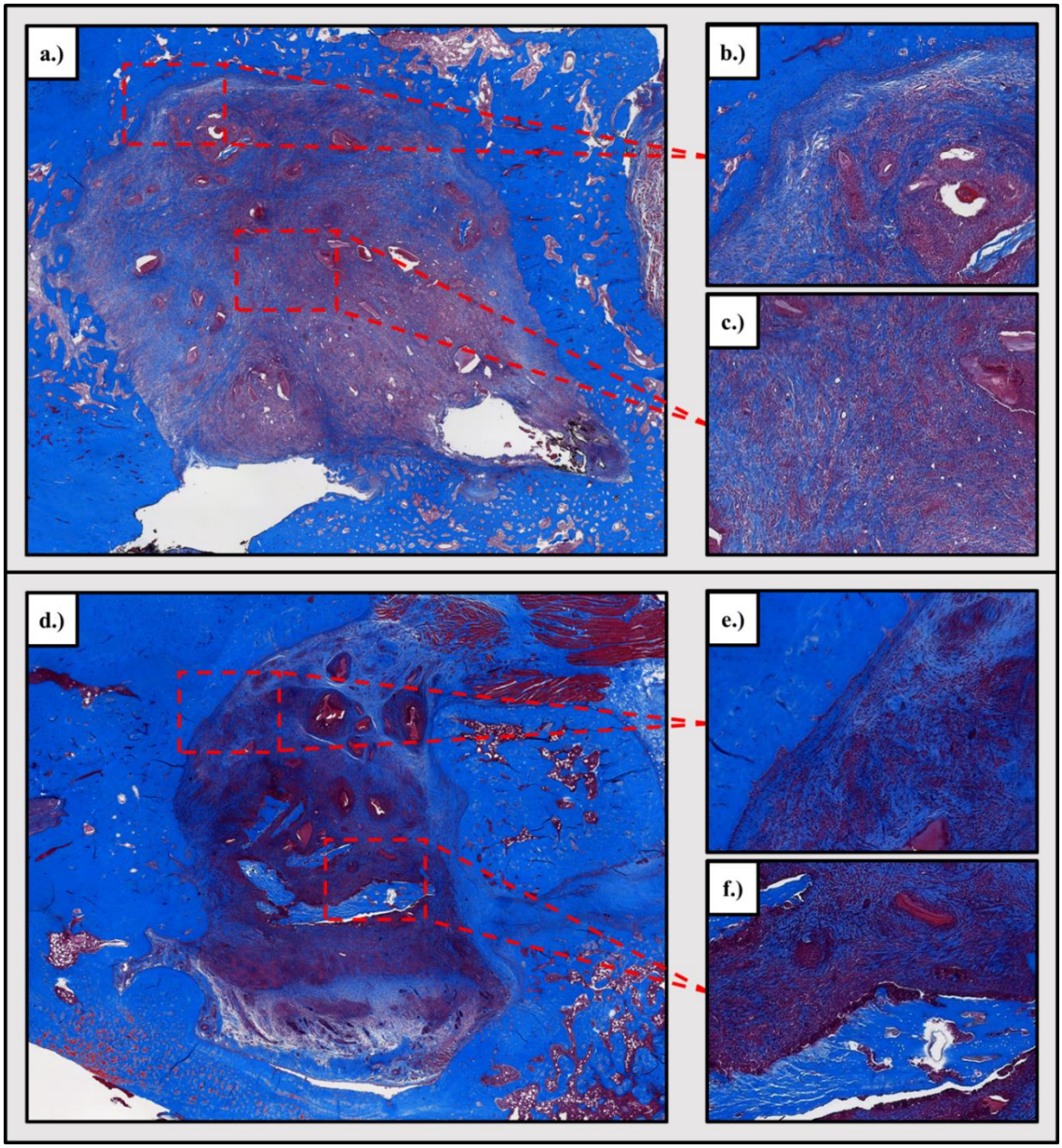

Figure 4.3. Masson's Trichrome images of M-1 at 1 and 2 months after implantation. Full defect region (a & d) derived from stitched 5x images and magnified regions depicting the defect border (b & e) and center (c & f) are shown.

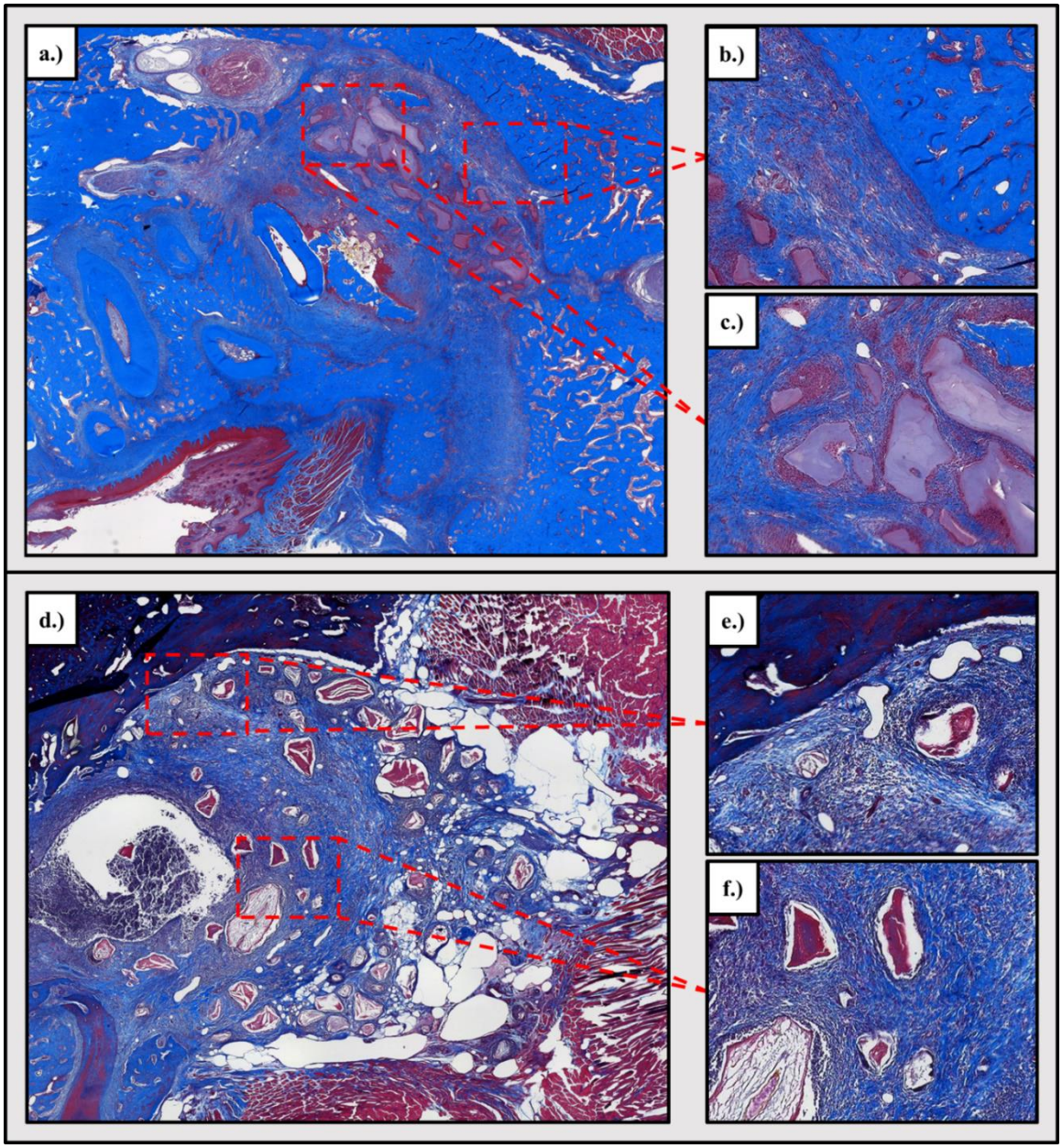

Figure 4.4. Masson's Trichrome images of Bio-Oss Collagen® at 1 and 2 months after implantation. Full defect region (a & d) derived from stitched 5x images and magnified regions depicting the defect border (b & e) and center (c & f) are shown.

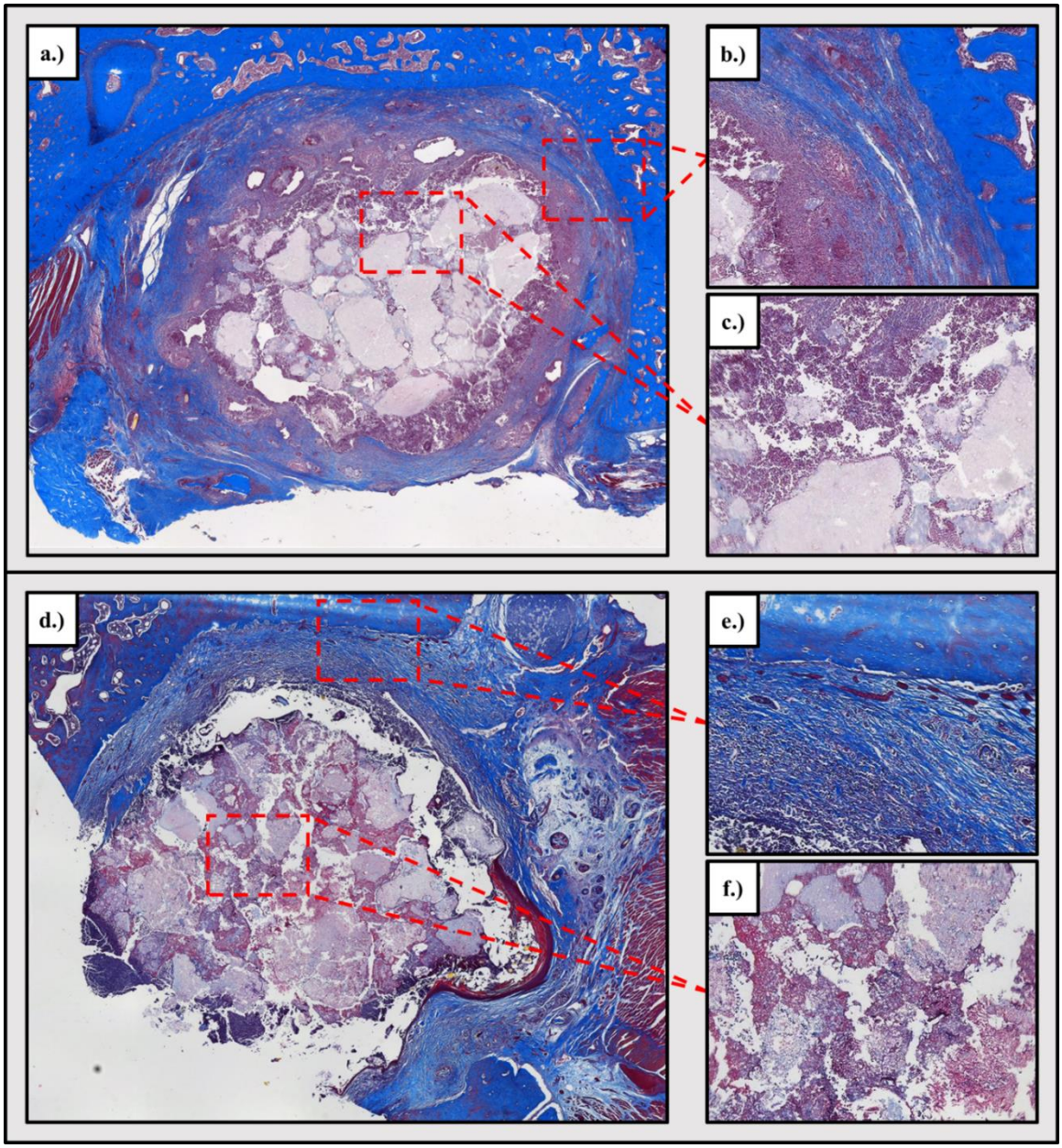

Figure 4.5. Masson's Trichrome images of Syntoss® at 1 and 2 months after implantation. Full defect region (a & d) derived from stitched 5x images and magnified regions depicting the defect border (b & e) and center (c & f) are shown.

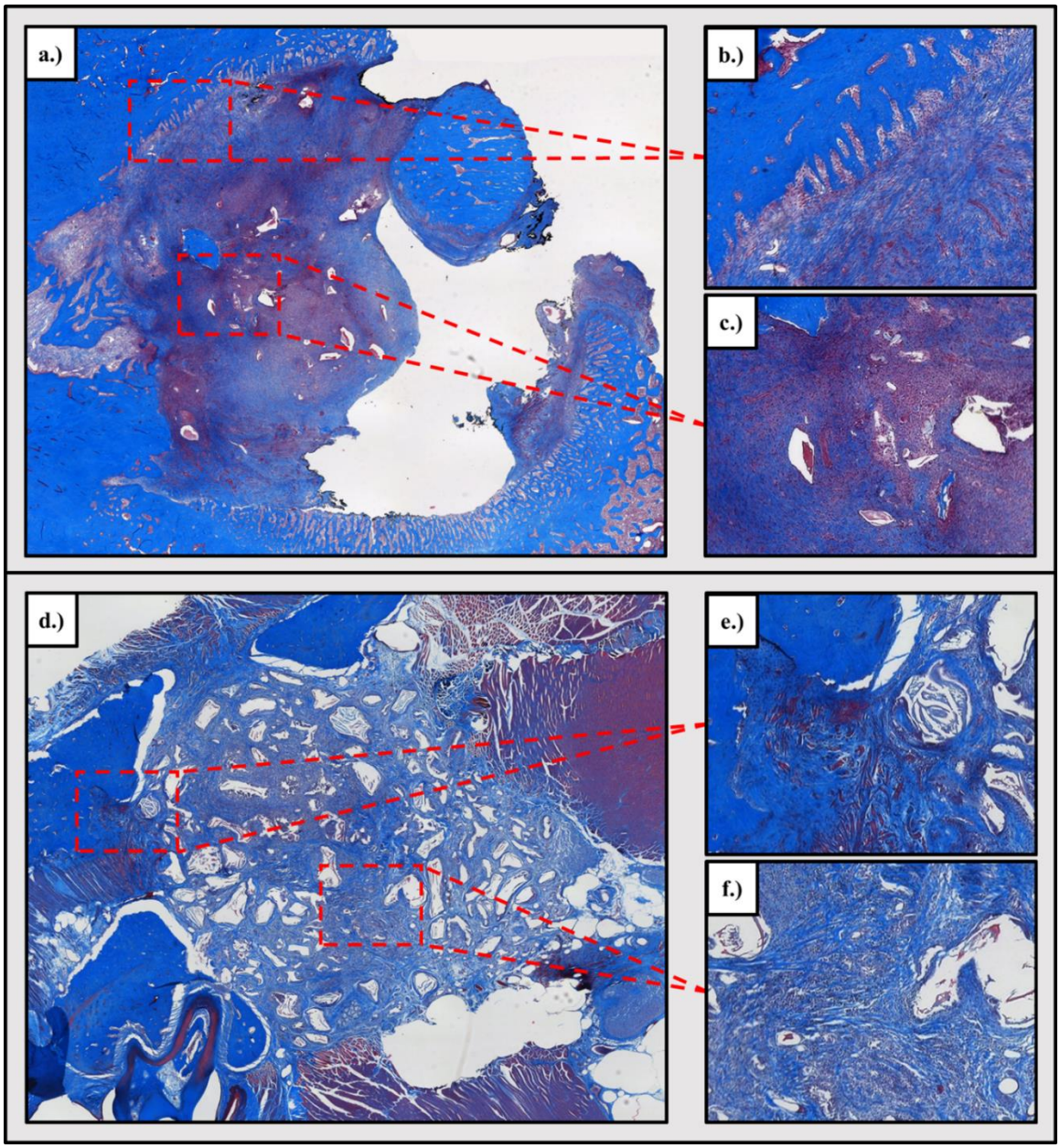

Figure 4.6. Masson's Trichrome images of S-1 at 1 and 2 months after implantation. Full defect region (a & d) derived from stitched 5x images and magnified regions depicting the defect border (b & e) and center (c & f) are shown.

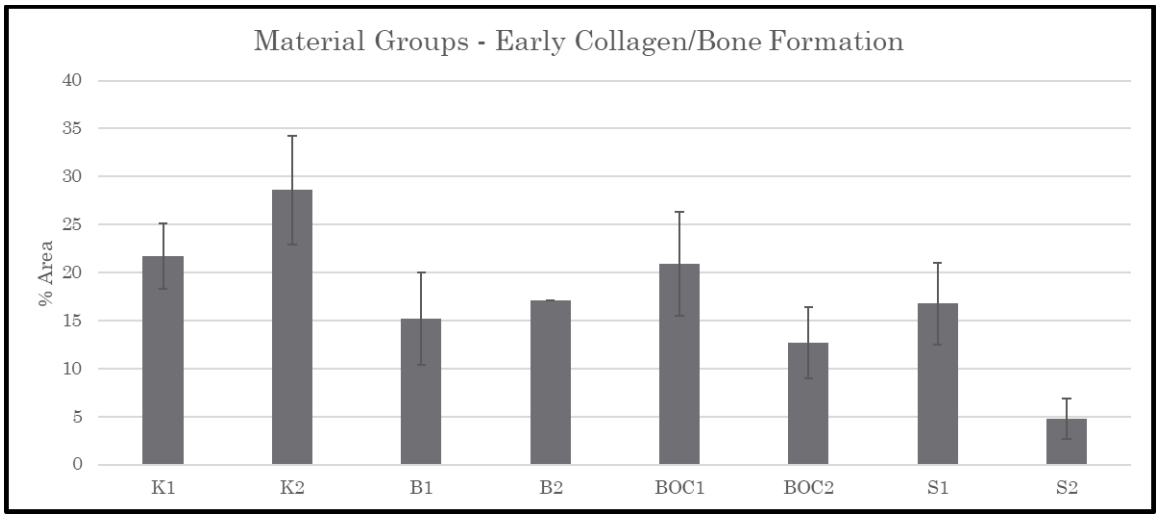

Figure 4.7. Graphical representation of early collagen/bone formation surface area data. Materials on left are test materials with M-1 scaffold treated samples indicated by (K) and S-1 indicated by (B), and predicate materials, BioOss Collagen® (BOC) and Syntoss® (S), on right. Numerical designation following letter code indicates study time point, either 1-month (1) or 2-month (2).

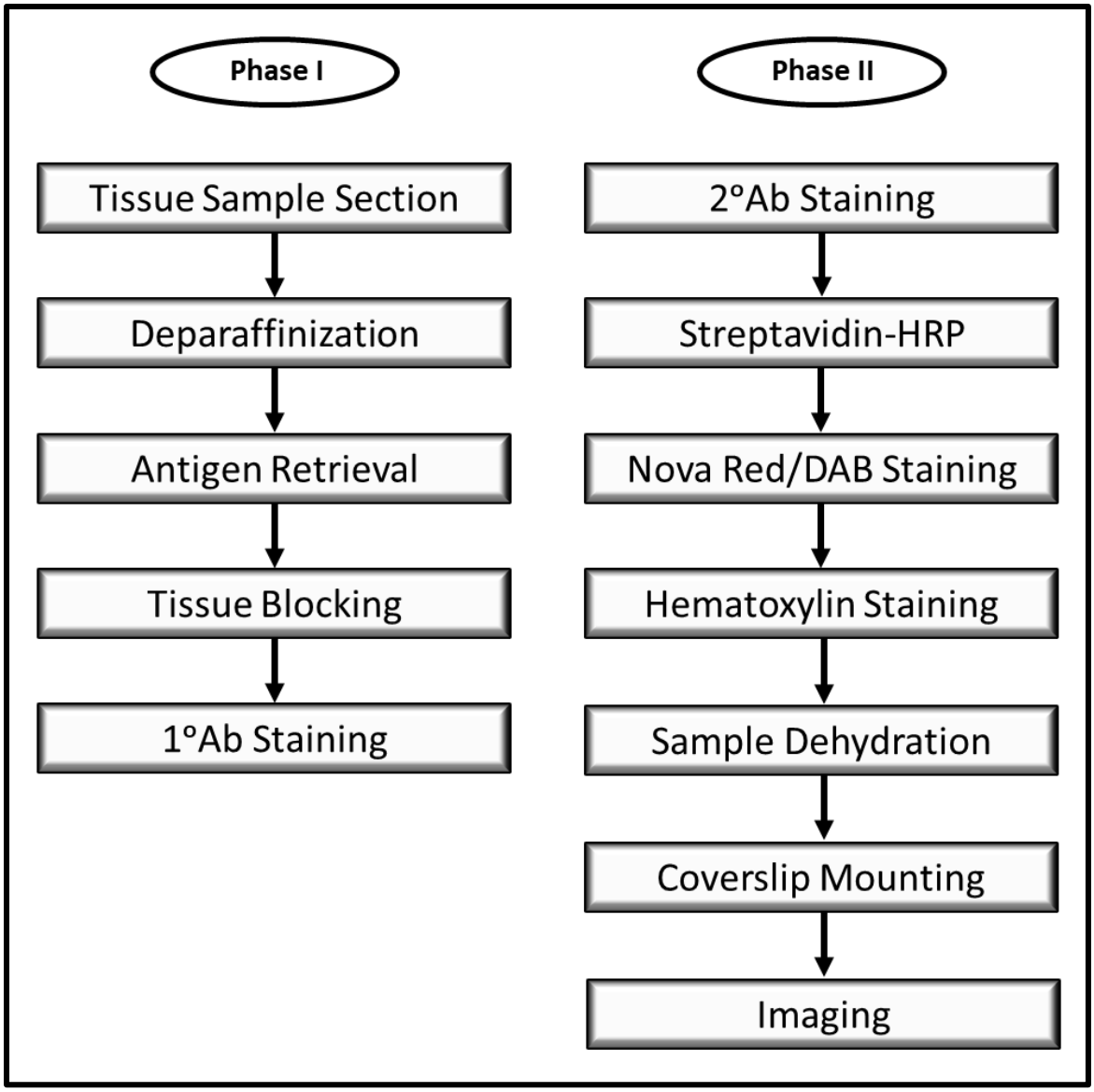

Figure 4.8. Overview of IHC protocol. (Phase I) Paraffin-embedded tissue samples were deparaffinized through xylene exposure followed by an ethanol rehydration gradient culminating in samples being placed in tap water. An antigen retrieval step using pH 6 citrate buffer at 80-85℃ was used along with 1% triton in PBS solution at room temperature to expose antigens on tissue surface for effective antibody binding. Prepped tissue was then blocked for endogenous hydrogen peroxidase (HRP) to eliminate background. Primary antibodies (°1 Ab) for target protein were applied to samples, which were then stored at 4℃ in a humid environment overnight. (Phase II) Samples were washed and biotinylated secondary antibodies (°2 Ab) targeting IgG of the °1 Ab host species were added. A streptavidin-HRP conjugate was then used to bind to biotin groups on tissue surface. Nova Red or DAB kits utilizing a hydrogen peroxide containing stain were applied and generated colorimetric reactions at the site of target proteins. A hematoxylin solution was used to provide background contrast for protein stains and samples were run though a dehydration process. Lastly, samples were mounted with a coverslip using limonene solution and imaged.

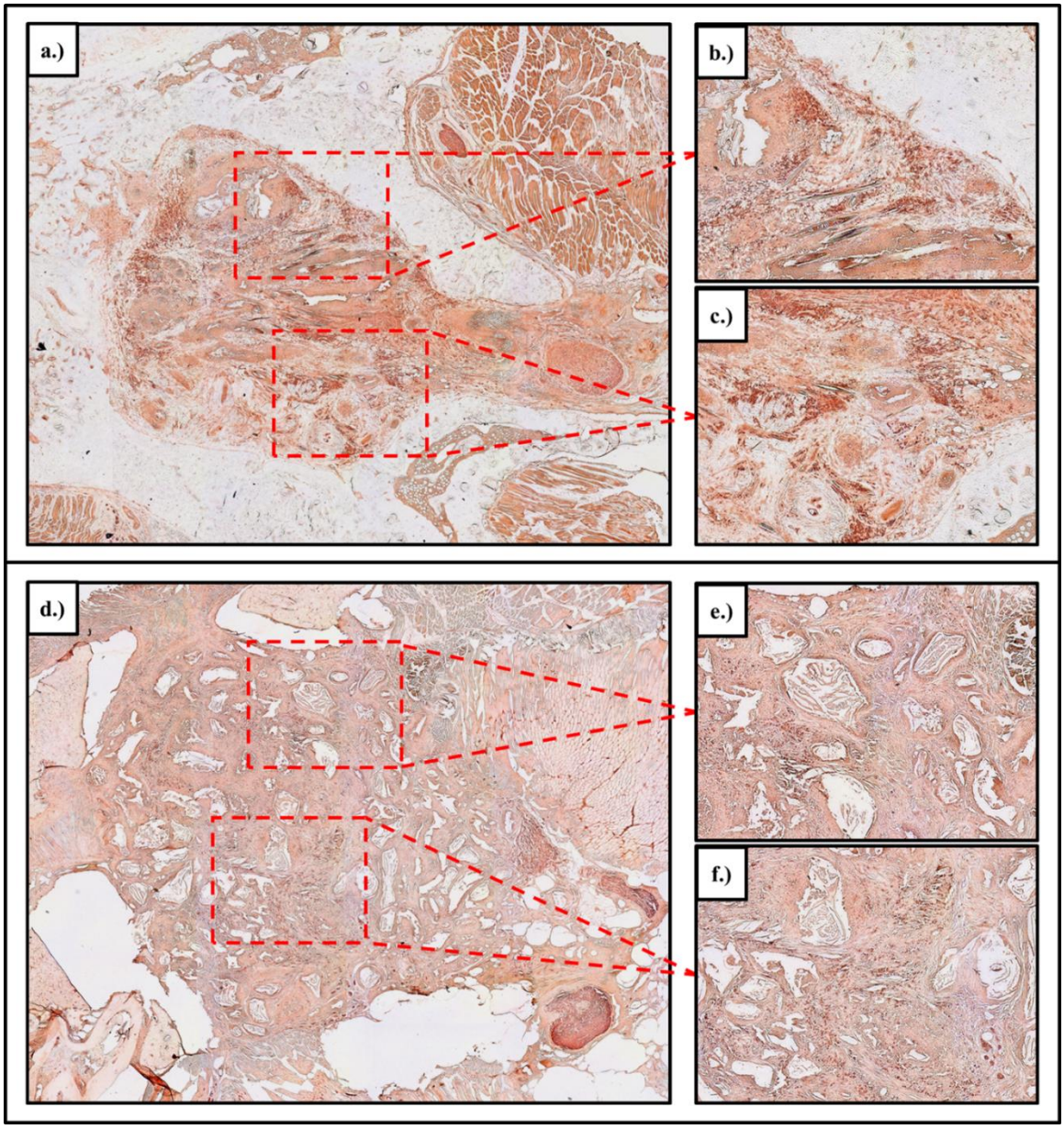

Figure 4.9. IHC staining for OPN in M-1 (a-c) and S-1 (d-f) samples at 2 months after implantation. Full defect region (a,d) derived from stitched 5x images and magnified regions of interest (b,c,f,e) are shown.

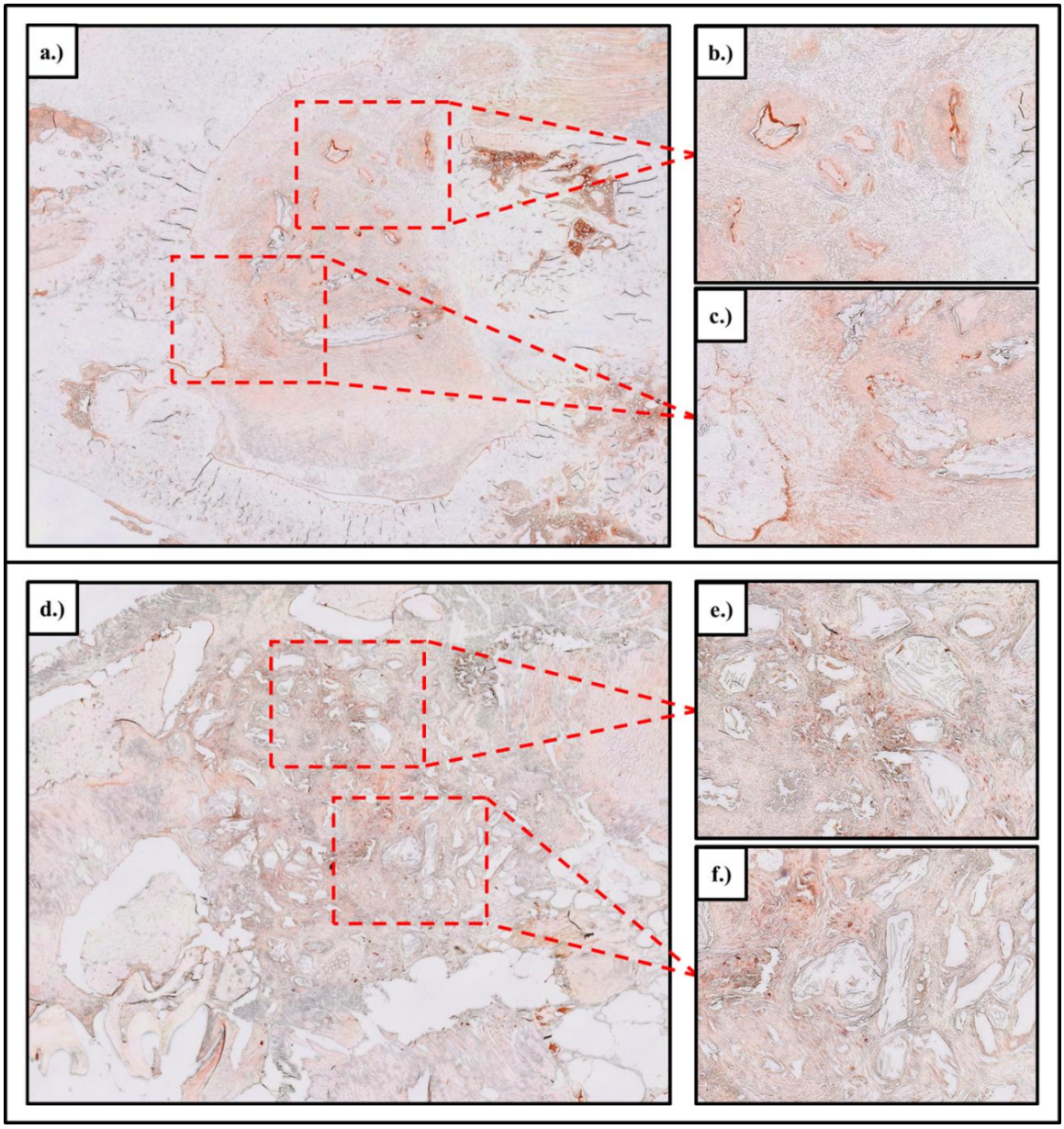

Figure 4.10. IHC staining for Sp7 in M-1 (a-c) and S-1 (d-f) samples at 2 months after implantation. Full defect region (a,d) derived from stitched 5x images and magnified regions of interest (b,c,f,e) are shown.

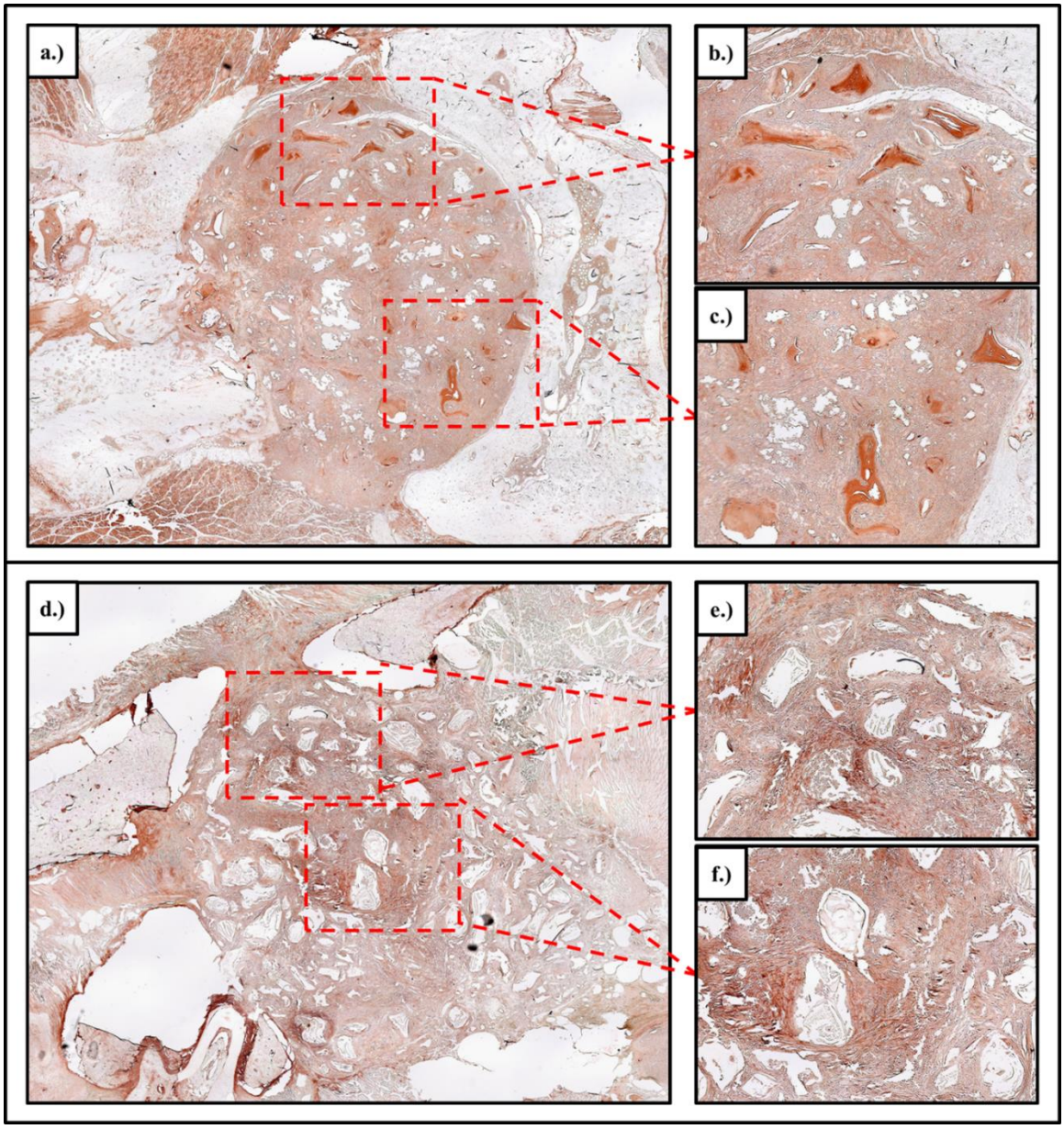

Figure 4.11. IHC staining for CD34 in M-1 (a-c) and S-1 (d-f) samples at 2 months after implantation. Full defect region (a,d) derived from stitched 5x images and magnified regions of interest (b,c,f,e) are shown.

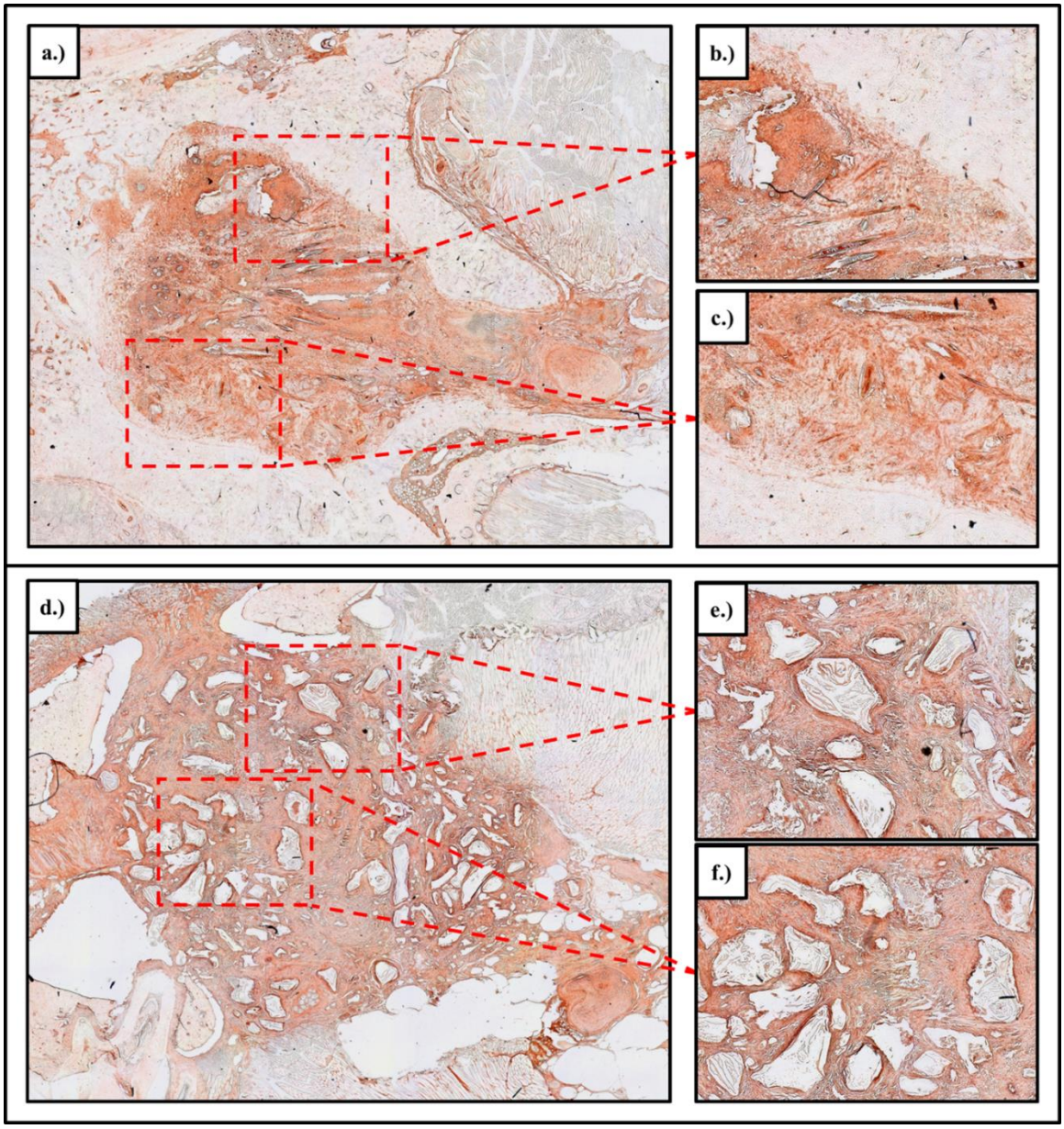

Figure 4.12. IHC staining for FN in M-1 (a-c) and S-1 (d-f) samples at 2 months after implantation. Full defect region (a,d) derived from stitched 5x images and magnified regions of interest (b,c,f,e) are shown.

CHAPTER V:
IN VIVO ASSESSMENT OF ADVANCED OSTEOBIOLOGICS PLATFORMS UTILIZING A RAT UNICORTICAL BONE DEFECT

Abstract

The field of bone tissue engineering has seen extensive focus on the development of novel and effective biomaterials that are capable of being applied through minimally invasive methods. These materials offer the potential to treat complex injuries while reducing major risk factors associated with surgical implantation, namely infection. The application of such advanced material designs will be largely dependent on the nature of the intended target defect. In this study two advanced material designs were examined for their cyto/biocompatibility characteristics. An expandable design, intended for applications that demand a void-filling material capable of providing mechanical stability to surrounding tissue through swelling pressure, was compared to a commonly used graft material, BioOss Collagen®, while two iteration of an injectable design, which offer the ability to stimulate accelerated or enhanced repair of fractures that can be stabilized without surgical intervention, were assessed in relation to an allogenic particulate graft material known as Veragraft®. The evaluated test articles maintained compositional properties similar to previously examined graft designs, thereby offering the promise of osteogiologic functional characteristics in addition to their application methods. Implementation of these biomaterials in a rat unicortical tibial defect demonstrated that the test articles were biocompatible and did not differ significantly from commonly used predicate devices in the formation of early collagen and bone structures within treated sites. Based on these findings, further evaluation of these advanced graft technologies will be pursued to more accurately determine their effectiveness as osteogenic platforms.

Introduction

As previously discussed, bone tissue is comprised of an intricate cellular matrix with hard mineral and soft organic regions that vary in ratio and distribution based on the type of bone and position within the structure. The complex and dynamic nature of this tissue provides bone with a high capacity for regeneration and reconstruction. However, despite this impressive natural reparative capacity, a lack of effective treatment or immobilization of the fracture/defect site can lead to abnormal growth following injury to tissue. For this reason, the use of graft materials is a common practice in treatment of such injuries, as it permits and promotes accelerated and improved repair. It has been demonstrated that the use of bone grafts offers the potential to enhance anatomical and functional integrity of the restored structure. The current gold standard for bone graft material, autogenous bone, can increase the risk of a procedure for the individual due to multiple surgical sites and potential for donor site morbidity. The focus of many current research efforts therefore has been to develop effective and relatively inexpensive graft designs capable of providing comparable results to autografts. Effective material designs should therefore maintain osteobiologic characteristics, namely osteo-conductive, osteo-inductive, and osseo-integrative potential (Hasan

et al., 2018). These properties will determine the capacity of the graft material to facilitate and promote bone growth, induce bone formation, and interact with surrounding tissues respectively. A previously examined scaffold, denoted in the previous chapters as S-1, and the modified fabrication method described in the previous chapter, M-1, demonstrated promise as osteogenic platforms in both *in vitro* and *in vivo* applications (Bow et al., 2019). To further explore the potential of such graft materials and the potential to develop relatively advanced materials with similar compositional elements, a comparative *in vivo* study was performed using multiple experimental advanced materials alongside commercially available graft materials to evaluate the biocompatibility and effectiveness of the test articles with relation to predicate devices.

Masson's trichrome and immunohistochemistry (IHC) assessment techniques were utilized as the primary means to evaluate the treated tissues. Trichrome imaging permitted evaluation of early collagen/bone surfaces within the treated defect regions, while ICH allowed detection of key proteins in the tissue associated with osteogenic and cell attachment functions, as well as their distribution and organization. Bio-markers for IHC were selected with a focus on examining proteins associated with osteogenesis, angiogenesis, and cellular attachment. Those chosen to evaluate osteogenesis included osteopontin (OPN), which is associated with early stages of bone development and osteoblastic activity, and BMP-2, which is strongly correlated with prolific bone development and mineralization. The cluster of differentiation (CD) markers CD34 and CD117 were used to assess the presence of progenitor cells as well as the ability of the graft materials to stimulate angiogenesis. Furthermore, CD117 serves as an indicator of the final stages of osteoblastic differentiation. Lastly, fibronectin (FN) and collagen II markers were utilized to determine any morphological and organization variations in the extracellular matrix architecture observed in the two treatment groups.

Observational comparisons of these key proteins within defect regions for test articles in relation to their respective predicate devices are anticipated to demonstrate the potential of these advanced materials as osteobiologic grafts. Furthermore, understanding of the handling techniques required for surgical application of these materials will be essential for development of materials with clinical translatability. Therefore, the primary objectives of the work described in this chapter are to verify the cytocompatibility/biocompatibility of the materials and detail the advantages and limitations of the current form of the test articles.

Advanced Materials

Super-hydratable Scaffold Design

A scaffold design comprised of nano-hydroxyapatite (nHA) and decellularized bone particles (DBPs) within a super-hydratable polymeric matrix was utilized as an osteogenic platform. The composite resembles the S-1 and M-1 scaffolds examined in previous studies (Bow et al. 2019; Jackson et al. 2018) in

compositional mineral additives, nHA and DBPs, yet employs a different degradable polyurethane (dPU) with enhanced hydrophilicity. This material design was designated as Expand-o-graft. Increased swelling capacity due to incorporation of this dPU enables this scaffold design to be delivered through minimal invasive procedures, as relatively small material pieces are capable of expanding to fill an entire defect. The proposed application would utilize a trocar device to implement an appropriately sized scaffold within the target defect, at which point absorption of *in situ* fluids were cause expansion of the material to effectively fill the void space (Chen, Yuen, & Li). Despite the differences in mechanical properties of this scaffold iteration, the cytocompatibility/biocompatibility characteristics are expected to echo those of previously assessed scaffold compositions, and therefore in vitro assessment for this material iteration was limited to a brief DiI fluorescent labeling assay to verify that cells are detected and proliferate within the matrix.

Injectable Scaffold Design

An injectable scaffold design was examined with two compositional variants. The basal construct for these materials consists of a thermosensitive polymer known as poloxamer 407 or Pluronic f127 solution at 30% weight by volume, which is capable of gelling from liquid to solid form as it approaches body temperature. Addition of nHA to this dynamic substrate provides the potential for the matrix to facilitate bone formation, as nHA has demonstrated osteo-inductive properties (Della Bella et al., 2018; Teng, Lee, Wang, Shin, & Kim, 2008), and integration with the surrounding tissue. A variation on this composite includes chitosan as an additive, which has demonstrated biocompatibility and potential as a natural adhesive (Georgopoulou et al., 2018; Li, Zhang, & Zhang, 2018; Park et al., 2009). These injectable material designs were designated as I-1 for the basal construct with nHA additive and I-2 for the basal construct with both nHA and chitosan additives. As the composites exist as low viscosity solutions at reduced temperatures, the ability to load the bone graft material into standard syringes therefore permits minimally invasive application to bone defects via hypodermic needle targeting (Coeshott et al., 2004; Julie Westerink et al., 2001). The substantial variations in material composition as compared to previously examined scaffold designs mandated that a more rigorous in vitro assessment be conducted to verify that the fabricated materials were non-cytotoxic prior to application in an *in vivo* model.

Predicate Device Comparisons

For evaluation of the super hydratable scaffold, a commonly implemented bone graft known as BioOss Collagen® was utilized. The composite consists of DBPs of bovine origin suspended within a porcine collagen matrix and has a wealth of literature describing its application *in vivo* (Miron et al., 2016; Sohn & Moon, 2018; Xu, Qi, Lin, Zhu, & He, 2019). The material is provided as a sterile block that can be cut to size according to the target defect. Since this scaffold does not

expand to the extent of the test article, it cannot be applied in the same minimally invasive fashion and requires full exposure of the defect for implantation.

To assess the cytotoxicity, biocompatibility, and effective regenerative capacity of the Pluronic f127-based composites a predicate device known as VeraGraft® was implemented. The commercially available allogenic bone graft product is produced and distributed by Avtec Surgical. The material is comprised of demineralized cortico-cancellous bone of human origin and comes contained in a sterile syringe for application. The size of the compositional particles (0.25-1.0 mm) prevent the deployment of the material through traditional syringe needle sizes yet can be extruded readily through the standard syringe bore-size. VeraGraft® dispenses as a thick putty consistency from its container, but upon contact with fluid converts to a low-viscosity liquid mixed with the bio-active particles (https://www.bonegrafting.com/veragraft-tm-en).

Advanced Material *In Vitro* Analysis

Caprine Mesenchymal Stem Cell Culture Parameters

To evaluate the cytocompatibility of the described advanced test articles it was determined that naïve caprine mesenchymal stem cells (cMSCs) would offer a more accurate representation of material effect as compared to the earlier utilized MC 3T3-E1 cells (ATCC) since these commercially available cells are pre-osteoblastic in nature. Bone marrow derived cMSCs (bmcMSCs) were extracted and isolated under an approved IACUC protocol and were expanded to generate a bank of cells below passage 5. Cells were seeded in tissue culture polystyrene-treated flasks and cultured at 37°C and 5% CO_2 in DMEM-F12 media with 10% fetal bovine serum and 1% amphotericin penicillin streptomycin. Media was replaced every 2–3 days, and the cells were passaged when they were approximately 70-80% confluent. Confluent cells were exposed to 0.05% Trypsin-ethylenediaminetetraacetic acid solution for 2 minutes at 37°C and collected. Cells were counted using a hemocytometer with Trypan Blue staining.

For viability and proliferation experiments to assess injectable material designs, cells were seeded at 1000 cells per well to a 96-well tissue culture plate and allowed to attach and proliferate for 24 hours. Injectable materials and their comparative predicate device were then added while in liquid state and placed into incubation conditions to cause gel formation. This process was conducted using DiI stained cells for tracking morphology over time and unstained cells for Calcein-AM staining and for MTS proliferation assessment.

For viability verification of cells on the super-hydratable scaffold design, material pieces were placed in wells of a 96-well non-tissue culture plate. Cells were then seeded to material samples at 1000 cells per well. Only DiI labeled cells were used for this assessment and fluorescent signal was monitored for morphological characteristics over time. As the primary function of this experiment was to verify that cells behaved similarly to previous scaffold designs, this was the sole *in vitro* assay conducted for this material design.

Viability and Proliferation

Calcein-AM staining, coupled with the quantitation of fluorescent intensity, was used to assess cell viability after exposure to materials, while MTS assay was implemented to determine impact on proliferation. For Calcein-AM fluorescence imaging cells were incubated in growth media for 7 days, at which point samples were washed to remove materials and reveal cells for staining and subsequent imaging. Cells were incubated with 0.1 mL of staining solution, containing 2 µg/ml calcein-AM reconstituted with dimethyl sulfoxide, at 37°C for 5 minutes. Fluorescent images of all samples were taken to verify the presence of cells and their viability.

Proliferation assessment using MTS assay for material exposed cells was conducted at 3, 7, and 9 days of culture growth. Briefly, MTS kit reagent (Promega) was added directly to cell cultures resulting in a colorimetric reaction due to the production of formazan crystals that is proportional to the density of the cell population in the well. Therefore, an increase in absorbance readings at subsequent time points would be indicative of healthy cellular proliferation.

Cell viability was confirmed on the I-1 and I-2 composites using Calcein-AM staining over a period of 7 days (**Figure 5.1**). MTS readings over the described time course revealed a relatively consistent absorbance value over the course of the study (**Figure 5.2**). As cells were determined to be healthy through Calcein-AM imaging, this plateauing of MTS values may indicate that, while the test articles are non-cytotoxic, they may not be conducive to *in vitro* proliferation. This may potentially be due to the materials obscuring surface area in the wells, which was not impeded in cell monolayer controls and those exposed to the predicate device, Veragraft®.

Lastly, DiI fluorescent monitoring for all test articles was conducted to verify cytocompatibility prior to in vivo application. Fluorescence was detected in samples cultured for 5 days furthering indicating that materials did not negatively impact cell viability.

Advanced Material *In Vivo* Analysis

Tibial Defect Model

As described in an earlier chapter Sprague Dawley rats were received and maintained at facilities for 7 days prior to surgeries for acclimation. Pre-surgical analgesic application of buprenorphine was administered, and animals were anesthetized with isoflurane delivered via inhalation for the duration of the surgery. Sterile prep of the surgery site was performed through removal of hair and application of 70% ethanol, chlorohexidine, and betadine solutions respectively. Surgical operations were then carried out. Briefly, linear incisions were made directly below the tibial stifle joints and muscle tissue was resected to expose the tibal crests. Unicortical defects were then generated at 3mm in diameter in the medial face of both tibias. Each resulting defect was filled with one test article, either the Expand-o-graft, I-1, or I-2, and the contralateral defect was treated with

that test article's respective predicate device, BioOss Collagen® for expandable scaffold and Veragraft® for injectables. As such, each animal permitted accurate comparative assessment by addressing potential animal-to-animal variation in implantation reaction. Following implantation, sites were closed through initial suturing of muscle layer and then of subcutaneous tissue. Animals were monitored closely to verify recovery and then transferred to housing room. Regular monitoring of animals was then carried out for 1-month post-operation. At 1-month post-operation animals were sacrificed as per protocol and CT scans of region of interest were taken. Treated tibias were then harvested from specimens for histological sectioning and staining, with tissue stored prior to sectioning in Decal A solution.

Advanced Material Handling

Surgical handling of the Expand-o-graft test article was largely similar to previously examined S-1 and M-1 scaffold designs; however, the expansion capacity of the construct due to the super-hydratable nature was a crucial consideration for *in vivo* application. Graft material was cut to approximately 2mm x 2mm x 2mm pieces to accommodate for swelling after contact with blood at defect site. Scaffolds were firmly placed within defects and allowed to undergo initial expansion to ensure that the material was not protruding from injury. Similar to previously assessed scaffolds, the Expand-o-graft maintained its structural integrity after exposure to in situ fluid. As observed in the mandibular in vivo assessment described in the previous chapter, the BioOss Collagen® scaffold, which is readily commercially available and commonly implemented for dental surgical applications, maintained its structural integrity when applied to the defects and was conducive to cutting and shaping. Both test article and predicate device proved easily manageable and convenient in surgical application.

The injectable test articles at first presented a unique challenge in prepping for surgical implementation yet were demonstrated to readily be applicable using a standard sterile syringe with 22.5-gauge needle. Bulk material sterilized through UV-radiation was stored at low temperatures to ensure low viscosity before mixing and drawing into sterile syringes. Needles were replaced with new sterile/capped needles and material samples were stored in clean containers at 4℃. On the day of surgery, materials syringes were placed on ice packs in an insulated container until needed. After defect generation, I-1 or I-2 material syringes were removed from cold chamber and 0.2cc of low viscosity was applied to site. The solutions were observed to rapidly gel within the site and did not appear to be readily disturbed when the muscle tissue was close above wound site. These injectable materials therefore proved to be relatively easy to handle and show a promising means for applying a scaffold with osteogenic components. Conversely, the compared predicate device, Veragraft®, was relatively difficult to handle compared to all other tested materials, as the original putty consistency bone particulate mix liquified upon contact with *in situ* fluids.

CT Analysis

CT scans were performed on animals after sacrificed at 1-month post-operation. 3D renders were generated and collected scans were evaluated by a certified radiologist for both quantitative and qualitative parameters. Measurements for area and density comprised the quantitative element and were coupled with a set of qualitative characteristics developed and employed in a previous study. These parameters include subjective rankings of 0 (negligible) to 3 (severe) for periosteal reaction, sclerosis, swelling, and mineralization, as well as healing with scores ranging from 0 (no closure) to 3 (completely healed).

CT imaging verified that defect generation was successful, and graft materials persist within the treated sites (**Figures 5.3-5.4**). Defects appeared to have largely healed with mineralized tissue formation observed in defect sites treated with the Expand-o-graft, BioOss Collagen®, and Veragraft® materials. Those treated with I-1 and I-2 demonstrated smooth surfaced and largely healed surfaces, which may in part have been due to spontaneous healing unimpeded by presence of a scaffold within the defect.

Histological Analysis

Histological sections were cut from paraffin-embedded decalcified tissue samples at 1-5um thickness. Sets of sections included one slide stained with H&E for general cellular reaction assessment, one slide stained with Masson's Trichrome for evaluation of present tissue types, and 3-5 unstained slides for immunohistochemistry (IHC). Masson's Trichrome stained slides will be used to generate semi-quantitative data for new early collagen/bone tissue surface area. Captured images are processed through ImageJ software to create binary masks highlighting tissue of interest, which can be subsequently measured as a ratio of highlighted area to total area.

Gross evaluation of H&E stained sections showed an absence of inflammatory signs indicating that all materials were biocompatible. Masson's Trichrome imaging resulted in observational differences in tissue content within the defect (**Figures 5.5-5.9**), yet ImageJ software assessment yielded no significant difference is the area of early collagen/bone structures between the Expand-o-graft, I-1, or I-2 are their respective predicate device. Though not significant in area coverage defects treated with all test articles appeared to demonstrate a highly organized formation of these early collagen/bone tissue fronts within the defect.

Immunohistochemistry Analysis

Unstained histological sections were subjected to deparaffinization and prepped for immune-staining to determine presence and abundance of specific proteins related to angiogenesis and bone formation. Prepped samples received primary antibodies for the marker of interest, which were then subjected to a biotinylated secondary antibody. A Nova Red kit utilizing horseradish peroxidase

(HRP) was then applied to stain samples and permit visualization of tissue surface proteins for image analysis.

Preliminary imaging of IHC stained sections showed promise in detecting specific markers within sample tissue and were used to observationally assess the distribution and organization of tissue surface proteins. Proteins associated with osteogenesis, angiogenesis, and cellular attachment were examined. These included the early-stage bone development marker OPN for early bone formation fronts, markers CD117 for progenitor cells and early vascular formation, and both collagen II and FN for cellular matrix organization within the defects (**Figures 5.10**).

Conclusion

The examined advanced materials demonstrated the unique ways in which basal scaffold components that have shown certain regenerative capacities, in this case osteogenic potential, can be implemented in relatively complex designs to target specific diseases or injuries. As determined through both *in vitro* and *in vivo* experimentation, the Expand-o-graft, I-1, and I-2 technologies all proved to be non-cytotoxic and biocompatible. Furthermore, CT and histological evaluation demonstrated that scaffold materials, with the exception of I-1 and I-2, maintain residual particulate within the defect at 1-month post-implantation. Though the injectable graft treated defects showed strong healing characteristics, this may in part be due to spontaneous healing that was not impeded by the presence of a solid graft material.

Both the super-hydratable and injectable graft designs were observed to handle well in surgical application, with the Expand-o-graft being readily cut and shaped to an appropriate size to accommodate swelling after fluid contact. I-1 and I-2 technologies were capable of being drawn into and dispensed from standard sterile syringes with a 22.5-gauge needle. Compared predicated devices were more variable, with BioOss Collagen® being easily manageable but Veragraft® displaying a liquifying characteristics upon contact with blood, which made this graft material difficult to maintain at site.

Successful detection of key proteins associated with osteogenic and cell attachment functions through IHC indicated that scaffold designs may also be capable of stimulating osteogenic repair of the treated site. The comparable intensity of the stain between defects treated with the Expand-o-graft and those treated with BioOss Collagen® represents a promising regenerative capacity for the test article design. Based on the compositional inclusion of nHA and chitosan in the I-1 and I-2 injectable iterations, it is anticipated that these materials will also demonstrate osteogenic potential; however, these analyses are still on-going.

The analytical techniques used to evaluate the *in vitro* and *in vivo* impact of these various osteogenic scaffold technologies have thus far focused on visual observations of biological systems, either through cell culture or harvested tissue, after exposure of that system to the material of interest. However, these methods do not offer a means of ascertaining the molecular mechanisms involved in

stimulating and promoting the observe effects. To address this this following chapter will utilize a multi-omics approach to determine potential pathway mechanisms impacted by exposure of naïve human cells to the previously discussed S-1 scaffold.

References

Bow, A., Newby, S., Rifkin, R., Jackson, B. K., Matavosian, A., Griffin, C., . . . Dhar, M. (2019). Evaluation of a Polyurethane Platform for Delivery of Nanohydroxyapatite and Decellularized Bone Particles in a Porous Three-Dimensional Scaffold. *ACS Applied Bio Materials, 2*(5), 1815-1829. doi:10.1021/acsabm.8b00670

Chen, H.-C., Yuen, D., & Li, S.-T. Evaluation of a self-expandable mineral-collagen composite implant as an osteoconductive scaffold for bone growth and regeneration in a rabbit femoral bone defect model. *Frontiers in Bioengineering and Biotechnology*. doi:10.3389/conf.FBIOE.2016.01.02718

Coeshott, C. M., Smithson, S. L., Verderber, E., Samaniego, A., Blonder, J. M., Rosenthal, G. J., & Westerink, M. A. J. (2004). Pluronic® F127-based systemic vaccine delivery systems. *Vaccine, 22*(19), 2396-2405. doi:https://doi.org/10.1016/j.vaccine.2003.11.064

Della Bella, E., Parrilli, A., Bigi, A., Panzavolta, S., Amadori, S., Giavaresi, G., . . . Fini, M. (2018). Osteoinductivity of nanostructured hydroxyapatite-functionalized gelatin modulated by human and endogenous mesenchymal stromal cells. *J Biomed Mater Res A, 106*(4), 914-923. doi:10.1002/jbm.a.36295

Georgopoulou, A., Papadogiannis, F., Batsali, A., Marakis, J., Alpantaki, K., Eliopoulos, A. G., . . . Chatzinikolaidou, M. (2018). Chitosan/gelatin scaffolds support bone regeneration. *Journal of Materials Science: Materials in Medicine, 29*(5), 59. doi:10.1007/s10856-018-6064-2

Hasan, A., Byambaa, B., Morshed, M., Cheikh, M. I., Shakoor, R. A., Mustafy, T., & Marei, H. E. (2018). Advances in osteobiologic materials for bone substitutes. *Journal of Tissue Engineering and Regenerative Medicine, 12*(6), 1448-1468. doi:10.1002/term.2677

Jackson, B. K., Bow, A. J., Kannarpady, G., Biris, A. S., Anderson, D. E., Dhar, M., & Bourdo, S. E. (2018). Polyurethane/nano-hydroxyapatite composite films as osteogenic platforms. *J Biomater Sci Polym Ed, 29*(12), 1426-1443. doi:10.1080/09205063.2018.1464264

Julie Westerink, M. A., Louise Smithson, S., Srivastava, N., Blonder, J., Coeshott, C., & Rosenthal, G. J. (2001). ProJuvant™ (Pluronic F127®/chitosan) enhances the immune response to intranasally administered tetanus toxoid.

Vaccine, 20(5), 711-723. doi:https://doi.org/10.1016/S0264-410X(01)00423-6

Li, Y., Zhang, Z., & Zhang, Z. (2018). Porous Chitosan/Nano-Hydroxyapatite Composite Scaffolds Incorporating Simvastatin-Loaded PLGA Microspheres for Bone Repair. *Cells Tissues Organs, 205*(1), 20-31. Retrieved from https://www.karger.com/DOI/10.1159/000485502

Miron, R. J., Zhang, Q., Sculean, A., Buser, D., Pippenger, B. E., Dard, M., . . . Zhang, Y. (2016). Osteoinductive potential of 4 commonly employed bone grafts. *Clinical Oral Investigations, 20*(8), 2259-2265. doi:10.1007/s00784-016-1724-4

Park, K. M., Lee, S. Y., Joung, Y. K., Na, J. S., Lee, M. C., & Park, K. D. (2009). Thermosensitive chitosan–Pluronic hydrogel as an injectable cell delivery carrier for cartilage regeneration. *Acta Biomaterialia, 5*(6), 1956-1965. doi:https://doi.org/10.1016/j.actbio.2009.01.040

Sohn, D. S., & Moon, Y. S. (2018). Histomorphometric study of rabbit's maxillary sinus augmentation with various graft materials. *Anat Cell Biol, 51*(Suppl 1), S1-s12. doi:10.5115/acb.2018.51.S1.S1

Teng, S. H., Lee, E. J., Wang, P., Shin, D. S., & Kim, H. E. (2008). Three-layered membranes of collagen/hydroxyapatite and chitosan for guided bone regeneration. *J Biomed Mater Res B Appl Biomater, 87*(1), 132-138. doi:10.1002/jbm.b.31082

Xu, A. T., Qi, W. T., Lin, M. N., Zhu, Y. H., & He, F. M. (2019). The optimization of sintering treatment on bovine-derived bone grafts for bone regeneration: in vitro and in vivo evaluation. *J Biomed Mater Res B Appl Biomater*. doi:10.1002/jbm.b.34387

Appendix

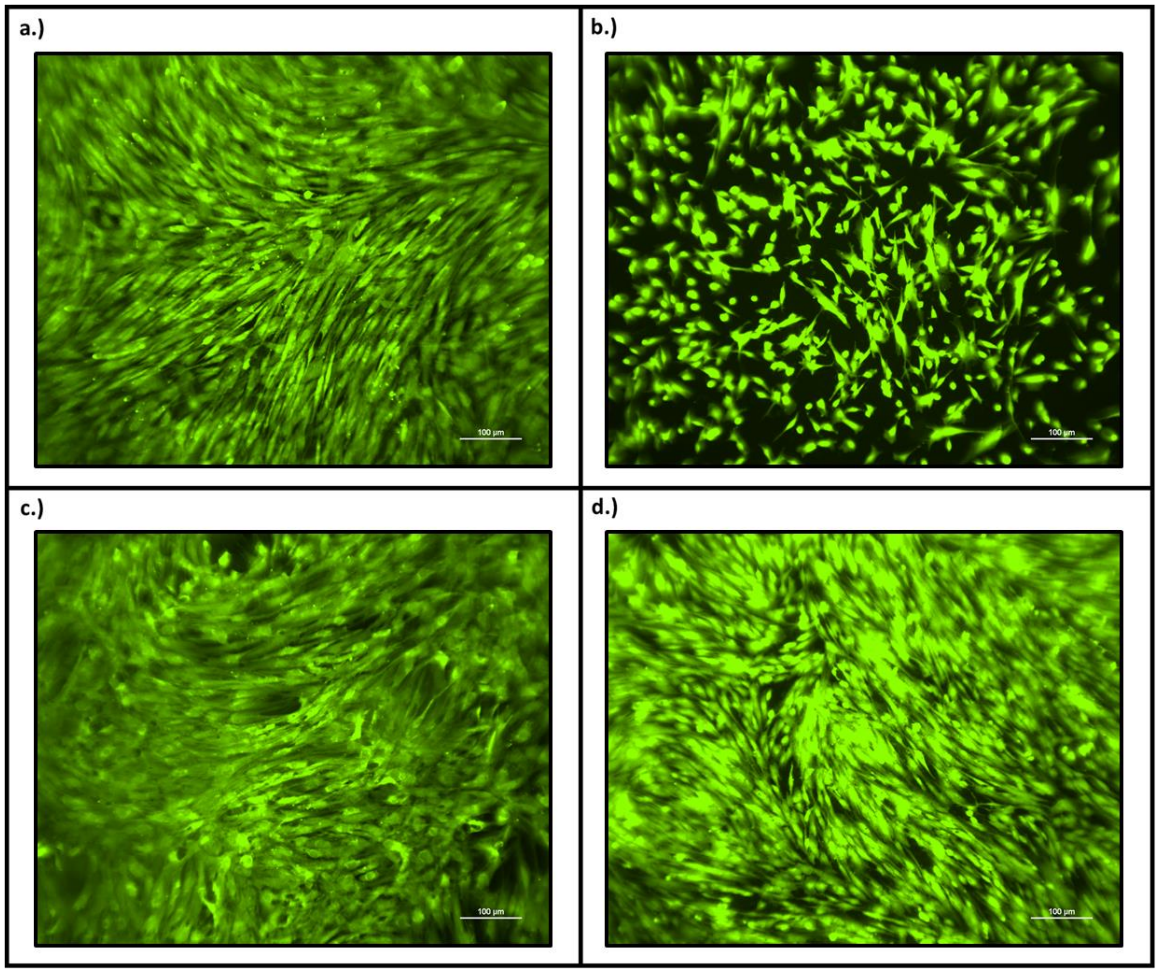

Figure 5.1. Calcein-AM imaging of bmcMSCs exposed and unexposed to injectable materials and corresponding predicate device. Uptake of staining agent is indicative of cell viability. I-1 (d) and I-2 (b) exposed cells were compared with Veragraft® predicate device (c) exposed cells and unexposed cell monolayers (a).

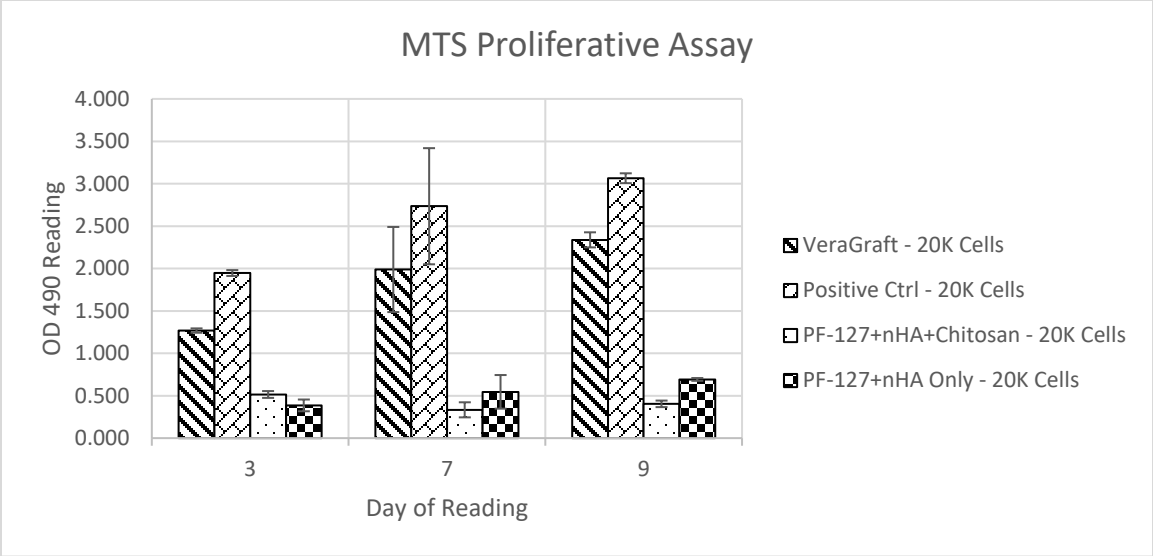

Figure 5.2. MTS proliferative assay for bmcMSCs seeded to injectable scaffold designs. Absorbance readings taken at day 3, 7, and 9 of culture growth were plotted to determine changes in cell density for I-1 and I-2 test articles as compared with predicate device and cell monolayer controls. Samples were run in triplicate.

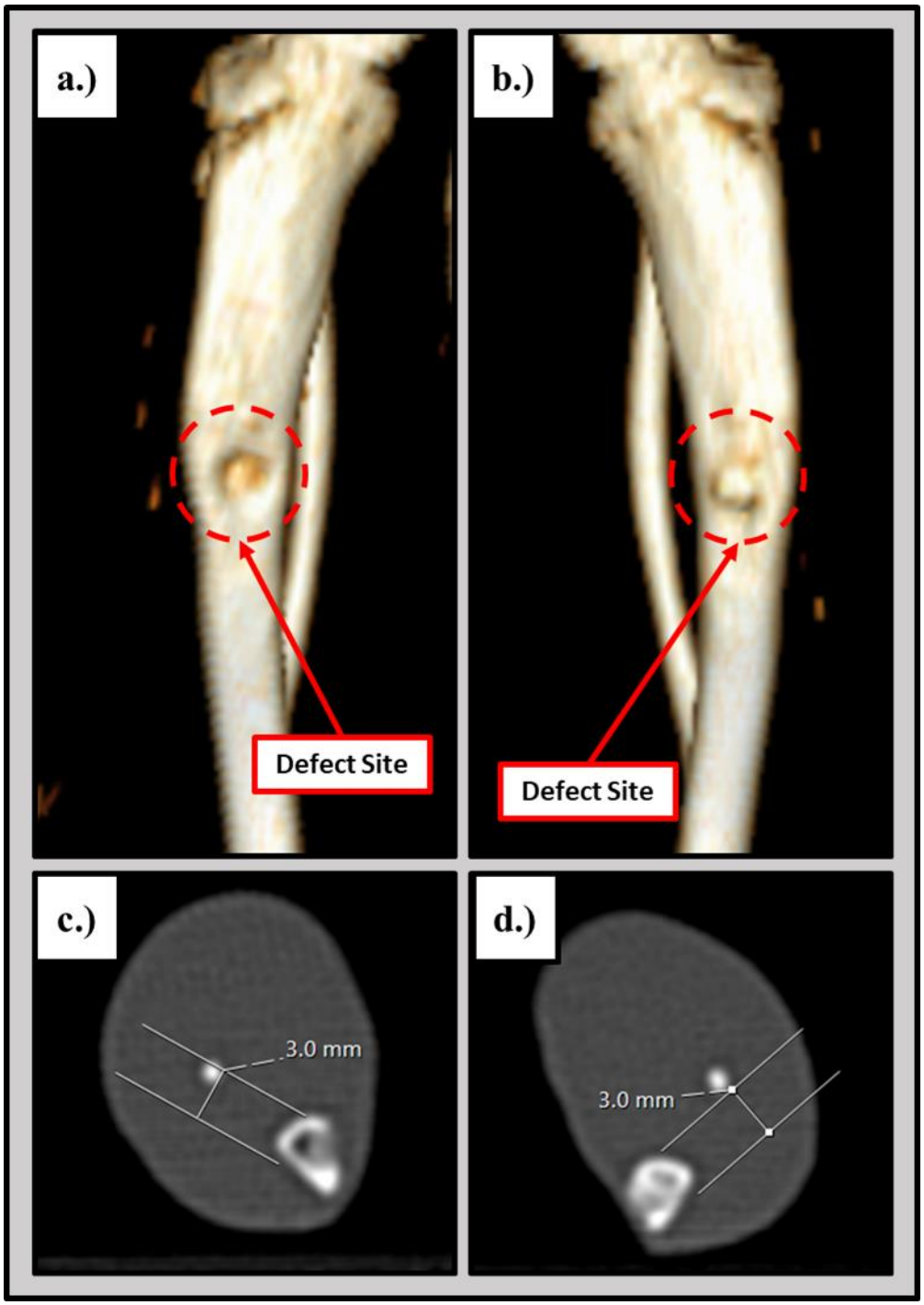

Figure 5.3. CT 3D renders (a,b) and cross-sectional images (c,d) for expandable design treated tibial defects. Expand-o-graft treated (a,c) and BioOss Collagen® treated defects (b,d) are shown.

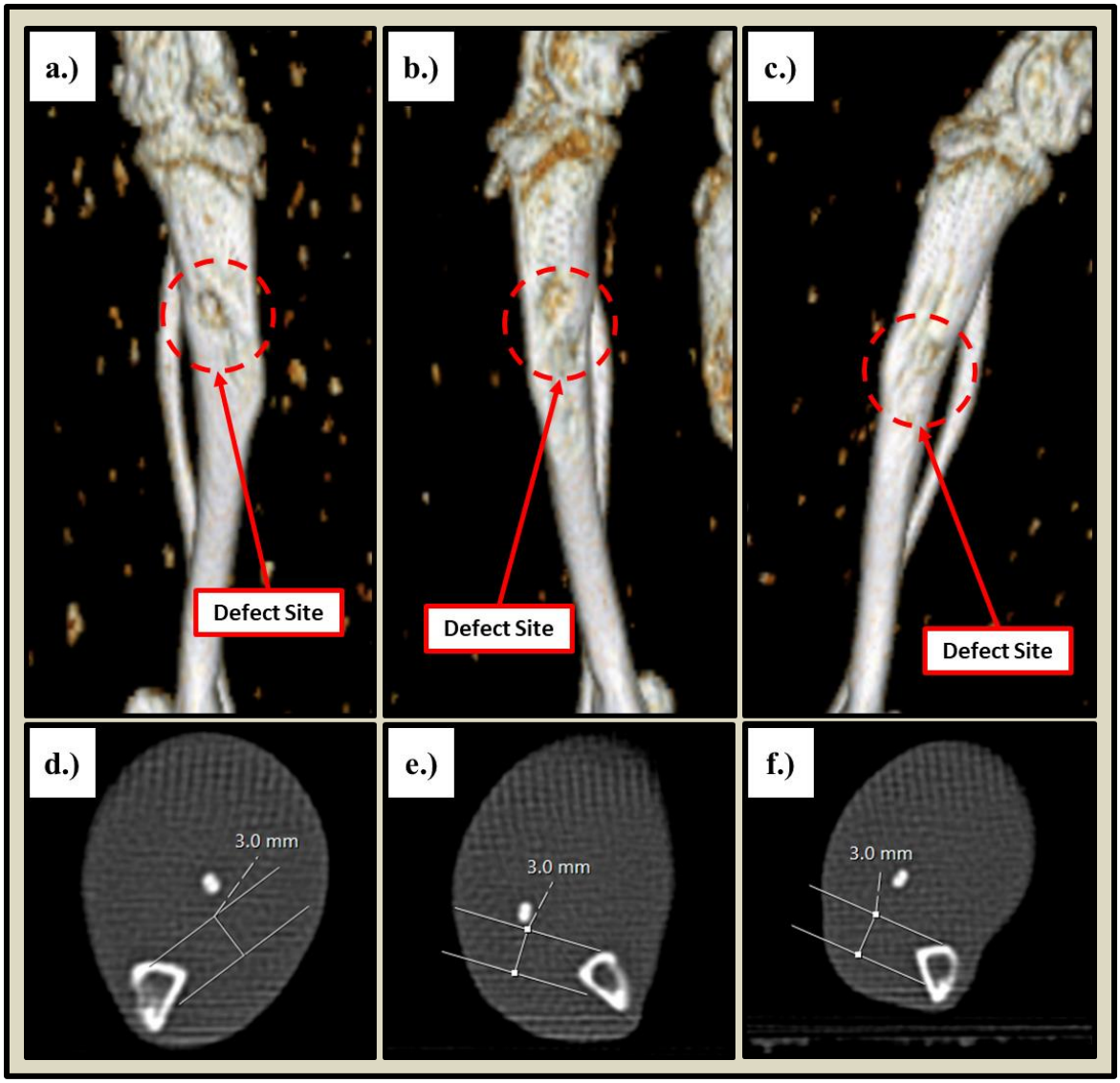

Figure 5.4. CT 3D renders (a-c) and cross-sectional images (d-f) for injectable design treated tibial defects. Veragraft® (a,d), I-1 (b,e), and I-2 (c,f) treated defects (b,d) are shown.

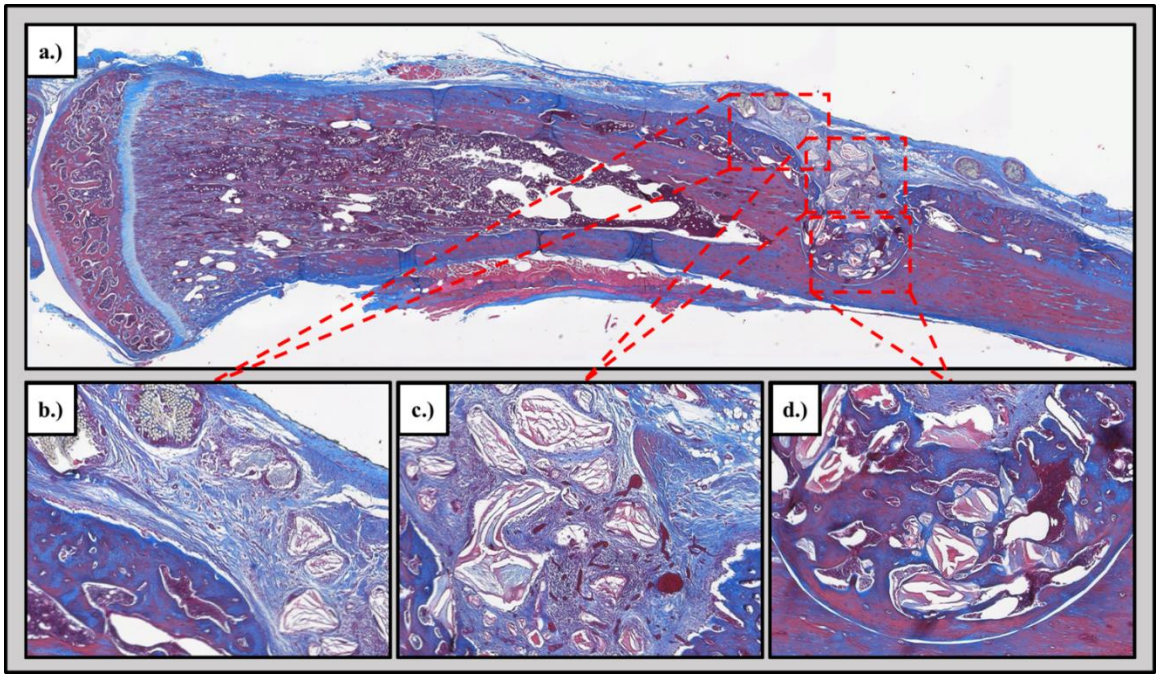

Figure 5.5. Masson's Trichrome Images of BioOss Collagen® treated defect. 5x magnification stitched composite image of tibia is shown (a) with magnified regions of interest within the defect boundary (b-d).

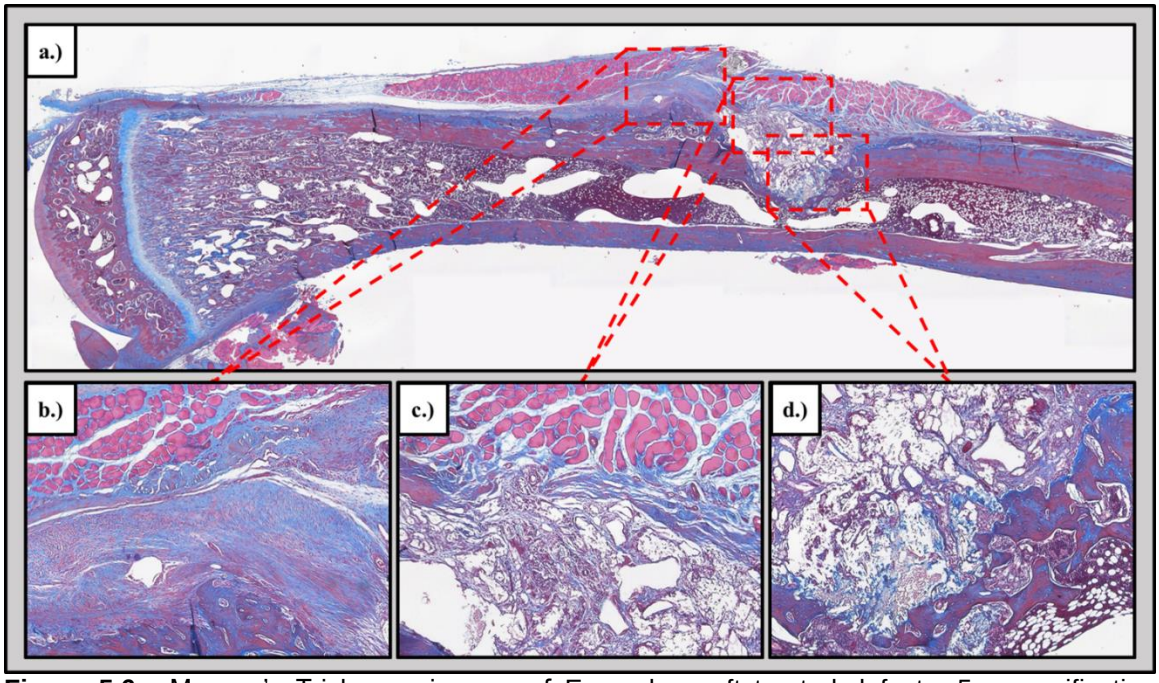

Figure 5.6. Masson's Trichrome images of Expand-o-graft treated defect. 5x magnification stitched composite image of tibia is shown (a) with magnified regions of interest within the defect boundary (b-d).

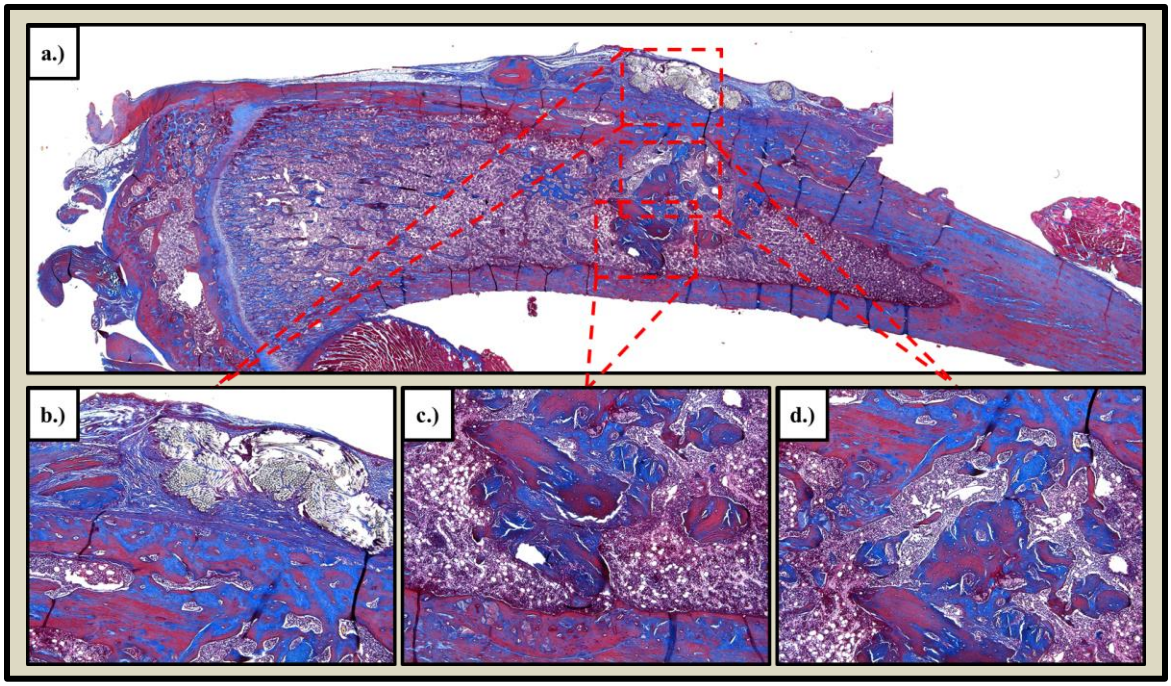

Figure 5.7. Masson's Trichrome images of Veragraft® treated defect. 5x magnification stitched composite image of tibia is shown (a) with magnified regions of interest within the defect boundary (b-d).

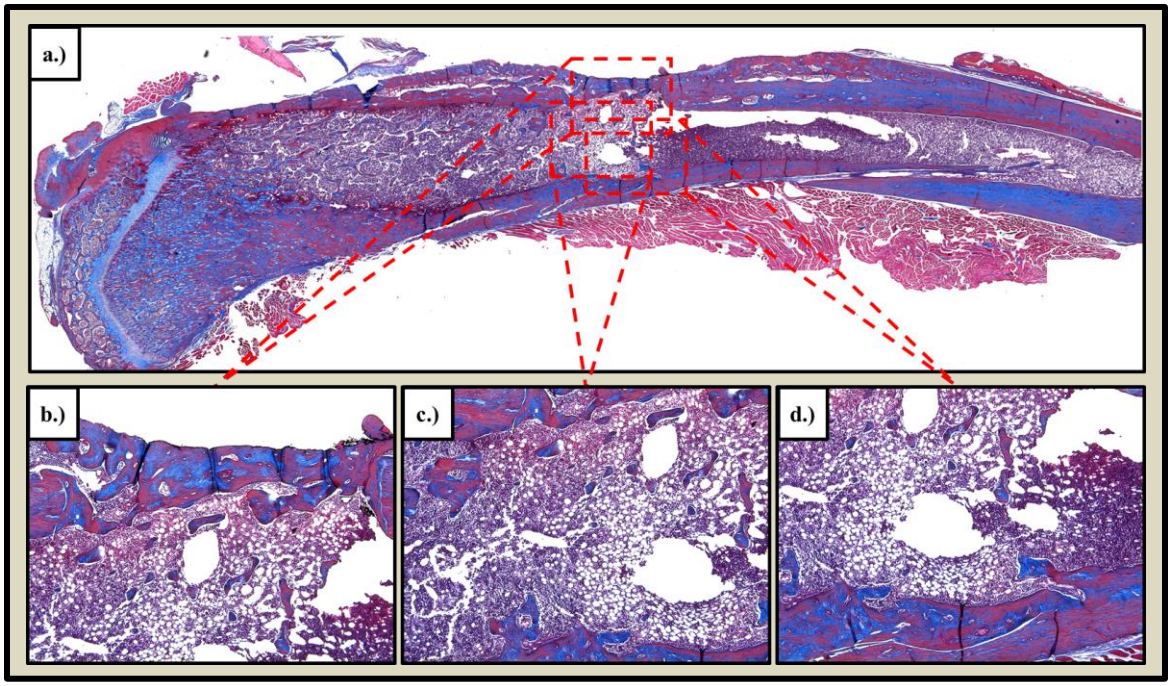

Figure 5.8. Masson's Trichrome images of I-1 treated defect. 5x magnification stitched composite image of tibia is shown (a) with magnified regions of interest within the defect boundary (b-d).

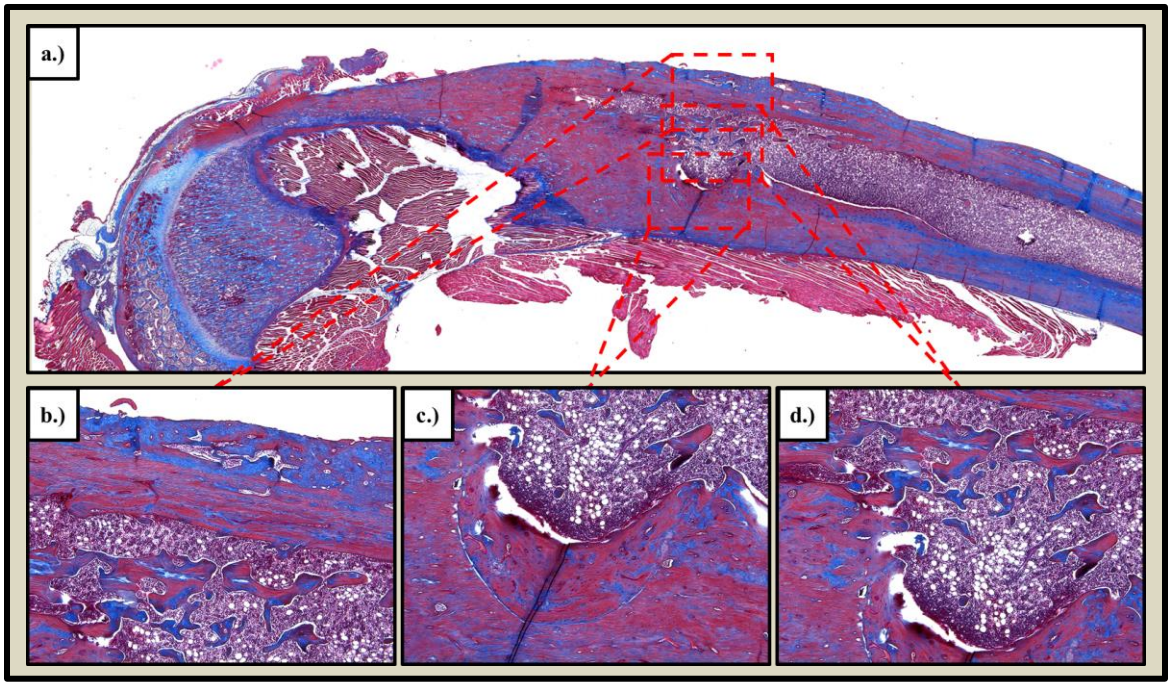

Figure 5.9. Masson's Trichrome images of I-2 treated defect. 5x magnification stitched composite image of tibia is shown (a) with magnified regions of interest within the defect boundary (b-d).

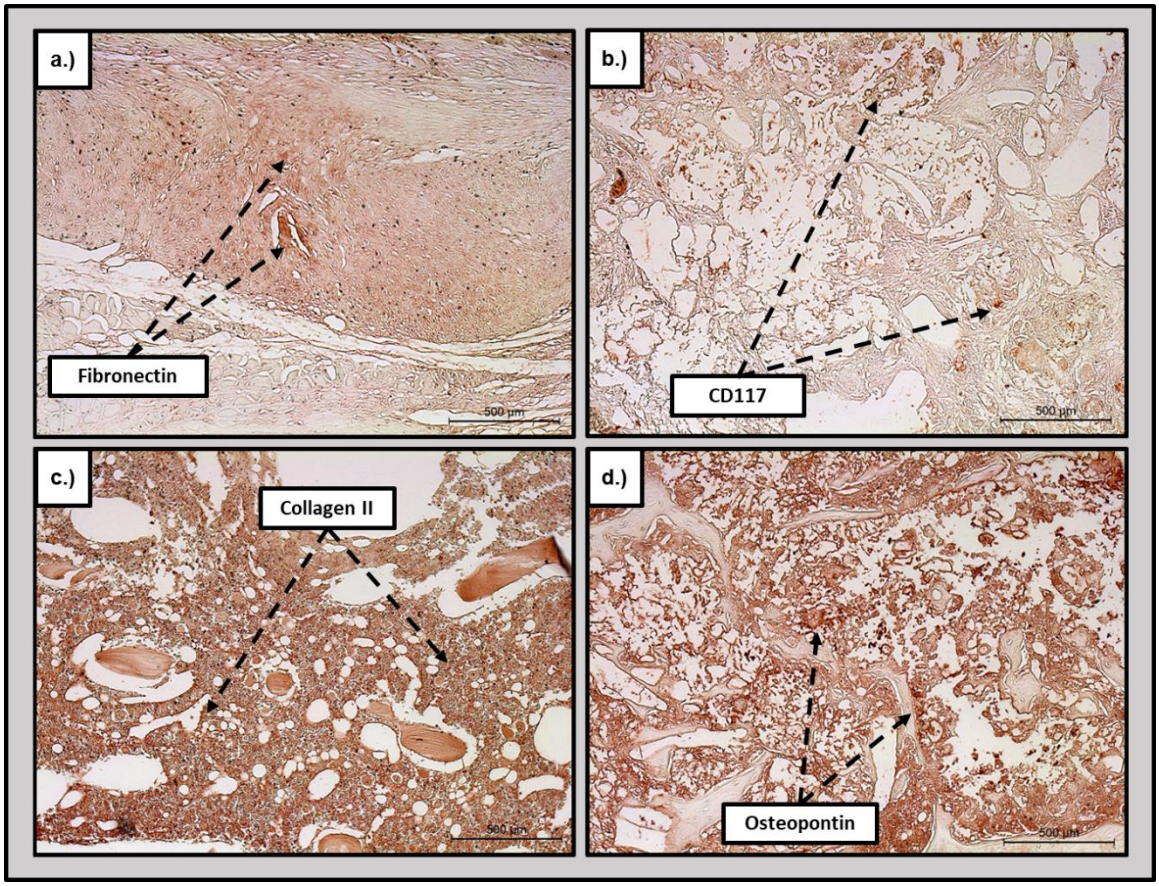

Figure 5.10. IHC imaging for Expand-o-graft treated tibial defects. 10x imaging of fibronectin (a), CD117 (b), collagen II (c), and osteopontin (d) staining within defect center.

CHAPTER VI:
MULTI-OMICS ASSESSMENT OF MOLECULAR MECHANISMS ASSOCIATED WITH ADHESION AND OSTEOGENIC FUNCTIONS OF HUMAN MESENCHYMAL STEM CELLS EXPOSED TO AN OSTEOBIOLOGIC PLATFORM

A version of this chapter is currently under submission by Austin J. Bow:

Bow, A.; Jackson, B; Griffin, C.; Howard, S; Castro, H; Campagna, S; Biris, A.; Anderson, D.; Bourdo, S.; Dhar, M. Multi-omics evaluation of adhesion and osteogenic mechanisms of human fat-derived mesenchymal stem cells on a polyurethane-nanohydroxyapatite nanocomposite.

This article was submitted for publication in the journal of Tissue Engineering Part A on November 5, 2019.

Abstract

The highly dynamic nature of bone represents one of the most impressive natural reparative tissue mechanisms, exhibiting constant remodeling through osteoblastic and osteoclastic activity in response to mechanical forces and injuries. However, it is precisely the complexity of this system that results in difficulties in developing effective grafting biomaterials for bone injuries that exceed the regenerative capacity of native bone. As the current gold standard, autologous tissue grafts, poses restrictive features including limited source materials and donor site morbidity, the design of easily synthesizable materials that facilitate repair comparable to autografts is essential. As previously reported, we have fabricated a multilayered nanocomposite comprised of polyurethane (PU) and nano-hydroxyapatite (nHA) films interspersed with decellularized bone particles (DBPs) for bone regeneration and have demonstrated it to be cytocompatible with murine osteoblasts *in vitro* and biocompatible, with osteobiologic characteristics, *in vivo*. To evaluate the underlying mechanisms of this biomaterial, the *in vitro* behavior of human fat-derived mesenchymal stem cells seeded onto these scaffolds was assessed using a combinatorial approach of transcriptomic and metabolomic analyses. Expression data from osteogenic and signal transduction gene arrays and small molecule concentrations, measured via liquid chromatography-mass spectrometry, were cross-examined using Integrated Molecular Pathway Level Analysis (IMPaLA), Database for Annotation, Visualization, and Integrated Discovery (DAVID), and ConsensusPathDB (CPDB) online tools to generate a fundamental collection of scaffold-influenced pathways. Results demonstrated up-regulation of key osteogenic, cellular adhesion, and cell signaling markers, and interactions between bone morphogenic protein (BMP), Hedgehog (HH), and Wnt signaling pathways were determined to be primary candidates for the osteobiologic mechanisms of the scaffold design. The detection of complimentary metabolites, such as ascorbate, further indicate that scaffolds generate intricate cellular environments, promoting cell attachment and subsequent osteo-differentiation. These data contribute to the understanding of cell recruitment, adhesion, and subsequent osteogenic signaling in the presence of this 3D nanocomposite scaffold.

Introduction

As discussed in previous chapters, the field of bone tissue engineering faces unique challenges in biomaterial design stemming largely from the highly dynamic nature of the target tissue, which boasts impressive natural reparative mechanics. Native bone undergoes continuous remodeling through osteoblastic and osteoclastic activity in order to accommodate for mechanical forces exerted on the body and provide structural support. For this reason, non-compromised bone tissue, as opposed to that observed in osteoporotic or geriatric individuals, is innately capable of repairing sizable injuries. However, for cases of tissue damage that result in defect sizes that exceed the reparative capacities of native bone, or for accelerated repair, the application of a graft material is necessary (Majidinia, Sadeghpour, & Yousefi, 2018). Currently the gold standard for such graft material is the use of autologous tissue, as this eliminates concerns of immunogenic reaction and provides an optimal substrate for cellular on-growth and eventual integration. Despite the superior reparative and restorative functions of autografts, implementation incurs an increased risk to patient due to the need for multiple surgical sites and donor site morbidity, as well as a reliance on a limited source material (Garcia-Gareta, Coathup, & Blunn, 2015). Therefore, the development and characterization of graft materials with similar or enhanced functionality and biocompatibility to autografts offer an attractive alternative (Araujo et al., 2019; Bow et al., 2019; Garcia-Gareta et al., 2015).

Scaffold constructs being designed for bone tissue engineering must display key osteobiologic characteristics including osteo-inductive, osteo-conductive, and osseo-integrative functions in order to facilitate effective repair of native tissue (Agrawal & Ray, 2001; Albrektsson & Johansson, 2001; Gao, Peng, Feng, & Shuai, 2017; Hasan et al., 2018). Osteo-induction indicates that the material is capable of stimulating exposed cells toward an osteogenic lineage (Garcia-Gareta et al., 2015). The osteo-conductivity of a material determines the ability of cellular communication across and through a substrate (Garcia-Gareta et al., 2015). Lastly, osseo-integration indicates the measure of cell migration and subsequent formation of mature bone tissue on the surface and throughout the matrix.

We have previously reported the fabrication of a nanocomposite, designated as S-1, comprised of nano-hydroxyapatite (nHA)/polyurethane (PU) film layers with interspersing layers of decellularized bovine bone particles (DBPs), which demonstrated biocompatibility and osteobiologic characteristics, both *in vitro* and *in vivo* (Bow et al., 2019; Jackson et al., 2018). Specifically, 8-week old Sprague Dawley rats had a significant increase in new bone formation over a 30-day period within unicortical tibial bone defects when treated with the nanocomposite. Based on these results, we next wanted to elucidate more precise mechanisms by which exposed cells are influenced. To accomplish this, a multi-omics approach utilizing analytical tools of transcriptomics and metabolomics was implemented (Araujo et al., 2019).

The use of various molecular analytical tools to assess the functions of biomaterials is an expanding and promising approach as the critical attributes of bone scaffolds previously described depend heavily on the cell-biomaterial interactions (Gao et al., 2017). Stimuli from surface topography or composition elements can drastically alter the influence of a material on exposed cells, leading to substantially different results both *in vitro* and *in vivo* (Jackson et al., 2018). Transcriptomics, the study of mRNA molecules and functional impact of their expression levels, offers the potential to observe the fundamental regulative capacities of cells through comparative assessment of gene expression (Ullah, Sittinger, & Ringe, 2013). The extraction and analysis of messenger RNA (mRNA) from cells exposed to various conditions, through generation of complimentary DNA (cDNA) and subsequent real-time polymerase chain reaction (qPCR), offers the potential to evaluate the effect of specific treatments on exposed cells by normalizing to an untreated control culture. Such methods have been utilized in studies focused on elucidating correlations between discrete material characteristics and biological responses of exposed cells in attempts to establish pathway libraries. These data can be used as a rationale to design biomaterials with specific topographies, architecture, and composition (Araujo et al., 2019).

Transcriptomic evaluation is further strengthened through supplementation with metabolomic data, which consists of small molecule concentrations often detected through mass spectrometry (Schrimpe-Rutledge, Codreanu, Sherrod, & McLean, 2016). Metabolites and their associated relative abundance can be detected in a wide variety of samples ranging from acellular materials to tissue biopsy samples, providing the potential for comparative analyses based on metabolite profiles. By cross-examining detected small molecules with expression data for up-regulated and down-regulated genes respectively, it is possible to develop a basic pathway(s) to describe the behavior of cells on scaffolds. Online databases, such as the Kyoto Encyclopedia of Genes and Genomes (KEGG) and Reactome, and tools for assessing connective elements within data sets, including Integrated Molecular Pathway Level Analysis (IMPaLA), Database for Annotation, Visualization, and Integrated Discovery (DAVID), and ConsensusPathDB (DPDB), can be used to generate basic pathway maps demonstrating the signals that are triggered when cells interact with scaffolds.

The use of naïve cells during *in vitro* examination of scaffold mechanisms provides a more relevant model, as pre-differentiated and immortalized cell lines may demonstrate expression profiles that reflect innate cell programming instead of material induced effects. Naïve cells alleviate this concern and permit accurate assessment of material impact on cellular activity. Furthermore, the use of human mesenchymal cells (MSCs) contributes a clinical translatability aspect, as the designed scaffold technology is intended for human medicine. Therefore, studies conducted to elucidate mechanisms of the biomaterial were facilitated using mesenchymal stem cells (MSCs) derived from human adipose tissue. MSCs are naïve, multi-potent cells with the potential to differentiate toward multiple lineages, namely osteocytes, chondrocytes, and adipocytes (Alghazali et al., 2017). These

cells therefore offer a unique potential as a reparative element, especially when coupled with a scaffold substrate, and have been implemented in a wide array of cell-based treatments (Majidinia et al., 2018). Seeding of these adipose-derived human MSCs (adhMSCs) onto the nanocomposite scaffold can thereby evaluate the effectiveness of the construct as an osteogenic platform capable of application as a cell-based therapy device (Majidinia et al., 2018). Our objective in the present study, based on data from previous studies, is to assess the interaction between human MSCs and the nanocomposite through variations in both the transcriptional and metabolite landscapes. Expression of genes associated with osteogenesis, cellular attachment, and signaling were examined for hMSC seeded nanocomposites and compared with hMSCs differentiated through a well-established method to assess scaffold impact. These data were then cross-examined with small molecule concentrations to elucidate potential candidate pathways of effect for the scaffold on exposed cells.

Human Mesenchymal Stem Cell *In Vitro* Work

Human Mesenchymal Stem Cell Isolation and Expansion

Adipose-derived human MSCs (adhMSCs) were collected and primary cultures were established using previously described methods (Alghazali et al., 2017). The stromal vascular fraction of cells which contain the non-hematopoietic mesenchymal stem cells were seeded in DMEM-F12 growth media containing 10% fetal bovine serum and 1% amphotericin penicillin streptomycin and expanded in vitro in tissue culture polystyrene flasks. Cells incubated at 37°C and 5% CO_2, with growth media replaced every 2-3 days, were enzymatically released from substrates with 0.05% Trypsin-EDTA upon reaching approximately 80% confluency and then allocated to tissue culture flasks for continued expansion, cryopreservation, or experimental set-ups. Cells were characterized and confirmed to be mesenchymal stem cells using previously described *in vitro* assays including tri-lineage differentiation (Alghazali et al., 2017).

Viability and Proliferation

1mm x 5mm x 5mm pieces of the nanocomposite scaffold material (Bow et al., 2019) were cut from bulk scaffold blocks to ensure that each piece fit into a single well of a 24 well plate. Each scaffold piece was placed into individual wells of a non-tissue culture plate and cell solutions were directly added to ensure cellular migration into nanocomposite pores through capillary action. Cells were seeded at a density of $4x10^4$ cells/scaffold for proliferation assessment and $5x10^5$ cells/scaffold for both gene expression and small molecule analyses. As previously observed, total RNA from cell/scaffold complexes at 5 days that had received media with osteogenic-inducing agents (growth media supplemented with 10mM beta glycerophosphate, 10nM dexamethasone, 100nM ascorbic acid) showed consistently poor yields (Bow et al., 2019). This indicated that stress factors due to conditions may negatively impact cell health, which was observed

in previous studies (Bow et al., 2019). As such, cell seeded scaffolds were exposed to growth media lacking osteo-differentiation additives. Media was refreshed every 2-3 days.

Quantitative analysis of Calcein-AM fluorescent staining was performed as previously described (Jackson et al., 2018) to determine cellular proliferation and viability on the scaffolds. Briefly, cell-seeded scaffolds were cultured in black-walled 24-well plates, preventing light refraction across wells during reading, and assessed in triplicate at 3, 5, and 7 days of growth. Samples were incubated in 0.5 mL staining solution, containing 2 µg/ml calcein-AM dimethyl sulfoxide mix in HBSS, at 37 °C for 5 minutes. Fluorescence intensity was quantitated using a plate reader set-up with an excitation wavelength of 485 nm and an emission wavelength of 528 nm. Normalized average fluorescent intensity values from each time point were plotted to generate a cellular proliferation curve.

Calcein-AM staining demonstrated an increased fluorescent intensity in cell-seeded scaffolds at day 7 that was significantly greater than days 3 and 5 (**Figure 6.1**). This increase over time indicates that scaffolds are cytocompatible.

Cytocompatibility

Cell adhesion and morphology on 3D scaffolds was assessed *in vitro* using previously described methods (Bow et al., 2019). Visualization of changes in cell morphology was performed using the fluorescent cytoplasmic stain, DiI. Cells seeded on scaffolds were compared to polystyrene tissue-culture dish controls, with cell-void scaffolds in media acting as negative controls.

In vitro evaluation of DiI stained cells demonstrated that cells adhered to the 3D scaffolds and exhibited clustering dynamics within 5-7 days of seeding, suggesting osteogenic differentiation (**Figure 6.2**). Cell behavior was similar to our observations on 2D PU/nHA films as described earlier (Jackson et al., 2018). Cells adhered and formed clusters on the 3D scaffolds within 5 days of seeding and in the absence of any differentiating reagents (dexamethasone, beta glycerophosphate and ascorbic acid). Monitoring of cellular morphology and proliferation through fluorescent microscopy demonstrated cell adhesion and supports cytocompatibility of the materials. Additionally, as described earlier, the mineral components of the scaffolds prevented the use of alizarin red and alkaline phosphatase staining, to demonstrate osteogenesis. Hence, morphological observations and analysis of gene expression were used for *in vitro* evaluation of scaffolds.

Transcriptomics

PCR Profiler Microarrays

Total RNA was extracted from the cell/scaffold constructs 5 days post seeding as described previously (Bow et al., 2019) and was analyzed for the expression of genes relating to osteogenesis and signal transduction (Ullah et al., 2013). Total RNA isolation was performed with Trizol extraction agent

(ThermoFisher) as per the manufacturer's protocol with modifications to increase the yield of RNA (Lee et al., 2018). cDNA was prepared using a Qiagen First Strand cDNA reverse transcription kit (Qiagen). A housekeeping RT^2 Profiler array (Qiagen) was used to ensure that the quality of isolated RNA.

Expression was then evaluated using Qiagen RT^2 Profiler arrays for human osteogenesis (PAHS-026Z) and signal transduction (PAHS-014Z) with 2ug of total RNA per array with approximately 20.8ng cDNA per PCR reaction, with samples run in triplicate.

Data Correlation

Relative fold differences in the gene expression and corresponding significance values were generated through Qiagen data center (https://www.qiagen.com/us/shop/genes-and-pathways/data-analysis-center-overview-page/). Expression of cells seeded on scaffold constructs for 5 days was compared to cell monolayers differentiated on polystyrene substrates for 21 days with osteo-differentiation media (Jackson et al., 2018).

Established techniques using cells cultured for 21 days with osteo-differentiation media were used as a positive control to assess cells seeded onto scaffolds and cultured for 5 days. RNA expression was compared using PCR evaluation of RNA, extracted and isolated from these cell cultures, and was carried out utilizing Qiagen RT^2 Profiler arrays for human osteogenesis and signal transduction pathways. Resulting expression fold changes and significance data between genes for samples were generated through Qiagen data center (https://www.qiagen.com/us/shop/genes-and-pathways/data-analysis-center-overview-page/). Fold change values and representative heatmaps for each array type are presented in **Figure 6.3**. Significantly upregulated genes, as designated by Qiagen Data Center output for genes with expression fold differences greater than 2, and their associated functions can be viewed in **Tables 6.1-6.4**. Notably, expression of RUNX2, an essential gene in regulating bone formation and remodeling, did not significantly differ from cell controls stimulated through well-characterized differentiation agents toward osteo-lineage. Furthermore, data from signal transduction arrays showed enhanced expression of genes related to oxidative stress, Notch, Hedgehog (HH), and hypoxia signaling pathways.

Metabolomics

LC-MS Analysis

Metabolite relative abundance profiles for cells exposed to scaffolds were compared with cell- and material-based controls to determine variations among groups. hMSCs seeded on material scaffolds for 5 days were compared to cell monolayers cultured on polystyrene substrates with and without osteo-differentiation media additives to evaluate concentration differences associated with the examined nanocomposite. Additionally, acellular scaffold samples both

exposed and not exposed to growth media were implemented to address metabolites attributed to the basal scaffold or media additives. Samples, in triplicate, were collected by scaping wells, adding HBSS, and pelleting suspended samples. Pellets were isolated and weighed before storage at -80°C with cell monolayer, dry material blanks, media-exposed material blanks, and cell-seeded material samples having weight ranges of 16.53-25.64mgs, 30.14-50.37mgs, 92.08-175.82mgs, and 165.30-191.71mgs respectively. Once all the samples were collected, the metabolites were extracted using a 20:40:40 solution of water/methanol/ acetonitrile with 0.1M formic acid following the procedure previously reported Lu, W. et al. 2008. Samples were sent to the Biological and Small Molecule Mass Spectrometry Core and the Department of Chemistry at the university of Tennessee, Knoxville for processing. Samples were reconstituted in ultrapure water and then ran on a liquid chromatography-mass spectrometer (LC-MS); they were separated on a Phenomonex Synergi Hydro RP column (100 mm x 2.0mm, 2.5 µm pore size, Phenomonex, Torrance, CA) using ultra high-pressure liquid chromatography. The mobile phases used to elute the metabolites were A) 97:3 water/methanol with 11mM tributyl amine and 15 mM acetic acid; and B) methanol. The 26-minute gradient, adapted from Lu, W. et al. 2010**,** was used with a flow rate of 0.2 mL/min. The gradient was as follows: 0 minutes, 0% B; 5 minutes, 20% B; 13 minutes, 55% B; 15.5 minutes, 95% B; 19 minutes, 0% B; 25 minutes, 0% B. The Exactive Plus Oribtrap Mass Spectrometer (Thermo Fisher Scientific, Waltham, MA) operated in negative mode with an electrospray ionization (ESI) probe; the scan range was set from 72 to 1,200 m/z while resolution was set to 140,000; the capillary temperature was set to 300°C. Once the raw files were obtained from the MS, the files were converted to mzML using an open source file converter. The mzML files were loaded into Metabolomic Analysis and Visualization Engine (MAVEN) where metabolites were chosen based on peak shape and signal-to-noise ratio. Metabolite intensities were recorded and normalized to sample weight.

Metabolite Data Analysis

Formatted data was uploaded to Metaboanalyst, an online metabolomic statistical analysis tool, to evaluate statistically significant variations among samples groups and generate visual representative figures. Partial least squares discriminant analysis (PLS-DA) performed on samples groups demonstrates similarity of within groups and significance between groups. Post-analysis heat maps offer a visual representation of metabolite variation that drive group differences in PLS-DA plot. Literature sources and KEGG database were then used to correlate detected metabolites and relative concentrations to potential metabolic pathways.

Assessment of small molecule abundance profiles utilizing sparse partial least squares discriminant analysis (sPLS-DA) showed that all samples groups were discrete and unique, with intra-group samples forming tight clusters. When comparing all study groups, it was determined that 18 metabolites were

significantly responsible for driving the separation of sample groups; however, separation of study groups into cell-oriented, hMSC monolayers with and with osteo-differentiation media addititves, and material-oriented, acellular scaffolds exposed and unexposed to growth media, sub-sets permitted more relevant comparisons due to initial sample characteristics, primarily weight and culture size. Sub-set groups both maintained the hMSC-seeded scaffold samples. Though groups remained discrete and unique when examined with sPLS-DA, it was observed that the metabolites responsible for the distinct grouping varied in both number and significance with 21 metabolites for cell-oriented and 15 metabolites for material-oriented samples (**Figures 6.4-6.5**). Generation of corresponding heatmaps for cell-oriented and material-oriented groups was performed by normalizing hMSC-seeded scaffolds to sub-group-specific controls, undifferentiated hMSC monolayers and acellular scafflds unexposed to growth media (**Figure 6.6**). The resulting heatmaps were assessed for metabolites of interest (MoIs), metabolites that may serve as corollary links to cellular and material mechanisms. For cell-oriented sub-set groups, comparisons in which both cell monolayers exposed to differentiation agents and cells seeded to scaffolds exhibited higher concentration than control samples, as well as those in which cell-seeded scaffolds alone displayed superior concentration, were selected as MoIs. The first of these relations being potentially indicative of an osteo-differentiation-related metabolite, and the second representing a scaffold-related metabolite. Similarly, MoIs from material-oriented sub-set groups were selected if a metabolite concentration was significantly different in cell-seeded scaffold samples compared to one or both control groups to examine changes due to cellular activity on constructs. Metabolites that demonstrated an increase in concentration in scaffold samples exposed to media as compared to dry scaffold samples were considered to be associated with components of media and were therefore not further examined.

Fundamental Pathway Development

Pathway Correlation Databases

Evaluation of molecular impact of the scaffold material on exposed cells was conducted through use of both IMPaLA (http://impala.molgen.mpg.de/) and the DAVID (https://david.ncifcrf.gov/) online software tools, with gene and metabolite inputs entered using Entrez IDs and KEGG IDs respectively.

For IMPaLA assessment, the detected metabolites were cross-examined with the up-regulated genes identified in osteogenic and signal transduction arrays. The generated list of pathways consists of pathway names, database source for pathway information, target genes involved in pathway, and target metabolites involved in pathway. Manual selection was performed to develop a discrete collection of pathways of interest (PoIs). PoIs containing greater numbers of target genes/metabolites were considered to be more relevance to material impact.

DAVID assessment was then performed for pathway enrichment based on functional categories, gene ontology, pathways, protein domains, and tissue expression characteristics based on the default statistical parameters (Dennis et al., 2003; Huang, Sherman, & Lempicki, 2008). Resulting PoIs are then divided into clusters based on pathway enrichment significance.

PoI collections generated through IMPaLA software can be observed in **Table 6.5**. Highly ranked PoIs for samples were largely associated with metabolic and signaling functions, including extracellular matrix organization and cell differentiation pathways. PoIs selected from clusters lists, created utilizing DAVID, are displayed in **Table 6.6** with pathway enrichment score, number of overlapping genes, and significance values. These generated PoIs demonstrate significant impact on bone mineralization, osteoblast differentiation, and osteoclast differentiation, which supports the osteogenic potential of the scaffold. Furthermore, cell signaling pathways, such as BMP signaling and cell-cell junction organization, compliment IMPaLA output and suggest that scaffolds facilitate cellular attachment and communication in addition to osteobiologic functions.

Network Mapping Software

Visualization of pathway connections for both gene and metabolite elements were facilitated through the use of CPDB (http://cpdb.molgen.mpg.de/). Network map construction using CPDB was used to illustrate intra-omic connection based on gene expression and metabolite concentration data respectively.

Observational assessment of intra-omic networks for gene expression and metabolite concentration data individually through CPDB demonstrated elements associated with osteogenic and cellular attachment functions (**Figures 6.7-6.8**). As in IMPaLA and DAVID assessments, CPDB generated for transcriptomic and metabolomic data demonstrate pathways closely associated with osteogenesis and cellular attachment. Mapped transcriptomic data (**Figure 6.7**) include pathways for cell differentiation, BMP signaling, and osteoclast differentiation, as well as extracellular matrix organization and focal adhesion pathways, and is reinforced by detection of fundamental metabolism functions and mineral absorption pathways through small molecule assessment with CPDB (**Figure 6.8**).

Conclusion

As expected, based on previous *in vitro* and *in vivo* studies, the 3D nanocomposite scaffold comprised of nHA/PU films interspersed with layers of DBPs, was cytocompatible with human adipose-derived MSCs. To elucidate the underlying mechanisms of this material, a combinatorial approach of transcriptomics and metabolomics was utilized. The scaffold demonstrated significant up-regulation of genes closely associated with osteogenesis and indicated that a combined interaction of multiple pathways may be responsible for the osteobiologic characteristics exhibited by the material (**Figure 6.9**). Specifically, the interaction of Hedgehog, Wnt, and BMP signaling pathways appear to play a crucial role in

stimulating exposed cells (Li et al., 2015). Members of the BMP family have been strongly correlated with osteogenesis and mineralization, in particular BMP-2/4/6/7, though recruitment of Smad 1/5/8, which interacts with Smad 4 to regulate gene expression. Up-regulation of BMP-2/4/6/7, BMP receptors, and Smad 1/4/5 may therefore provide evidence for activation of this pathway (Beederman et al., 2013; Wang et al., 2014). Additionally, coordination of this BMP signaling with both Wnt and Hedgehog signaling pathways are indicated by increased expression of essential pathway elements including PTCH1, Gli1, and Wnt5A (James et al., 2012). Hedgehog, as well as Notch, signaling mechanisms have been previously demonstrated to have vital roles in bone remodeling and development through modulation of osteoblast and osteoclast activity (Regan & Long, 2013; Yang, Andre, Ye, & Yang, 2015). The described pathways culminate in up-regulation of vital transcription factors, RUNX2 and Sp7, shown to elicit pro-osteogenic and anti-adipogenic characteristics (Chi, Liu, Xing, & Tian, 2016; James, 2013). This results in the enhanced production of key proteins for OB differentiation and ossification, including SPP1 and BGLAP (Hishida, Nishizuka, Osada, & Imagawa, 2009), both of which were up-regulated. As the expression of RUNX2 is similar between material-seeded cells and osteo-differentiated cultures, expression difference in other osteo-related targets may represent the mechanisms by which scaffold induces exposed cells toward an osteogenic lineage in 5 days. Furthermore, hypoxia signaling and oxidative stress may also play important roles in facilitating the osteo-inductive capacity of the scaffold, as these have been linked to skeletal development and bone promoting functions. Hypoxia signaling has been shown to have a role in the formation of endochondral bone, as well as the potential to modulate bone formation through manipulation of oxygen sensing (Yellowley & Genetos, 2019); while oxidative stress, relating to an imbalance between generated radical oxygen species (ROS) and available counteracting antioxidants, has demonstrated substantial influence on bone remodeling functions through suppression of osteoblast activity, temporarily reducing mineralization capacity and promoting resorption dynamics (Domazetovic, Marcucci, Iantomasi, Brandi, & Vincenzini, 2017). These data combined with the up-regulation of genes associated with cellular attachment functions, including cell-cell and cell-extracellular matrix (ECM) adhesion/communication mechanisms, indicate that scaffold constructs facilitate cellular infiltration, attachment, and proliferation with subsequent stimulation of osteogenesis.

By correlating the transcriptomic data with detected metabolite concentrations in cell-seeded scaffolds, fundamental pathways were constructed that appear to further support the function of scaffolds as osteogenic platforms. Particularly the detection of ascorbate, a small molecule strongly associated with osteogenesis, in scaffold samples at markedly lower concentrations than those in scaffold blanks may indicate utilization of the metabolite by seeded cells. Xanthine concentration levels detected in cell-seeded scaffolds may also correlate to upregulation of oxidative stress pathway genes. Importantly, overlay of multi-omic data through IMPaLA software revealed that overlapping regions between gene

expression and metabolite concentrations were related to primarily cellular metabolism and signaling functions, which demonstrates that scaffolds are capable of facilitating cell-cell communication and supporting intricate intra-structural cell networks.

As expected, the results of this study demonstrate that the scaffold material is both biocompatible and maintains osteogenic properties. Evaluation of the transcriptional landscape for scaffold exposed hMSCs as compared with cells differentiated on polystyrene further indicated this osteogenic potential in the up-regulation of expression in genes strongly associated with pro-osteogenic and cell attachment functions. Fundamental pathway analysis of expression data revealed interactions among BMP, HH, and Wnt signaling mechanism as primary candidates for the osteobiologic characteristics of the material. Among these, HH appears to play a particularly crucial role, and thus will be the target of future studies, which will implement HH-specific PCR profiler arrays (Qiagen) and inhibition assays to elucidate precise mechanisms.

The pro-osteogenic potential of the scaffold indicates that it may serve as an effective scaffold for both long and flat bone injuries, as it is capable of facilitating cellular in-growth and subsequent ossification. Further evaluation of scaffolds as delivery vehicles for drug and cell-based treatments are expected to yield enhanced osteobiologic graft treatments. Furthermore, application of similar experimental approaches for tissue samples from *in vivo* analyses of this material may provide invaluable insight as to its impact on native tissue, which is essential for translation to clinical applications.

References

Agrawal, C. M., & Ray, R. B. (2001). Biodegradable polymeric scaffolds for musculoskeletal tissue engineering. *J Biomed Mater Res, 55*(2), 141-150.

Albrektsson, T., & Johansson, C. (2001). Osteoinduction, osteoconduction and osseointegration. *Eur Spine J, 10 Suppl 2*, S96-101. doi:10.1007/s005860100282

Alghazali, K. M., Newby, S. D., Nima, Z. A., Hamzah, R. N., Watanabe, F., Bourdo, S. E., . . . Biris, A. S. (2017). Functionalized gold nanorod nanocomposite system to modulate differentiation of human mesenchymal stem cells into neural-like progenitors. *Sci Rep, 7*(1), 16654. doi:10.1038/s41598-017-16800-9

Araujo, R., Carneiro, T. J., Marinho, P., da Costa, M. M., Roque, A., da Cruz, E. S. O. A. B., . . . Gil, A. M. (2019). NMR metabolomics to study the metabolic response of human osteoblasts to non-poled and poled poly (L-lactic) acid. *Magn Reson Chem*. doi:10.1002/mrc.4883

Beederman, M., Lamplot, J. D., Nan, G., Wang, J., Liu, X., Yin, L., . . . He, T. C. (2013). BMP signaling in mesenchymal stem cell differentiation and bone formation. *J Biomed Sci Eng, 6*(8a), 32-52. doi:10.4236/jbise.2013.68A1004

Bow, A. J., Newby, S., Rifkin, R., Jackson, B., Matavosian, A., Griffin, C., . . . Dhar, M. (2019). Evaluation of a polyurethane platform for delivery of nanohydroxyapatite and decellularized bone particles in a porous three-dimensional scaffold. *ACS Applied Bio Materials*. doi:10.1021/acsabm.8b00670

Chi, B., Liu, G., Xing, L., & Tian, F. (2016). [RESEARCH PROGRESS OF Hedgehog SIGNALING PATHWAY IN REGULATING BONE FORMATION AND OSTEOGENIC DIFFERENTIATION OF BONE MESENCHYMAL STEM CELLS]. *Zhongguo Xiu Fu Chong Jian Wai Ke Za Zhi, 30*(12), 1545-1550. doi:10.7507/1002-1892.20160318

Dennis, G., Sherman, B. T., Hosack, D. A., Yang, J., Gao, W., Lane, H. C., & Lempicki, R. A. (2003). DAVID: Database for Annotation, Visualization, and Integrated Discovery. *Genome Biology, 4*(9), R60. doi:10.1186/gb-2003-4-9-r60

Domazetovic, V., Marcucci, G., Iantomasi, T., Brandi, M. L., & Vincenzini, M. T. (2017). Oxidative stress in bone remodeling: role of antioxidants. *Clin Cases Miner Bone Metab, 14*(2), 209-216. doi:10.11138/ccmbm/2017.14.1.209

Gao, C., Peng, S., Feng, P., & Shuai, C. (2017). Bone biomaterials and interactions with stem cells. *Bone Research, 5*, 17059. doi:10.1038/boneres.2017.59

Garcia-Gareta, E., Coathup, M. J., & Blunn, G. W. (2015). Osteoinduction of bone grafting materials for bone repair and regeneration. *Bone, 81*, 112-121. doi:10.1016/j.bone.2015.07.007

Hasan, A., Byambaa, B., Morshed, M., Cheikh, M. I., Shakoor, R. A., Mustafy, T., & Marei, H. E. (2018). Advances in osteobiologic materials for bone substitutes. *Journal of Tissue Engineering and Regenerative Medicine, 12*(6), 1448-1468. doi:10.1002/term.2677

Hishida, T., Nishizuka, M., Osada, S., & Imagawa, M. (2009). The role of C/EBPdelta in the early stages of adipogenesis. *Biochimie, 91*(5), 654-657. doi:10.1016/j.biochi.2009.02.002

Huang, D. W., Sherman, B. T., & Lempicki, R. A. (2008). Systematic and integrative analysis of large gene lists using DAVID bioinformatics resources. *Nature Protocols, 4*, 44. doi:10.1038/nprot.2008.211 https://www.nature.com/articles/nprot.2008.211#supplementary-information

Jackson, B. K., Bow, A. J., Kannarpady, G., Biris, A. S., Anderson, D. E., Dhar, M., & Bourdo, S. E. (2018). Polyurethane/nano-hydroxyapatite composite films as osteogenic platforms. *J Biomater Sci Polym Ed, 29*(12), 1426-1443. doi:10.1080/09205063.2018.1464264

James, A. W. (2013). Review of Signaling Pathways Governing MSC Osteogenic and Adipogenic Differentiation. *Scientifica (Cairo), 2013*, 684736. doi:10.1155/2013/684736

James, A. W., Pang, S., Askarinam, A., Corselli, M., Zara, J. N., Goyal, R., . . . Soo, C. (2012). Additive effects of sonic hedgehog and Nell-1 signaling in osteogenic versus adipogenic differentiation of human adipose-derived stromal cells. *Stem Cells Dev, 21*(12), 2170-2178. doi:10.1089/scd.2011.0461

Lee, S. J., Yi, T., Ahn, S. H., Lim, D. K., Kim, S. N., Lee, H. J., . . . Kwon, S. W. (2018). Comparative study on metabolite level in tissue-specific human mesenchymal stem cells by an ultra-performance liquid chromatography

quadrupole time of flight mass spectrometry. *Anal Chim Acta, 1024*, 112-122. doi:10.1016/j.aca.2018.04.018

Li, L., Dong, Q., Wang, Y., Feng, Q., Zhou, P., Ou, X., . . . Luo, J. (2015). Hedgehog signaling is involved in the BMP9-induced osteogenic differentiation of mesenchymal stem cells. *Int J Mol Med, 35*(6), 1641-1650. doi:10.3892/ijmm.2015.2172

Lu, W., Bennett, B. D., & Rabinowitz, J. D. (2008). Analytical strategies for LC–MS-based targeted metabolomics. *Journal of Chromatography B, 871*(2), 236-242. doi:https://doi.org/10.1016/j.jchromb.2008.04.031

Lu, W., Clasquin, M. F., Melamud, E., Amador-Noguez, D., Caudy, A. A., & Rabinowitz, J. D. (2010). Metabolomic Analysis via Reversed-Phase Ion-Pairing Liquid Chromatography Coupled to a Stand Alone Orbitrap Mass Spectrometer. *Analytical Chemistry, 82*(8), 3212-3221. doi:10.1021/ac902837x

Majidinia, M., Sadeghpour, A., & Yousefi, B. (2018). The roles of signaling pathways in bone repair and regeneration. *J Cell Physiol, 233*(4), 2937-2948. doi:10.1002/jcp.26042

Regan, J., & Long, F. (2013). Notch signaling and bone remodeling. *Curr Osteoporos Rep, 11*(2), 126-129. doi:10.1007/s11914-013-0145-4

Schrimpe-Rutledge, A. C., Codreanu, S. G., Sherrod, S. D., & McLean, J. A. (2016). Untargeted Metabolomics Strategies-Challenges and Emerging Directions. *J Am Soc Mass Spectrom, 27*(12), 1897-1905. doi:10.1007/s13361-016-1469-y

Ullah, M., Sittinger, M., & Ringe, J. (2013). Extracellular matrix of adipogenically differentiated mesenchymal stem cells reveals a network of collagen filaments, mostly interwoven by hexagonal structural units. *Matrix Biol, 32*(7-8), 452-465. doi:10.1016/j.matbio.2013.07.001

Wang, R. N., Green, J., Wang, Z., Deng, Y., Qiao, M., Peabody, M., . . . Shi, L. L. (2014). Bone Morphogenetic Protein (BMP) signaling in development and human diseases. *Genes & Diseases, 1*(1), 87-105. doi:https://doi.org/10.1016/j.gendis.2014.07.005

Yang, J., Andre, P., Ye, L., & Yang, Y.-Z. (2015). The Hedgehog signalling pathway in bone formation. *International journal of oral science, 7*(2), 73-79. doi:10.1038/ijos.2015.14

Yellowley, C. E., & Genetos, D. C. (2019). Hypoxia Signaling in the Skeleton: Implications for Bone Health. *Curr Osteoporos Rep, 17*(1), 26-35. doi:10.1007/s11914-019-00500-6

Appendix

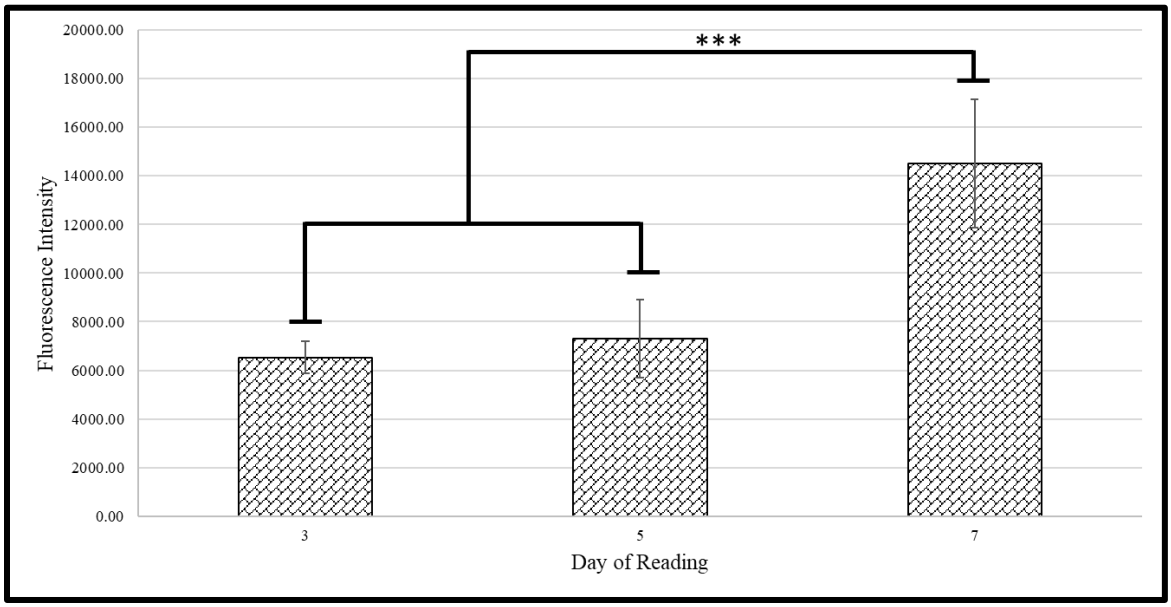

Figure 6.1. Calcein-AM proliferation assay conducted at day 3, 5, and 7 time points. Fluorescent intensity measurements output by plate reader are normalized to blank scaffold readings. The significant increase in fluorescence intensity between day 7 readings and previous time points is indicates by asterisks.

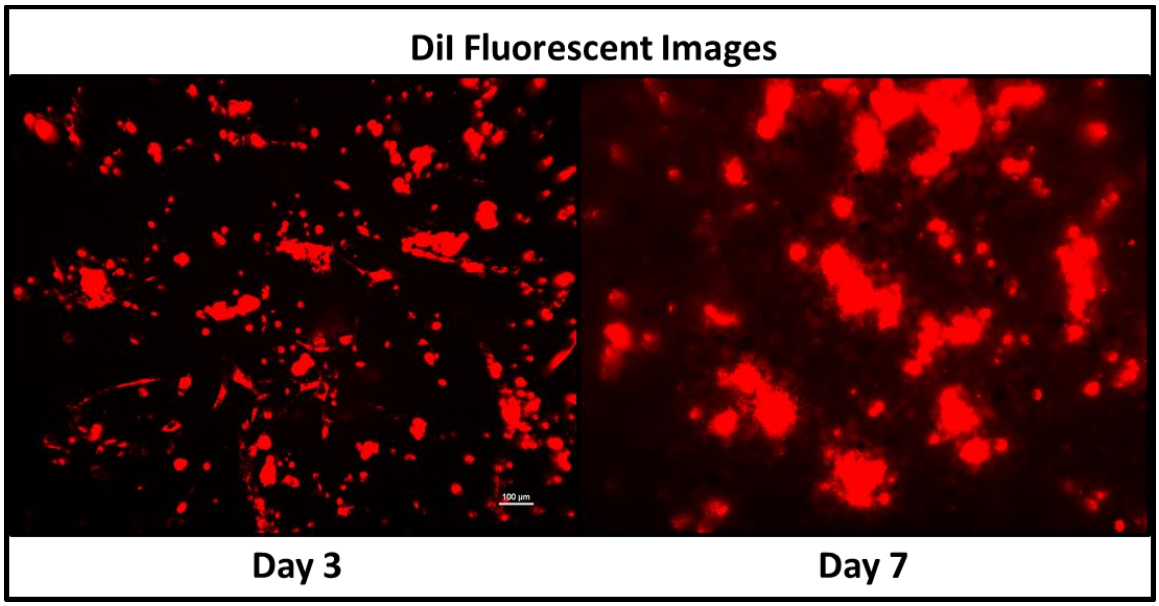

Figure 6.2. DiI fluorescent images of cells seeded to scaffolds at day 3 and 7 time points.

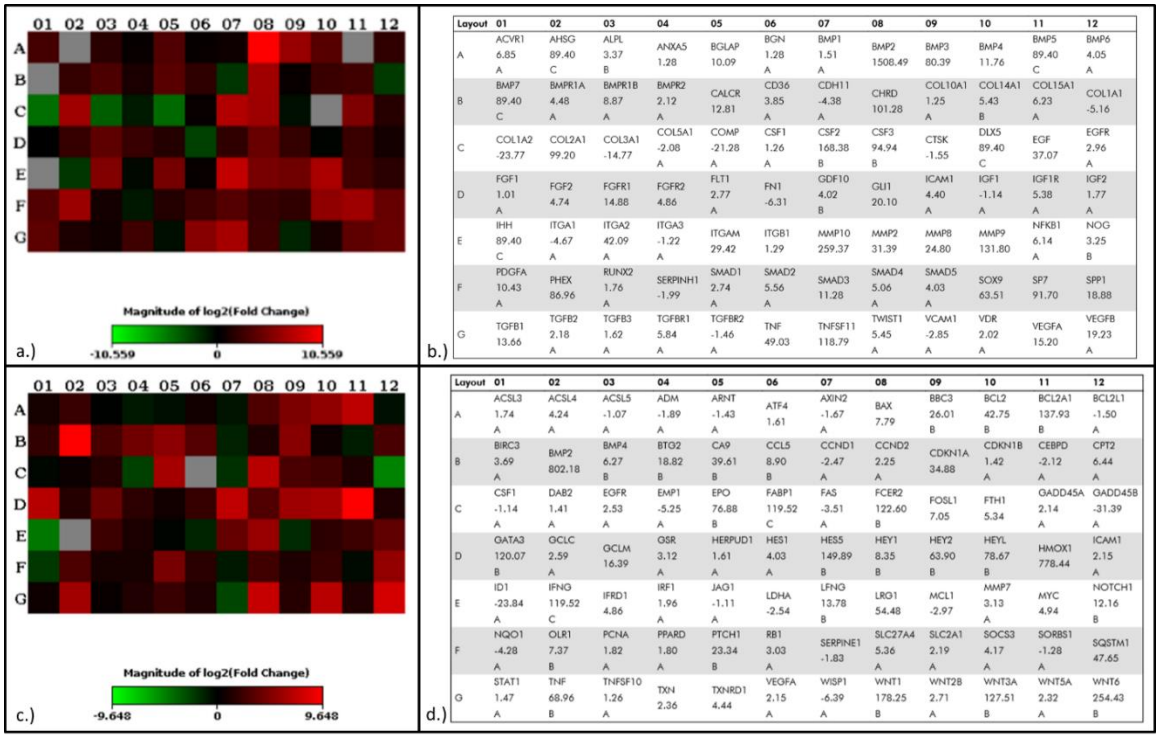

Layout	01	02	03	04	05	06	07	08	09	10	11	12
A	ACVR1 6.85 A	AHSG 89.40 C	ALPL 3.37 B	ANXA5 1.28	BGLAP 10.09	BGN 1.28 A	BMP1 1.51 A	BMP2 1508.49	BMP3 80.39	BMP4 11.76	BMP5 89.40 C	BMP6 4.05 A
B	BMP7 89.40 C	BMPR1A 4.48 A	BMPR1B 8.87 A	BMPR2 2.12 A	CALCR 12.81	CD36 3.85 A	CDH11 -4.38 A	CHRD 101.28	COL10A1 1.25 A	COL14A1 5.43 B	COL15A1 6.23 A	COL1A1 -5.16
C	COL1A2 -23.77	COL2A1 99.20	COL3A1 -14.77	COL5A1 -2.08 A	COMP -21.28 A	CSF1 1.26 A	CSF2 168.38 B	CSF3 94.94 B	CTSK -1.55	DIX5 89.40 C	EGF 37.07	EGFR 2.96 A
D	FGF1 1.01 A	FGF2 4.74	FGFR1 14.88	FGFR2 4.86	FLT1 2.77 A	FN1 -6.31	GDF10 4.02 B	GLI1 20.10	ICAM1 4.40 A	IGF1 -1.14 A	IGF1R 5.38 A	IGF2 1.77 A
E	IHH 89.40 C	ITGA1 -4.67 A	ITGA2 42.09 A	ITGA3 -1.22 A	ITGAM 29.42	ITGB1 1.29	MMP10 259.37	MMP2 31.39	MMP8 24.80	MMP9 131.80	NFKB1 6.14 A	NOG 3.25 B
F	PDGFA 10.43 A	PHEX 86.96	RUNX2 1.76 A	SERPINH1 -1.99	SMAD1 2.74 A	SMAD2 5.56 A	SMAD3 11.28	SMAD4 5.06 A	SMAD5 4.03 A	SOX9 63.51	SP7 91.70	SPP1 18.88
G	TGFB1 13.66	TGFB2 2.18 A	TGFB3 1.62 A	TGFBR1 5.84 A	TGFBR2 -1.46 A	TNF 49.03	TNFSF11 118.79	TWIST1 5.45 A	VCAM1 -2.85 A	VDR 2.02 A	VEGFA 15.20	VEGFB 19.23 A

Layout	01	02	03	04	05	06	07	08	09	10	11	12
A	ACSL3 1.74 A	ACSL4 4.24 A	ACSL5 -1.07 A	ADM -1.89 A	ARNT -1.43 A	ATF4 1.61	AXIN2 -1.67 A	BAX 7.79	BBC3 26.01 B	BCL2 42.75 B	BCL2A1 137.93 B	BCL2L1 -1.50 A
B	BIRC3 3.69 A	BMP2 802.18	BMP4 6.27 B	BTG2 18.82 B	CA9 39.61 B	CCL5 8.90 B	CCND1 -2.47 A	CCND2 2.25 A	CDKN1A 34.88	CDKN1B 1.42 A	CEBPD -2.12 A	CPT2 6.44 A
C	CSF1 -1.14 A	DAB2 1.41 A	EGFR 2.53 A	EMP1 -5.25 A	EPO 76.88 B	FABP1 119.52 C	FAS -3.51 A	FCER2 122.60 B	FOSL1 7.05	FTH1 5.34	GADD45A 2.14 A	GADD45B -31.39 A
D	GATA3 120.07 B	GCLC 2.59 A	GCLM 16.39	GSR 3.12 A	HERPUD1 1.61 A	HES1 4.03 A	HES5 149.89 B	HEY1 8.35 B	HEY2 63.90 B	HEYL 78.67 B	HMOX1 778.44	ICAM1 2.15 A
E	ID1 -23.84 A	IFNG 119.52 C	IFRD1 4.86	IRF1 1.96 A	JAG1 -1.11 A	LDHA -2.54	LFNG 13.78 B	LRG1 54.48	MCL1 -2.97	MMP7 3.13 A	MYC 4.94	NOTCH1 12.16 B
F	NQO1 -4.28 A	OLR1 7.37 B	PCNA 1.82 A	PPARD 1.80 A	PTCH1 23.34 B	RB1 3.03 A	SERPINE1 -1.83	SLC27A4 5.36 A	SLC2A1 2.19 A	SOCS3 4.17 A	SORBS1 -1.28 A	SQSTM1 47.65
G	STAT1 1.47 A	TNF 68.96 B	TNFSF10 1.26 A	TXN 2.36	TXNRD1 4.44	VEGFA 2.15 A	WISP1 -6.39 A	WNT1 178.25 B	WNT2B 2.71 A	WNT3A 127.51 B	WNT5A 2.32 A	WNT6 254.43 B

Figure 6.3. Heatmap (a,c) and gene primer layout with expression values (b,d) generated from human osteogenesis (a-b) and signal transduction arrays (c-d). Heatmaps utilize a Log2 scale and represent expression fold changes in cell-seeded materials relative to differentiated cell monolayers. Complimentary gene primer lists display numerical expression fold change values for heatmaps with associated rankings shown directly below values. Rankings are assigned via Qiagen Data Center processing and indicate the quality of the expression relationship based on cycle threshold (Ct) values of PCR runs. Primary attention was given to unranked and rank “A” genes, as these were most reliable values.

Table 6.1. List of up-regulated genes associated with human skeletal development, categorized by function.

Function	Gene	Fold Relation	Function	Gene	Fold Relation
Ossification	ACVR1	6.8474	Cartilage Condensation	BMPR1B	8.8697
	BGLAP	10.0949		COL2A1	99.1968
	BMP2	1508.4894		SOX9	63.5090
	BMP3	80.3869	Osteoclast Differentiation	BGLAP	10.0949
	BMP4	11.7579		TNF	49.0287
	BMP6	4.0527		TNFSF11	118.7861
	BMPR1A	4.4760	Osteoblast Differentiation	ACVR1	6.8474
	BMPR1B	8.8697		BGLAP	10.0949
	BMPR2	2.1222		BMP2	1508.4894
	CHRD	101.2812		BMP4	11.75.79
	COL2A1	99.1968		BMP6	4.0527
	EGFR	2.9599		BMPR1A	4.4760
	FGF2	4.7422		BMPR1B	8.8697
	FGFR2	4.8643		BMPR2	2.1222
	GDF10	4.0247		CHRD	101.2812
	GLI1	20.0967		FGF2	4.7422
	IGF1R	5.3848		FGFR2	4.8643
	MMP2	31.3898		GDF10	4.0247
	MMP8	24.7992		GLI1	20.0967
	MMP9	131.8014		NOG	3.2465
	NOG	3.2465		SMAD1	2.7363
	SMAD1	2.7363		SMAD3	11.2789
	SMAD3	11.2789		SP7	91.7025
	SOX9	63.5090		SPP1	18.8813
	SP7	91.7025		TWIST1	5.4474
	SPP1	18.8813	Other Skeletal Development Genes	ALPL	3.3688
	TGFB1	13.6632		FGFR1	14.8826
	TGFB2	2.1819		TGFBR1	5.8383
	TNFSF11	118.7861			
	TWIST1	5.4474			

Table 6.2. List of up-regulated genes associated with human bone mineral metabolism, categorized by function.

Function	Gene	Fold Relation
Bone Mineralization	ACVR1	6.8474
	BGLAP	10.0949
	BMP2	1508.4894
	BMP4	11.7579
	BMP6	4.0527
	BMPR1A	4.476
	BMPR1B	8.8697
	BMPR2	2.1222
	FGFR2	4.8643
	SMAD3	11.2789
	SOX9	63.509
	TGFB1	13.6632
	TWIST1	5.4474
Calcium Ion Binding & Homeostasis	BGLAP	10.0949
	CALCR	12.8073
	EGF	37.0711
	FGF2	4.7422
	MMP2	31.3898
	MMP8	24.7992
	TGFB1	13.6632
	VDR	2.0217

Table 6.3. List of up-regulated genes associated with human cell adhesion molecules, categorized by function.

Function	Gene	Fold Relation
Cell-Cell Adhesion	BMPR1B	8.8697
	COL14A1	5.4348
	COL2A1	99.1968
	EGFR	2.9599
	ICAM1	4.4042
	SOX9	63.5090
	TGFB1	13.6632
	TNF	49.0287
	TNFSF11	118.7861
Cell-ECM Adhesion	CD36	3.8519
	COL2A1	99.1968
	ITGA2	42.0944
	ITGAM	29.4233
	SMAD3	11.2789
Other Cell Adhesion Molecules	BGLAP	10.0949
	COL15A1	6.2285
	TNF	49.0287

Table 6.4. List of up-regulated genes from associated with human signal transduction pathways, categorize by function.

Function	Gene	Fold Relation	Function	Gene	Fold Relation
Hedgehog Signaling	BCL2	42.7478	TGFβ Signaling	IFRD1	4.8605
	BMP2	802.1775		MYC	4.9398
	BMP4	6.2670	WNT Signaling	FOSL1	7.0508
	PTCH1	23.3353		CCND2	2.2519
	WNT1	178.2524		MMP7	3.1335
	WNT2B	2.7090		MYC	4.9398
	WNT3A	127.5080	NFκB	BCL2A1	137.9286
	WNT5A	2.3205		BIRC3	3.6921
	WNT6	254.4276		CCL5	8.9039
Oxidative Stress	FTH1	5.3435		ICAM1	2.1452
	GCLC	2.5867		IFNG	119.5202
	GCLM	16.3866		TNF	68.9643
	GSR	3.1191	Notch Signaling	HES1	4.0309
	HMOX1	778.4413		HES5	149.8918
	SQSTM1	47.6513		HEY1	8.3462
	TXN	2.3583		HEY2	63.9015
	TXNRD1	4.4417		HEYL	78.672
Hypoxia Signaling	CA9	39.6096		LFNG	13.7794
	EPO	76.8751		NOTCH1	12.1631
	HMOX1	778.4413			
	SLC2A1	2.1852			
	VEGFA	2.1452			

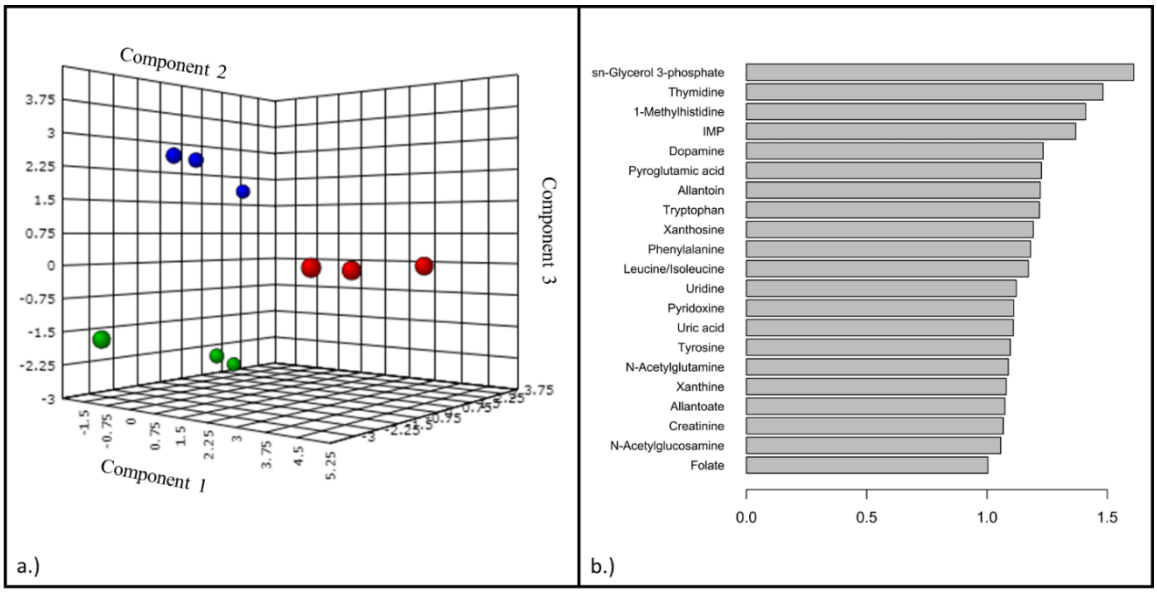

Figure 6.4. sPLS-DA plot and driving metabolites for cell-based group. sPLS-DA plot (a) demonstrating discrete cluster separation for metabolomic concentration assessment of cell-based subset group with differentiated (green) and undifferentiated (blue) hMSCs on tissue culture substrates compared to hMSC-seeded (red) scaffolds. 21 metabolites driving separation (b) observed in sPLS-DA plot.

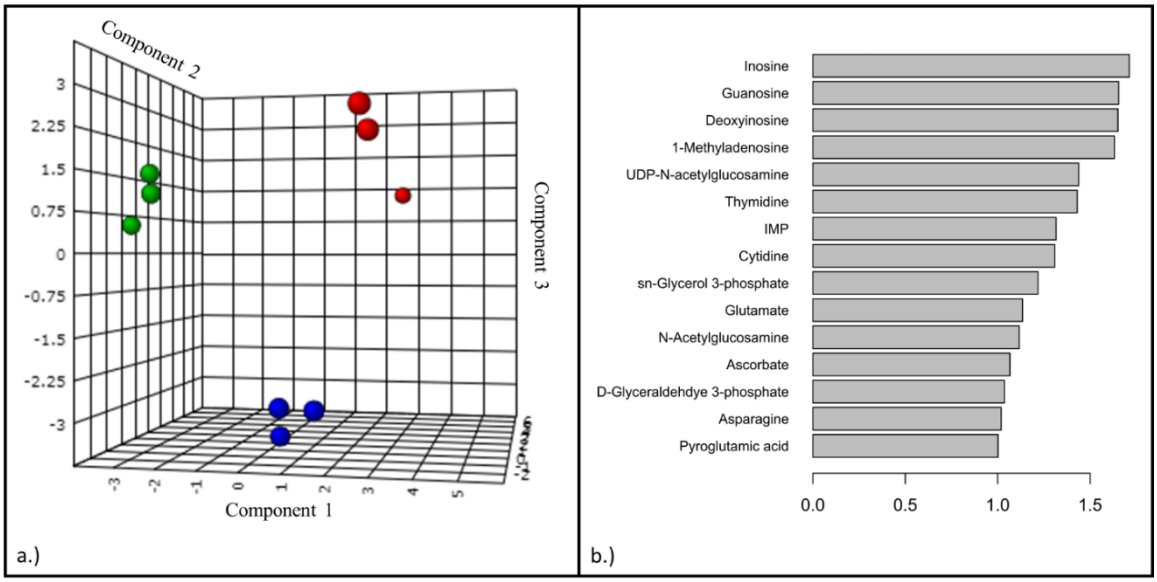

Figure 6.5. sPLS-DA plot and driving metabolites for material-based group. sPLS-DA plot (a) demonstrating discrete cluster separation for metabolomic concentration assessment of material-based subset group with dry (red) and media-exposed (green) scaffolds compared to hMSC-seeded (blue) scaffolds. 15 metabolites driving separation (b) observed in sPLS-DA plot.

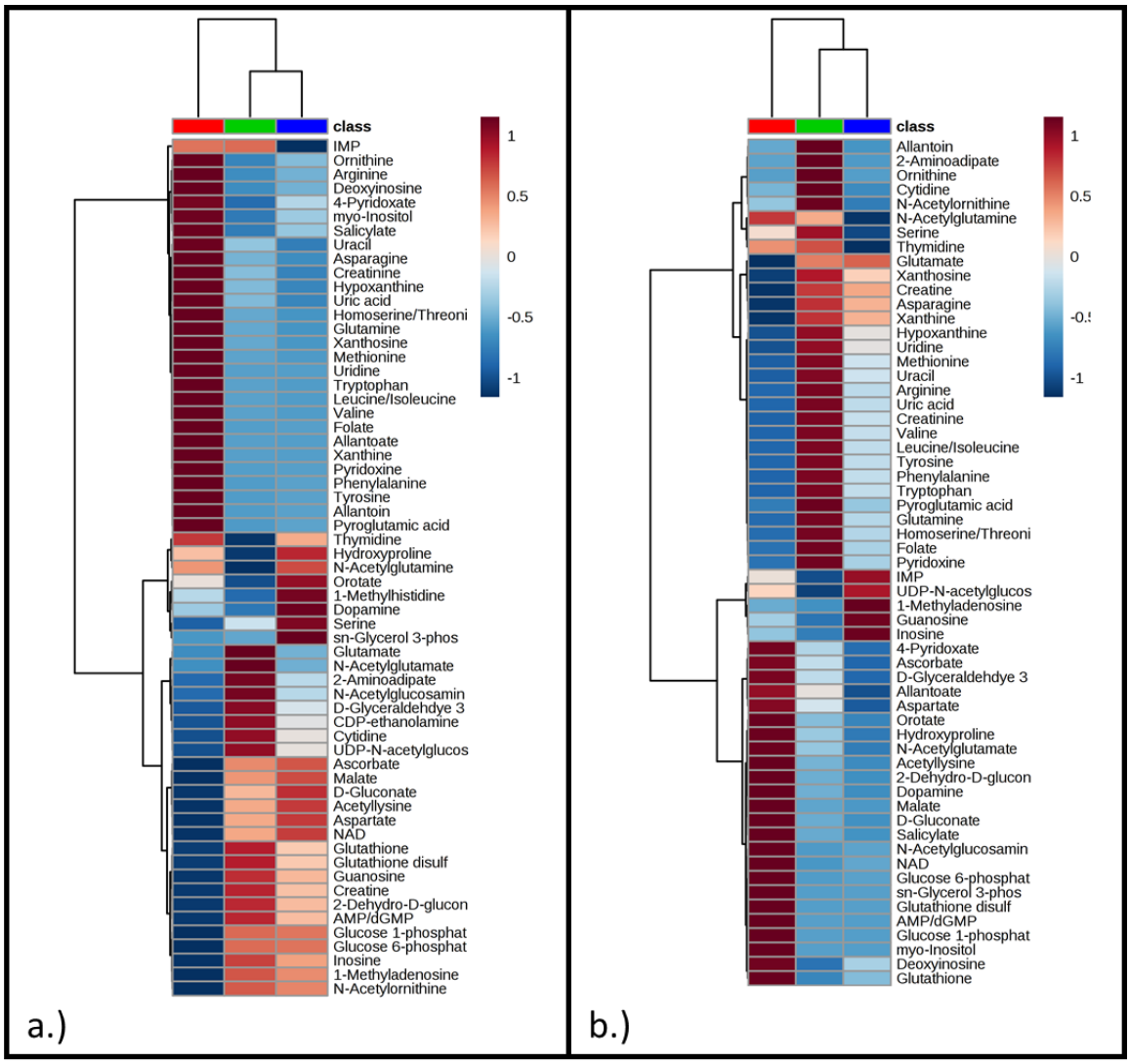

Figure 6.6. Heatmaps depicting metabolite abundance variations. Metabolite abundance variations among both cell-based (a), with differentiated (green) and undifferentiated (blue) hMSCs on tissue culture substrates compared to hMSC-seeded (red) scaffolds, and material-based (b) sub-set groups, with dry (red) and media-exposed (green) scaffolds compared to hMSC-seeded (blue) scaffolds. Log scale used for relative abundance is Log2.

Table 6.5. Pathways of interest list generated using IMPaLA software. Pathways are listed based on number of overlapping elements, both up-regulated genes and detected metabolite, in descending order. Source information for pathways is derived from KEGG, Reactome, and Wikipathways databases.

Pathway Name	Overlapping Genes	Overlapping Metabolites
Signal Transduction	TGFB1; BMP2; BMPR2; IGF1R; NOG; EGF; CALCR; PDGFA; EGFR; SPP1; NFκB; ITGA2; MMP9; BMPR1A; SMAD1; SMAD2; SMAD3; SMAD4; SMAD5; VEGFA; VEGFB	N-Acetylglucosamine; UDP-N-Acetylglucosamine; Dopamine; NAD+; Glutamate
Signaling by Receptor Tyrosine Kinases	PDGFA; EGFR; EGF; SPP1; FLT1; VEGFA; IGF1R; ITGA2; MMP9; VEGFB	NAD+
Signaling by TGF-beta Family Members	TGFB1; BMP2; SMAD2; BMPR1A; BMPR2; SMAD1; NOG; SMAD3; SMAD4; SMAD5	NAD+
Extracellular Matrix Organization	TGFB1; COL2A1; PDGFA; ITGAM; SPP1; BMP2; BMP4; ICAM1; ITGA2; MMP9	Ascorbate
Gene Expression (Transcription)	TGFB1; EGFR; BMP2; SMAD3; SMAD1; SMAD2; BGLAP; SMAD4; SP7; VEGFA	Glutathione Disulfide; Glutathione; Ascorbate; Glutamate; NAD+
Generic Transcription Pathway	TGFB1; EGFR; BMP2; SMAD3; SMAD1; SMAD2; BGLAP; SMAD4; SP7; VEGFA	Glutathione Disulfide; Glutathione; Glutamate; NAD+
Metabolism of Proteins	TGFB1; SPP1; BMP4; SMAD3: SMAD1; SMAD2; BGLAP; SMAD4; ALPL	Glucose 1-phosphate; Asparagine; Valine; Glutamate; NAD+; Inosine; N-Acetylglucosamine; UDP-N-Acetylglucosamine
Post-translational Protein Modification	TGFB1; SPP1; BMP4; SMAD3: SMAD1; SMAD2; BGLAP; SMAD4; ALPL	N-Acetylglucosamine; UDP-N-Acetylglucosamine; Glucose 1-phosphate; NAD+; Glutamate
Differentiation Pathway	TGFB1; PDGFA; BMP4; EGF; TNFSF11; NOG; VEGFA	Ascorbate
HIF-1 Signaling Pathway	EGFR; FLT1; EGF; NFκB; IGF1R; VEGFA	Ascorbate
Developmental Biology	SMAD3; ITGA2; SMAD4; EGFR; SMAD2	Glutamate
MAPK Family Signaling Cascades	PDGFA; EGFR; EGF	Glutamate
MAPK1/MAPK3 Signaling	PDGFA; EGFR; EGF	Glutamate
RAF/MAP Kinase Cascade	PDGFA; EGFR; EGF	Glutamate
Vitamin B12 Metabolism	NFκB; ICAM1	Ascorbate; NAD+; Creatinine
Signaling by NOTCH	EGFR; EGF	N-Acetylglucosamine; UDP-N-Acetylglucosamine
Collagen Formation	COL2A1; MMP9	Ascorbate
Signaling by GPCR	EGFR; CALCR	Dopamine; NAD+; Glutamate
GPCR Downstream Signaling	EGFR; CALCR	Dopamine; Glutamate; NAD+
Cellular Responses to External Stimuli	NFκB	Glutathione Disulfide; Glutathione; NAD+
Cellular Responses to Stress	NFκB	Glutathione Disulfide; Glutathione; NAD+
cAMP Signaling Pathway	NFκB	Dopamine
Collagen Biosynthesis and Modifying Enzymes	COL2A1	Ascorbate
Protein Digestion and Absorption	COL2A1	Asparagine; Valine; Glutamate

Table 6.6. Pathways of interest list generated using DAVID software for up-regulated genes from osteogenesis and signal transduction arrays. Pathways and associated overlapping genes and significance values are displayed. Benjamini scores represent a statistical correction of p-values to minimize false discovery rate.

Pathway	Overlapping Genes	p-value	Benjamini
TGF-beta Signaling Pathway	18	1.10E-17	1.60E-15
Cellular Response to BMP Stimulus	11	2.80E-16	1.20E-13
Positive Regulation of Pathway-restricted SMAD Protein Phosphorylation	12	9.30E-16	2.70E-13
BMP Signaling Pathway	13	5.40E-15	1.10E-12
Signaling Pathways Regulating Pluripotency of Stem Cells	18	9.10E-14	4.30E-12
Positive Regulation of Bone Metabolism	9	9.50E-12	1.00E-09
Positive Regulation of Osteoblast Differentiation	10	2.60E-11	2.30E-09
Extracellular Space	41	2.80E-22	4.10E-20
SMAD Protein Signal Transduction	12	2.00E-11	2.80E-12
Negative Regulation of Canonical Wnt Signaling Pathway	5	1.10E-02	9.70E-02
Growth Factor	14	1.40E-14	7.50E-13
Osteogenesis	5	1.90E-05	2.20E-04
Positive Regulation of Ossification	4	3.10E-05	6.20E-04
Osteoclast Differentiation	10	1.20E-05	1.20E-04
FOxO Signaling Pathway	10	1.50E-05	1.30E-04
Adherens Junction	7	1.20E-04	7.20E-04
Cell-cell Junction Organization	3	4.00E-03	4.10E-02
Angiogenesis	11	2.80E-07	9.00E-06

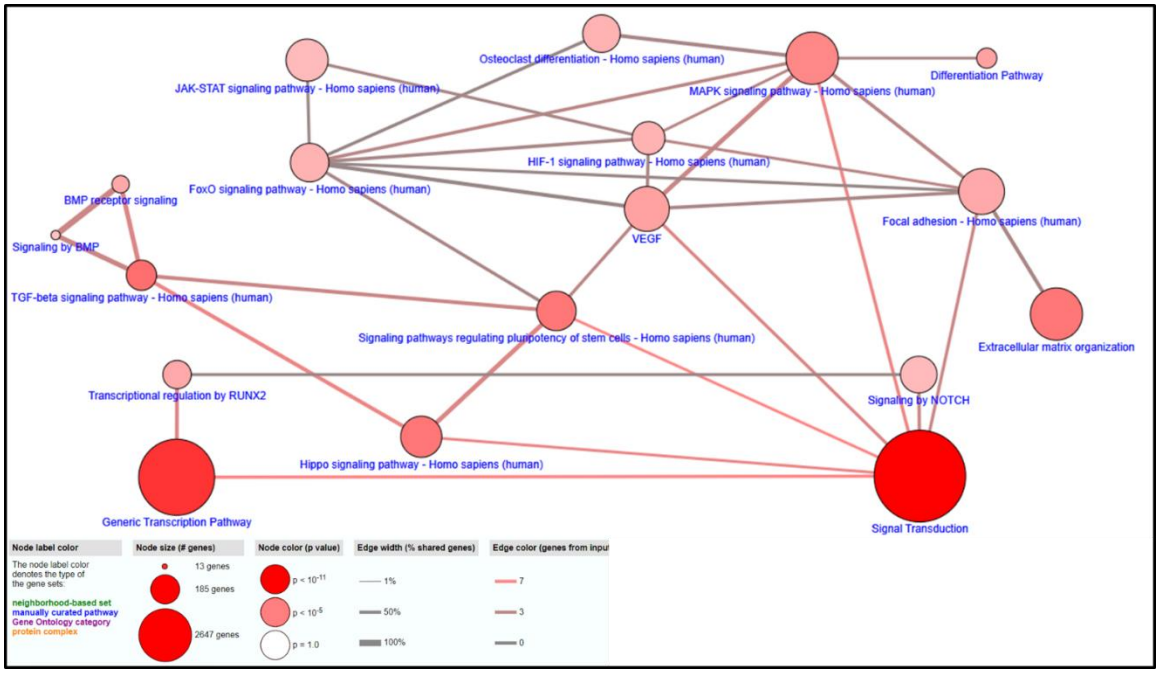

Figure 6.7. ConsensusPathDB network map generated from up-regulated osteogenesis and signal transduction array expression data. Pathway elements were selected from generated list based on significance (p-value<0.01) and relevance to utilized arrays. Pathway connective elements were filtered for at least a 0.15 overlap and 2 overlapping agents.

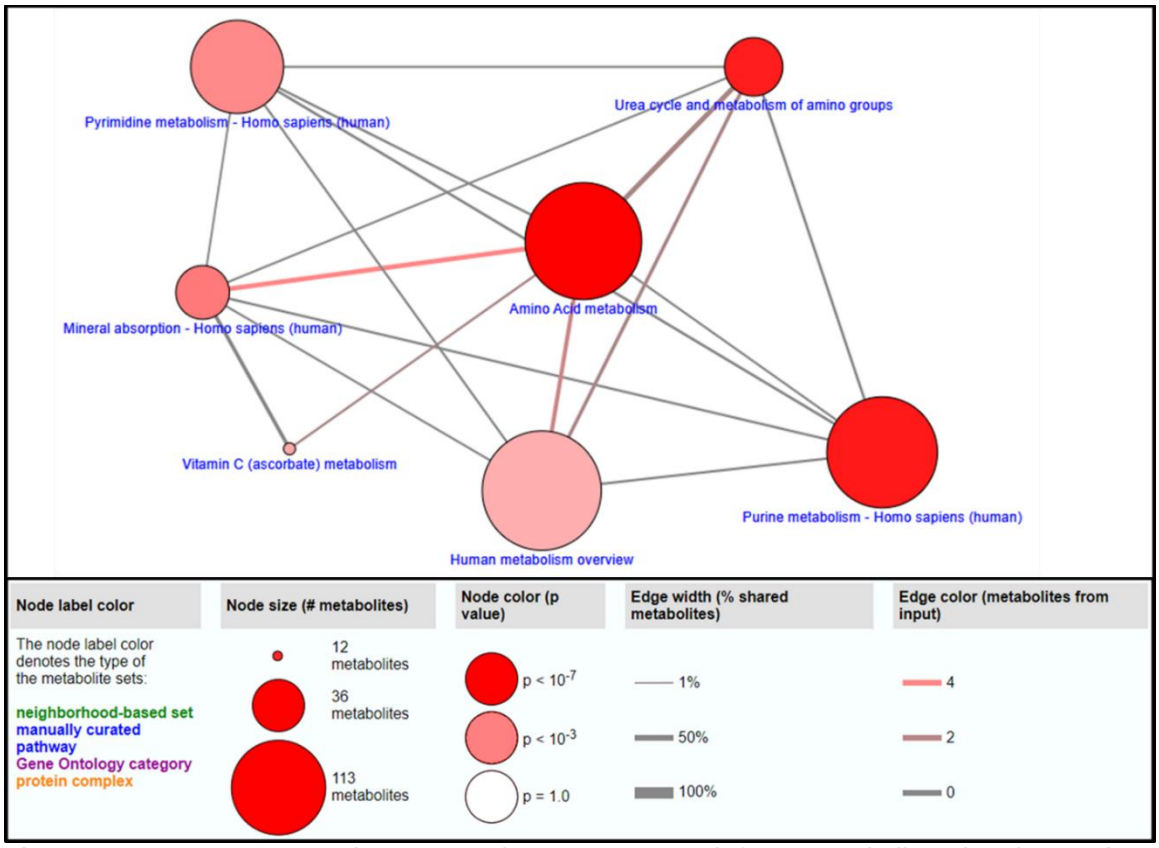

Figure 6.8. ConsensusPathDB network map generated from metabolite abundance data. Pathway elements were selected from overview based on significance (p-value<0.01).

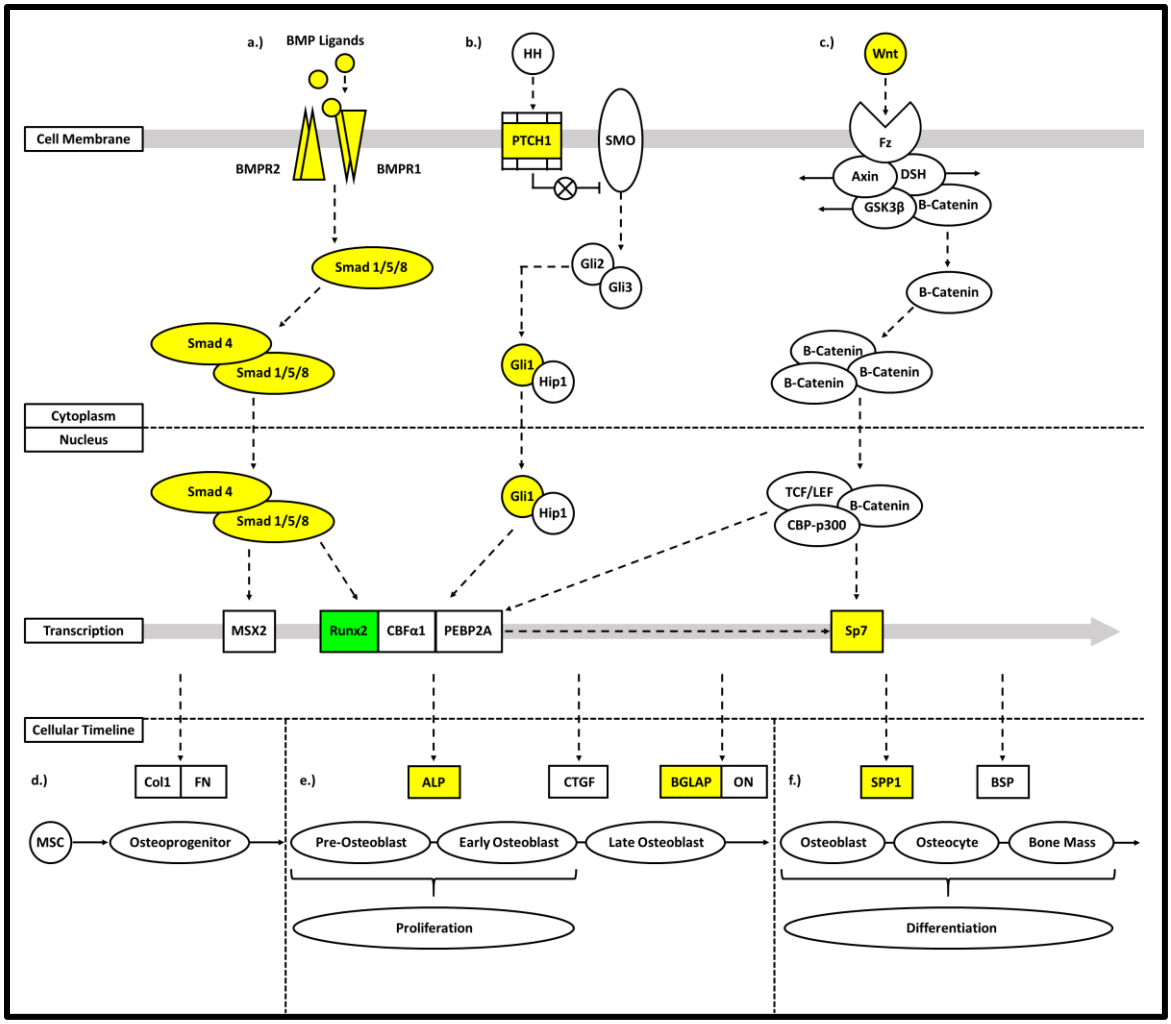

Figure 6.9. Osteogenic signal pathway interaction schematic. Pathways for BMP, HH, and Wnt signaling are shown with up-regulated genes highlighted in yellow and the similarly expressed Runx2 in green. a.) BMP ligands bind with BMP receptor subunits stimulating Smad 1/5/8 to couple with Smad 4. b.) HH binding to PTCH1 surface protein prevents inhibition of SMO, permitting production of Gli2/3 and subsequent transcription of Gli1 and Hip1. c.) Wnt interacting with Fz surface protein leads to release and subsequent accumulation of β-Cantenin, which then couples with TCF/LEF and CBP-p300. a-c.) BMP, HH, and Wnt pathways culminate in up-regulation of crucial osteogenic transcription factors including Runx2 and Sp7. d.) Naïve MSCs are stimulated via matrix proteins toward osteo-lineage and differentiate to osteoprogenitor cells expressing primary cell attachment proteins including collagen 1 (Col1) and fibronectin (FN). e.) Induction of osteoprogenitor cells by osteo-related transcription factors results in early maturation stages for osteoblastic (OB) cells promoting proliferation and expression of alkaline phosphatase protein (ALP). Late-stage development of OB cells show increased expression of osteocalcin (BGLAP) and osteonectin (ON) proteins. f.) Mature OBs demonstrate reduced proliferative characteristics and enhanced expression of osteopontin (SPP1) protein. Matrix mineralization through OB activity during differentiation toward osteocytes results in bone mass formation.

CHAPTER VII:
CONCLUSIONS AND FUTURE DIRECTION

Introduction

The work comprised in these chapters represents the extensive research conducted to examine the biological impact of a novel osteobiologic graft and its various iterations. A vital first step in this process was the development of basic cell culture work practices, which would lay the foundation for many of the crucial experimental steps to come. Initial work with MC 3T3-E1 cells provide invaluable experience and served as the basis for future work with multiple naïve primary cell lines. Observations of these immortalized cells also worked to establish a morphological baseline for cell monolayers on tissue-treated polystyrene surfaces prior to test element exposure. As shown in **Figure 7.1**, cell seeding density experiments were performed to assess the optimal density for cell controls in future experiments, comparing cell monolayers to material-seeded cells. This evaluation was comprised of morphological and proliferative assessment techniques using Calcein-AM staining and an MTS assays kit respectively.

Introduction of the early-stage iterations of the graft fabricated and provided by the collaborative research team at the University of Arkansas at Little Rock (UALR), polyurethane (PU) films impregnated with varying percentages of nano-hydroxyapatite (nHA), was conducted to determine which films should be utilized in the 3D scaffold fabrication process. The selection of superior film ratios was dependent on the morphology and proliferative characteristics of material-seeded cells as compared with monolayer controls. This was done to ensure that the selected material was non-cytotoxic and did not prevent cell proliferation. Additionally, attention was given to any perceived evidence of potential osteogenic effects exhibited on material-seeded cells, as the compositional inclusion of nHA was anticipated to imbue the material with an osteo-inductive capacity. Unfortunately, both the PU and nHA components interfered substantially with the MTS proliferation assay and osteogenic potential assay, Alizarin Red staining, respectively. The results of the MTS assay were determined unreliable based on observed healthy cell populations on films, apart from the 60/40 PU-nHA film, through Calcein-AM and DiI fluorescent imaging in spite of the contradictive low MTS absorbance values, which would appear to indicate low cell population numbers and potential cell death. It was postulated that the formazan crystals produced in reaction to the MTS reagent, which are responsible of the measured colorimetric intensity, were in some way trapped within the polymeric matrix preventing release into media and subsequent analysis. Similarly, the Alizarin Red staining assay, commonly used to determine if a material or additive has an osteogenic impact on cells, was rendered ineffectual by the nHA content of the films. As this stain targets mineralized regions by binding to calcium within the extracellular matrix, the presence of a calcium phosphate (CaP) rich mineral in the material resulted in extensive background staining that completely obscured assessment of the seeded cells. The intensity of this background staining was associated with the percentage of incorporated nHA in a given film with increased compositional nHA resulting in more prolific sample staining (**Figure 7.2**). To

circumvent these challenges, a Calcein-AM fluorescent assay (Crisan et al., 2015) was conducted to verify viability and track proliferation characteristics for material-seeded films, while a morphometric assessment was performed using a DiI fluorescent marker to track the development of nodules that correlated to mineralized clusters observed in films without nHA content. The results of these studies, discussed in *Chapter II*, indicated that two of the film iterations, the 80/20 and 90/10 PU-nHA compositions, were promising candidates for fabricating a multi-layered osteobiologic platform, as both film iterations displayed cytocompatibility and did not impede cell growth/proliferation. Furthermore, these iterations appeared to demonstrate some osteo-inductive characteristics, particularly the 80/20 material.

After selection of candidate films, multi-layered scaffold designs based on each film were fabricated as described in *Chapter III*, with 80/20-derived scaffolds designated as S-1 and 90/10-derived scaffolds as S-2. A cursory *in vitro* examination of the scaffolds was conducted to verify that the final compositions, which now included decellularized bone particles (DBPs), maintained cytocompatibility. This was done by imaging of DiI labeled cells seeded to constructs and demonstrated cells were capable of migrating in materials and proliferating, though clarity of imaging suffered due to challenges associated with intra-scaffold imaging for largely opaque 3D structures. Additionally, RNA was isolated from cell-seeded material samples to evaluate expression of a couple key osteogenic genes, which demonstrated expression of both the early bone marker osteopontin (OPN) and the mineralization marker osteocalcin (OCN). This indicated that both scaffolds maintained osteogenic capacities, particularly in the case of the S-1 iteration. The process of extracting and isolating total RNA from these scaffolds again provided challenges due to material composition. As described in an article by Lee et al. (Lee, 2011), the presence of CaP materials during RNA extraction can complicate the procedure due to binding and trapping of RNA by CaP particles. Therefore, a modified extraction method was utilized in which the phenolic agent Trizol (Thermo Fisher Scientific) is added in two stages, the first being for the initial extraction from the material and the second directly following sonication. This method resulted in substantial improvements to both yield and purity of isolated RNA and used for all future RNA extractions dealing with these scaffold designs.

Following these *in vitro* assessments, the materials were then further examined *in vivo* using a rat unicortical tibial bone defect to observe the effects of the materials in a complex biological environment. One of the generated defects at 3mm in diameter were treated with one of the material iterations, while the contralateral limb defect was left untreated for control. At one-month post-implantation animals were sacrificed, CTs were performed, and samples were collected for histology. Based on the results of both CT and histological assessments, it was determined that both scaffolds were biocompatible and maintained osteobiologic properties. Notably, the S-1 iteration appeared to demonstrate enhanced osteogenic functions as compared to its sister scaffold, as

evident in the significant levels of new bone formation over control samples. As a whole the described unicortical tibial defect model proved sufficient for biocompatibility assessment, yet comprehensive assessment of osteobiologic characteristics such as osseo-integration and tissue in-growth were difficult to discern, essentially given that the controls for this study appeared to undergo spontaneous healing over the timeframe. Therefore, an alternative model implementing a truly critically-sized defect was determined necessary to assess accurately the function of this graft design in repair and restoration of bone tissue.

The S-1 scaffold, being isolated as the primary candidate for futures evaluation, was subsequently examined in a comparative study alongside a modified version of itself and two common applied predicated devices. The modified version, designated as M-1, implemented an alternative fabrication method. Both scaffolds, as discussed in *Chapter IV*, were applied to a critically-size bone defect in rats. A 5mm diameter defect generated in the mandible these rats were filled with one of four graft materials, either S-1, M-1, BioOss Collagen®, or Syntoss®. These animals were then sacrificed at 1- and 2-month timepoints, with CTs performed and samples then extracted for histology. Maintained biocompatibility of both test articles was confirmed, and a significant level of early collagen/bone formation was observed via Masson's Trichrome staining assessment in M-1 indicated that this modified variant of S-1 may offer superior attributes for an osteobiologic platform. Immunohistochemistry (IHC) of tissue sections further supported this potential, as key proteins for osteogenic and cell attachment functions were observed throughout scaffold treated defects. These proteins including OPN, Sp7, CD34, and fibronectin (FN), illustrated the capacity of the scaffold designs to facilitate tissue ingrowth, promote osteogenic activity, and stimulate extracellular matrix development throughout the defect. Conversely, Syntoss® treated defects appeared to only demonstrate healthy integration with native tissue at the material boundaries, while the scaffold interior showed poor cellular activity. Similarities in performance of the test articles with samples treated with BioOss Collagen® proved promising due to this predicate device's documented effectiveness in treating bony defects (Miron et al., 2016; Sohn & Moon, 2018; Xu, Qi, Lin, Zhu, & He, 2019). As compared with the unicortical tibial defect study, the mandibular defect model appeared to offer a more comprehensive means of assessing the effectiveness of scaffold designs. The consistent boundaries and critical-size of the defects allowed to ease of evaluating attributes such as osseo-integration with the native tissue and tissue in-growth to graft matrix. Furthermore, the application of IHC in samples from this model proved an efficient method of comparing both protein expression and organization/distribution throughout the defect region.

The fabrication of multiple advanced bone tissue engineering materials by the UALR research team presented an interesting challenge, and the unicortical tibial defect was again utilized as the primary purpose of the study was to determine if the novel osteobiologic platforms were biocompatible. Additionally, attributes of the two material designs made them inherently unsuitable for the

earlier described mandibular model. The advanced material designs, as discussed in *Chapter V*, were divided into an iteration of the earlier S-1 and M-1 scaffolds that employed a super-hydratable PU, which allowed for dramatic material swelling on contact with material, and two iterations of an injectable scaffold based on a thermosensitive polymer known as Pluronic f-127. A brief *in vitro* assessment of these materials to verify that they were non-cytotoxic was performed and demonstrated that materials were suitable for *in vivo* application. While the expandable design, designated as Expand-o-graft, was able to be cut and sized as previous scaffolds in the surgical theater, the enhanced swelling characteristics demanded that the scaffold size be appropriately reduced as compared with the 3mm bore defect to prevent protrusion of the material from the defect or damage to surrounding bone due to mechanical pressure. The thermosensitive injectable materials, designated as I-1 for the iteration containing the basal construct with nHA additive and I-2 for the iteration with this composition plus a quaternized chitosan additive, was drawn into standard 1cc syringes with a 22.5-gauge needle at low temperature and then UZ-irradiated to sterilize. These material aliquots were then kept cold in surgical theater until needed. The injected material within the defect site was observed to gel rapidly and maintained position largely during closure of muscle layer. Both material designs, the expandable and injectable, were observed to be biocompatible and did not differ significantly from compared predicates, BioOss Collagen® and Veragraft® respectively, in CT or histological data. These osteobiologic platforms demonstrate advanced methods of application that focus on the ability to implement graft technologies through minimally invasive techniques, and therefore demand further examination for determining osteogenic potential.

The observed osteogenic effects of the earlier iterations of the osteobiologic platform, S-1 from *Chapters 3-4*, piqued interest in elucidating the potential molecular mechanisms involved. As discussed in *Chapter VI*, a multi-omics approach was utilized to determine candidate pathways induced by scaffold exposure to naïve cells. Transcriptomics using gene arrays acquired from Qiagen was combined with the ever-growing field of metabolomics to generate gene expression and metabolite abundance profiles for naïve cells seeded to scaffolds and cell monolayers that had been exposed to osteo-differentiation agents. A comparison of these profiles utilizing available online databases and pathway mapping tools then permitted the selection of pathways of interest for future examination. Specifically, the interactions of the bone morphogenic protein (BMP), Wnt, and Hedgehog (HH) pathways appeared to be primary candidates for continued studies. Furthermore, the availability of HH-specific gene expression profiler arrays by Qiagen offers an attractive opportunity to verify this pathways significance in the scaffolds osteogenic influence on naïve cells. This assessment of molecular mechanisms associated with these osteobiologic grafts will constitute an intensive process but will elucidate invaluable information for graft technologies intended for application in human medicine.

Future Research

The ever-expanding field of biomaterial research and design affords a wealth of opportunities to both develop and improve on existing technologies. Within the field of bone tissue engineering alone are a vast number of graft designs utilizing varying source material and demonstrating substantially differing levels of effectiveness for repair and restoration of tissue. The application of material constructs that resemble bone in structure or chemical make-up have been attractive alternatives to the use of autologous grafts, due to heightened risk to patients. However, these graft technologies are largely ineffectual for treating or preventing injuries caused by diseases such as osteoporosis, in which bone tissue becomes brittle and relatively fragile due to upregulated osteoclastic activity and propensity of naïve cells to mature toward adipocytes as opposed to osteocytes. These complex systems require more advanced approaches, as graft materials applied to fractures in these conditions may be capable of facilitating integration with native tissue or promoting new bone development. For this reason, graft designs for such challenges may likely require the inclusion of stimulatory elements such as protein or gene therapy approaches.

Of particular interest based on my previous studies with the earlier discussed biomaterials, is the incorporation of an injectable matrix capable of then stimulating surrounding tissue to produce therapeutic levels of a given protein or proteins. Exploration into literature surrounding the application of chemically-modified RNAs (cmRNAs) or modified-mRNAs (mmRNAs) appears to offer a promising means for such stimulation of native tissue (Badieyan et al., 2016; Badieyan & Evans, 2019; Balmayor et al., 2016; Balmayor et al., 2017; Evans, 2012). However, extensive research will be required to determine the optimal combination of material and coded proteins to elicit the desired rescue of tissue subject to these systemic diseases such as osteoporosis and may offer more rapid potential in coupling with current scaffold designs for enhanced guided bone regeneration. As this method may alleviate the complications associated with adding supra-natural doses of exogenous protein to scaffold designs, this would be a means of fabricating highly effective osteobiologics.

Conclusion

As discussed earlier, the work comprised in this document (**Figure 7.3**) represents an extensive process for assessing the biological impact of an osteobiologic technology, and steps through the stages associated with *in vitro* and *in vivo* characterization of cyto/biocompatibility and osteogenic capacity. Research efforts to examine the molecular mechanisms responsible for observed osteogenic effects of the studied grafts are on-going and studies hold invaluable information for the development of materials in the field of bone tissue engineering.

References

Badieyan, Z. S., Berezhanskyy, T., Utzinger, M., Aneja, M. K., Emrich, D., Erben, R., . . . Plank, C. (2016). Transcript-activated collagen matrix as sustained mRNA delivery system for bone regeneration. *J Control Release, 239*, 137-148. doi:10.1016/j.jconrel.2016.08.037

Badieyan, Z. S., & Evans, T. (2019). Concise Review: Application of Chemically Modified mRNA in Cell Fate Conversion and Tissue Engineering. *Stem Cells Transl Med*. doi:10.1002/sctm.18-0259

Balmayor, E. R., Geiger, J. P., Aneja, M. K., Berezhanskyy, T., Utzinger, M., Mykhaylyk, O., . . . Plank, C. (2016). Chemically modified RNA induces osteogenesis of stem cells and human tissue explants as well as accelerates bone healing in rats. *Biomaterials, 87*, 131-146. doi:10.1016/j.biomaterials.2016.02.018

Balmayor, E. R., Geiger, J. P., Koch, C., Aneja, M. K., van Griensven, M., Rudolph, C., & Plank, C. (2017). Modified mRNA for BMP-2 in Combination with Biomaterials Serves as a Transcript-Activated Matrix for Effectively Inducing Osteogenic Pathways in Stem Cells. *Stem Cells Dev, 26*(1), 25-34. doi:10.1089/scd.2016.0171

Crisan, L., Crisan, B., Soritau, O., Baciut, M., Biris, A. R., Baciut, G., & Lucaciu, O. (2015). In vitro study of biocompatibility of a graphene composite with gold nanoparticles and hydroxyapatite on human osteoblasts. *J Appl Toxicol, 35*(10), 1200-1210. doi:10.1002/jat.3152

Evans, C. H. (2012). Gene delivery to bone. *Adv Drug Deliv Rev, 64*(12), 1331-1340. doi:10.1016/j.addr.2012.03.013

Juliana Tsz Yan Lee, W. H. T., King Lau Chow. (2011). Simple Modifications to Standard TRIzol® Protocol Allow High-Yield RNA Extraction from Cells on Resorbable Materials. *Journal of Biomaterials and Nanobiotechnology, 2*, 41-48. doi:10.4236/jbnb.2011.21006

Miron, R. J., Zhang, Q., Sculean, A., Buser, D., Pippenger, B. E., Dard, M., . . . Zhang, Y. (2016). Osteoinductive potential of 4 commonly employed bone grafts. *Clinical Oral Investigations, 20*(8), 2259-2265. doi:10.1007/s00784-016-1724-4

Sohn, D. S., & Moon, Y. S. (2018). Histomorphometric study of rabbit's maxillary sinus augmentation with various graft materials. *Anat Cell Biol, 51*(Suppl 1), S1-s12. doi:10.5115/acb.2018.51.S1.S1

Xu, A. T., Qi, W. T., Lin, M. N., Zhu, Y. H., & He, F. M. (2019). The optimization of sintering treatment on bovine-derived bone grafts for bone regeneration: in vitro and in vivo evaluation. *J Biomed Mater Res B Appl Biomater*. doi:10.1002/jbm.b.34387

Appendix

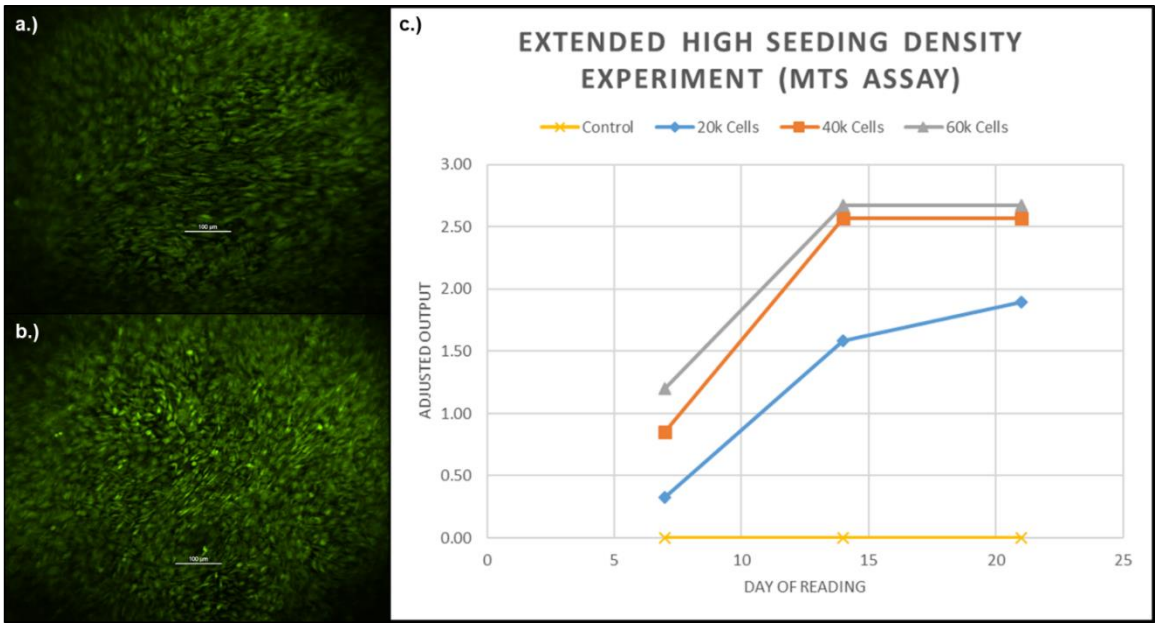

Figure 7.1. Early in vitro MC 3T3-E1 cell seeding density optimization. Morphological and proliferative assessment of varying densities of MC 3T3-E1 on tissue-treated polystyrene surfaces to determine optimal seeding density for future experiments. Calcein-AM staining of 20,000 cells (a) and 60,000 cells (b) per well of a 24-well tissue culture plate were examined using an MTS proliferation assay (c) in which the control comprised of empty plate wells.

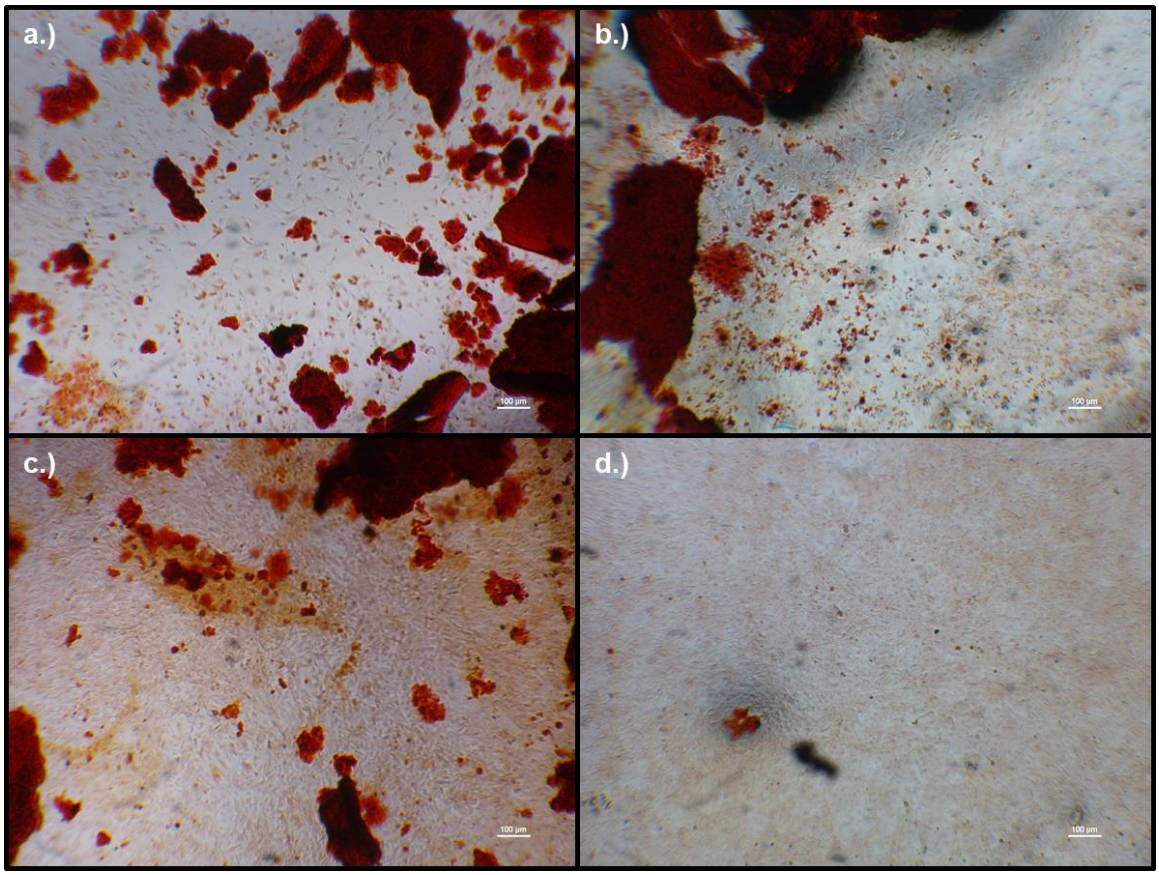

Figure 7.2. nHA content interference with Alizarin Red staining. Deep red staining of nHA content of the films can be observed and background intensity was related to the percentage of nHA within matrices as evident in observations of 60/40 (a), 70/30 (b), 80/20 (c), and 90/10 (a) PU-nHA compositions.

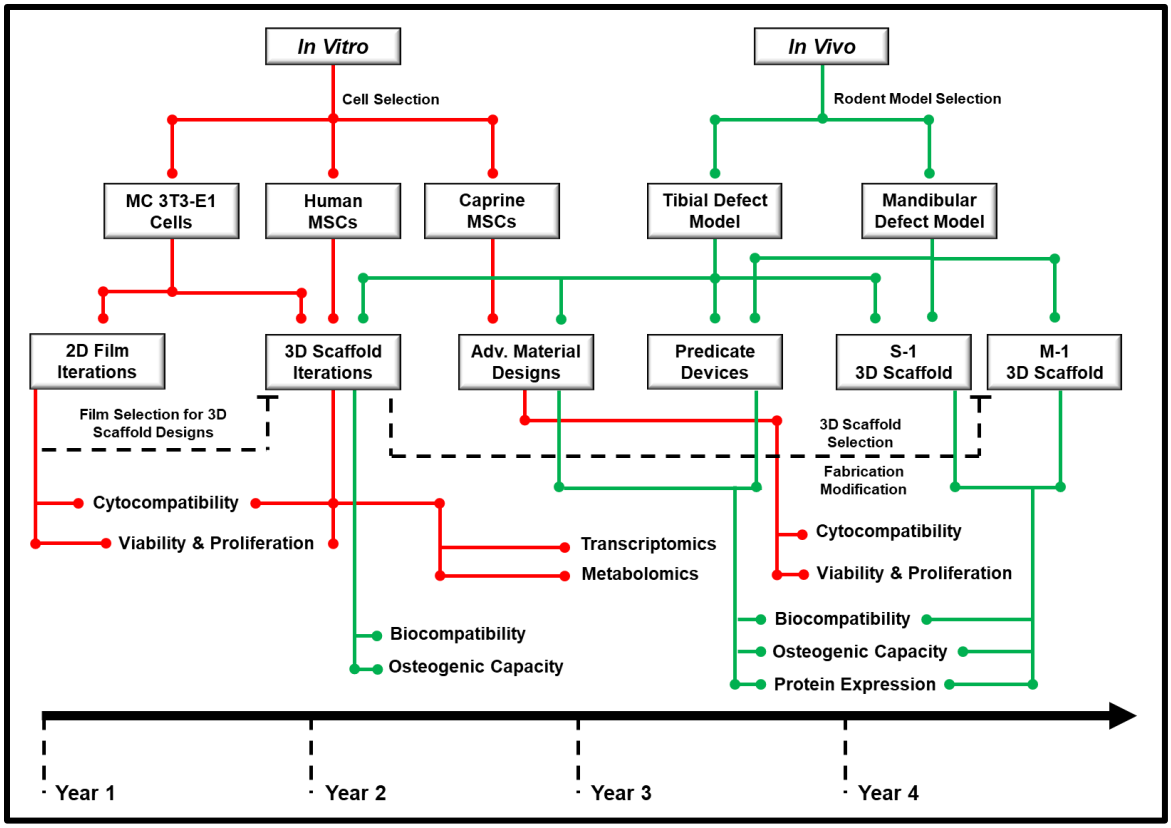

Figure 7.3. Research workflow overview. In vitro and in vivo experimental set-up and objectives are plotted along research timeline to demonstrate general progression of studies.

VITA

Austin J. Bow, born in November 1992, attended the Tennessee Governor's Academy (TGA) from August 2009 to May 2011 where he took college level math and science-based courses through the University of Tennessee, Knoxville (UTK) for credit. He then was accepted to and attended the UTK for Biomedical Engineering. In May of 2015 he graduated with his Bachelor of Science degree for Biomedical Engineering and proceeded to apply for graduate programs. In January of 2016, Austin began his pursuit of a PhD under the mentorship of Dr. Madhu Dhar in the Comparative and Experimental Medicine (CEM) program at the UTK. His studies focused on the application and design of biomaterial and cell-based regenerative medicine therapies, specifically targeting bone tissue. He has written and submitted his dissertation for review, for a planned graduation in December of 2019.

During his time in graduate school, Austin has had two publications, with one as a first author. These publications constitute *Chapters II and III*, in this work. Additionally, the content covered in Chapter I and VI has been submitted as two separate works to the journal of Drug Metabolism Reviews and Biomaterials respectively. Apart from journal articles, he has presented a collection of poster and oral presentations at symposia and conferences hosted by the CEM department at UTK, the Tissue Engineering and Regenerative Medicine International Society (TERMIS), and the Military Health System Research Symposium (MHSRS).